THE RUNBOT: ENGINEERING CONTROL APPLIED TO REHABILITATION IN SPINAL CORD INJURY PATIENTS

Lin Meng

Submitted in fulfilment of the requirements for the degree of
Doctor of Philosophy (PhD)

School of Engineering
College of Science and Engineering
University of Glasgow

August 2015

Abstract

Human walking is a complicated interaction among the musculoskeletal system, nervous system and the environment. An injury affecting the neurological system, such as a spinal cord injury (SCI) can cause sensor and motor deficits, and can result in a partial or complete loss of their ambulatory functions. Functional electrical stimulation (FES), a technique to generate artificial muscle contractions with the application of electrical current, has been shown to improve the ambulatory ability of patients with an SCI. FES walking systems have been used as a neural prosthesis to assist patients walking, but further work is needed to establish a system with reduced engineering complexity which more closely resembles the pattern of natural walking.

The aim of this thesis was to develop a new FES gait assistance system with a simple and efficient FES control based on insights from robotic walking models, which can be used in patients with neuromuscular dysfunction, for example in SCI.

The understanding of human walking is fundamental to develop suitable control strategies. Limit cycle walkers are capable of walking with reduced mechanical complexity and simple control. Walking robots based on this principle allow bio-inspired mechanisms to be analysed and validated in a real environment. The Runbot is a bipedal walker which has been developed based on models of reflexes in the human central nervous system, without the need for a precise trajectory algorithm. Instead, the timing of the control pattern is based on ground contact information. Taking the inspiration of bio-inspired robotic control, two primary objectives were addressed. Firstly, the development of a new reflexive controller with the addition of ankle control. Secondly, the development of a new FES walking system with an FES control model derived from the principles of the robotic control system.

The control model of the original Runbot utilized a model of neuronal firing processes based on the complexity of the central neural system. As a causal relationship between foot contact information and muscle activity during human walking has been established, the control model was simplified using filter functions that transfer the sensory inputs into motor outputs, based on experimental observations in humans. The transfer functions were applied to the RunBot II to generate a stable walking pattern. A control system for walking was created, based on linear transfer functions and ground reaction information. The new control

system also includes ankle control, which has not been considered before. The controller was validated in experiments with the new RunBot III.

The successful generation of stable walking with the implementation of the novel reflexive robotic controller indicates that the control system has the potential to be used in controlling the strategies in neural prosthesis for the retraining of an efficient and effective gait. To aid of the development of the FES walking system, a reliable and practical gait phase detection system was firstly developed to provide correct ground contact information and trigger timing for the control. The reliability of the system was investigated in experiments with ten able-bodied subjects. Secondly, an automatic FES walking system was implemented, which can apply stimulation to eight muscles (four in each leg) in synchrony with the user's walking activity. The feasibility and effectiveness of this system for gait assistance was demonstrated with an experiment in seven able-bodied participants.

This thesis addresses the feasibility and effectiveness of applying biomimetic robotic control principles to FES control. The interaction among robotic control, biology and FES control in assistive neural prosthesis provides a novel framework to developing an efficient and effective control system that can be applied in various control applications.

Acknowledgement

Firstly, I would like to thank Dr. Bernd Porr and Dr. Henrik Gollee for their supervision throughout my PhD. Their supports, encouragement and ideas have helped to guide me through the process. Much of what I have learned over the past four years is attributed to you and you have my sincere thanks.

I must thank all my colleagues in the Centre of Rehabilitation Engineering, who are always on my side and keep me smile, especially: Bethel Osuagwu, Margaret Armentano and Sarah Comincioli. I would like to acknowledge Catherine A.Macleod of the University of Strathclyde in our collaboration. The human studies you have done is fundamental in the whole project, and I really enjoyed the hours we spent together to make Runbot walk using human data. I must express my gratitude to the help of electronics technician Tom OHara, all mechanical technicians who made the robots real, and ladies in the financial office. All your work was extremely valuable to my research. To all volunteers who took part in the human study I would to extend my thanks. Thank you for your time and patience. Your participations let me be able to finish the human experiment in two weeks.

I would like to acknowledge the Lord Kelvin Smith Scholarship for the financial support to allow me to conduct this PhD.

Last but not the least, the whole-hearted support of my friends and family throughout this PhD has meant a lot to me. Thank you for your love and patience. Your support has helped me to get through the tough periods in my PhD.

Author's Declaration

I declare that, this thesis is the result of the author's original research, and has not been submitted for examination which leds to the award of a degree.

Lin Meng

August 2015

Contents

List of Tables

List of Figures

Abbreviations

AEA Anterior Extreme Angle.

AIS ASIA Impairment Scale.

AL Adaptive Learning.

ANN Artificial Neural Network.

ASIA American Spinal Injury Association.

BF Biceps Femoris.

BWS Body Weight Support.

CNS Central Nervous System.

CPG Central Pattern Generator.

DoF Degree of Freedom.

EMG Electromyography.

ESW Early Swing.

FDA Food and Drug Administration.

FES Functional Electrical Stimulation.

FF Flat Foot.

FSC Finite State Control.

FSM Finite State Machine.

FSRs Force Sensitive Resistors.

GA Genetic Algorithm.

GUI Graphical User Interface.

HO Heel Off.

HS Heel Strike.

HZD Hybrid Zero Dynamics.

IA Induce Acceleration.

IL Inductive Learning.

iSCI imcomplete Spinal Cord Injury.

LG Lateral Gastrocnemius.

LMN Lower Motor Neuron.

LMS Least Mean Squares.

LSW Late Swing.

MaxTC Maximal Threshold Current.

MinTC Minimal Threshold Current.

PNS Peripheral Nervous System.

PTC Perception Threshold Current.

QF Quadriceps Femoris.

RF Rectus Femoris.

RL Reinforcement Learning.

SCI Spinal Cord Injury.

TA Tibialis Anterior.

TO Toe Off.

ZMP Zero Moment Position.

Chapter 1

Introduction

1.1 Background

Human walking results from the complicated interaction between the nervous system, the musculoskeletal system and the environment. The coordination of muscle activity and limb movement is required for stable locomotion, where gait phases and spatial information from the environment are provided by the Peripheral Nervous System (PNS) via sensory feedback. The theory of "Limit Cycle Walking" regards the walking gait as a repetitive motion of steps [4]. The walking gait could be simplified as a periodic sequence of movements.

Dynamic walkers with proper mechanical design and biologically inspired control model benefited from human walking to achieve a stable walking with low energy consumption, reduced computation cost and good adaptivity to disturbances. The RunBot is a bipedal robot driven by simple reflexes without precise trajectory algorithms and is inspired by human reflex mechanisms as shown in Fig. 1.1 [5, 6, 7]. Phases are switched by the ground contact information.

The robotic controller has potential use in the development of gait rehabilitation strategies for patients with Spinal Cord Injury (SCI) as the system follows the control of human walking without complex algorithms. However, the lack of ankle control in the existing robotic controller requires a new controller to be created with additional ankle control. An understanding of human walking control based on knowledge of the RunBot system is needed to complete the reflexive robotic controller. The idea is to map sensory inputs to motor outputs by studying the relationship between foot contact information and muscle activity. A closed loop system can then be created with a minimalist approach. Conversely, the RunBot could be a tool in a realistic environment to test biological models for walking.

To understand the context of the research, it is important to understand the concept of SCI and the rehabilitation strategies for regaining walking ability thereafter. The problems related to

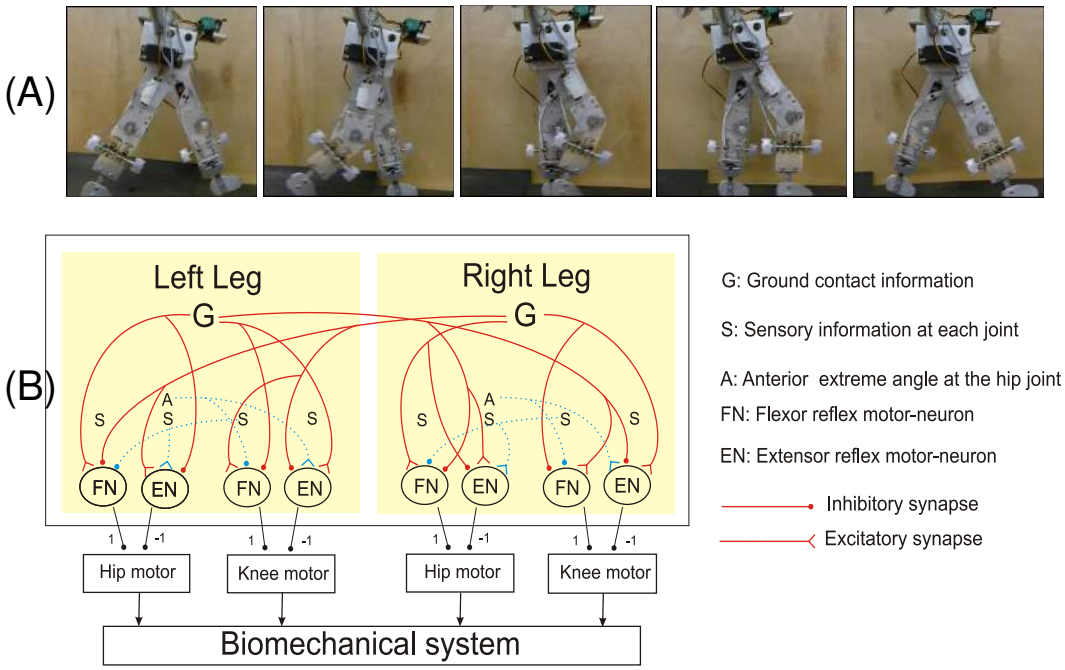

Figure 1.1: RunBot achieves stable cycle walking with the implementation of a neural reflexive controller. Ground contact information triggers the extensors of the ipsilateral leg and the flexors of the contralateral leg. (A) Photographs of RunBot's gait cycle and (B) the neural reflexive controller used by RunBot to generate walking.

gait rehabilitation approaches are discussed. In addition, the mechanism of human walking control and how this knowledge was to be used in the development of a novel FES system will be presented first. The chapter also outlines the aims and structure of this thesis.

1.2 Spinal Cord Injury

SCI is a trauma to the spinal cord which results in sensory and motor deficits, and autonomic dysfunction [8]. The extent of disability depends on the severity and level of the injury to the spinal cord. The neural damage can be temporary or permanent and the SCI can be defined as complete or incomplete. The ASIA's International Classification of SCI is used as a measurement to describe the level of damage and completeness of the injury as well as an evaluation of recovery.

Humans have 33 vertebrae in the spine, consisting of 7 cervical vertebrae, 12 thoracic vertebrae, 5 lumbar vertebrae, 5 sacral vertebrae and 4 coccygeal vertebrae [9]. As shown in Fig. 1.2, intervertebral discs exist in the cervical, thoracic and lumbar vertebrae, while the sacral and coccygeal vertebrae in adults fuse to form two bones known as the sacrum and the coccyx. There are 31 pairs of spinal nerves consisting of 8 cervical nerve pairs (C1-C8), 12 thoracic pairs (T1-T12), 5 lumbar pairs (L1-L5) and 1 coccygeal pair.

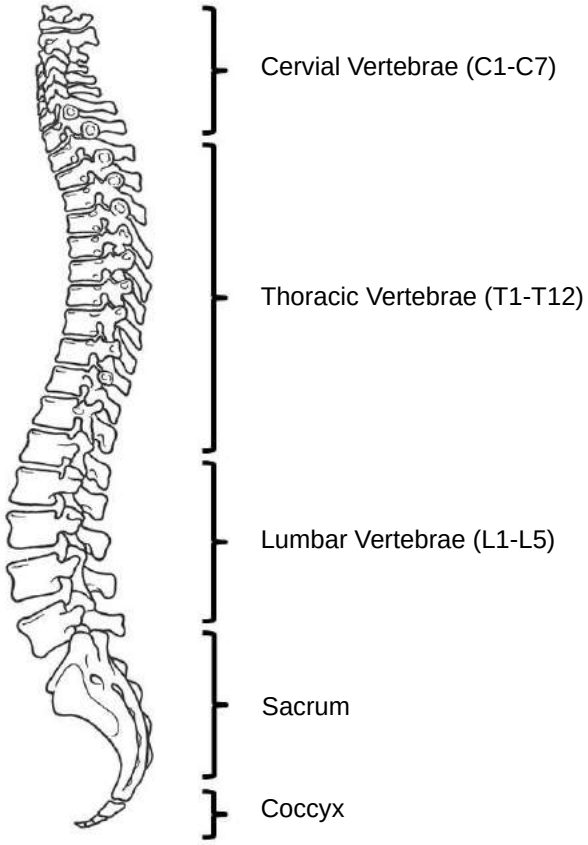

Figure 1.2: Levels of the spinal cord.

SCI is categorised into five levels (A to E) outlined in the ASIA classification form (Fig. 1.3 and Tab. 1.1). According to the ASIA scale complete SCI, classified as ASIA Impairment Scale (AIS) A, is an injury resulting in the total loss of sensory and motor function emanating from the S4-S5. If there is sensory or motor function preserved below the injury, it is defined as incomplete SCI. Function recovery in the first few months after injury has been observed in a significant proportion of patients, especially those with incomplete SCI initially assessed as AIS B and C [8]. More than 50 % of patients with an incomplete sensory lesion (AIS B) regain a certain amount of their ambulatory function, and 75 % of patients with an incomplete motor lesion (AIS C) become ambulatory by discharge [10, 11]. Improved locomotion post injury demonstrates that the adaptivity of the neural circuits preserved in the spinal cord could reproduce sensorimotor function, which is known as “neuroplasticity” [12]. Mechanisms within the spinal cord could also play a role in enabling movements, such as gait change in reaction to muscle spasticity.

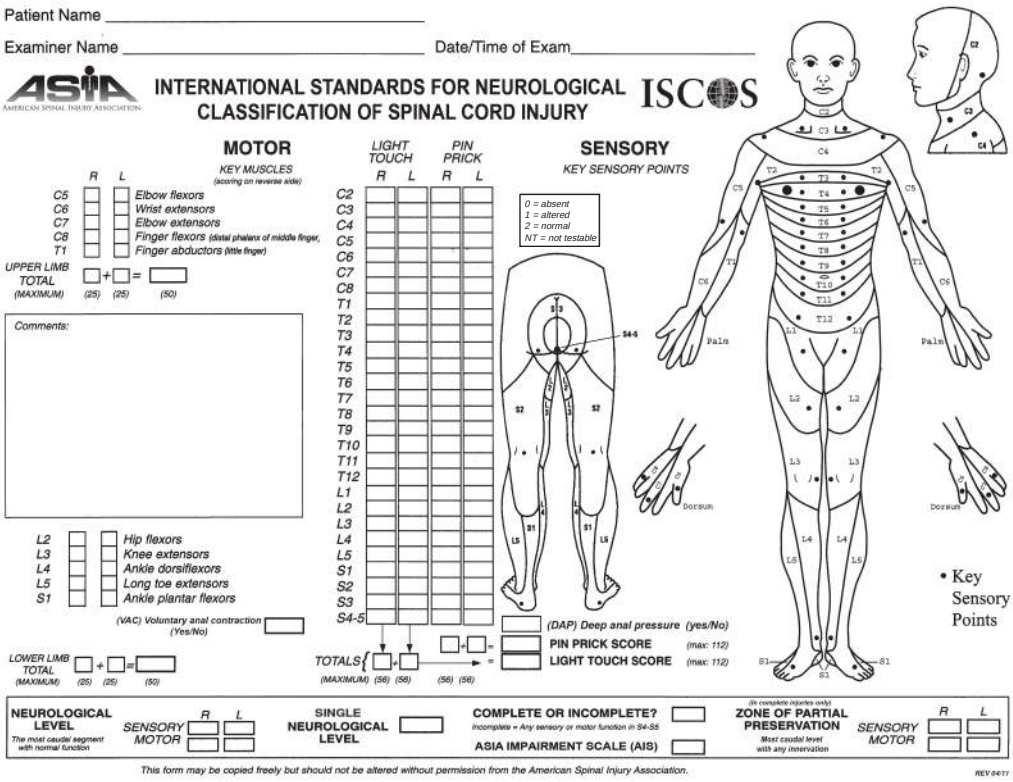

Figure 1.3: ASIA Impairment Scale scoring sheet [2].

Table 1.1: ASIA Impairment Scale

Grade	Description
A	Complete: No sensory or motor function preserved in the sacral segments S4-S5
B	Incomplete: sensory but not motor function preserved below the neurological level and extending through the sacral segment S4-S5
C	Incomplete: motor function preserved below the neurological level; most key muscles have a grade <3
D	Incomplete: motor function preserved below the neurological level; most key muscles have a grade >3
E	Normal sensory and motor functions

1.2.1 Gait Rehabilitation

Limitations of over-ground walking in patients with SCI includes: 1) reduced coordination, 2) leg paresis, and 3) impaired balance [13]. The rehabilitation of patients with SCI aims to

improve locomotive function and facilitate neuroplasticity for the recovery of motor function. Conventional rehabilitation strategies, such as bracing and walking aids, primarily provide compensation for deficits to accomplish mobility and strengthen muscles above the level of the lesion. These strategies are designed to promote maximum muscle capacity and to compensate the absence or weakness of the muscles. The compensatory model may not influence the recovery of the nervous system. New approaches facilitate locomotor recovery by using locomotion training that optimises sensory inputs related to locomotion [14]. These approaches provide sensory inputs associated with a motor task to let the nervous system within the spinal cord learn how to respond to the sensory signals again. The incorporation of sensory inputs related to locomotion can improve the walking ability of patients after SCI on a treadmill or overground [15, 16, 17].

Current therapeutic rehabilitation approaches includes treadmill, Body Weight Support (BWS), robotic orthoses and FES [8]. One of the most common rehabilitation approaches is physiotherapy for patients with SCI to regain muscle function by using repetitive and intensive gait practises on a treadmill. BWS is widely used to provide a safe and efficient environment for locomotion training. Partial BWS can be incorporated in therapeutic strategies to enhance the strength of weight-bearing muscles. Robotic orthoses, such as Lokomat (Hocoma AG, Volketswil, Switzerland), can provide assistance during training by relieving the therapists from the tedious work of moving the limbs for patients during the treadmill training [18]. Unlike other therapeutic approaches FES is a technique applied on muscles to elicit motor responses by electrical stimulation for patterned locomotion. The rehabilitation strategies usually involve a combination of different approaches.

1.3 Functional Electrical Stimulation

FES is a technique that applies electrical currents to neural tissues for the purpose of restoring functional movement. Electrical stimulation artificially replaces absent or weak muscle contractions [19]. FES systems have been utilised as neural prostheses which replace the conventional braces for walking. FES is recommended by Kakulas [20], who reported that the electrical stimulation contributes to retaining neurological functions and modulating reflexes to the normal state. For instance, in paralysed limbs of patients with SCI, there are more type II muscle fibres (white, fast, anaerobic) than type I (red, slow, aerobic) due to muscle atrophy. The electrical stimulation can increase type I muscle fibres to a normal distribution and further increase muscle contraction and resistance to fatigue [21]. It has been speculated that activity-dependent neural adaptation training could be important for the development and recovery of sensorimotor functions. The electrical stimulation of the muscles can be coordinated within the gait cycle by incorporating appropriate sensory feedback to

facilitate cortical reorganisation [22]. The FES is beneficial to patients with incomplete SCI who have intact Lower Motor Neuron (LMN) (T4-T12) and good upper body strength [19].

Since 1960 Kantrowitz [23] proposed that patients can achieve standing by applying stimulation to the quadriceps muscles bilaterally, numerous worldwide studies investigated the use of FES for patients with SCI to stand and walk. The outcomes had limited success due to physiological and engineering reasons, such as high energy expenditure, slow walking speed, lack of balance, inadequately coordinated muscle activation, the system with heavy battery etc [19]. Although the clinical significance of FES has been proven in standing and walking for patients with SCI, FES walking systems can not replace the wheelchairs as the main mobility aid for patients with SCI. Many surface FES system have been tested and only one FES system ParaStep is approved by Food and Drug Administration (FDA) and available in the commercial market. Implanted FES systems have been developed since the 1980s by using percutaneous electrodes for stimulation, which enable better activation of deep muscles and reliable muscle contractions. Several implanted FES systems were designed and tested in clinical trials but were finally abandoned due to inadequate muscle selectivity [24, 25]. Hybrid systems combining FES with a gait orthosis have been investigated but not reached the commercial market yet. The majority of FES devices in the market are open-loop. The high energy expenditure, engineering complexity and inadequate coordination of muscle activation limit the routine use of FES walking system [26]. Thus, it is fundamental to explore an approach for FES control that is in real-time, robust, computationally efficient and adaptive to voluntary limb movements from the patient.

1.4 Motivation

An ideal FES system should work perfectly parallel with the human nervous system. Further understanding on the control of human walking is needed. The project was inspired by the concept of the original RunBot [7], which instead of attempting to understand the mechanisms of walking in detail, obtained a stable walking cycle by generating a motor output with a simple foot contact input in a neural processing model. The model proposed by Geng [7] was based on theoretical biology in humans. The nervous system in humans is still not fully understood in terms of locomotion control, however, the system can be treated as a black box. If the foot contact information can be related to muscle activity, the processing in the nervous system can be simply regarded as a transfer function that translates sensory information into muscle activation during walking. The coordination of muscle activations that drive hip, knee and ankle joints during walking can be determined. Knowledge of how sensory feedback relates to muscle activation during walking could be used in FES for SCI rehabilitation. A simple biological-inspired robotic approach used in the development of an

FES control system may assist in regaining walking ability and facilitate neuroplasticity in the spinal cord.

1.5 Aim and Objectives

The final aim of this thesis was to develop a simple and efficient FES control model with the potential to be used to assist walking in patients with SCI. By taking inspiration from the reflexive mechanism used by the RunBot [6], the reflexive control model will firstly be improved based on transfer functions derived from human studies. Here the relationship between foot contact information and muscle activation will be studied in collaboration with colleagues at the University of Strathclyde. In contrast to the original reflexive controller [6], the novel reflexive control model will include the ankle action and use transfer functions instead of neuronal processing. The feasibility of the model will be tested in a bipedal walker, RunBot III. An FES controller will be created based on the robotic reflexive controller, and the FES walking system will be developed and tested in able-bodied participants.

The objectives required to complete this PhD project were to:

1. Create a novel reflexive controller consisting of hip, knee and ankle joints based on transfer functions derived from human data where foot sensory information is related to muscle activations and further joint movements.

2. Improve the mechanism of the RunBots. To test the biological control principles, a series of the RunBot will be designed. The mechanism of the robot is firstly improved by implementing a compliant knee joint. An actuated ankle joint is then included in the RunBot III for the creation of a fully actuated bipedal walker so that the novel reflexive controller can be tested.

3. Develop an FES system. The FES system will be built up based on the concept of the robotic system while the FES control is transferred from the robotic reflexive controller.

4. Evaluate the FES system. The feasibility and effectiveness of the system will be investigated in experiments with able-bodied participants.

1.5.1 Thesis Outlines

These aims and objectives will be addressed in chapters of this thesis. The thesis is structured as below:

Chapter 2: A thorough background will be given in this chapter with a literature review on neural control in human walking. Subsequently, the concept of using robots to solve biological problems will be discussed alongside an overview of the current research in dynamic walkers. Studies investigating FES control for walking are then reviewed in this chapter, with a particular focus on Finite State Control (FSC) methods. The open questions and possible development to improve the efficiency of the technique will be presented.

Chapter 3: This chapter is the preliminary study of biological inspired robotic control. The knee mechanism of the RunBot II is firstly improved to obtain a more human-like knee movement within gait cycle and reduce force impact to the knee when the heel strikes the ground. A simplified reflexive controller with filter functions will be created and implemented in the RunBot II. The feasibility of the transfer function that translates the sensory input to motor output is discussed in this chapter.

Chapter 4: Following the preliminary studies, this chapter focuses on creating a new reflexive controller featuring ankle control for the completion of the control model illustrating human walking. Based on the causal relationship between foot contact information and muscle activation measured by Electromyography (EMG), transfer functions are analysed which translate the foot contact to motor control by determining the sensory triggering of flexion/extension in the hip, knee and ankle joints during walking. A minimal and reflexive control model for walking is outlined and implemented in the RunBot III. The results are discussed in this chapter.

Chapter 5: This chapter introduces a novel reliable gait phase detection system, which will provide correct trigger timing for FES control. The methodology for detecting gait phases and generating trigger impulses at phase transition events by using the foot contact and hip angular position is the focus of this chapter. The reliability of the system is investigated. This chapter also includes a small study of optical motion tracking as a reference system in the experiment.

Chapter 6: This chapter includes a description of the multichannel FES walking system and the FES control principles. The feasibility of using this system for walking assistance is demonstrated with 7 able-bodied participants. The effectiveness of the system is evaluated in the experiments.

Chapter 7: This chapter is a discussion of the main outcomes of the research. The main contributions of the approach are summarised from the aspects of biological inspired robotic engineering and the FES control for gait rehabilitation based on robotic control. Possible future research is recommended, such as further development of a commericial system.

1.6 Contributions

1. A novel compliant knee joint is designed by taking the inspiration of a sagittal model of the patellofemoral joint. It is shown that a compliant knee significantly improves walking performance of the RunBot II resulting in a more robust and human-like knee movement during the swing phase. The results of this study suggest that the stiffness in the compliant knee could affect walking speed of the robot. It illustrates the significance of the mechanism to dynamic walkers.

2. A novel reflexive controller is developed based on the causal relationship between the foot contact information and muscle activity in human data and associated filter functions. It is the first attempt to involve ankle control in the reflexive control model to establish fully actuated ankle movement during walking gait without precise trajectory algorithms. It is shown that the use of the controller in the RunBot III enables the robot to generate a stable walking pattern. Furthermore, the bio-inspired mechanism for controlling walking is validated by using the robot in the real environment.

3. A novel gait phase detection system utilises the foot contact information and hip sagittal angle with a novel rule-based finite state machine algorithm to distinguish the gait cycle into five phases and generate triggering impulses for gait events. Demonstration of the feasibility and reliability of the system is a necessary first step towards the development of FES walking system as a novel gait assistive neural prosthesis.

4. A novel FES protocol for gait assistance is developed and implemented in a real-time multi-channel FES walking system. A novel FES control inspired by the control of the RunBot III has a hierarchical structure consisting of finite state control at the high level and responses generated by filter functions at the low level. Eight muscles in two legs are stimulated in the coordination and synchronisation during walking gait in the system. The feasibility of using the FES protocol to assist walking is also demonstrated in the experiment of able-bodied participants.

The author was independently responsible for the mechanical design and build of the RunBot II and III. In the collaboration with Catherine A.Macleod at the University of Strathclyde transfer functions were extracted from human walking data and successfully implemented in the reflexive controller of the RunBot II promoting stable limit cycle walking. A novel control model where the control of ankle movement was first included in a purely reflexive controller was completed by the author based on the results of the collaborative study. An FES strategy for walking was created based on the inspiration of the control of the RunBot III. A novel FES system was designed and built by the author.

Publications

[1] C A Macleod, L Meng, B A Conway, and B Porr. Reflex control of robotic gait using human walking data. *PloS ONE*, 9(10):e109959, 2014.

[2] L Meng, C A Macleod, B Porr, and Gollee H. Application of reflex control to the ankle using human walking data. *In Preparation*.

[3] L Meng, B Porr, and Gollee H. Bio-inspired reflexive controlled biped robot with compliant knee joint. *Ready to submit*.

[4] L Meng, B Porr, and Gollee H. A novel multichannel functional electrical stimulation walking system based on bio-inspired reflexive robotic control. *In Preparation*.

[5] L Meng, B Porr, and Gollee H. Variable knee stiffness in bipedal walking. In *8th IEEE EMBS UK & Republic of Ireland Postgraduate Conference on Biomedical Engineering and Medical Physics.*, 2014.

[6] L Meng, B Porr, and Gollee H. Multichannels functional electrical stimulation walking system inspired by pure reflexive controller. In *25th Congress of the International Society of Biomechanics*, Glasgow, 2015.

Chapter 2

Literature Review

The literature review first describes the current understanding of neutral control in human walking where the reflexes are particularly emphasised as the main motivation of my PhD research. Research in passive dynamic walking and further limit cycle walking is discussed. Based on these studies we address how robotic walkers have solved the problem of control in bipedal walking with appropriate self-mechanism and how the robotic control system can benefit from the mechanism in human walking. Moreover, we explain how the knowledge of reflexive mechanism can be applied in the development of biped walkers. A comprehensive review of FES for the restoration of the ambulatory ability of spinal cord injured patients is given, especially focusing on the control methods. Furthermore, whether the strategy of reflexive robotic control can be adapted into a novel controller for a FES-assistive walking device is presented with the aim of providing a simple and efficient control to patients for improving functional walking ability.

2.1 Human locomotion control

Human walking is a complicated task requiring the coordination of muscle activities on different joints. Central Nervous System (CNS) is responsible for generating the muscle activity, coordinating the muscle activities, and adjusting it to the environment [27]. The CNS consists of two levels of control systems: the top level of CNS is the brain and the low level is the spinal cord. The reduced degree of freedom is controlled by the top level of the CNS (brain), while the flexibility of muscle activity is left controlled by the low level of the CNS (spinal cord) [28]. It is suggested that the spinal cord significantly contributes to the alternate flexion and extension of leg muscles during human walking.

Evidences on the spinal cord control of locomotion in invertebrates and vertebrates have come in the recent decades [29, 30, 31, 32, 33]. The first study reported by Brown [29]

demonstrated that antagonist muscle activity was evoked in invertebrates after deafferentation. Fedirchuk et al. [32] demonstrated that alternating activity of antagonist muscles was evoked in the acute spinalised monkeys by applying monoaminergic drug clonidine, and suggested that a spinal network exists for the generation of rhythmic activity. The spinal circuit can work without any supraspinal or peripheral sensory inputs in cats [34]. Evidences are accumulated for the existence of spinal circuitry in humans [35, 36]. For instance, the stepping responses were found in infants in all range of ages [37]. As the movement of the infants is mainly controlled by the brainstem and spinal cord due to the incomplete development of the corticospinal tract, it is reasonable to suggest that the brainstem and the spinal cord contribute more to the stepping response in infants. The neural control mechanism in infants is similar to the mechanisms found in cats. Another study showed that motor output from spinal circuitry is significantly dependent on peripheral sensory information in adults [38]. However, studies of patients with SCI show that the rhythmic pattern could be generated in the spinal cord of humans in some circumstances. Kuhn [39] observed the "spontaneous rhythmic stepping like movement" occasionally in one patient with SCI. Bussel et al. [35] demonstrated that the alternating flexor/extensor reflexes were observed in a patient. Dimitrijevic et al. [36] found that the application of electrical stimulation on the spinal cord of patient with complete SCI is able to trigger locomotion-like activity. Overall, a spinal cord network for rhythmic generation exists in humans and can be activated in some circumstances.

2.1.1 Central Pattern Generators (CPGs)

The existence of CPG has been well studied in both vertebrates and invertebrates [34, 40, 41, 42, 43]. Most studies on CPG in mammals are from cats. Brown [44] showed that cats with a transected spinal cord and cut dorsal roots could still generate a rhythmic alternating contraction of ankle plantarflexor and dorsiflexor muscles on a treadmill. The EMG of muscles during locomotion indicates that CPG could switch on and off muscle activities, and thus control the rhythmic locomotor movement. The CPG in the spinal cord are capable of producing rhythmic locomotion pattern without sensory inputs from the limbs or descending commands from the brain [45]. It appears that the CPG provides an open-loop control of locomotion.

The simplest model of CPG is the "half-center oscillator" proposed by Brown [44]. In the model, two neurons (flexor and extensor) are connected via reciprocally inhibitory connections. Each neuron is connected with an excitatory input. The two neurons alternatively inhibit each other by evoking reciprocal inhibition. The reciprocal coupling between the extensor and flexor motor neurons generates alternating patterns of activity.

Despite the simplicity of the "half-center oscillator" model, the structure of CPG locomotion control could be more complicated. Grillner [46] proposed a unit oscillator model of pattern

generation. Each unit oscillator model is a simple network for one joint movement control, which contributes to complex movements like walking by coupling multiple unit oscillators in limbs. This system is more flexible to generate different behaviours by adjusting the setting of unit oscillators with sensory inputs.

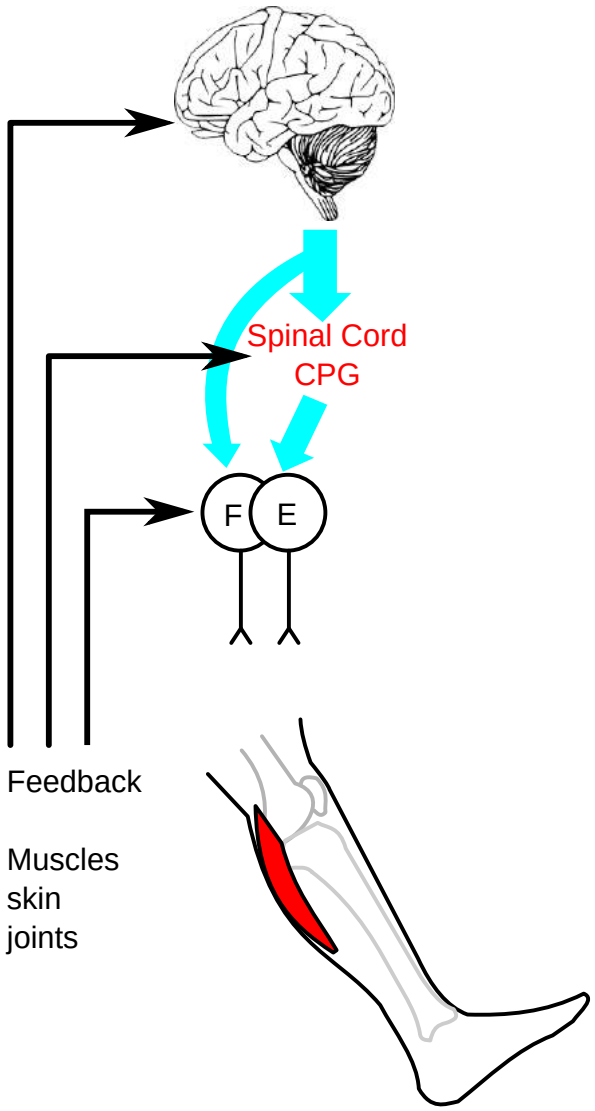

Figure 2.1: Overivew of central control structure with CPG circuitry in the spinal cord of human walking [27]. The integration of different levels of the central nervous system generates the central control of human walking. The CPG in the spinal cord is capable of generating the basic rhythmic locomotion which is controlled by supraspinal (brain stem and motor cortex) and sensory afferent feedback from the joint. The sensory afferent feedback is involved in all levels of the central nervous system.

It is theorised that sensory afferents from the skin of the foot and muscles regulate the rhythmic locomotor movements via reflex pathways to motor neurons with the CPG in the spinal circuit. Denervated spinal cats were not capable of placing the foot correctly on the ground while spinal cats with intact cutaneous sensors could recover correct foot placement during the stance phase [47, 48]. Further study in [49], spinal cats after partially denervation

were still capable of adapting locomotion with minimal cutaneous input. Thus, cutaneous inputs play an essential role in the correction of the foot position during the stance phase or to respond to sudden perturbations [50]. Load receptor feedback converges in the CNS to generate rhythmic locomotion output commands [51]. Signals from the ankle extensor determine the length of the stance phase [52], as the ankle unloading during the late stance phase decreases the signal of the ankle extensor and further initiates the swing phase. Hip position-related afferent inputs contribute to the initiation of different gait phases, especially the swing phase [53]. Therefore, sensory afferent has a global function on initiating rhythmic patterns as well as timing or resetting the rhythmic locomotor [27] as shown in Fig. 2.1.

CPGs have been well documented in vertebrates and invertebrates with vast evidence for CPGs and control models, which suggests that human would have a similar pattern generating structure. For decades, studies have documented that the neuronal pathways and motor control also exist in the human spinal cord. The pathways that produce responses for disynaptic reciprocal Ia inhibition, autogenic Ib inhibition, recurrent inhibition and the flexion reflex have been distinguished in humans [30, 54, 55, 56, 57]. Therefore, no direct evidence has been found to prove the existence of CPGs in humans after excluding reflex and supraspinal processes. One obvious difference between human CPGs and those in animals is that humans become completely paralysed after complete SCI and no recovery of locomotion is observed for years [58]. Eidelberg et al. [59] showed that Macaque monkeys with spinal cord transections could not generate stepping locomotion by utilising the same methodology that has been used in cat studies. However, stepping-like rhythmic locomotion could be generated in incomplete SCI [39] or by applying electrical stimulation to the spinal cord [36]. Thus, these studies indicate that if CPGs are present in the human spinal cord, then it is more dependent on intact peripheral feedback and supraspinal control.

2.1.2 Reflex circuits in locomotion

“The simplest motor actions are reflexes, mediated by relatively straightforward circuitry in the spinal cord.” - by Nicholls et al. [60].

Shik and Orlovsky [61] proposed that two mechanisms are responsible for interlimb coordination during locomotion. One is the interaction between the spinal automatisms where each automatism receives sensory afferent information from the specific limb. Another one consists of reflexes that do not affect the spinal automatism but directly influence motor neurons. Locomotion control can thus be hypothesised as a chain of reflexes. Different afferents have been studied to determine their roles during walking. The understanding of the reflex function is required to improve neuronal networks and models. In this section, we will address the function of reflexes based on studies in cats and humans.

Stretch reflex

Stretch reflex responses arisen from muscle afferents, especially group Ia, were investigated as they have an essential role of walking in animals. Lundberg [62] proposed that proprioceptive reflexes from muscle spindle Ia afferent and Golgi tendon organ Ib afferent contribute to "sculpture" the complex muscle activation patterns in real locomotion.

Akazawa et al. [63] studied stretch reflexes during locomotion in cats and observed that the stretch reflexes in the soleus muscle were deeply modulated during the step cycle while they peaked during the stance phase and were small during the swing phase. Capaday and Stein [64] did the same study on human and observed that the soleus H-reflex was large during the stance phase and small during the swing phase of human walking. Kearney et al. [55] studied the ankle passive-walking movements driven by a hydraulic actuator and observed that the pulse disturbance generated a large reflex torque during the early stance phase and little torque during the late stance and swing phase. Yang et al. [65] designed an experiment in which a mechanical dorsiflexion driven by a pneumatic actuator was applied to the foot during the stance phase of the walking and observed a velocity-sensitive reflex response in the soleus muscle. They calculated that the component of reflex response could account for 30-60 $\%$ of the muscle activation. It suggests that the function of phase-dependent stretch reflex contributes to stabilisation and body loading response during the early stance phase.

When the foot loses contact with the ground, the afferent of muscle stretch sensor signaling the limb position plays an important role in locomotion occurrence [53]. Early experiments done by Brown [29] showed that holding to extend the hindlimb of spinal cats efficiently triggered the hindlimb flexion. The sensorimotor interaction in infants is remarkably similar to that in cats [66]. The disturbance generated by grasping the limb for a short time in the swing phase resulted in a prolonged stance phase of the contralateral limb and a delayed swing phase. The load added to the limb by pushing down the pelvic during the stance phase prolonged this phase and delayed the swing phase. Pang and Yang [67] indicated the inverse relationship between the hip position and load contributing to regulate the transition from the stance to the swing phase.

Load receptor reflex

Proprioceptive inputs from muscle group I, especially Golgi tendon organ Ib afferent, play a fundamental role in regulating the step and rhythm [52]. In "foot-in-the-hole" experiments where cats make a step through a trap, the muscle activation was proportional to the sensory feedback [68]. Similar studies in humans [56, 57] showed that the EMG in extensor muscles decreases when unloading the subjects or specific muscles with mechanical methods. Hence, Sinkjær et al. [57] concluded that muscle afferent Ib input significantly contributes to ankle

plantarflexor activations in the stance phase. Dietz [69] suggested that load receptors in the extensor muscles regulate the stance phase during human walking. Adding load during human walking increases extensor activity and thus prolong the duration of the stance phase. The gait adaptation was investigated by applying different speeds to each leg and adjusting load weight [70]. The results showed that adjusting body loading weight significantly improved the adjustment of treadmill speed, suggesting a major functional role of load receptor in gait locomotion.

Cutaneous reflex

In studies about contributions of cutaneous sensory inputs to locomotion [49, 71, 72], cutaneous nerves that innervate the hindfeet were removed and the denervated cats performed normal walking on the treadmill. The results of kinematic and EMG pattern showed the adaption to the denervation leading to a decrease in the swing phase and an increase in the double stance phase. However, ladder, beam, up or down-hill walking never returned to complete normal even after 3-7 weeks recovery. It is thus reasonable to suggest that cutaneous input plays an essential role to adjust walking on a step by step basis. Denervated cats were not capable of placing the foot correctly on the ground while spinal cats with intact cutaneous sensors could recover correct foot placement during the stance phase in studies of Barbeau and Rossignol [47] and Belanger et al. [48]. Furthermore another study showed that spinal cats after partial denervation were still capable of adapting locomotion with a minimal cutaneous input [49]. Therefore, the cutaneous input is fundamental for gait rehabilitation after spinal injury.

The same stimulus may elicit a response in the flexor or extensor muscles depending on the gait phases. A mechanical stimulus to the dorsum of the foot in the swing phase triggers an additional flexion of muscles, results in a prominent flexion in the knee, ankle and hip joints, and thus clears the foot over to the obstacle [73]. The same mechanical stimulus does not evoke the flexor muscles in the stance phase, in contrast, an increase of reflex amplitude in extensor muscles was observed [74]. A similar study has been done in humans [75]. A foot tripping mechanical disturbance was applied in the early and late swing phases during walking. An elevating strategy emerged from the perturbation in the early swing phase, with a short latency response in the BF and a later response in the RF of the ipsilateral limb, meanwhile, short latency responses in the extensor muscles of the contralateral limb were evoked. On the other hand, a lowering strategy was elicited by the same perturbation in the late swing phase to let the foot touch the ground faster.

Cutaneous reflexes arising from electrical stimulation have been studied and showed the phase-dependent modulation of reflex responses (reviewed in [76]). Nociceptive electrical stimulation during walking causes phase-depended responses that induce withdraw reflexes

in the swing phase and increase the extensor responses during the stance phase. Tibial nerve stimulation yields an increased ankle extension in the late swing phase, whereas it causes an increased activity in the TA muscle for ankle flexion from the stance to swing transition to remove the foot [76]. Stimulation of superficial peroneal nerve results in a reduction in the TA muscle activation which mechanically transfers a plantarflexion in the early swing. A study of stimulating the sural nerve to innervate the lateral side of the foot showed a suppression in the gastrocnemius medialis and soleus muscle activities, which results in dorsiflexion and eversion of the foot during the stance phase [77]. In contrast, the response in the TA was suppressed in the early swing phase.

In summary, cutaneous inputs perform phase-dependent roles in facilitating or inhibiting locomotion. However, it suggests that cutaneous inputs contribute more significantly to correct the position of the foot during the stance phase or respond to sudden perturbations [50], such as obstacles, mechanical stimulation or electrical stimulation.

Reflex functions during human locomotion

In previous sections, it has been shown that reflexes have task-, phase- and context-dependency to adjust motor control during human walking. The functions of reflexes during locomotion are drawn and summarised by Zehr and Stein [3] as shown Fig. 2.2. The gait cycle will be divided into four phases and described respectively here.

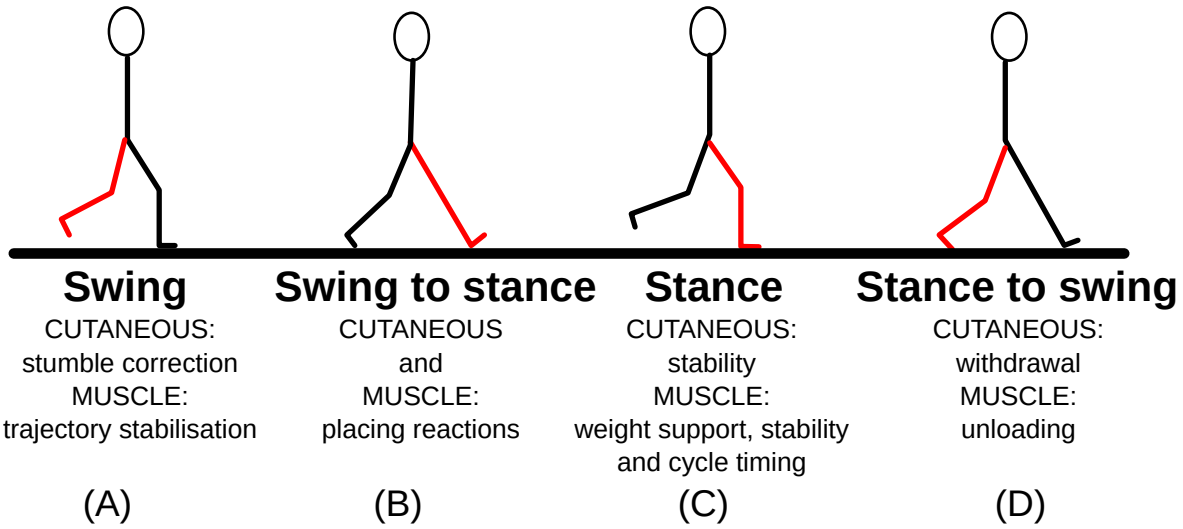

Figure 2.2: The main functional roles of reflexes during gait walking [3].

Swing Phase

In the swing phase, reflexes arise due to electrical [76] or mechanical stimulations [75, 78] of the foot dorsum to overcome the perturbance in the swing and stance limb. The stimulus triggers an elevating strategy where flexor muscles of the ipsilateral limb and extensors in

muscles of the contralateral limb correct the perturbance. If the perturbance is not sensed by the cutaneous sensory afferent in the foot, for instance, hit an obstacle, muscle stretch reflexes generate the ankle dorsiflexion and knee flexion to maintain the swing leg movement [66]. Thus, reflexes act to correct the stumbling and stabilise the swing leg. Despite that, muscle afferents signaling the hip position during normal locomotion provide fundamental information when the foot loses contact with the ground [67].

Swing to stance

The reflex from tibial nerve stimulation is observed to be essential in a reaction to the initiation of foot contact with the ground [76]. Dietz et al. [79] demonstrated a similar reaction observed by holding the limb for a short time during the late swing phase, where short latency responses arise in the TA and RF muscles of the ipsilateral leg and the gastrocnemius medialis and RF muscles in the contralateral leg. The "lower strategy" described by Eng et al. [75] is consistent with the finding in Dietz et al. [79]. As shown in Fig. 2.2B, cutaneous and muscle reflexes are essential in reaction to place the foot during the swing to stance phase.

Stance

The stretch reflexes and load receptor reflexes from muscle afferents contribute to force generation for forward body propulsion during the stance phase [56]. To walk on an uneven surface ground, cutaneous reflexes help to correct the foot position by adjusting the ankle motion [76]. Hence, in Fig. 2.2C, muscle reflexes are responsible for weight support and cycle timing while cutaneous reflexes act for the gait stabilisation.

Stance to swing

The load receptor reflexes arising from the unloading of ankle extensor muscles trigger the flexors of the limb and start the swing phase [54]. Perturbances during the stance phase, like adding load to the ankle extensor [80] or pushing down the pelvis [67], may prolong the stance phase. The cutaneous reflex from the tibial nerve stimulation activates the ankle flexor from the stance to swing phase so that the limb withdraws from the ground [76]. As shown in Fig. 2.2D, load receptor reflexes contribute to affect the timing of the gait cycle, and the cutaneous reflexes act in withdrawal reaction.

2.1.3 Summary

The sensory feedback from the PNS to the spinal cord or higher centers are integrated by the CNS to generate output signals to motorneurons in muscles. Spinal circuits are responsible for the basic rhythmic generation [27]. Bernstein [28] suggested that the reduced degree of freedom is controlled by the top-level CNS (supraspinal) while the flexibility of muscle activity is left controlled by the low level CNS (spinal cord). In the current view, there are

two hypotheses of human locomotion. The first hypothesis is that CPGs provide rhythmic activation to the extensor and flexor muscles for the generation of walking movements with essential reflex regulation from sensory afferent feedback. The second hypothesis is that human locomotion is a consequence of a chain of reflexes. Both hypotheses place the emphasis on the fundamental role of spinal reflexes in gait locomotion. The reflexes contribute to the timing of the step cycle, the adaption of gait pattern and reaction to perturbance by regulating the motor neuron outputs. Three main types of reflexes, namely cutaneous reflexes at the skin of the foot, load receptor reflexes and stretch reflexes from muscle afferents, appear to be essential. Their functional roles during locomotion were reviewed in this section. Task- and phase-dependent cutaneous reflexes contribute significantly to responses to the sudden disturbances [75, 76] and stabilisation [50]. Load receptor reflexes play an important role in regulating the time of step cycle [56, 57]. Stretch reflexes regulate the muscle activations during locomotion [62], especially for body loading during the stance phase [63].

Knowledge of reflexes could help us to simplify the control of locomotion as reflexes connect sensory feedback directly to motor activations bypassing central inputs.

2.2 Bioinspired robotic control

Research in robots with human-like gait patterns have potential benefits ranging from the robotic applications, insights in dynamic control systems to knowledge for the human locomotion restoration. The approach is to study human locomotion by designing and testing walking control models in robots.

2.2.1 Dynamic walking

Previous bipedal robots demonstrated stable and versatile motions based on the Zero Moment Position (ZMP) control. This control paradigm is inefficient as it requires precise and frequent responses of its actuators and the energy consumption is high. A promising control paradigm to address these issues is “passive dynamic walking” [81]. In contrast to mainstream robots, passive dynamic walkers are able to walk down a slope without any active control.

McGeer [81] described gait as a natural repetitive motion so that the bipedal locomotion control could be simplified into one step control. The first 2D passive dynamic walker designed by McGeer [81] as shown in Fig.2.3A has two favorable features: inherent stability and low energy consumption. Garcia et al. [82] demonstrated the simplest walking model based on the straight-legged bipedal model of McGeer [81] (Fig. 2.4). The model walks down a slope whose angle is γ with gravitational acceleration g. The stance leg rotates like an inverted

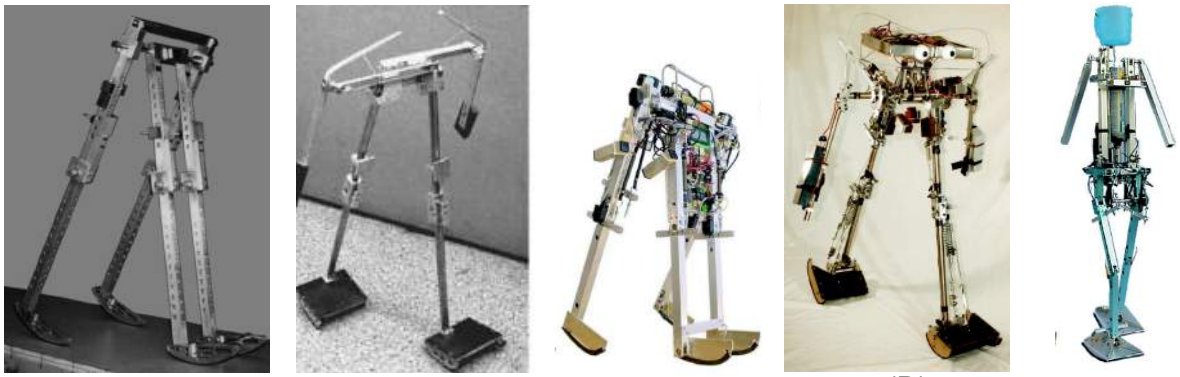

Figure 2.3: A series of bipedal dynamic walkers. (A) A close copy of McGeer's 2D passive dynamic walker with knees [82]. (B) First 3D passive dynamic walker built by Collins et al. [83]. (C) 2D passive dynamic walking robot Mike with pneumatic McKibben muscles at hip [4]. (D). The Cornell biped with actuated ankle joints via a spring [84]. (E) The Delft biped Denise with 2D hip actuation[85].

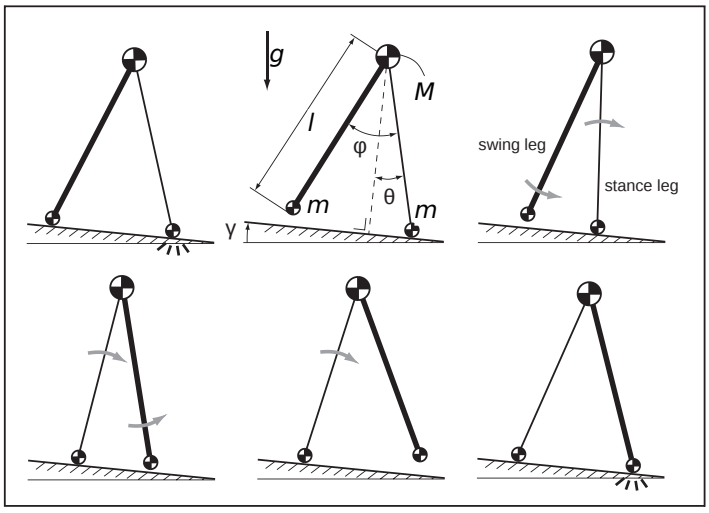

Figure 2.4: A typical walking step of the simplest walking model [82].

pendulum after the foot strikes the slope while the contralateral leg swings forward. One step is finished when the swing leg's foot hits the slope. Heel striking at the end of every step causes a loss of energy which is compensated by the gravitational acceleration g. A periodic walking motion without actuation results from the model.

Collins et al. [83] built the first 3D passive dynamic walker as shown in Fig. 2.3B where curved feet and mechanically constrained arms were used to obtain stable walking. The bipedal walker preserved the strengths of McGeer's passive dynamic walker. To demonstrate that the gravitational acceleration is not essential to the human-like properties of passive dynamic walkers, researchers at the University of Delft built a series of powered bipedal robots (Fig. 2.3C-F), substituting gravitational power with small amounts of ankle or hip actuation [84, 86, 87]. As the bipedal walkers have actuators, they are not purely passive

dynamic walkers anymore and thus falls in the category of "Limit Cycle Walkers".

Hrmzl and Moskowitz [88] proposed the concept of limit cycle walking even earlier than passive dynamic walking. Most research on passive dynamic walking follows the core of "limit cycle walking" to analyse the walking motion as a limit cycle. However, there has not been a clear definition of limit cycle walking until 2007. An exact definition of limit cycle walking is presented by Hobbelen [4]: "*Limit cycle walking is a nominally periodic sequence of steps that is stable as a whole but not locally stable at every instant in time*".

2.2.2 Bio-inspired robot control model

The control in biped robots is challenging due to inherent instability when the robot stands on a single leg and the center of gravity is behind the supporting foot. The unilateral foot contact makes the system underactuated. This would cause instability and tipping-over during the stance phase. The classical solution is to maintain the center of mass (CoM) fallen in the convex hull of the foot support area, so-called static walking [89]. This approach is being abandoned because robots can only achieve very slow speed and robot-like walking. A more sophisticated method proposed is the ZMP [90]. In this control architecture, the total angular moment at the ground remains zero. The ZMP is used as a stability criterion to prevent the underactuation problem. This concept forms the basis of the mainstream human-like robots [91, 92, 93].

Although this method has been impressively applied to a series of humanoid robots, accurate position control which is necessary for these robots is not inherent in human walking. Humans are capable of walking without accurate trajectory control. It suggests that this accurate control is unnecessary, and would result in redundant, complicated, and inefficient walking robots. The concept of dynamic walking is promising because of its efficiency and simplicity. McGeer [81] showed that a passive dynamic walker is capable of stable walking with a proper mechanical design. The outcomes from limit cycle walking indicate that complex locomotion control can be simplified [6, 84, 86, 94].

CPG control in robots

As gait is described as a natural repetitive motion of a dynamic system, a stable limit cycle is established with an appropriate interaction between the nervous system and the musculoskeletal system. The locomotion control based on the knowledge of the sensorimotor interaction was proposed by Taga et al. [95]. The simulation results showed that the oscillator controller and mechanical system were dynamically coupled to generate a stable limit cycle walking. The approach is promising to solve the problem: "To achieve a robust and adaptive behavior while coordinating a redundant high Degree of Freedom (DoF) system under

the strong effect of physical body dynamics" [96]. CPG-controlled bipedal locomotion has been studied in simulation [96, 97, 98, 99, 100, 101]. These studies show that simple oscillator systems lead to improved stability of the walker due to modification of step periods by sensory feedback. In a typical CPG-based locomotion model, each joint is controlled by a Matsuoka oscillator as shown in Fig. 2.5B. Each joint consists of two motor neurons, a flexor and an extensor, where the outputs of each motor neurons map a joint torque. Coupling between joints allows the oscillators to entrain in appropriate phases related to each other. The large number of parameters in the CPG network are determined by using Genetic Algorithm (GA) or Reinforcement Learning (RL).

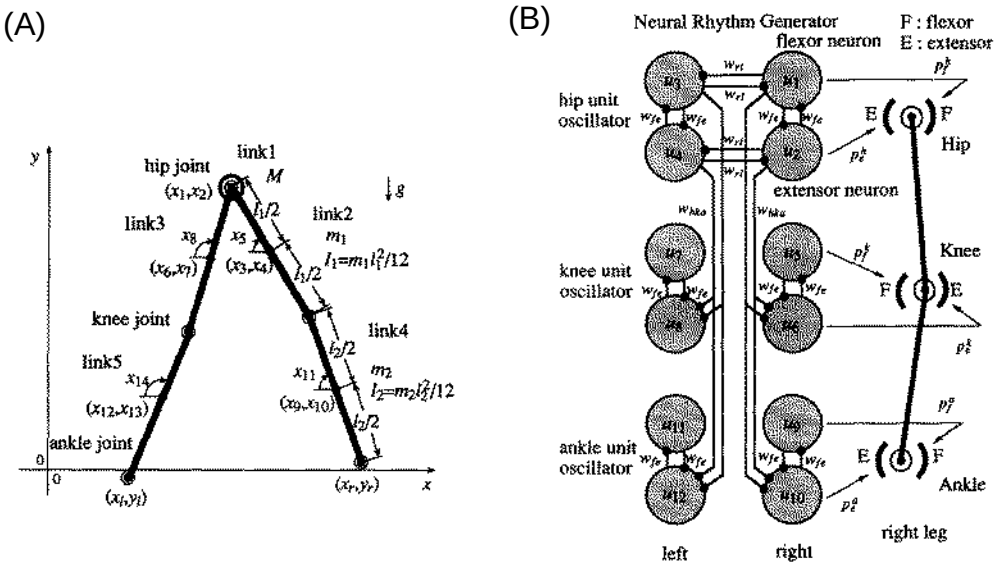

Figure 2.5: (A) Neuromechanical model presented by Taga et al. [95]. (B) The body consists of six joints, while each joint contains one Matsuoka oscillator. Joints are connected by weak coupling. Outputs of the oscillators are applied as joint torques. Feedbacks from joint angular positions are used to entrain the CPG outputs.

Numerous biped walkers were implemented based on principles of CPGs [94, 99, 101, 102, 103, 104, 105, 106]. Most CPG models are used as an alternative to methods based on Finite State Machine (FSM) and pre-designed joint trajectories, for instance, ZMP-based control [104], Hybrid Zero Dynamics (HZD) [105, 106], virtual model control [102], etc. Thus precise modeling and complicated computations are still necessary for these approaches. On the other hand, biped walkers employing non-linear oscillators modulated by foot sensory feedback are able to achieve a stable limit cycle walking with no precise joint trajectories [94, 103], such as Jena walker [94]. The robot is constructed by three passive segments. The hip joint is directly driven by a sine oscillator reset by the foot strike signal while the knee and ankle joints are driven passively via springs. The biped walker performs stable limit cycle walking with different speeds by tuning oscillator frequency and leg stiffness.

Reflex control in robots

van der Linde [107] suggested that self-organising walking control is not necessary by demonstrating that stable walking can be obtained by varying muscle activation or reflex parameters. Muscle reflexes are not only involved in disturbance responses but also play an important role in biological locomotion [108]. Geyer and Herr [109] proposed a biped walking control model using pure reflex signals in a human musculoskeletal simulation model. The reflexes modify muscle activations furthermore joint and leg compliance to allow the model to achieve a stable ballistic walking cycle. The joints are driven by a reflex chain, rather than CPG. The study shows the reflex circuit is able to independently generate appropriate muscle activation for each phase.

The combination of CPG with reflexes has been tested in robots. Klein [110] proposed a neurobotic model for proper locomotion control in robots. In the model, descending signals generated by the CPG are modulated by reflexes to produce phase-dependent reflex responses to drive locomotion. The study shows that the reflexes have a greater contribution in the control of the locomotion as they are responsible for approximately 80% of the robot walking.

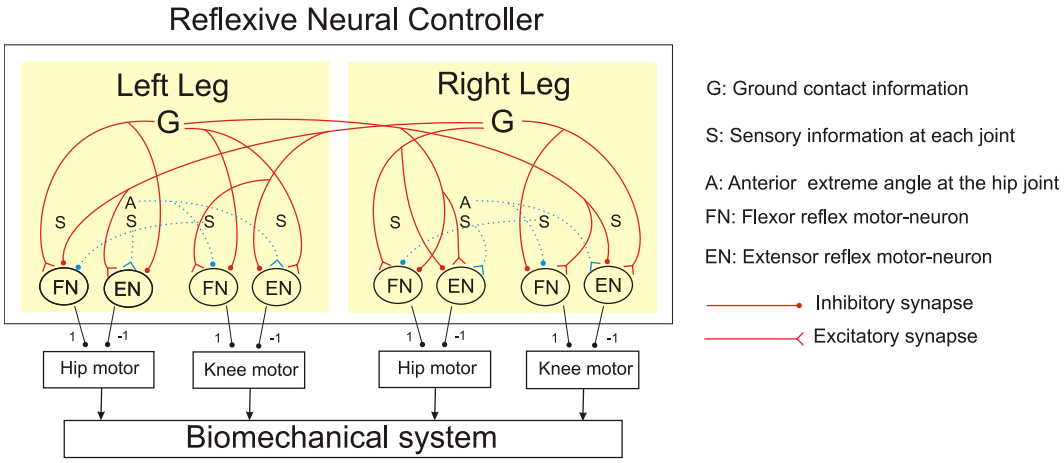

Figure 2.6: The reflexive neural controller on original RunBot [6].

Walking with a pure reflexive system has been used in a few bipedal robots [6, 108]. The original RunBot built by Geng et al. [6] is the first dynamic biped walker exclusively controlled by a pure reflexive controller. Fig. 2.6 illustrates how the reflexive controller is used to generate the locomotion of the robot. The controller has a hierarchical structure with monosynaptic reflex where the sensor neuron contacts motor neuron directly. Each joint consists of two reflexes, the extensor and flexor reflexes. Ground contact G works for switching phases of each limb. Hip stretch receptors signal the position of the limbs which triggers the knee extensor reflexes during the late swing phase. Local reflex circuits in the joint prevent the hyperflexion or extension by switching off the actuation. The pure reflexive controller

involves no explicit mechanisms for global stability control of the biped. The simplified control structure makes the original RunBot obtain a very fast walking speed of 3.5 leg-length per second. The achievement indicates the potential utilisation of reflexive mechanisms in further robotic control.

2.2.3 Interaction between robotics and biology

In above subsections, recent studies showed that the approaches implementing dynamic walking with biologically inspired control have great benefits because of lower energy consumption, robustness, and reduced computational cost. Conversely, biological studies could be inspired from robotics research. Robots provide a scientific tool for real environments to verify biological hypotheses [111]. For instance, Ijspeert et al. [112] used a tetrapod robot to validate the hypothesis in their mathematical model that the CPG model is capable of generating forward motion. Simulation models can be tested when they are implemented on a real body and established in a real environment by using robots. Using robots contributes to letting one comprehensively understand the functions of a system, like the locomotion system in human[113].

2.2.4 Summary

In this section, we reviewed the research in the development of bipedal walking robots. First, we demonstrated the concepts of passive dynamic walking and limit cycle walking. The performances of dynamic walkers showed that proper mechanical design contributes significantly to locomotion control. Second, we reviewed the biologically inspired control models based on CPGs and reflexive mechanisms. Reflex signals are essential to modulate the outputs generated by the CPG [110]. The pure reflexive controller allowing the original RunBot to walk at a fast speed without precise joint trajectories shows the significant contribution from reflexes to locomotion control and that CPGs are not necessary. Thirdly, we discussed the benefit of using robots in biological studies. The use of the control models in robots can help us to understand human walking better. There are mutual benefits between robotics and biology research.

2.3 Functional electrical stimulation

Voluntary muscle contraction in Fig. 2.7A is activated by descending motor outputs from the CNS. A lesion in the spinal cord blocks the CNS pathway in the spinal cord of patients. As seen in Fig.2.7B, the application of electrical current on the paralysed muscles can innervate

motor neurons to produce muscle contraction, and then substitute the role of descending motor outputs from the CNS. FES is a technique for the restoration of functional movements lost in neurologically impaired patients. The purpose of FES is to "enable function by placing or assisting a person's voluntary ability" [114]. As the aim of FES is to let subjects achieve the desired function, FES systems are usually called neural prostheses.

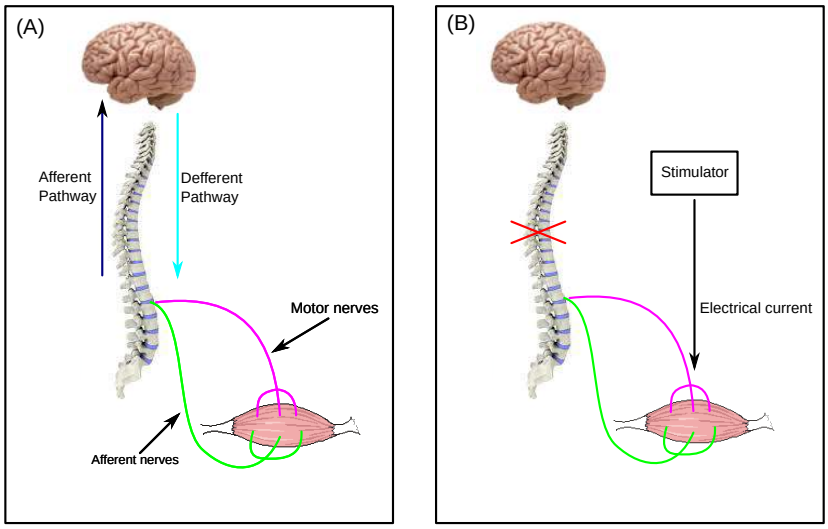

Figure 2.7: Schematic explanation of FES. The figure indicates the natural pathways for voluntary muscle contraction (A) and the FES solution when a lesion interrupts the spinal cord (B).

Stimulation may be applied in three ways. Firstly, implanted systems where the electrodes are implanted in the motor nerves are designed for long-term use. The stimulator implanted in the body receives power and commands via a radio-frequency link from an external control unit. Secondly, a percutaneous system uses intramuscular electrodes piercing the skin and attaching to the muscles. The percutaneous electrodes are able to activate deep muscles and reduce pain through avoiding stimulating sensory neurons on the skin. But there is a high risk of infection and failure if the electrodes are poorly maintained [115]. Thirdly, transcutaneous systems use adhesive surface electrodes placed on the skin over the "motor points" of selected muscle. It is difficult to activate isolated contraction or deep muscles due to the size of the electrodes. Knowledge and patience are required to locate appropriate locations to obtain the desired responses. However, the unique advantages of using surface electrodes, that are an easy application, relatively cheap price, and no requirement of surgery, make them widely utilised in therapeutic applications and commercial devices.

During the last four decades, FES has been utilised for functional restoration of the upper limb, lower limb, bladder and bowel, and respiration, thus enhancing the life quality of patients with SCI. Research of FES application to lower extremity focuses on three aspects: correction of drop foot, maintenance and transfer of standing posture, and restoration of walking[114].

Positive therapeutic effects of FES walking-assisted systems in hemiplegic and paraplegic patients have been reported in recent decades. The therapeutic benefits include increased blood flow to the lower extremities [116], lower heart rate at subpeak work intensities [117], and reduced spasticity [118]. It was found that task-oriented stimulation therapy can help the CNS replace the lack of descending neural pathways as the CNS in acute SCI rats preserves a capability to respond to peripheral stimulation [119]. It suggested that the stimulation of muscle afferents during voluntary motion is potentially important for the restoration of locomotion.

In this section, we will start with a brief background review of FES-assisted walking systems. The types of systems and control methods will be discussed.

2.3.1 A Brief history of FES-assisted Walking

Kantrowitz [23] first reported that the FES application enabled an SCI patient to stand. Also in the 1960s, Liberson et al. [120] developed the first portable device to prevent the foot from dragging in the swing phase. The first FES system for restoration of walking in paraplegic patients was proposed by Kralj et al. [121] based on the simple on-off stimulation protocols. The stimulation of several channels is controlled by the patient through two push buttons attached to the left and right handles of a walking frame.

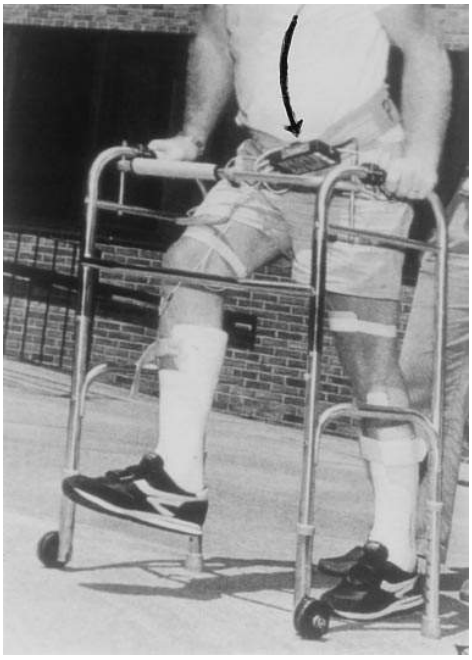

Figure 2.8: The Parastep I ambulation system used by a T9 paraplegic patient [117].

The final goal of a FES-assisted walking system is to enable complete spinal cord injured patients to walk again. Pioneering work by Bajd et al. [122] introduced the technique of the

hand switch to control the transition from stance phase to swing phase for respectively eliciting knee extensor in the stance phase and knee flexor in the swing phase. The hand switch was controlled by the therapist or embedded into the support frame or crutches for patient's self-control. The only FDA-approved FES walking system was built based on this technique [117]. Parastep-I system consists of a portable stimulator with a microprocessor, a walker for patient support, and 6 channels of bilateral adhesive electrodes. The quadriceps muscle and common peroneal nerves are chosen for reflex withdrawal, and the gluteus maximus muscle is selected if needed for further hip flexion. The patient wore the microprocessor/stimulator on his waist and used the hand switch built in the walker to control the stimulation as shown in Fig. 2.8. The results showed that patients can stand and walk at least a short distance of 30 feet. Researchers at the Cleveland VA Medical Center synchronised complicated lower limb muscles by activating up to 48 muscle based on the set-up rules according to gait phases[24], where the stimulation modes were chosen by the patient through a hand-controlled switch.

Manual control is the simplest approach to controlling the timing of stimulation during the gait cycle. However, this approach requires the continuous attention from the subject, and would result in abnormal synchronisation with gait events. Moreover, it is only suitable for single event control. Therefore, the concept of automatic FES control was proposed to synchronise the control of multiple muscles within the gait cycle. Sensory inputs are necessary for the determination of gait phases. Several control methods have been presented based on the integration of FES and different sensors ranging from the simple switch placed in the foot insole to gyroscopes, accelerometers, EMG, etc. Chen et al. [123] presented a method in which the stimulation of muscle on the affected leg is controlled by a switch placed on the heel of the unaffected foot. FSRs embedded in shoe insoles were used to detect gait phases (heel strike and toe off) in real-time based on set-up rules [124]. Williamson and Andrews [125] designed a gait phase detector using a cluster of accelerometers attached to the shank for the stance and swing phase detection. A reliable gait phase detection system consisting of the combination of FSRs in the shoe insole and gyroscope sensor detects four gait phases for the timing control of electrical stimulation sequences [126]. Pappas et al. [126] demonstrated that the system works robustly on different terrains with the combination of various sensor inputs. Kojović et al. [127] used the FSRs placed on the heel and metatarsal head and accelerometers attached to the shank as sensory inputs to generate stimulation sequences for four muscles based on the rules learned from the human data. The combination of artificial sensors substituting biological sensors has been widely utilised in automatically timing the gait events in FES-assistive walking systems. These approaches are promising due to the reliable performance of sensors. Despite these advantages, the available triggering methods are not suitable for our FES system requirement due to different sensory inputs we selected. Therefore, progress must be pursued to design a novel gait phase detection system for FES walking application which comprises of FSRs embedded in the shoe insole for foot

contact detection and a motion tracking sensor measuring hip angular position.

2.3.2 Control methods

FES control is still the most challenging step in designing clinical FES devices. Several important challenges are presented in the control [128]. The first challenge is that the response of stimulated muscle is nonlinear and time-varying, including muscle fatigue. Secondly, motor reflexes are unpredictable which might impede the walking. Spasticity in SCI increases the difficulty in predicting joint movements. Thirdly, the time delay between stimulation and muscle contraction needs to be considered in the processing system.

The use of FES compensates for sensorimotor pathologies in hemiplegia and paraplegia. The neuroprostheses are artificial control systems that assist or replace the role of the CNS of humans, where muscles are activated by electrical stimulation generated with the integration of sensory feedback from artificial sensors or the human body's physiological sensors. Hence, closed-loop control and sensory feedback are usually incorporated in FES systems.

Popović [129] suggested the biologically-inspired control is the most promising method for restoring functional movement. When the intention of the user is detected, a programme from models of movements is selected by a feedback system, which is equivalent to biological control in the brain stem and spinal cord. The discrete model based on the central nervous system consists of two aspects: sensory feedbacks for timing and separate activities at the joint level. Thus FSC is known as a well-suited method for the discrete control. The concept of FSC for gait control was proposed in 1960s [130]. A finite state controller usually consists of input events, output events, states and state transition function. The system behaviour can be characterised by a series of states. A state transition occurs when finite state machine switches between states corresponding to current inputs and current state.

The fundamental characteristic of FSM is the sequential operation, which makes the method suitable for gait control as human gait consists of a sequential pattern of movements [131] as shown in Fig. 2.9. The system output (gait event detection or FES) is determined by the current state of the system incorporating with temporal sensory inputs. The rules in FSC fall into two categories: heuristically defined by a manual control (like "hand-crafted"), and automatic generation by machine learning algorithms.

Basic FES systems use single event-triggered control. For instance, the application of electrical stimulation is controlled by the foot switch placed in the insole [120] for drop foot prevention. The stimulated muscle contraction is thus synchronised with specific events within the gait cycle, like heel strike, toe off, etc. However, the timing of the stimulation would be disrupted due to erroneous detection of gait sensors. The finite state controller for gait rehabilitation was first presented by Tomović and Mcghee [130]. Following this

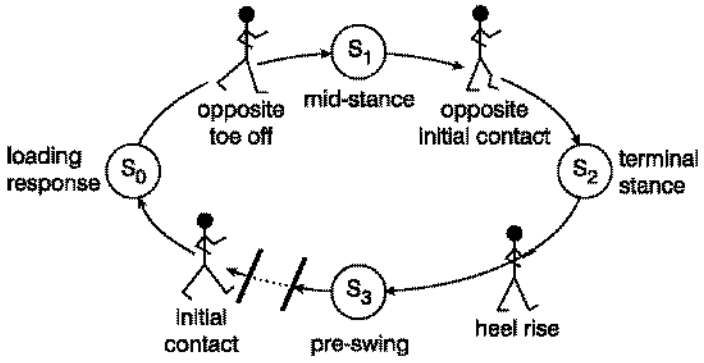

Figure 2.9: A finite state model of human gait walking. The states represent phases of the gait cycle, namely loading response, mid-stance, terminal stance, pre-swing. Gait events cause the state transition illustrated using stick figures [131].

paradigm, the first finite state controller implemented in neuroprostheses with hand-crafted systems was proposed by Andrews et al. [132], where gait events were manually identified by the expert. Numerous applications of similar finite state controllers to FES system for spinal cord injured patient have been done [132, 133].

In such "hand-crafted" FSC systems, both considerable time and expertise are required. However, if available time or expertise is limited, using an automatic technique has its advantages. Therefore, machine learning approaches, like Inductive Learning (IL), Adaptive Learning (AL), Artificial Neural Network (ANN), have been used with the incorporation of FSC through training. Kirkwood et al. [134] presented a method for automatic gait phases classification by using IL algorithm. The efficient rules were learned from training data measured from a spinal cord injured patient during manually controlled FES-assisted walking. Kostov et al. [135] demonstrated that ANN can be used to generate stimulation sequences by offline supervised training. Kostov et al. [135] compared IL and ANN methods and demonstrated that the learning process of IL was relatively faster than the ANN due to the generation of simpler and explicit decision rules. More studies reported the use of IF-THEN rule-based control in the coordination of FES in walking-assisted neuroprostheses [127, 136, 137]. For instance, Kojović et al. [127] developed a sensor driven IF-THEN rule-based control for four channels stimulation in a neuroprosthesis. The IF-THEN rules were created via mapping input data (kinematic and FSRs data) to output data (EMG) through IL algorithm. The IF-THEN rules switch the stimulation of the muscles on and off. Less than 5mins are required to set up the system showing the feasibility of this technology.

The use of fuzzy control has been used to detect gait phases in FES application [138]. Five gait phases were detected in three paraplegic subjects by a fuzzy logic system. Fuzzy logic methods are suitable for gait detection because they are less sensitive to sensor noise and vari-

ability comparing with the traditional classification. Fuzzy control is an advanced method based on FES.

The successful application of FSC in neuroprostheses demonstrates that the technology is a powerful mean to control gait by interpreting sensory feedback with the current state of the system. The advantage of using FSC is that it relatively alleviates the problems related to individual sensor noise. FSC is an effective control technology for the synchronisation of FES, however, it is not suitable for regulating FES parameters. Thus, hierarchical finite state controllers are used for open-loop or closed-loop FES control to regulate FES parameters. FES developments follow an evolutionary process towards an ideal neuroprosthesis which can be perfectly integrated with a human system. Based on studies to date, FSC as a descending control model, plays an essential role in the control of FES systems [131].

2.3.3 Summary

The brief history of FES-assisted walking systems was reviewed in Section 2.3.1. It is clear that the incorporation of artificial sensory feedback, like accelerometers, gyroscopes, EMG, and FSRs, substitutes the role of biological sensory feedback for the timing of electrically stimulated muscle contractions. An ideal neuroprosthesis with FES can support the human motor system. In the process towards the final goal of neuroprosthesis design, a well-suited method for mimicking descending control in human CNS is known as FSC [131]. Thus we illustrated studies of the implementation of FSC in FES-assisted walking system in Section 2.3.2. The FSC methods fall into two main categories: the first one has its rules heuristically defined through expertise like "hand-crafted" while the second one has its rules automatically generated by machine learning algorithm. The finite state controllers generated by machine learning have advantages, like less time required for preparation, less expertise knowledge needed to set up rules. However, the limitation of FSC is that this technology is for a high-level state control and not suitable for regulating low-level FES parameters. A simple and efficient FES controller integrating FSC for state detection with analogue control to regulate low-level FES parameters is still required to be further investigated and developed.

2.4 Research hypothesis

The main hypothesis of this thesis is that a biologically inspired robotic model can be successfully implemented as an FES-assisted system. The main motivation is that robotic control and human locomotion control would benefit from the interdisciplinary research of biology and engineering. Human walking is a sophisticated process with the interaction of CNS and PNS. Circuits in the spinal cord at the bottom level of the CNS generate basic units

for rhythmic locomotor movements [27]. Reflexes including load receptor and stretch reflexes play an important role during locomotion. The biologically inspired controller based on reflexive mechanism implemented with the dynamic walker can achieve stable limit cycle walking [6]. The collaboration with C.A.Macleod at the University of Strathclyde verifies the hypothesis that a causal relationship exists between foot load information and muscle activation (EMG) [139]. Based on the mapping of foot load information and muscle EMG, it is hypothesised that limb movement can be further mapped with foot load information. Hence, a new reflexive controller for hip, knee and ankle joints will be created based on derived transfer functions between foot load information and muscle activation in humans. As human can be regarded as an "ideal robot" in a natural environment, it is assumed that a robotic control model can be applied to externally control human locomotion. Thus, the reflexive controller is expected to be a promising novel control for FES-assisted walking due to its simplicity and effectiveness on gait control.

Chapter 3

Preliminary investigation into bio-inspired reflexive controlled biped robot with compliant knee joint

3.1 Introduction

Biped walking requires a sophisticated interplay of neuronal and mechanical control where the mechanical system feeds back to the motor neuron in a closed loop. However, it is possible to establish a walking gait just by setting up a purely mechanical system. This class of biped robots emulating human-like walking by means of a mechanical system are called "passive dynamic walkers" which can walk down a slope without any actuations [81] demonstrating that large part of the walking cycle is generated by the mechanical system. For walking on level ground, actuation is required in order to inject energy [140] and to let the robot adapt to a range of terrains. Careful design of the mechanical system is important to reduce the complexity of the neuronal control system. It is possible to develop a bipedal walking robot which has an improved mechanical system while the neuronal control is kept as simple as possible.

While passive dynamical walkers exhibit impressive human-like walking, these walkers have been designed with rigid legs. The design lacks important aspects of human anatomy while both muscles and tendons have elastic properties [141]. Compliance of robotic joints can take advantage of the natural limb and joint dynamics, and thus contribute to better mechanical properties for interactions with natural environments. It has been proven that compliant legs should improve the robustness and velocity of bipedal walking [142], and this will be the main focus of this chapter.

The human musculoskeletal system allows to adapt leg stiffness to different gaits and ter-

rains. Understanding its mechanisms is essential to establish adaptive robotic locomotion. Pneumatic artificial muscles have been designed to mimic muscles properties by van der Linde [143]. Walking robots constructed with pneumatic muscles proposed in recent years [85, 144, 145] can be considered as potential mechanical models to study the muscle functions in human walking. However, these robots can not achieve human-like speed due to sluggish responses of pneumatic muscles. Another approach that is simple but adapts human-like structures for locomotion by using springs to mimic the passive properties of muscle [94, 103, 146, 147, 148]. The springs are crucial to absorbing shocks and storing energy during gait [146]. A physical passive dynamic runner with knees suggests that a certain amount of computation can be offloaded from the neuronal control to the mechanical components [148]. A minimalist model of a compliant leg structure with bi-articular tension springs has been investigated to generate walking and running by tuning leg stiffness [94]. The actuators are usually located on the torso in order to reduce the weight of the legs, and so the knees are passively driven via elastic elements whereas the leg is regarded as a linear spring [94, 103, 146].

The original RunBot's gait trajectories are not planned but emerge from its neuromechanical properties [5]. A well-designed mechanical structure allows the robot to exploit its natural dynamics during walking and thus greatly simplifies the control structure which requires no precise trajectory control during dynamic walking. However, the robot exhibits an imbalance between neuronal and mechanical biological realism. First, the neuron model in the reflexive controller retains some physical properties, but reflexes in motor neurons driven by sensor neurons during walking are still not fully understood in current research. Secondly, a rigid actuated knee design brought about a jerk-like knee motion during dynamic walking which is not biologically realistic.

In this chapter, we continue the tradition of emphasising the biomechanics and present a further simplified reflexive controller which has been implemented on a novel biped dynamic walker with a compliant knee structure. Instead of attempting a neuronal controller on incomplete knowledge of the neuronal processes, we implemented the control algorithm as a black box which generates the coordinated muscle reflex responses [149]. A compliant knee was designed based on the human musculoskeletal knee system. The principles are based on the sagittal plane model of the patello-femoral joint in humans [150]. This new robot establishes close to human-like stable biped walking combining biomechanical "self-computation" with a purely reflexive controller. We are going to summarise briefly its properties and its limitations which will be addressed in this chapter.

3.2 Methods and Materials

3.2.1 Bio-inspired compliant knee design

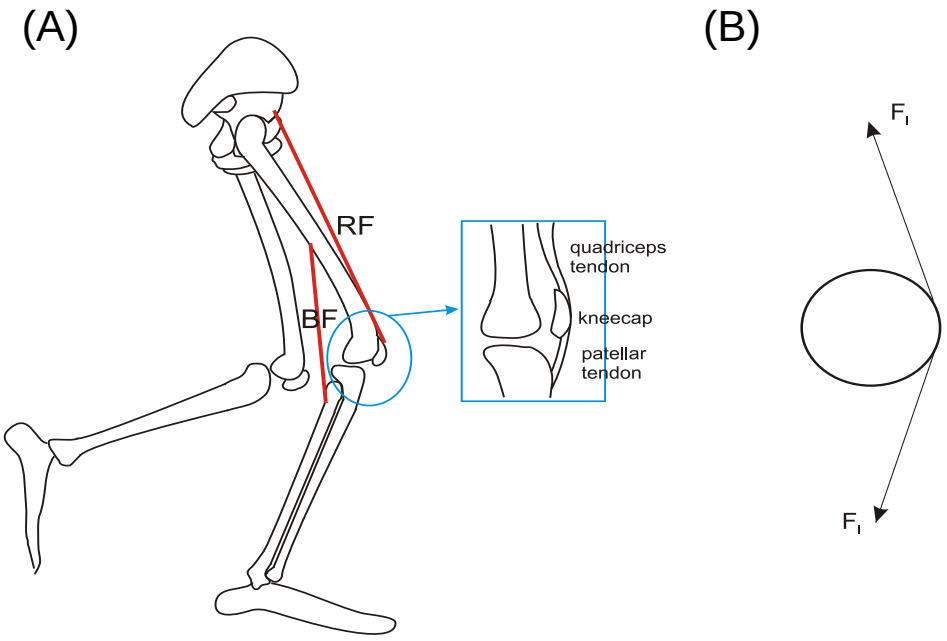

Figure 3.1: (A) The anatomical structure of the human knee. The existence of the patella (kneecap) significantly benefits the extensor mechanism that is driven by the Quadriceps Femoris (QF), while the Biceps Femoris (BF) dominates the knee flexion. (B) The simple sagittal model of the patello-femoral joint[150] describes the joint as a frictionless pulley changing the direction of the force applied on the tibia according to the knee flexion angle.

In order to arrive at our new mechanical design of the RunBot, we need to review the anatomy of the human knee which consists of the femoral condyles, tibial plateau and patella. The knee is stabilised on the posterior side by the BF and the gastrocnemius muscles. The extensor mechanism of the knee consists of Quadriceps Femoris (QF), quadriceps tendon and the patellar ligament. The anterior surface of the patella is convex and covered by the quadriceps tendon which continues distally to become the patellar ligament (see Fig. 3.1A). The existence of the patella provides great mechanical benefit during the extension of the knee and dynamic stability [151]. The sagittal plane model of the patello-femoral joint was simply described as a frictionless pulley changing the direction but not the magnitude of the quadriceps tension force applied on the tibia independent of the knee flexion angle [150], which has been proven to be comprehensive and valid in human experiments [152].

A two-dimensional model of the patello-femoral joint was adopted in the prototype of RunBot II to establish a more human-like knee extension mechanism and further enhance the walking performance. Our new compliant knee as shown in Fig. 3.2 is a hinge joint where the knee motor mounted on the upper leg drives the joint via springs. A frictionless pulley

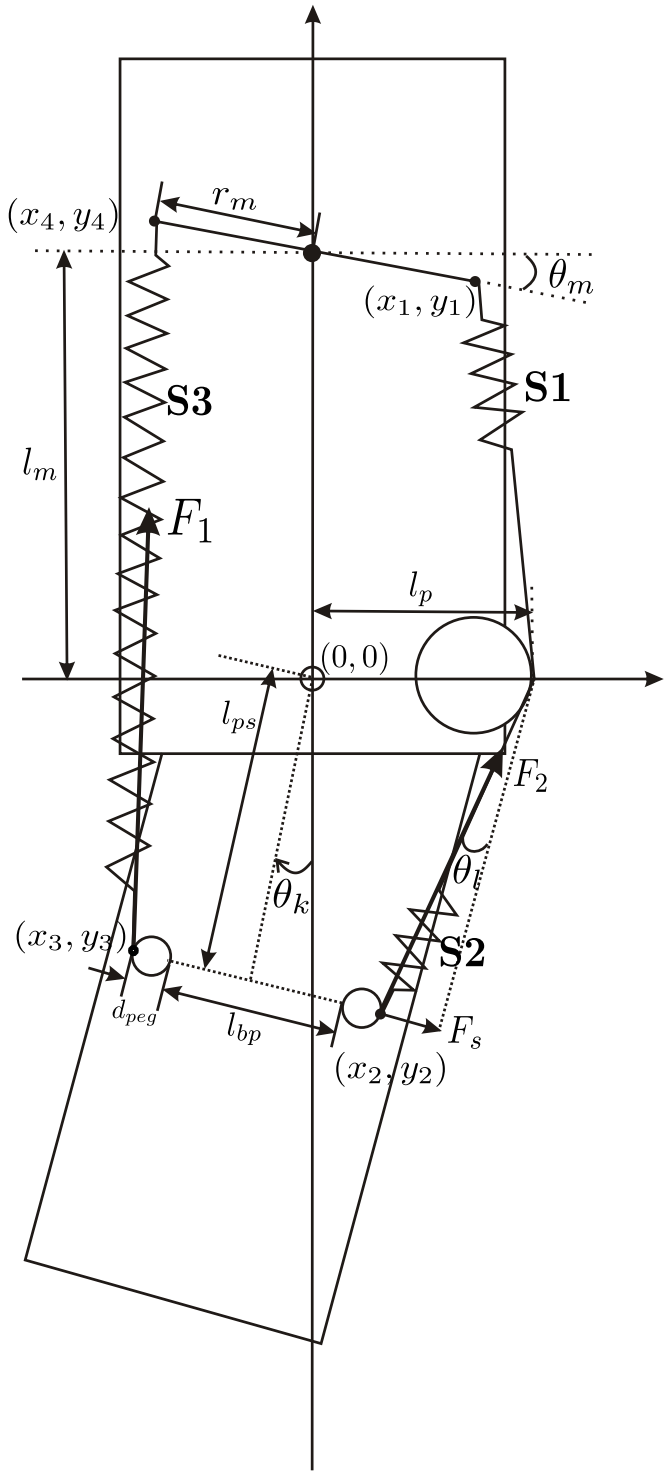

Figure 3.2: The geometric model of knee joint of RunBot II. l_m is the distance between the knee motor and the knee joint, l_{ps} is the distance between the knee joint and perpendicular line of the shank where the springs are attached to the lower leg. l_{bp} is the distance between the two points where the extensor and flexor strings are attached. r_m is the radius of the lever holding the flexor and extensor springs on the knee motor. d_{peg} is the diameter of the tuning peg shaft, θ_m is the knee motor angle, θ_k the knee angle, the l_p distance between the patellar tendon contact and the joint centre, θ_l the orientation angle between the tendon spring S2 and the parallel line of the shank.

level with the centre of the joint changes the direction of the extensor tension which mimics the function of the patella in humans. While the motor emulates the active properties of the muscles, the springs S1, S2 and S3 mimic the muscle passive properties as muscles have linear, spring-like properties [153]. S1 and S2 are utilised as the QF muscle and the patellar ligament. Another spring S3 is placed at the posterior side working as the BF muscle to drive the knee flexion. A mechanical stop is designed to prevent knee hyperextension.

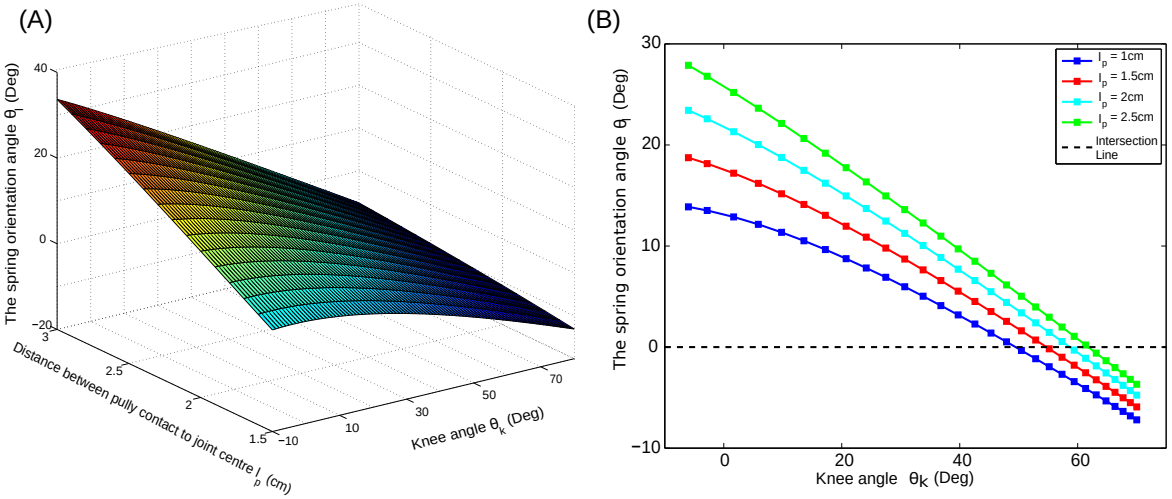

Figure 3.3: The magnitude of θ_l between the tendon and the perpendicular line of the shank as a function of knee flexion angles θ_k for different distances of the pulley l_p measured from the joint centre. (A): 3D plot. (B): plot of θ_l and θ_k produced by the distance of 1cm, 1.5 cm, 2 cm, 2.5 cm between the pully and joint centre.

A first crucial parameter is the exact position of the patella which is defined by the distance between the patellar tendon contact and the joint centre and is called l_p. This distance determines the relationship between the orientation angle θ_l of the spring S2 and the knee angle θ_k which is an important feature of the human knee extension mechanism and is shown in Fig. 3.3. During human knee flexion, the patella ligament is directed anteriorly in the first 70 degrees of knee flexion and posteriorly between 70 and 120 degrees, and the maximal anterior oriented angle is smaller than 30 degrees [152]. According to the above description, the optimal value of the distance between the point where the tendon contacts the pulley and the joint centre l_p was determined as 2.5 cm.

3.2.2 The reflexive controller

Human walking is hierarchically controlled at several levels of the CNS, namely the spinal cord, the brainstem and the cerebral cortex. The spinal cord generates the basic control unit for rhythmic locomotion, for instance, walking, running, etc. It uses peripheral feedback in the legs to automatically control the legs and respond to sudden disturbances.

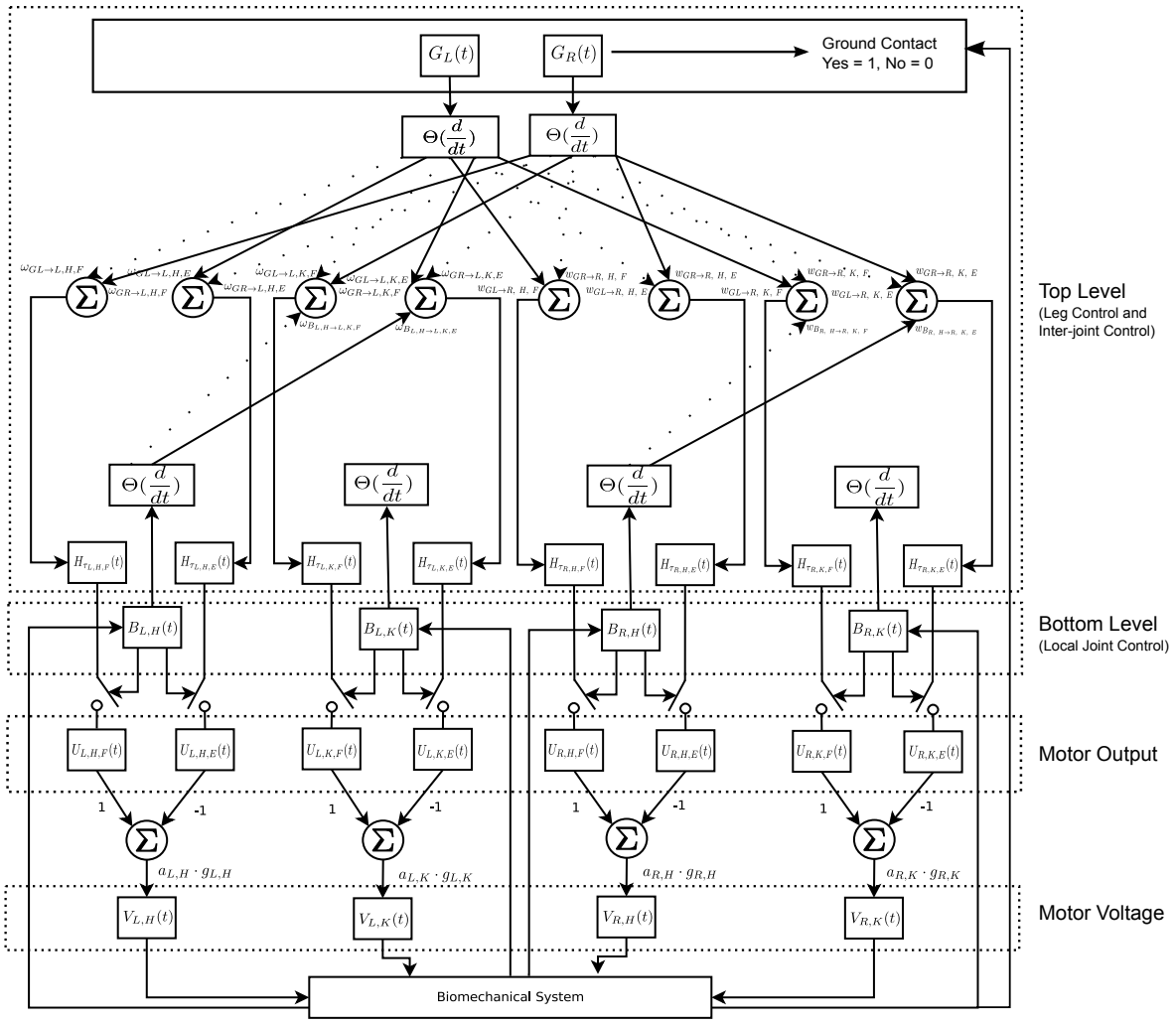

Figure 3.4: The control diagram of the reflexive controller. The dashed lines mean that contributions of sensory feedback to the motor neurons are zero. $G_{L/R}$ are the signals from the ground contact sensors. $\Theta(d/dt)$ is the rectified derivative of the ground contact providing a delta pulse at the moment of the heel strike. $\sum$ are summation nodes integrating the different sensor inputs. $H_{\tau_{L/R,\ H/K,\ F/E}}$ are low-pass filters creating smooth responses from the delta or step like inputs. $B_{L/R,K/H}$ provide outputs from the stretch receptors based on the knee and hip angles. $U_{L/R,\ H/K,\ F/E}$ are the motor outputs. The motor voltages applied on the motors $V_{L/R,\ H/K}$ are obtained by multiplying the gain coefficients $a_{L/R,\ H/K} \cdot g_{L/R,\ H/K}$.

The reflexive locomotion controller is built based on the spinal reflex mechanism in human locomotion [154] and is shown in Fig. 3.4. It will be explained in detail, starting with its hierarchical structure. Three loops are established: leg control, intra-joint control, and joint control.

1. Leg control: cutaneous sensory input from the feet switch phases (stance or swing) of each leg, excite the flexor (or extensor) of each joint and reciprocally inhibit the extensor (or flexor) of the same joint.

2. Inter-joint control circuit elicits an extensor reflex at the knee when the ipsilateral hip reaches the Anterior Extreme Angle (AEA).

3. Local joint control arises from local reflex which inhibits the motor when the joint reaches its extreme angle positions.

We are now going to describe the different building blocks of our reflexive controller in details.

Filter functions

Geyer and Herr [109] proposed a muscle-reflex model in which the human leg mechanics can be encoded into autonomous muscle reflexes. This study indicates the possibility to relate individual motor neuron output to mechanical function. Instead of using neuronal processing [6], filter functions are utilised to generate the reflex responses elicited by sensory inputs [149].

For instance, a spinal reflex output U excited by sensory input G can be modelled as a filtering operation: $U = H * \Theta(\dot{G})$ where

$$H(t) = \frac{2\sqrt{3}}{\tau} e^{\frac{-1.5t}{\tau}} sin(\frac{\sqrt{3}t}{2\tau}) \tag{3.1}$$

is a 2nd order low-pass Bessel filter with maximally flat group delay and time constant τ. This filter type was chosen because it has no undershoot and can be modelled efficiently by an IIR filter. We use the rise time t_r ($t_r = 0.6046\tau$) to describe the response time of the burst activity from the excitation to obtaining the maximum amplitude. Details on how filter parameters were chosen are provided in the results section. For filter functions we use in general the capital letter H and its indices define its motor output: left/right leg and knee/hip.

Gait generation via sensory feedback

The walking gait is primarily established by the ground contact information ($G_{L/R}$) which pushes the system from one gait phase to the next one. When the foot touches the ground, the sensory input activates the extensors of the ipsilateral leg and the flexors of the contralateral leg. With the help of the ground contact information, all but one motor outputs can be generated. Only for the knee extension during the late swing phase, we require the hip sensory feedback $\Theta(\dot{B}_{L/R,H})$ which provides an excitatory signal to the ipsilateral knee extensor.

Stretch receptors

Stretch receptors play a significant role in animal locomotion control. When the limb reaches the extreme positions, its stretch receptors will send signals to reset the phase of its controller. In our case the stretch receptor provides a signal in Eq. 3.2 that leads to a local reflex which inhibits the motor output to mimic the inhibition of the alpha motor neuron. Some biologically inspired robots use the leg's anterior extreme position and posterior extreme position to trigger specific phases of locomotion [155]. We define the outputs of our stretch sensors $B_{L/R,\ H/K}$ as:

$$
\begin{aligned}
B_{L/R,\ H} &= \begin{cases} 1 & \theta_{L/R,\ H,\ F} < \phi_{L/R,\ H} < \theta_{L/R,\ H,\ E} \\ 0 & \text{otherwise} \end{cases} \\
B_{L/R,\ K} &= \begin{cases} 1 & \theta_{L/R,\ K,\ E} < \phi_{L/R,\ K} < \theta_{L/R,\ K,\ F} \\ 0 & \text{otherwise} \end{cases}
\end{aligned}
\tag{3.2}
$$

where $\phi_{L/R,\ H/K}$ are the real-time angular positions of hips and knees and $\theta_{L/R,\ H/K,\ F/E}$ are the threshold positions for hips and knees. Generally for the stretch receptors we use the capital letter B and its indices indicate if they are related to the left/right and knee/hip angle.

Extensor/flexor signal generation

Each joint consists of one extensor and one flexor which inhibits each other reciprocally. All motor outputs consisting of both extensor ($U_{L/R,\ H,\ E},\ U_{L/R,\ K,\ E}$) and flexor ($U_{L/R,\ H,\ F}$,

$U_{L/R,\ K,\ F}$) reflexes are generated via sensory inputs as shown in Eq. 3.3:

$$
\begin{aligned}
U_{L,\ H,\ F} =& B_{L,\ H} H_{\tau_{L,\ H,\ F}} * (w_{GL\to L,\ H,\ F}\Theta(\dot{G}_L) + w_{GR\to L,\ H,\ F}\Theta(\dot{G}_R)) \\
U_{L,\ H,\ E} =& B_{L,\ H} H_{\tau_{L,\ H,\ E}} * (w_{GL\to L,\ H,\ E}\Theta(\dot{G}_L) + w_{GR\to L,\ H,\ E}\Theta(\dot{G}_R)) \\
U_{L,\ K,\ F} =& B_{L,\ K} H_{\tau_{L,\ K,\ F}} * (w_{GL\to L,\ K,\ F}\Theta(\dot{G}_L) + w_{GR\to L,\ K,\ F}\Theta(\dot{G}_R) \\
&+ w_{B_{L,\ H\to L,\ K,\ F}}\Theta(\dot{B}_{L,\ H})) \\
U_{L,\ K,\ E} =& B_{L,\ K} H_{\tau_{L,\ K,\ E}} * (w_{GL\to L,\ K,\ E}\Theta(\dot{G}_L) + w_{GR\to L,\ K,\ E}\Theta(\dot{G}_R) \\
&+ w_{B_{L,\ H\to L,\ K,\ E}}\Theta(\dot{B}_{L,\ H})) \\
U_{R,\ H,\ F} =& B_{R,\ H} H_{\tau_{R,\ H,\ F}} * (w_{GR\to R,\ H,\ F}\Theta(\dot{G}_R) + w_{GL\to R,\ H,\ F}\Theta(\dot{G}_L)) \\
U_{R,\ H,\ E} =& B_{R,\ H} H_{\tau_{R,\ H,\ E}} * (w_{GR\to R,\ H,\ E}\Theta(\dot{G}_R) + w_{GL\to R,\ H,\ E}\Theta(\dot{G}_L)) \\
U_{R,\ K,\ F} =& B_{R,\ K} H_{\tau_{R,\ K,\ F}} * (w_{GR\to R,\ K,\ F}\Theta(\dot{G}_R) + w_{GL\to R,\ K,\ F}\Theta(\dot{G}_L) \\
&+ w_{B_{R,\ H\to R,\ K,\ F}}\Theta(\dot{B}_{R,\ H})) \\
U_{R,\ K,\ E} =& B_{R,\ K} H_{\tau_{R,\ K,\ E}} * (w_{GR\to R,\ K,\ E}\Theta(\dot{G}_R) + w_{GL\to R,\ K,\ E}\Theta(\dot{G}_L) \\
&+ w_{B_{R,\ H\to R,\ K,\ E}}\Theta(\dot{B}_{R,\ H}))
\end{aligned}
\tag{3.3}
$$

Here w are the weights of the connections between the sensor inputs and the motor outputs,

$$
w = \begin{array}{c} \\ G_L \\ G_R \\ B_{L,H} \\ B_{R,H} \end{array}
\begin{array}{c}
\begin{array}{cccccccc} L,H,F & L,H,E & R,H,F & R,H,E & L,K,F & L,K,E & R,K,F & R,K,E \end{array} \\
\left(\begin{array}{cccccccc}
0 & 1 & 1 & 0 & 0 & 0.3 & 1 & 0 \\
1 & 0 & 0 & 1 & 1 & 0 & 0 & 0.3 \\
 & & & & 0 & 1 & & \\
 & & & & & & 0 & 1
\end{array}\right)
\end{array}
\tag{3.4}
$$

The rows in equation describes the target motor outputs ($U_{L/R,\ H/K,\ F/E}$) and the sources of the columns are the foot sensory signals ($G_{L/R}$) and hip joint stretch receptor signals ($B_{L/R,H}$).

Motor outputs

The value of the motor output after being multiplied by a gain coefficient and a rotation direction indicator is sent to the servo amplifier to drive the joint motor directly. Thus, the

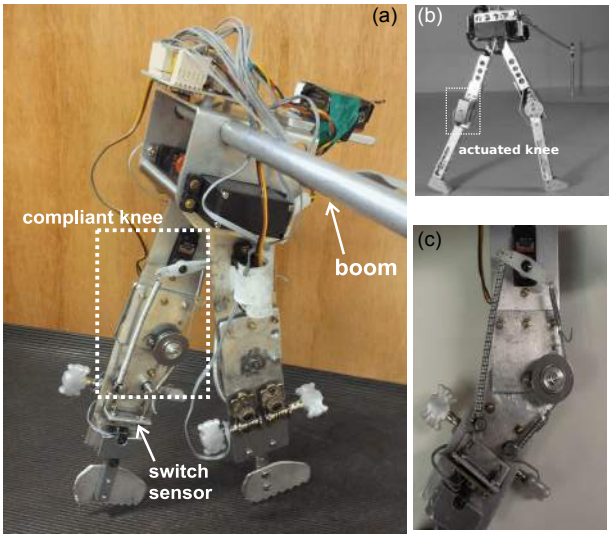

Figure 3.5: (A) RunBot II with compliant knee structure. (B) The original RunBot with directly actuated knee joint designed by Geng et al. [6]. (C) The compliant knee in the RunBot II.

voltages applied on each joint motor of RunBot II are described as follows:

$$\begin{aligned} V_{L,\,H} &= s_{L,\,H} \cdot a_{L,\,H} \cdot g_{L,\,H} \cdot (U_{L,\,H,\,F} - U_{L,\,H,\,E}) \\ V_{R,\,H} &= s_{R,\,H} \cdot a_{R,\,H} \cdot g_{R,\,H} \cdot (U_{R,\,H,\,F} - U_{R,\,H,\,E}) \\ V_{L,\,K} &= s_{L,\,K} \cdot a_{L,\,K} \cdot g_{L,\,K} \cdot (U_{L,\,K,\,F} - U_{L,\,K,\,E}) \\ V_{R,\,K} &= s_{R,\,K} \cdot a_{R,\,K} \cdot g_{R,\,K} \cdot (U_{R,\,K,\,F} - U_{R,\,K,\,E}) \end{aligned} \tag{3.5}$$

where $a_{L/R,\,H/K}$ presents the coefficient of the servo amplifier. $g_{L/R,\,H/K}$ stands for the output gain of the motor outputs. $s_{L/R,\,H/K}$ indicates the rotation direction of the motor (see Appendix.A for the specific values).

3.2.3 The RunBot II

The RunBot II is a planar bipedal walker as shown in Fig. 3.5A. The robot consists of four actuated joints. Two hips are actuated by DC servo motors HS-625MG (Hitec RCD, USA) directly while two compliant knees are actuated by DC servo motors HS-85+MG (Hitec RCD, USA) via springs (see Fig.3.5C). The standard controllers of all servo motors were removed and the control voltages are applied directly to the motors. The motor positions are measured via the potentiometers of the servos. Micro-switches (microswitch, Maplin, UK) are used to detect ground contact. Flat serrated feet are mounted on rigid ankles. A summary of the robot's dimensions is given in Table.3.1.

A USB-DUX-D data acquisition device (Incite Technology Ltd, UK) is utilised as the interface between a computer running Linux and the RunBot II. Six input channels are used for

Table 3.1: Specification of RunBot II

Parameters	Value
Mass(g)	552
Thigh(cm^3)	4 $\times$0.2$\times$ 11
Shank(cm^3)	4 $\times$0.2$\times$ 10
Foot(cm^3)	5 $\times$0.2$\times$ 3
Height(cm)	30

the locomotion control. Four input channels measure the motor angles $\phi_{L/R,\ H/K}$ and two contact switches $G_{L/R}$ detect the foot contacts. The control programme is written in C++ using the comedi library (www.comedi.org). The sampling rate was 200 Hz. Four analogue outputs ($V_{L/R,\ H/K}$) with an output range of $\pm 4.096V$ of the USB-DUX-D are fed into a power amplifier with a gain of 2.3 and then used to drive the four motors respectively.

3.2.4 The experimental setting

The experimental setting is as shown in Fig. 3.6. A boom of 1m length constrains the RunBot II's walking to a circular path and prevents it falling to the side. A counter weight is mounted on the other side of the boom to balance part of the weight of RunBot II. A camera (Color Camera Board L79AB) is fixed on the boom for video capturing when the robot walks on its the circular path. The right knee motion was tracked with the help of colour markers around the knee joint and the image analysis was performed with openCV and a custom C++ programme.

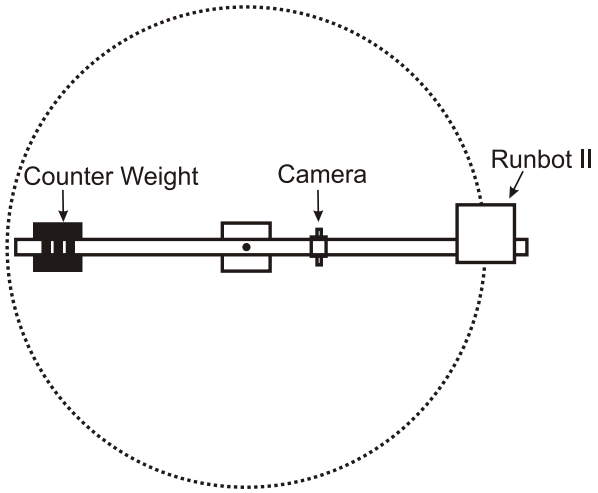

Figure 3.6: The experimental setting of RunBot II walking in a circular path.

3.3 Results

3.3.1 Parameters optimisation

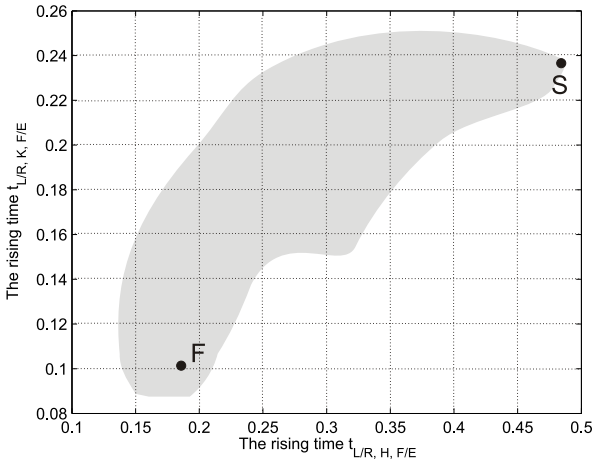

Figure 3.7: Regions of stable walking as a function of the rise time of the knee transfer function $t_{r_{L/R,K,F/E}}$ and the rise time of the hip transfer function $t_{r_{L/R,H,F/E}}$. The shaded area represents the parameter combinations in which the robot performs stable walking. Point F represents the optimal parameters for the fastest speed, while the parameter pair related to the slowest speed is represented by point S.

Two parameters required more detailed investigation and were systematically varied: the rise time of the hip filter functions ($t_{r_{L/R,H,F/E}}$) and knee filter functions ($t_{r_{L/R,K,F/E}}$) when the gain coefficients for hip and knee motors are determined. It was found that stable gaits can be achieved in a considerable large range of these two parameters as shown in Fig. 3.7. The fastest speed (0.2969 ± 0.0049 m/s, point F Fig. 3.7) was achieved when the rise time of the knee function $t_{r_{L/R,K,F/E}}$ was set to 0.107 s and the rise time of the hip function $t_{r_{L/R,H,F/E}}$ was set to 0.175 s. The optimised parameter values were used in the following experiments.

3.3.2 Dynamics of walking

In this section, we are going to describe how walking is generated by the interplay between the electrical and the mechanical system. Fig. 3.8 shows one step which is illustrated in conjunction with the data flow diagram shown in Fig. 3.4:

1 The Heel Strike (HS) of the left foot (Fig. 3.8A(1)) causes the signal G_L to switch from 0 to 1 and back to 0 at liftoff. Its rectified derivative $\Theta(\dot{G}_L)$ excites both the extensors of the hip and knee of the left leg $U_{L,\ H/K,\ E}$ and the flexors of the right leg $U_{R,\ H/K,\ F}$ according to Eq. 3.3. The motor voltages are calculated by Eq. 3.5 and then sent to the motors (Fig. 3.8B). In this part of the gait cycle, the left leg is essentially straight and the robot slowly falls forward being supported by the left leg.

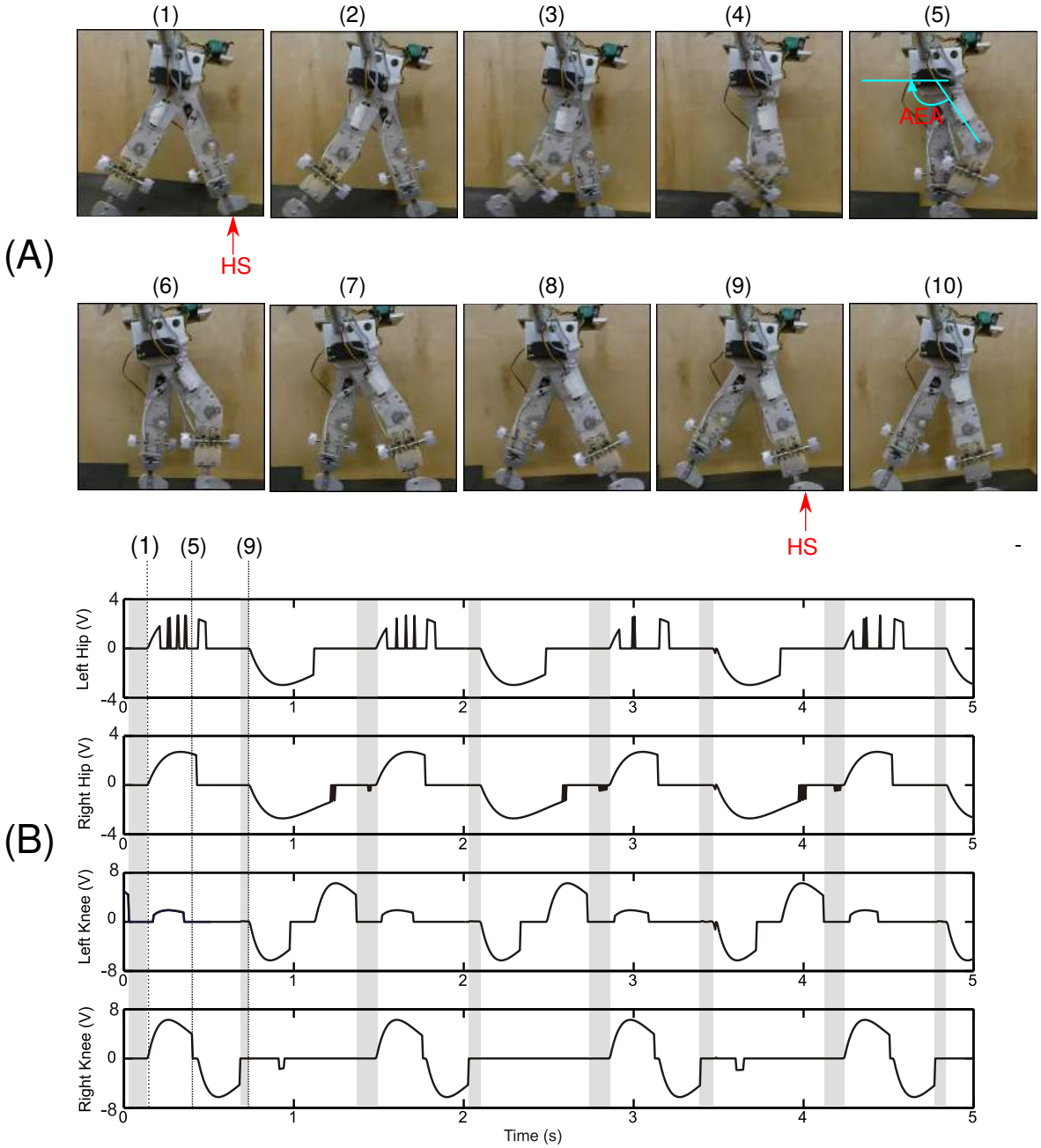

Figure 3.8: (A) Series of frames of one walking stride. The interval time between every two adjacent frames is approximately 0.083 ms. One step starts when the foot of the stance leg heel strikes the ground. (B) Motor voltages of all joints. During one period of every gait cycle (grey area), all four motor voltages remain zero, and the robot moves passively.

2 When AEA has been reached by the ipsilateral hip as shown in Fig.3.8 A(5), its stretch receptor signal $\Theta(\dot{B}_{R,\,H})$ activates the knee extensor $U_{R,\,K,\,E}$ to straighten the knee during the late swing phase. The knee extension is achieved by the force exerted from the knee motor applied to the lower leg via the springs S1 and S2. The effect of spring stiffness to the walking pattern will be investigated systematically in section 3.3.3 below.

3 At the moment the right foot touches the ground, the roles of left and right feet are swapped and a new step starts.

Furthermore, the stretch receptor signals $B_{L/R,\,H/K}$ switch the motor voltages to zeros when the hips and knees reach the minimum or maximum thresholds. Thus, the RunBot II is a passive dynamic walker during this period as all four motors are switched off shown as grey parts in Fig. 3.8B, which means the biomechanism of the robot still "computes" a part of the walking gait.

In the next section, we are going to investigate how spring stiffness in the knee extensor influences the timing of the swing phase, walking speed, and the performance of a stable gait.

3.3.3 The effect of knee extensor stiffness on walking performance

To study how the stiffness of the springs responsible for knee extension influences the walking performance of the RunBot II, we tested six different stiffnesses (see Tab. 3.2). The range of the spring stiffness was 0.18-1.17 N/mm. "Inf" means that a stiff string was used instead of a spring representing an extreme condition of the spring stiffness. The springs were selected so that a stable walking pattern was possible. All springs were shorter than 15 mm because of the size limit of the mechanical knee structure. The trials were all carried out under the same experimental condition and control parameters.

Table 3.2: The spring stiffness chosen in the experiment

	SP01	SP02	SP03	SP04	SP05	SP06	NOSP
Stiffness (N/mm)	0.18	0.29	0.38	0.63	0.85	1.17	Inf

The performance of the RunBot II corresponding to various spring stiffness of the knee extensions is shown in Fig. 3.9. A clear dependency between the spring stiffness and average speed is observed in Fig. 3.9. The robot achieved the fastest speed (0.2975$\pm$0.0078 m/s)) when the spring SP03 (0.38 N/mm) was utilised in both the S1 and S2 positions of the

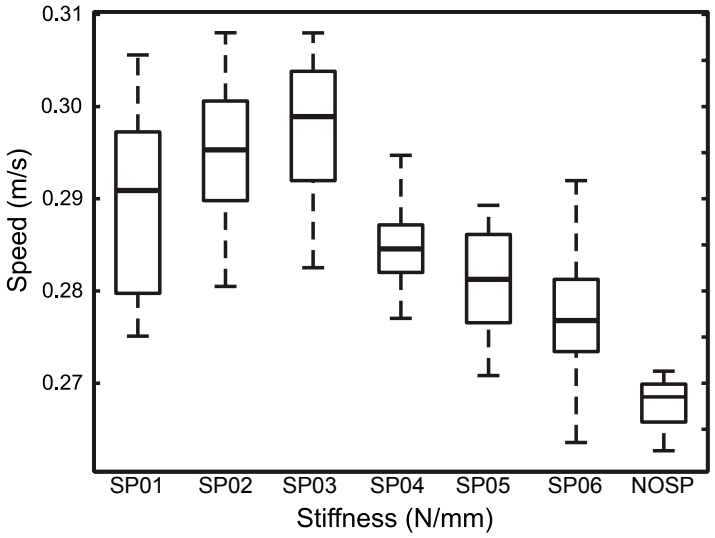

Figure 3.9: Boxplot of speed results with variable spring stiffness (n=20) where the speed result was calculated as the circumference of the cycle path divided by the time for completing one cycle path walking.

Table 3.3: P-values of two-sample t-test results of walking speeds when different springs were implemented at S1 and S2. Bold indicates significant difference (P¡0.05).

	SP01	SP02	SP03	SP04	SP05	SP06	NOSP
SP01		0.0767	**0.0065**	0.0868	**0.0014**	**5.555e-05**	**8.680e-12**
SP02			0.2705	**1.366e-05**	**2.895e-07**	**1.460e-08**	**1.617e-16**
SP03				**1.519e-06**	**2.249e-09**	**1.824e-10**	**1.144e-18**
SP04					**0.0283**	**6.442e-04**	**2.594e-14**
SP05						0.0909	**1.473e-14**
SP06							**1.269e-06**

compliant knee structure and walked at the slowest speed when the stiff string (“Inf”) was used. We can tell from Tab. 3.3 that the robot walking performance with the stiff string (“Inf”) is significantly different to the ones with the tendon springs (P¡0.05). Moreover, there are also significant differences among the speed groups using springs as tendons. The result indicates that the spring stiffness in the compliant knee structure has a significant effect on biped robotic walking.

To gain a better understanding of how the spring stiffness in the compliant knee affects the walking performance of the RunBot II, force F_s which is perpendicular to the shank and contributes to the knee extension was calculated within the gait cycle based on the geometric model of the compliant knee joint [1] (see Fig. 3.2). We see from Fig. 3.10A that the force F_s increases when the spring stiffness of S1 and S2 increases and that it is strongest when

[1]Note that there is no analytical solution possible for this setup.

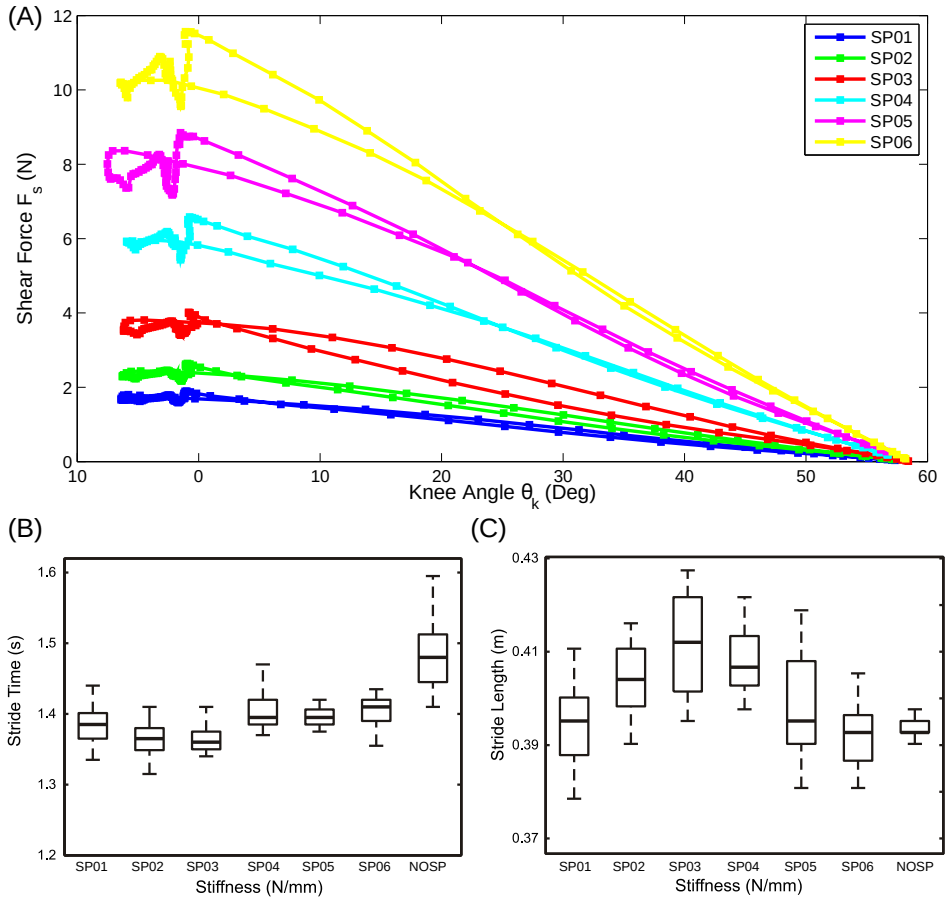

Figure 3.10: (A) The plot shows the average shear forces F_s in one gait cycle versus the knee angular position when different springs were used. The F_s is the vertical force applied to the shank by the extensions of springs S1 and S2, and responsible for knee extension. (B) The boxplot of stride time with variable spring stiffness (n=20). (C) The boxplot of average stride length results with variable spring stiffness (n = 20) where the average stride length was calculated as the circular circumference divided by stride number in one circle path.

the knee is straight and weakest when the knee is flexed. As shown in Fig. 3.8B, when the hip achieves its AEA, the knee extensor is activated and the hip motor voltage falls to zero. During this period, the hip is passively driven by the force F_s while the knee extends and causes a backward shift of the centre of the gravity. An overly excessive force F_s may cause a strong gravity centre shift and thus results in a longer time to shift the gravity centre back to its equilibrium position. This can explain the longer stride time in Fig. 3.10B and the smaller average stride length in Fig. 3.10C in the case of the stiff string compared to the ones with the tendon springs. On the other hand, a small F_s may cause insufficient knee extension and lead to a small stride length and slow speed.

To analyse the dynamic stability of the RunBot II using different springs, phase plots of knee angular velocity versus the angular position were generated in Fig. 3.11. We can see that our reflexive control system successfully produces stable limit cycles. Fig. 3.11C showing the phase plot with the use of the spring SP03 demonstrates that the limit cycles are less affected

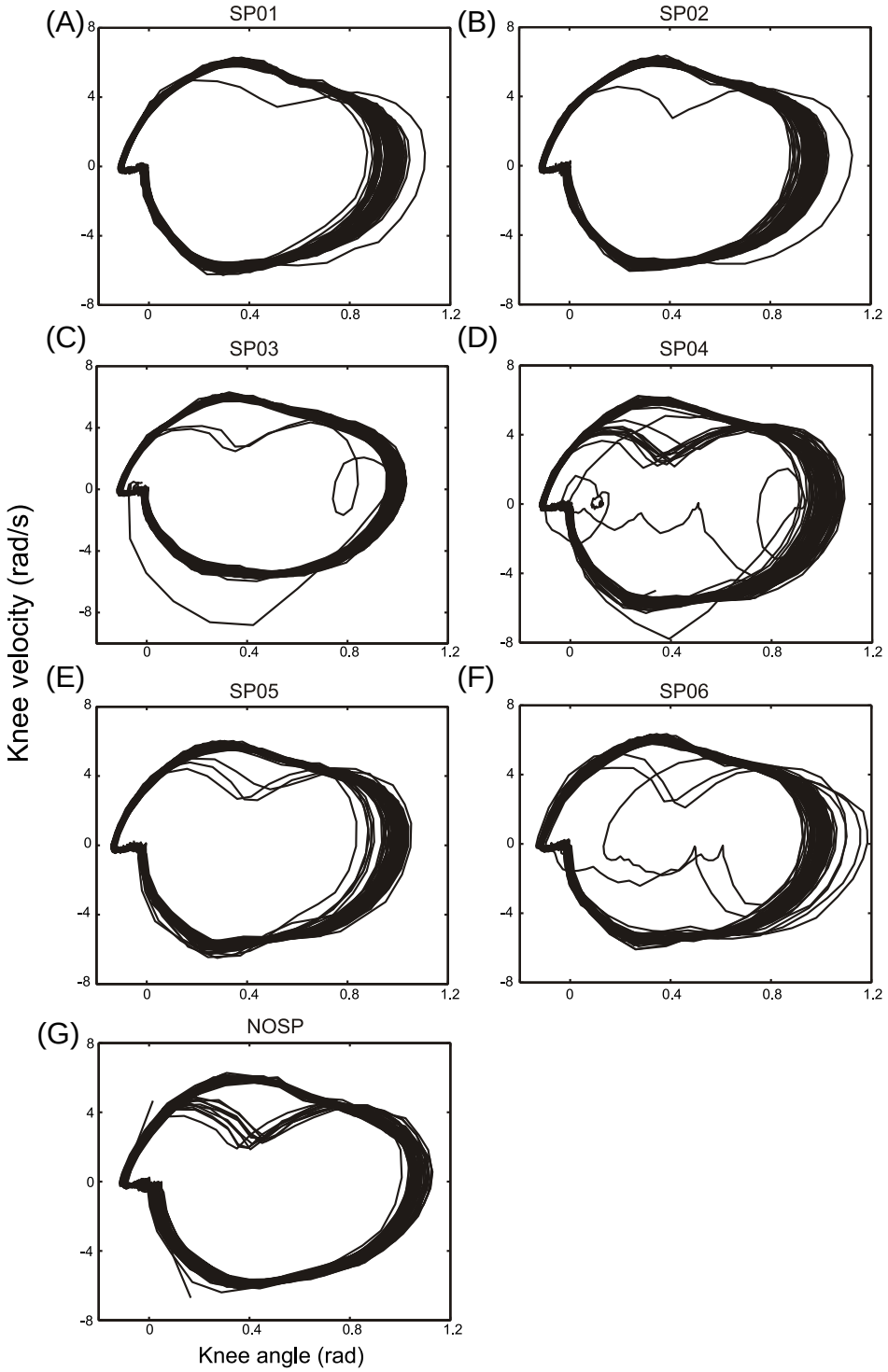

Figure 3.11: Phases plots of knee angular velocity versus angular position. Knee angle was calculated from the positions of markers around the knee joint in video camera tracking over twenty complete rotations of the circular path.

by perturbations than using the other springs sets and appear most stable.

As a next step, we look at the knee angle against different moments of the gait cycle which is shown in Fig. 3.12. During the stance phase, human exhibits a slight knee flexion and

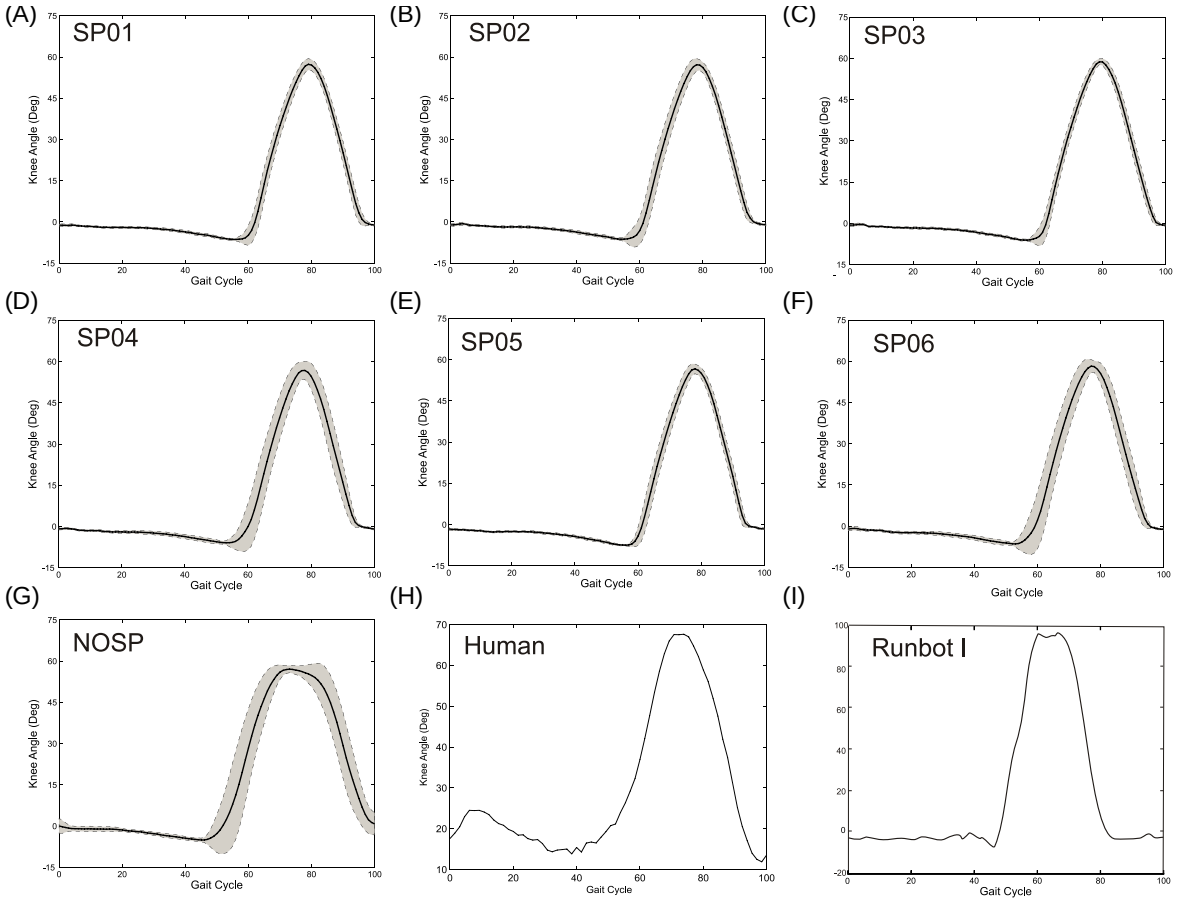

Figure 3.12: Plots of knee angle tracking during the gait cycle for different springs (A-F), rigid tendon (G), for human walking (H) and for the original RunBot (I). The grey areas indicate the standard deviation.

extension which can be seen in (H) whereas the RunBot II rotates like a rigid inverted pendulum keeping the knee straight. However, the RunBot II with the compliant knee achieves a smooth human-like knee movement during the swing phase similar to the human knee motion (H) during walking [156] compared to the jerky knee motion of the original RunBot (I) [7] (It has been permitted to replot data by Vaughan et al. [156] and Geng [7]).

Another point of interest is the knee angle curve (Fig. 3.12G) where a rigid tendon has been used. The flat peak during knee flexion in the swing phase is due to the knee flexing to its maximal angle without any delay caused by springs and remaining in this state before the hip reaches the AEA. This is similar to the knee motion of the original RunBot with actuated knee joint (Fig. 3.12I).

3.4 Discussion

3.4.1 Locomotion control using a reflexive controller

Human walking is characterised by a smooth, regular and repeating movement [156]. A stable limit cycle is established with an appropriate interaction between the nervous system and the musculoskeletal system, which has oscillatory characteristics. The CNS generates the signals that control the major muscle groups in the legs [157] where each joint is controlled by a single neural controller via muscle groups [158], while each muscle has its own specific pattern of activity during separate phases of the step cycle [76, 159]. Afferents play an important role in shaping the rhythmic pattern, controlling phase transitions and reinforcing the ongoing activity [160]. It is suggested that all the biological models for walking should incorporate sensory feedback but also use them to govern state- or phase-dependent modulation during locomotion [161]. For example, the innervating cutaneous afferents in the skin of the foot trigger phase transition between the swing and stance phase [76, 162]. The afferents from muscles that signal the hip joint position excite the knee extensor of the swing leg to extend the swing leg [158].

Numerous bipedal walkers were implemented based on principles of CPGs [94, 97, 105, 106, 163, 164, 165, 166]. A few biped robots employed non-linear oscillators modulated by sensory information [94, 166]. However, most CPG systems use approaches such as ZMP-based control [163], the HZD approaches [106], virtual model control [164], etc. Thus precise modelling and complicated computations are still necessary in these models. Our robot does not rely on precise models but rather is a stable limit cycle system.

In contrast to the original RunBot [5], filter functions were utilised in the controller instead of biologically inspired neuronal processing. We have chosen low-pass filter responses because of their prevalence in biological systems [149, 167]. The parameters were determined in an iterative optimisation process as outlined in section 3.3.1. Our study shows that it is possible to treat the complex neuronal processing as a black box utilising filter functions as transfer functions between sensory input and motor output.

3.4.2 Robotic walking compared to human walking

The RunBot II achieves a human-like walking performance in the swing phase as shown in Fig. 3.13. The initial HS occurs at 0% while the opposite HS occurs at 50% of the gait cycle. The hip movement in the sagittal plane can be seen as a single, sinusoidal curve. The hip movement of RunBot II satisfies all crucial factors of human hip motions: 1) Maximum hip flexion occurs in the terminal swing phase. 2) maximum hip extension occurs at the opposite HS [168]. The knee movement in humans can be separated into two flexion waves.

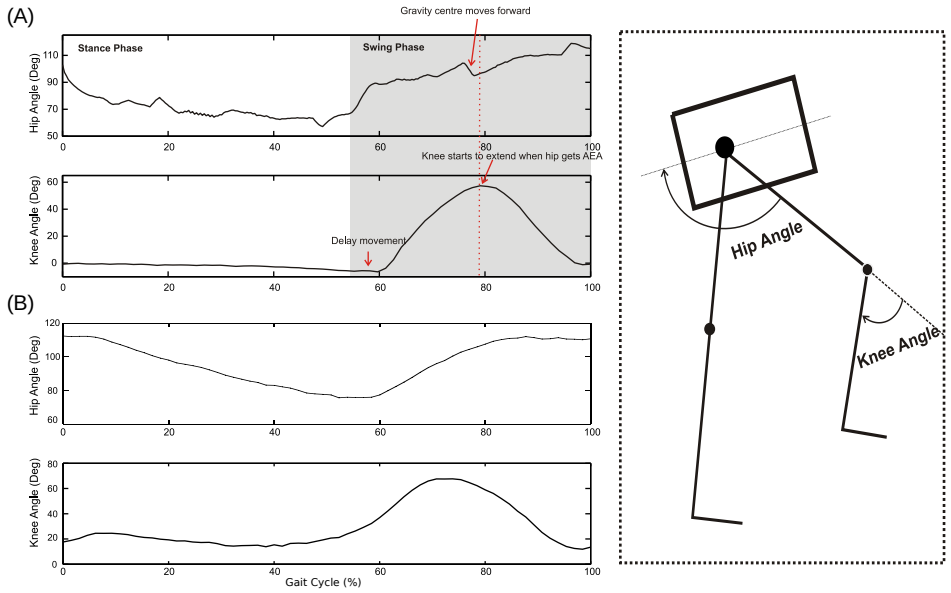

Figure 3.13: Kinematic comparison of RunBot II and human. (A) The angular position of hip joint and knee joint on the right leg in RunBot II within one gait cycle. (B) The angular position of hip joint and knee joint of the right leg in human within one gait cycle [156].

The flexion wave in the swing phase is necessary to clear the foot off the ground which begins at the late stance phase when the heel rises off the ground. The rapid knee flexion effectively shortens the limb to prevent foot-dragging. The knee then extends and achieves a full extension prior to next ipsilateral HS. Humans have a small knee flexion in the stance phase as well, which occurs after the HS. This flexion absorbs the shock for bearing the body weight and preventing excessive vertical translation of the centre of body mass and reaches its peak at the opposite Toe Off (TO). The knee extends in mid-stance by the extension force created by the QF. RunBot II lacks the knee flexion in the stance phase so that the leg swings as a rigid inverted pendulum due to the mechanical stop in the compliant knee structure without shock absorption after the HS. Compared to compliant knee joints without a mechanical stop [94, 166] the compliant knee structure of the RunBot II provides a better body weight acceptance and less vertical translation of the center of body mass.

3.4.3 Speed variation

It is well known that speed can be controlled by means of ankle push-off, body pitch angle and step length. A few limit cycle walkers show that varying hip joint velocities, like “Spring Flamingo” [102] and the original RunBot [6], changes the walking speed. Walking and running can be generated by tuning the amplitude and frequency of a simple CPG oscillator [94]. In the present study, the speed under the same control scheme and the environment is variable in a specific range because the biomechanism “self-computes” a significant part of the walking movement. It is also observed that the speed can be changed by varying the time

constants of the filter functions, especially the time constant of the hip transfer functions. The speed results show that the response speed of motor-neuron output determines the walking speed.

3.4.4 Compliant knee structure

Compliant knee structures have been employed in a number of biped robots aiming to mimic the human leg muscular architecture [85, 87, 94, 144, 169, 170]. There have been a variety of different approaches to achieve compliant control of knees, like using straps [169] or pneumatic artificial muscles [87, 144, 170], which are able to provide a large force with a light weight mechanism and the stiffness is adjustable by control. However, the precise timing control is unavailable due to their compliant characteristics, and it is impossible to achieve a human-like speed [144].

A geared electrical DC motor connected to the joint through an elastic component (usually a spring) has been proven to be an attractive candidate for biped robots [141]. Passive compliance is achieved by inserting a linear spring between the actuator and the effector. Joint compliance becomes a function of the robotic mechanism and is thus not controllable. This might be a disadvantage from a traditional robotic perspective, but it can be adopted in limit cycle walkers such as the RunBot II as no precise trajectory control is required.

To reach a better biological realism we have added a pulley modelling the patellar function so that the torque generated is properly dependent on the angle of the knee. This could still be improved by making the pulley sliding up and down as observed in a real knee. The human knee is a synovial joint where the patella "slides" on the surface of the femur during various knee angles and acts more like a "level" to alter the magnitude and direction of the force transmitted from the quadriceps tendon to the patellar ligament tendon [171]. This is a complicated mechanism for a robot which probably causes more problems than advantages and has been omitted in our design. The experimental results show the feasibility of enhancing the walking performance by applying a simple knee mechanism.

A robot with spring-like legs could generate stable walking over a range of different leg stiffness [142], and even achieve different gait patterns like running and walking [94, 166]. However, to our knowledge we are the first who have examined the relationship between the knee stiffness and the walking speed. The experimental results show that the walking speed is sensitive to the change of knee stiffness and a clear dependency between the stiffness and speed has been observed in Fig. 3.9. In this chapter, we have taken a purely experimental approach which had its limitations. A wider parameter regime could have been explored with simulations using springs which couldn't have been used due to their practical sizes, however, this would be a research in future.

3.5 Summary

In this chapter, we have presented a walking robot with a compliant knee and benchmarked the walking performance against different levels of stiffness. We concluded that a compliant knee significantly improves walking performance. Our knee mechanism was implemented with the help of a single motor located on the hip segment and controls the angle of the knee with the help of three springs. This setup allows simultaneous control of the knee angle and its compliance. A frictionless pulley over the front of the knee joint mimics the function of the patella in the human knee by changing the direction of the extension force. Two parallel spring groups are used to connect the motor with the joint. The springs S1 and S2 work as the QF and the patellar ligament. Another spring S3 mimics the property of the BF. Using a compliant knee structure results in a more robust and smoother knee movement during the swing phase. From a mechanical perspective, the compliant knee protects the knee motor from the HS and thus allows for a substantially longer lifetime of the robot.

Instead of implementing a biologically realistic network on the basis of incomplete data about it we rather have opted here for an abstract controller using filter functions instead. Processing of the signals only involves low-pass filtering [149, 167] and linear summation. The study suggests the feasibility of using filter function between the sensory input and motor output in the reflexive controller to establish stable walking.

The original RunBot was the fastest bipedal walking robot in the world which has a relative speed of 3.5 leg/second. The RunBot II has a slower speed which is approximately 40% compared to the original one mainly because of the compliant knee structure in Fig. 3.12 which won not allow to inject more energy into the system. In humans a substantial amount of the active work during walking is performed in the ankle. For instance, the ankle dorsiflexor plays a pivotal role for the forward propulsion in the stance phase. The ankle push-off is the main principle of gait to smooth the transition from the double support to the swing phase [172]. Therefore, the ankle actuation will be considered in future work to improve the walking speed and obtain a more realistic walking gait.

Chapter 4

Robotic reflexive controller derived from human data

4.1 Introduction

Human walking is a complex task, involving the interaction between the nervous system and biomechanical system. The flexibility and adaptivity of human gait pattern are the results of the integrated activity of spinal neuronal circuitries, sensory feedback signals and descending supraspinal motor commands. Two different explanations for the creation of the rhythms underlying the locomotion were proposed. The thought that CPG is primarily responsible for generating the motor patterns with the rhythmic movements has been the dominant paradigm over the recent decades [173, 174, 175]. CPGs are the basic function units regulated by sensory feedback from peripheral receptors to control the motor patterns and generate smooth locomotion. CPGs have been identified in mammals like cats but no data in experimental procedures can conclusively describe the existence of CPGs in humans [176]. Thus, an alternative view that rhythm motions are the result of a chain of reflexes where sensory feedback plays a significant role, triggering switches in different locomotion patterns [177] is used in this work.

As walking is a technically challenging problem in robotics, benefits have been found in integrating experimental studies of human locomotion and physiology with robot design and construction [155]. In the last two decades, researchers have attempted to design walking controllers for bipedal robots based on the organisational and architectural principles of neural circuits. Most bio-inspired biped walkers generated the rhythmic pattern motion by CPGs controllers without [178, 179, 180] or with sensory feedback signals [69, 94, 103, 105, 181] which have been suggested to play a significant role in modifying and stabilising rhythmic movements. The original RunBot [6] was the first dynamic biped robot exclusively controlled by a pure reflexive controller, where the pure reflexive controller involves no explicit

mechanisms for the global stability control of the biped.

As we know, in humans a substantial amount of the active work during walking is performed in the ankle. For instance, the ankle dorsiflexor plays a pivotal role for the forward propulsion in the stance phase. The ankle push-off is the main principle of gait which smooths the transition from the double stance phase to the swing phase [172]. Passive dynamic walkers established stable walking on the level ground with the addition of ankle actuation [182] which indicates that the ankle actuation also contributes significantly to the robotic walking. However, to our knowledge there is no ankle control model proposed based on reflexive mechanisms.

In this chapter, we will present a novel reflexive control model with the addition of ankle control. The central work is to investigate the control between the sensory inputs and motor outputs. In Section 4.2, the causal relationship between foot contact information and motor activation (muscle activation EMG in human) were studied. The transfer function was calculated from human walking data and extracted according to the function of each muscle. A closed-loop system was created with the transfer functions translating the sensory signals into the muscle activations. The optimised transfer functions would be replaced with IIR filter functions due to the 2nd order low-pass filter property of the transfer functions. The new reflexive controller was drawn from the human study. The control model was applied to the latest version of the robots, RunBot III, in which the actuated ankle joints are implemented. The hardware of the robot is introduced in Section 4.3. The results are described in Section 4.4.

4.2 Reflexive controller with ankle control

Investigation of neuromuscular coordination control in locomotion requires a thorough knowledge of basic variables which characterise the locomotion. The kinematic and muscle activity of the ankle and foot during human walking are described in this section first. We point out that sensory feedback, especially foot contact or loading information, is a significant input which can be integrated to generate motor activation in muscle. The causal relationship between sensory input and muscle EMG was studied in human walking experiments. We present a reflexive control model based on transfer functions derived from human walking data.

4.2.1 Foot and ankle kinematics during human walking

A clear understanding of ankle kinematics during walking is crucial to building a biological inspired ankle control model. The foot-ankle joint is a complex joint which contributes

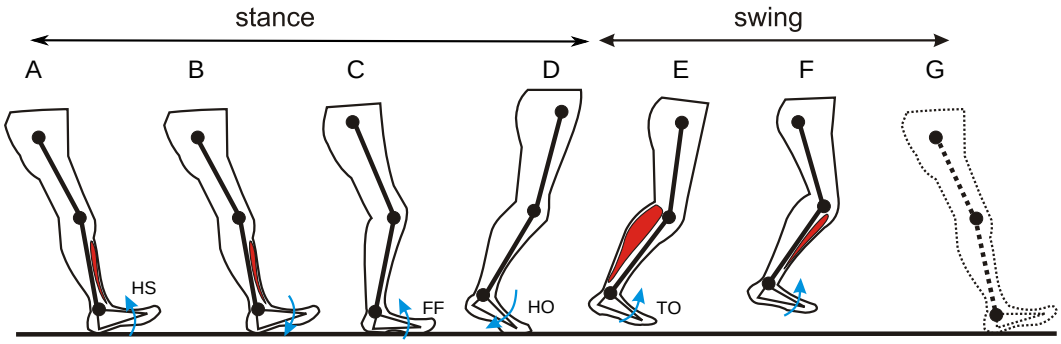

Figure 4.1: Position of the right leg during a gait cycle. The stance phase starts when the ipsilateral foot heel strikes the ground. The ankle joint plantarflexes to lower the foot toward the ground. When the tibia rotates over the foot, the ankle joint starts to dorsiflex. A major plantarflexion initiates after heel off and last until toe off. During swing the ankle moves back to dorsiflexion so that the forefoot clears the ground. Note: HS = heel strike, FF = flat foot, HO = heel off, TO = toe off.

significantly to various motion activities. A typical gait cycle is shown in Fig. 4.1 [183]. At HS, the ankle joint is either in its neutral position or slightly dorsiflexed. During the loading response of the gait cycle (0-10%), the ankle has a tendency of dorsiflexion due to loading body weight. Then the foot flexes forward until it touches the ground (Flat Foot (FF), Fig. 4.1C). At the FF the foot stays on the ground, the lower limb rotates forwards like an inverted pendulum, and the ankle is slightly dorsiflexed by the limb motion. After HO the ankle begins the plantarflexion regarded as ankle push-off as shown in Fig. 4.1D. The heel reaches the highest placement before TO. After the TO, the foot dorsiflexes to clear the ground during the swing phase, prepares to touch the ground again and starts a new stride, Fig. 4.1E-G .

4.2.2 Sensorimotor interaction

Sensory feedback contributes to motor control in two ways [154]: Firstly, it is an integrated part which generates motor command of muscle activation in natural movements. A clear drop in EMG after the unloading of the ankle plantarflexor was observed when the ankle dorsiflexors were blocked by local lidocaine injection or the skin of the foot was anesthetised [57]. Load afferent (Group II afferent) contributes to 50% of muscle activity in the stance phase, indicating that sensory afferents contribute significantly to motor activation during unperturbed human walking. Secondly, a reflex is excited when external disturbances occur to correct the movement and avoid falling. Cutaneous reflexes are phase-modulated during the gait cycle. For example, tibial nerve stimulation causes plantarflexion at the late swing phase but elicits dorsiflexion during the late stance phase [76]. The extensor muscle exhibits a reflex response by a cutaneous stimulus at the late swing and early stance phases, while the extensor reflex response is inhibited during the mid-stance phase [184]. These studies sug-

gest that sensory feedback is essential to compensatory reactions to external disturbances. Overall, sensory feedback significantly contributes to natural human locomotion and generates reponses to unexpected environmental events.

Muscle activity is a combined effect of all the synaptic inputs to the motor neurons [185]. The human foot is the only physical contact between the human body and the environment, sending spatial-location information back to the CNS during locomotion. Sensory feedback is significant in retaining balance [186], postural control [187, 188] and locomotion [76, 189]. To investigate the control principles between the sensory signals and ankle movements, we studied the causal relationship between the sensory information and motor activation in human muscle activation (EMG). With this knowledge we can create an abstract and closed-loop controller based on human walking data.

4.2.3 Transfer functions derived from human walking data

The original RunBot adapted a biologically inspired controller, where motor neuron outputs were generated by sensor neuron inputs with the help of neuronal firing processing [6]. The CNS is highly complicated with numerous unknown variables and the location of the origin of walking is controversial, meaning that a robot with neural networks is unsustainable and redundant. Our aim is to create an abstract and analogue close-loop controller that can be implemented in a robot and FES system. To establish this, it was necessary to investigate the causal relationship between foot contact information and muscle activation.

The study of transfer functions relating sensory information and muscle activation during human walking has been done in the collaboration with Catherine A. Macleod and the University of Strathclyde. Ten subjects participated at the Department of Biomedical Engineering, University of Strathclyde. The data collection comprised muscle EMG and foot contact information during treadmill walking. Four muscles were chosen due to their different roles in the gait cycle: two muscles (TA and LG) in the shank and two (BF and RF) in the thigh. FSRs (Interlink Electronics, CA, USA) were embedded in standard shoe insoles at four different positions (toe, 1st metatarsal, 5th metatarsal, and heel). All data was recorded with a sampling frequency of 1kHz using the USB-DUX Sigma data acquisition device (Incite Technology Ltd, Stirling, UK).

Adaptive filtering

An adaptive filter was used to derive the transfer function for each recorded muscle. The EMG signals were filtered by a band-pass filter (50-200Hz), full-wave rectified and filtered (6Hz) to obtain the linear envelop of the EMG signals. The EMG and FSRs sequences were divided into strides and scaled to 0 to 100 for eliminating the effect of various speeds.

The estimated EMG output signal of each muscle was generated by using the Least Mean Squares (LMS) approach through the convolution of the filter impulse response with a typical FSRs contact signal [190]. The filter impulse response $h_{L/R,mus,CH/IH/IT}$ converged after 100 times of iterative learning, where the length of the filter is two strides. A half Hanning window was used to extract filter coefficients for one stride. To compensate for the difference in foot contact sensory feedback between the human and robotic systems, the filter coefficients $h_{L/R,mus,CH/IH/IT}$ from the human data were convolved with the average FSR signals $\overline{FSR}_{CH/IH/IT}$ in two strides, Eq. 4.1. Therefore the response of the transfer function is equivalent to applying a typical FSR signal measured in gait but the RunBot can use an impulse signal to trigger the response. The values of the transfer function are normalised to 0 and 1.

$$H_{L/R,mus,CH/IH/IT} = h_{L/R,mus,CH/IH/IT} * \overline{FSR}_{CH/IH/IT} \tag{4.1}$$

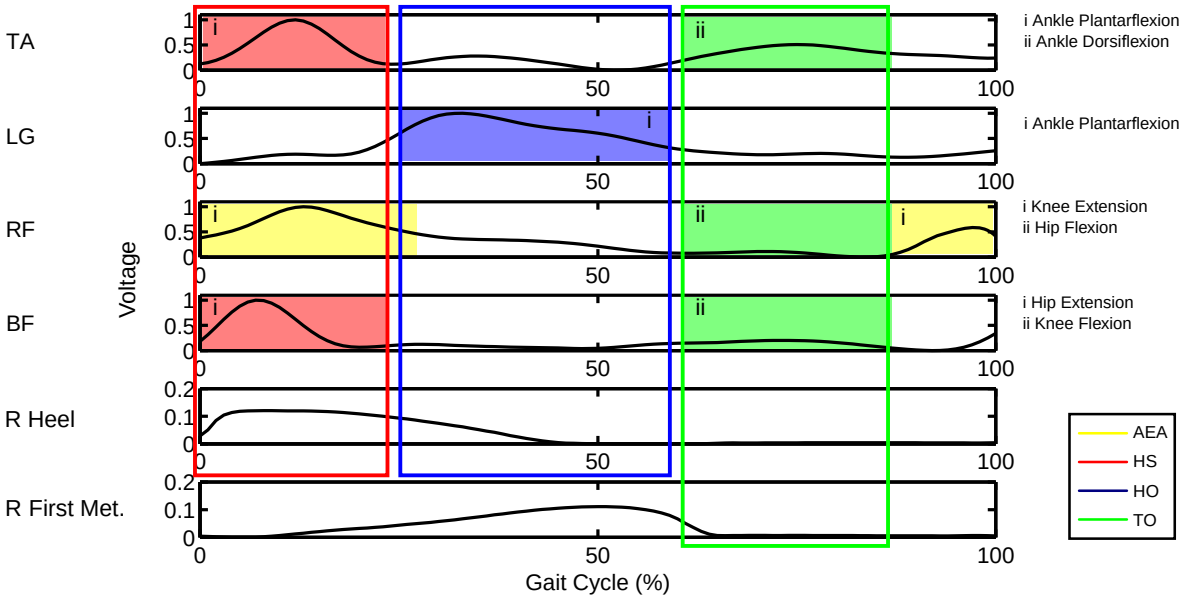

Figure 4.2: Transfer functions between foot contact information and muscle activity. The diagram indicates how the muscle EMG signals are triggered and related to the sensory information.

Extracting transfer functions

The key is to define the transfer functions related to activation and suppression of motor neuron pools, which bears the relationship of the biomechanical movements. The transfer functions related to the joint movements can be separated. It is essential to define the sensory feedback signal that is responsible for triggering the transfer functions. The function of each muscle on the joints is summarised in Tab. 4.1. The transfer functions of hip and knee joints

Table 4.1: Relating the muscle transfer functions to motor control

Transfer Function	Motor Control
$H_{L/R,BF,IH}$	Hip extension during the stance phase (IH)
$H_{L/R,RF,IH}$	Hip flexion during the swing phase (IH)
$H_{L/R,RF,CH}$	Knee extension during the late swing and stance phase (CH)
$H_{L/R,BF,IT}$	Knee flexion during the early swing phase (IT)
$H_{L/R,LG,IT}$	Knee flexion during the swing phase (IT)
$H_{L/R,LG,IH}$	Ankle dorsiflexion during the late stance phase (IH)
$H_{L/R,TA,IH}$	Ankle dorsiflexion during the stance phase (IH)
$H_{L/R,TA,IT}$	Ankle plantarflexion during the swing phase (IT)

IH = Ipsilateral Heel, CH = Contralateral Heel, IT = Ipsilateral Heel.

(flexion/extension) were successfully applied to the RunBot II (details in [139]). It is proof of the concept that the reflexive control model using human data can generate stable walking of the robot. The concern in this study was to relate muscle activity to foot contact information and create a closed-loop control system using the cutaneous feedback from the foot to elicit muscle activations that can be applied to the robotic control.

Rectus Femoris (RF)

RF is a bifunctional muscle responsible for hip flexion in the swing phase and knee extension in the late swing and stance phase. Two peaks are observed in the RF transfer function, Fig. 4.2C. One peak corresponds to the hip flexion relating to the ipsilateral TO. Another peak, which coincides with the late swing, is identified as the activity related to the knee extension. It is observed that the knee extension at the late swing phase does not follow any foot contact as it occurs before ipsilateral HS. In accordance with the reflexive neuronal controller implemented in the RunBot II decribed in Chapter 3, we assumed that the AEA of the hip activates the RF muscle for knee extension. As shown in Fig. 4.3, the transfer functions are derived following Eq. 4.2 and 4.3.

$$H_{L/R,RF,HF}(t) = \begin{cases} H_{L/R,RF,IH}(t + t_{RF,IH,start}) & 0 \leq t \leq (t_{RF,IH,end} - t_{RF,IH,start}) \\ 0 & \text{otherwise} \end{cases} \tag{4.2}$$

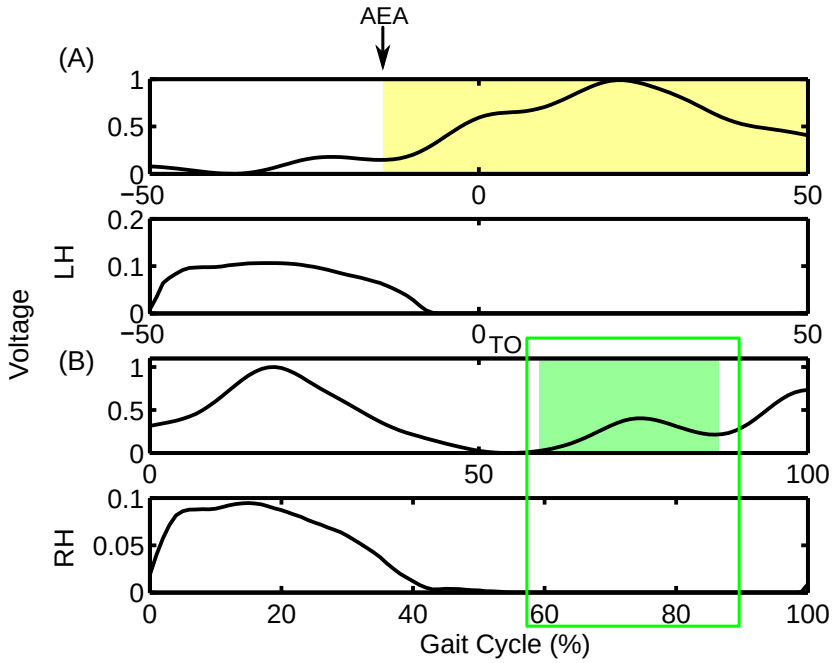

Figure 4.3: Transfer functions of the RF muscle generated using the FSR signals $\overline{FSR}_{CH}$ and $\overline{FSR}_{IH}$ respectively. Plots are taken from one subject as an example. The different colours demonstrate the sensory signals which are used for each muscle activation. The $h_{L/R,RF,CH}$ in (A) shows that the RF muscle has muscle activation arising from the AEA (yellow) and continuing during the stance phase, while a relatively small peak is observed in the $h_{L/R,RF,IH}$ (B) elicited at toe off (green, approximately 60% in normalised gait cycle).

$$H_{L/R,RF,KE}(t) = \begin{cases} H_{L/R,RF,CH}(t + t_{RF,CH,start}) & 0 \leq t \leq (t_{RF,CH,end} - t_{RF,CH,start}) \\ 0 & \text{otherwise} \end{cases} \tag{4.3}$$

Where $t_{RF,IH,start}$ and $t_{RF,CH,start}$ are ipsilateral TO and AEA respectively, $t_{RF,IH,end}$ is the ipsilateral AEA and $t_{RF,CH,end}$ is the contralateal HS. L = Left, R = Right, HF = Hip Flexion, KE = Knee Extension, CH = Contralateral Heel, IT = Ipsilateral Toe.

Biceps Femoris (BF)

The BF muscle responds to hip extension in the stance phase and the knee flexion in the swing phase. By comparing the BF transfer function with the foot contact information as shown in Fig. 4.4, the muscle activity can be identified following the ipsilateral HS for the hip extension and ipsilateral TO for knee flexion. The extracted transfer functions are as follows:

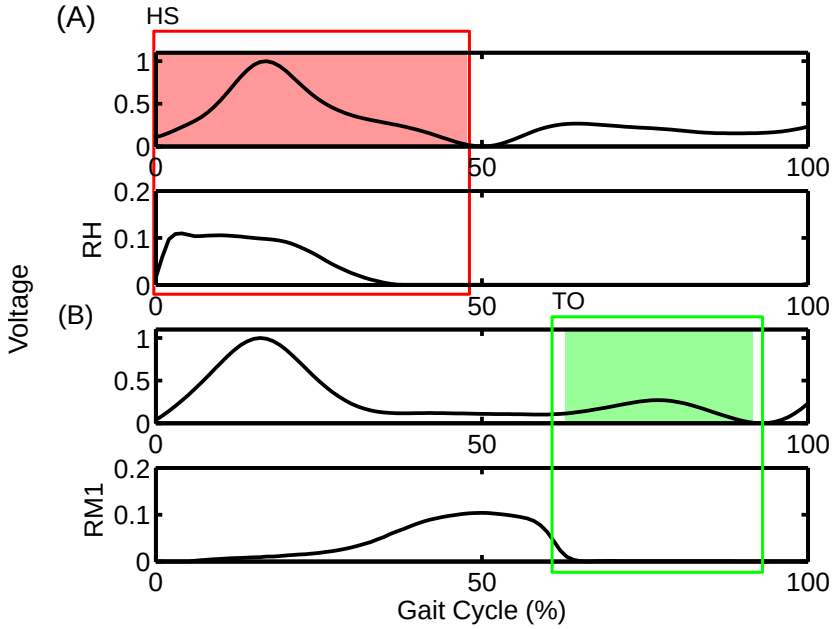

Figure 4.4: Transfer functions of the BF muscle generated using the FSR signals $\overline{FSR}_{IH}$ and $\overline{FSR}_{IT}$ respectively. Plots taken from one subject as an example. The different colours demonstrate the sensory signals which are used for each muscle activation. The $h_{L/R,BF,IH}$ in (A) shows that the BF muscle has muscle activation arising from the ipsilateral heel contact and continuing until the contralateral heel strike (red), while a relatively small peak is observed in the $h_{L/R,BF,IT}$ (B) elicited at ipsilateral toe off (green, approximately 60% in normalised gait cycle).

$$H_{L/R,BF,HE}(t) = \begin{cases} H_{L/R,BF,IH}(t + t_{BF,IH,start}) & 0 \leq t \leq (t_{BF,IH,end} - t_{BF,IH,start}) \\ 0 & \text{otherwise} \end{cases} \tag{4.4}$$

$$H_{L/R,BF,KF}(t) = \begin{cases} H_{L/R,BF,IT}(t + t_{BF,IT,start}) & 0 \leq t \leq (t_{BF,IT,end} - t_{BF,IT,start}) \\ 0 & \text{otherwise} \end{cases} \tag{4.5}$$

Where $t_{BF,IH,start}$ is the ipsilateral heel contact, $t_{BF,IH,end}$ is the contralateral heel contact, $t_{BF,IT,start}$ and $t_{BF,IT,end}$ are the ipsilateral toe off and AEA. L = Left, R = Right, HE = Hip Extension, KF = Knee Flexion, IH = Ipsilateral Heel, IT = Ipsilateral Toe.

Lateral Gastrocnemius (LG)

The LG transfer functions of all subjects are shown in Fig. 4.5. The LG muscle is primarily responsible for ankle plantarflexion but also takes part in knee flexion [191]. In most subjects, a peak is observed during late stance phase when the LG muscle shortens to plantarflex the

ankle joint. This generates an explosive push-off force after heel off during walking gait. The ankle push-off generated by the muscle is the main principle of gait which smooths the transition from double support to the swing phase [172]. The transfer function for the ankle plantarflexor elicited by HO is as Eq. 4.6. It should be noted that although the contraction of the LG also induced knee flexion in this period, only ankle plantarflexion is concerned as the primary muscle function. Another peak activity is also observed in a few subjects during early stance phase, which may be caused by the LG muscle lengthening while the hip extends backwards. As the eccentric muscle activation is not considered as voluntary contraction, this part of the LG transfer function is not considered in this case. The LG muscle is inactive during the swing phase in Fig. 4.5.

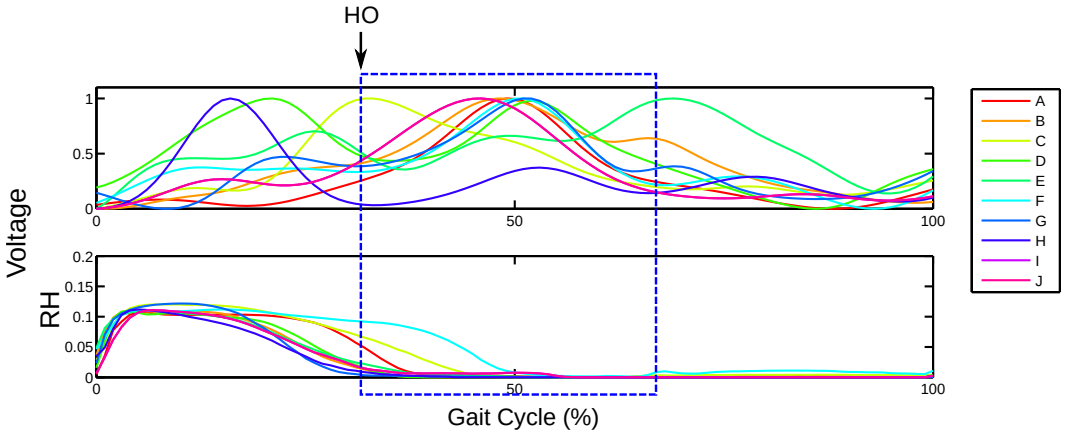

Figure 4.5: Transfer function of the LG muscle generated using the FSR signals $\overline{FSR}_{IH}$. Plots taken from all subject (A to J). The $h_{L/R,LG,IH}$ shows that the BF muscle has muscle activation arising from the ipsilateral heel off and continuing until the ipsilateral toe off.

$$H_{L/R,LG,AP}(t) = \begin{cases} H_{L/R,LG,IH}(t + t_{LG,IH,start}) & 0 \leq t \leq (t_{LG,IH,end} - t_{LG,IH,start}) \\ 0 & \text{otherwise} \end{cases} \tag{4.6}$$

Where $t_{LG,IH,start}$ is the ipsilateral HO, and $t_{LG,IH,end}$ is determined as the ipsilateral TO. L = Left, R = Right, KF = Knee Flexion, AP = Ankle Plantarflexion, IH = Ipsilateral Heel, IT = Ipsilateral Toe.

Tibialis Anterior (TA)

The TA muscle has two functions in human walking. The muscle is responsible for the ankle dorsiflexion during the swing phase to clear the foot off the ground. It was also found that the muscle generates a peak activity during early stance after HS, to generate the force to lower the foot. During this period, the muscle works as a reverse muscle - a plantarflexor [192].

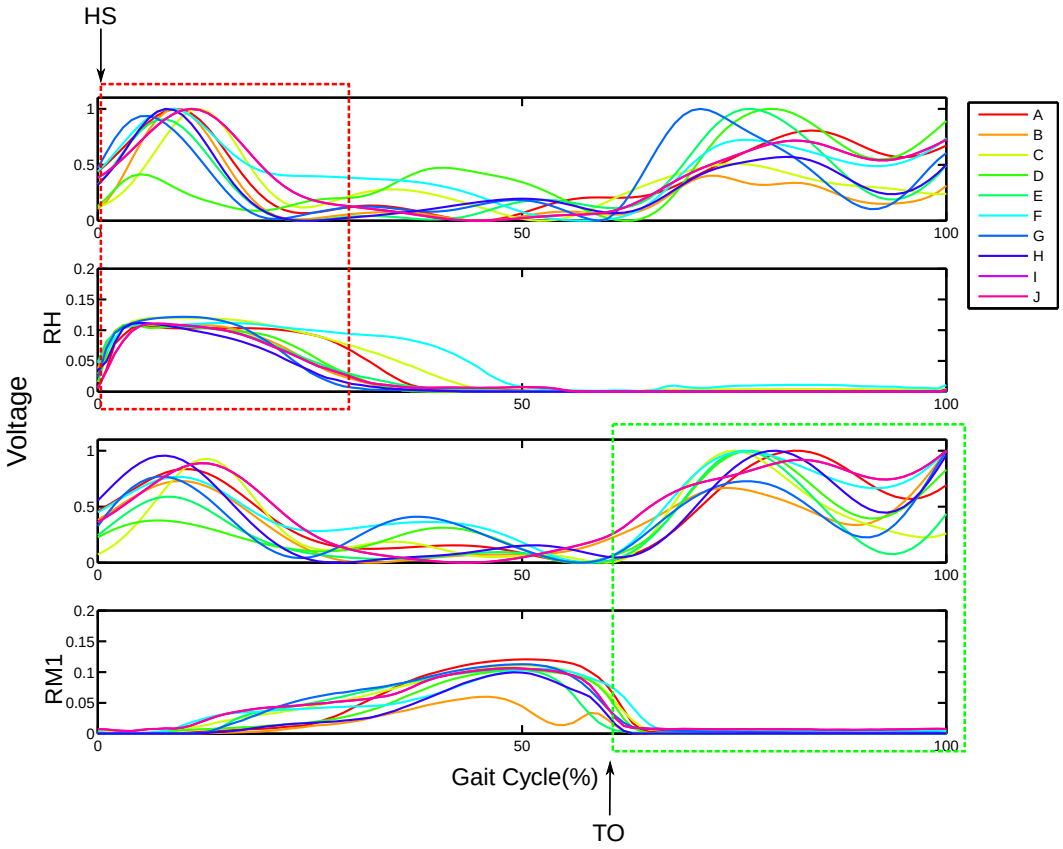

Figure 4.6: Transfer functions of the TA muscle generated by using the FSR signals $\overline{FSR}_{IH}$ and $\overline{FSR}_{IT}$ respectively. Plots are taken from all subject (A to J). Two peaks are observed in the TA transfer functions. One peak arising with the ipsilateral heel strike is responsible for reverse ankle plantarflexion. Another peak relates to the ipsilateral toe off.

Two peaks were observed in the TA transfer functions in Fig. 4.6. Following the ipsilateral HS, a peak is elicited in the TA muscle, which acts for reverse ankle plantarflexion. Another peak is closely related to the ipsilateral TO, corresponding to ankle dorsiflexion during the swing phase. Thus, two transfer functions relating to muscle functions for ankle movement were derived from the TA transfer functions $H_{L/R,TA,IH}$ $H_{L/R,TA,IT}$ respectively, see Eq. 4.7 and 4.8.

$$H_{L/R,TA,AD}(t) = \begin{cases} H_{L/R,TA,IT}(t + t_{TA,IT,start}) & 0 \leq t \leq (t_{TA,IT,end} - t_{TA,IT,start}) \\ 0 & \text{otherwise} \end{cases} \tag{4.7}$$

$$H_{L/R,TA,AP}(t) = \begin{cases} H_{L/R,TA,IH}(t + t_{TA,IH,start}) & 0 \leq t \leq (t_{TA,IH,end} - t_{TA,IH,start}) \\ 0 & \text{otherwise} \end{cases} \tag{4.8}$$

Where $t_{TA,IH,start}$ and $t_{TA,IT,start}$ are the ipsilateral HS and ipsilateral TO respectively. $t_{TA,IH,end}$ and $t_{TA,IT,end}$ are the ipsilateral HO and ipsilateral HS respectively. L = Left, R = Right, AP = Ankle Plantarflexion, AD = Ankle Dorsiflexion, IT = Isilateral Toe, IH = Ipsilateral Heel.

Transfer functions related to the joints

After relating each muscle activation to specific sensory feedback, mainly foot contact information, the sensory feedback was used to activate the muscle via the transfer functions while the muscle contraction drives the movements of the joints. These muscle transfer functions need to be translated to joint controls first to create a abstract closed-loop control system.

- Hip joint. The hip comprises of two motion during walking - the hip flexion and extension. The BF muscle drives the hip extension after the ipsilateral HS, while the hip flexion is driven by the RF muscle during the early swing phase immediately after ipsilateral TO. Thus two muscle transfer functions are used to control the hip flexion and extension respectively as follows:

$$H_{L/R,H,F} = H_{L/R,RF,HF} \tag{4.9}$$

$$H_{L/R,H,E} = H_{L/R,BF,HE} \tag{4.10}$$

- Knee joint. Two muscles in our study are responsible for knee movement. A peak is observed in the BF transfer functions correlating to the knee flexion in the swing phase, Eq. 4.11. The RF muscle contracts to extend the knee during the late swing and stance phase so that the RF transfer function is used as the transfer function for knee extension, Eq. 4.12.

$$H_{L/R,K,F} = H_{L/R,BF,KF} \tag{4.11}$$

$$H_{L/R,K,E} = H_{L/R,RF,KE} \tag{4.12}$$

- Ankle joint. Both TA and LG muscle contribute to ankle movement in the sagittal plane. The transfer functions relating foot contact information to muscle activity were defined in the previous subsection. The ankle plantarflexes toward the ground from HS to HO by the TA muscle to allow body loading during the stance phase. Another plantarflexion tha is driven by the LG is not triggered by foot contact information but rather by the ipsilateral heel off information. Thus, two transfer functions, $H_{L/R,TA,AP}$

and $H_{L/R,LG,AP}$ are adapted respectively correlating with different sensory feedback information, Eq. 4.13. The ankle dorsiflexion is acted by the TA to clear the foot off the ground during the swing phase. The transfer function relating to the ankle dorsiflexion is defined in Eq. 4.14.

$$\begin{aligned} H_{L/R,A,P_{HS}} &= H_{L/R,TA,AP} \\ H_{L/R,A,P_{HO}} &= H_{L/R,LG,AP} \end{aligned} \tag{4.13}$$

$$H_{L/R,A,D} = H_{L/R,TA,AD} \tag{4.14}$$

The negative values of the curve fitted transfer function were excluded to zeros. Each transfer function was then normalised to a value range between 0 to 1.

Filter function optimisation

The muscle response with a characteristic shape could closely match the impulse time curve of a damped, linear second order differential system [193]. The second order model behaves like a low-pass filter that produces a delay between the neuronal excitation and the activate state of the muscle [149]. The muscle transfer functions were optimised by using curve fitting to remove the artifacts of the EMG transfer functions [139]. The curved fitted transfer function needed to be resampled at the specific sampling frequency to fit the mechanical system of the RunBot II. In this study, a second order low-pass Bessel filter as described in Eq. 4.15 was used to optimised the muscle transfer functions instead of the curve fitting approach as the transfer function between the sensor neuron and motor unit action potential is a second order damped system [149]. The impulse response of the filter function could be modelled efficiently by adjusting the cut-off frequency f_c and gain coefficient g. The utilisation of filter functions would significantly improve the efficiency of adapting the control system to different applications, for instance, the robotic control, FES control, etc.

$$H(t) = g(\frac{1}{\tau} e^{\frac{-1.5t}{\tau}} sin(\frac{\sqrt{3}t}{2\tau})) \tag{4.15}$$

Where g is the amplitude fitted variable, or gain to normalise the amplitude. τ is the time constant of a second order low-pass Bessel filter, $\tau = \frac{1}{2\pi f_c}$.

The motor actions have been related to muscle activations derived from the muscle transfer functions, suggesting that the joint movements are activated and inhibited by sensory feedback consisting of the foot contact information or the hip AEA signal. The t_{start} and t_{end} of muscle transfer functions are summarised in Tab. 4.2. The impulse response of filter function has been used to curve fit the desired characteristics of the average muscle transfer function

in the least-square sense by adjusting the time constant τ. The resulting transfer function $\widehat{H}$ was normalised to a value range between 0 and 1. The filter functions within one gait cycle are shown in Fig. 4.7 and parameter values are listed in Tab. 4.3.

Table 4.2: A summary of t_{start} and t_{end} of transfer functions related to joint movements.

Muscle	Transfer function	t_{start}	t_{end}
TA	$H_{TA,AP}$	HS	HO
	$H_{TA,AD}$	TO	HS
LG	$H_{LG,AP}$	HO	TO
RF	$H_{RF,HF}$	TO	AEA
	$H_{RF,KE}$	AEA	HO
BF	$H_{BF,HE}$	HS	HO
	$H_{BF,KF}$	TO	AEA

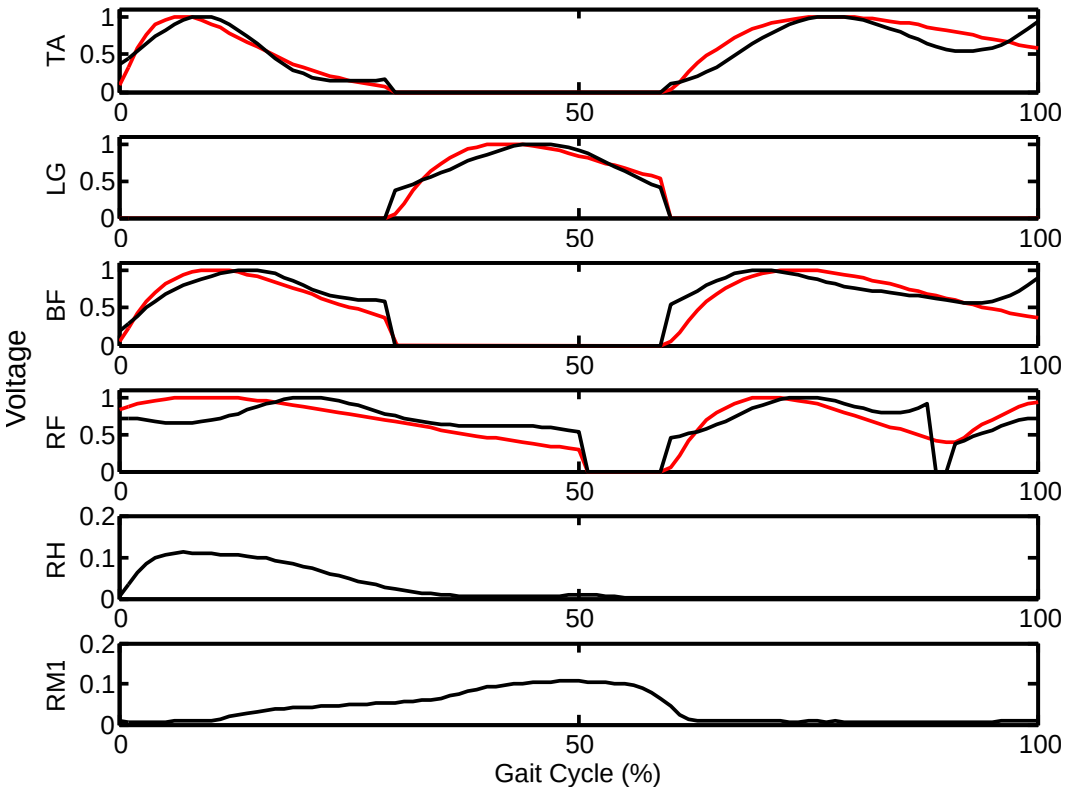

Figure 4.7: Plots of filter functions to one stride. Each impulse response of the filter function (red) curve fits the corresponding average muscle transfer function from all subjects (black).

Table 4.3: Results of filter functions for each joints. The filter function is used to curve fit the characteristics of the muscle functions in the normalised gait cycle.

Muscle	Filter Function	f_c	g	Sum of squared error (SSR)
TA	$\widehat{H}_{A,P_{HS}}$	1.45	1.5750e+01	2.6119e-01
	$\widehat{H}_{A,D}$	0.55	4.1408e+01	1.0731
LG	$\widehat{H}_{A,P_{HO}}$	0.80	2.8468e+01	3.7403e-01
BF	$\widehat{H}_{H,E}$	0.95	2.3984e+01	9.2681e-01
	$\widehat{H}_{K,F}$	0.70	3.2537e+01	1.5976
RF	$\widehat{H}_{H,F}$	0.90	2.5319e+01	1.9918e-01
	$\widehat{H}_{K,E}$	0.50	4.5533e+01e	2.1720

4.2.4 The robotic reflexive controller

Dynamic walkers that can walk with reduced mechanical complexity and little or no control have been developed in recent decades [81]. The compliant ankle equipped in the bipedal robots consists of rotational or extension springs to generate passive ankle torques, mainly during the stance phase [94, 194]. A strong limitation of the passive ankle joint is that a significant amount of active work during human walking is performed in the ankle. In contrast, the effect of the actuated ankle and flat foot on the energy of limit cycle walkers and their disturbance rejection have been studied by Hobbelen and Wisse [195]. Local feedback in the ankle and from the hip angle are used to modulate the ankle torque throughout the stance phase. A fully actuated ankle control model without any precision trajectories has not been explored. The purely reflexive controller has been successfully implemented in the original RunBot [6] and the RunBot II discussed in Chapter 3, where ground contact information is mainly used to trigger flexor/extensor reflexes in the legs and further drive the motors without any precision control algorithms. The successful implementation of transfer functions derived from human data to the RunBot II demonstrates that the causal relationship between the foot contact information and muscle activation can be extracted and applied to a robotic model[139]. A novel reflexive control including ankle control was created based on our previous human study in this chapter.

In Section 4.2.3, the sensory information was related to muscle activation and furthermore to the joint movement. The muscle transfer functions were extracted corresponding to the functions of the muscles and then the transfer functions for joint control ($\widehat{H}_{H,F}$, $\widehat{H}_{H,E}$, $\widehat{H}_{K,F}$, $\widehat{H}_{K,E}$, $\widehat{H}_{A,D}$, $\widehat{H}_{A,P}$) were identified. The HS triggers the extensors of the hip, knee and ankle plantarflexor at the initiation of the stance phase. The flexors of the joints are elicited by the TO signal that indicates the start of the swing phase. The unloading information HO is used

to activate another ankle plantarflexor during the stance phase. The knee extensor during the swing phase is the only exception as it is not related to the foot contact information. It has been discussed in [139] that the knee extensor could be related to the hip AEA.

It has been noticed that the toe contact information, or rather the TO information, is an essential sensory signal as it indicates the start of the swing phase. Although there was no sensor detecting toe contact and the foot was designed as a whole rigid body in the RunBot II, the contralateral HS was utilised as the trigger of the swing phase of the leg [139]. Therefore, the contralateral HS is still used instead in the new reflexive controller.

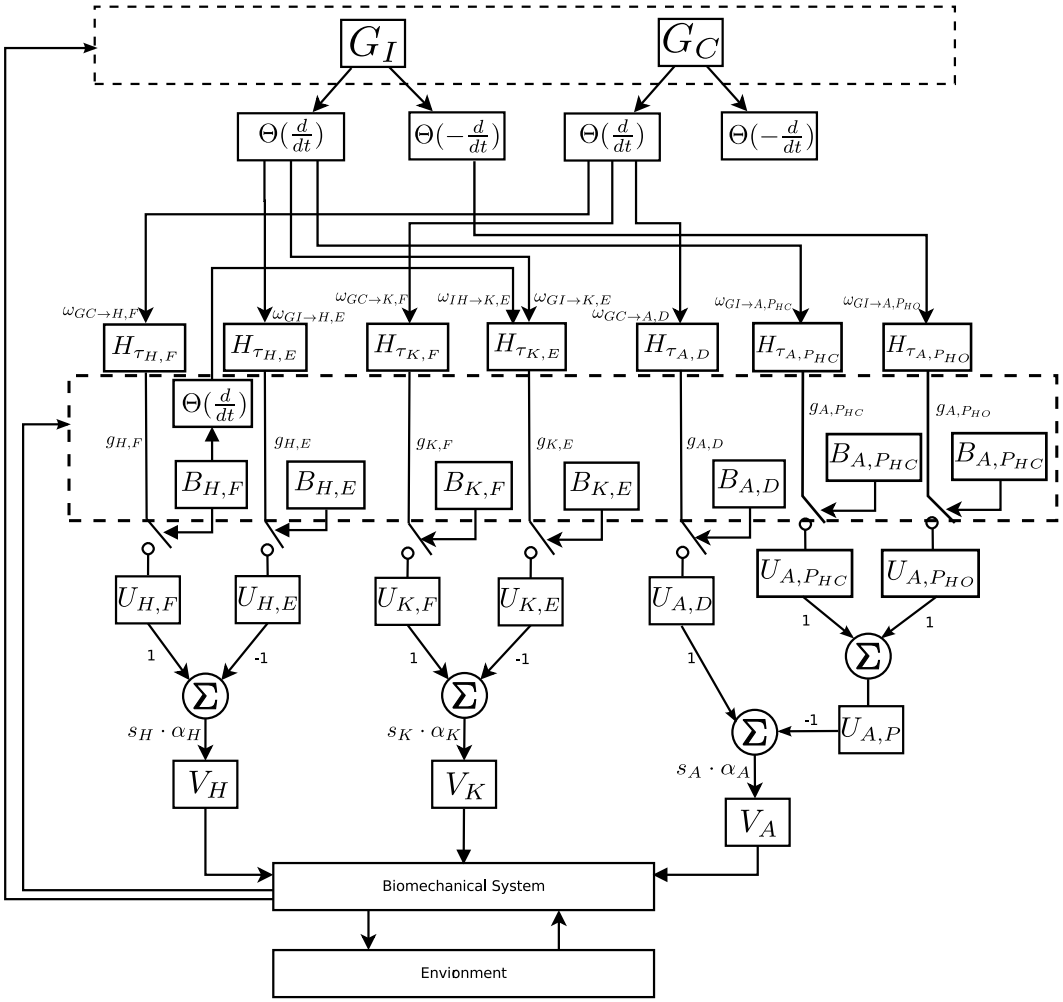

Figure 4.8: The control diagram of the reflexive controller. $G_{I/C}$ are the signals from the ground contact sensors of the ipsilateral and contralateral leg. $\Theta(d/dt)$ is the rectified derivative of the ground contact providing a delta pulse at the moment of the heel contact. $\Theta(-d/dt)$ is the rectified derivative of the ground contact providing a delta pulse at the moment of the heel uncontact. Σ is summation node integrating the sensory inputs. Filter functions H are used to create responses with impulse inputs. The impulse responses are normalised by multiplying with the gain coefficients g. B provide local reflexes from the stretch receptors based on the joint angles. U are motor outputs. V are motor voltages obtained by multiplying motor outputs U with $s \cdot \alpha$.

A full mathematical data flow diagram is shown in Fig, 4.8. The hip and knee control are consistent with the previous model. The control part has a hierarchical structure with three local loop controls: leg control, intra-joint control and joint control. The cutaneous sensory input from the foot indicating the loading information excites the extensors of the ipsilateral leg and flexors of the contralateral leg, so called leg control. In intra-leg control, when the hip joint achieves its extreme angular position during the swing phase, the hip AEA signal will activate an extensor reflex at the ipsilateral knee joint. The local joint reflex arises in joint control to inhibit the motor output to prevent the hyperflexion or hyperextension of the joint.

Like with the hip and knee joint, the ankle joint consists of one plantarflexor and one dorsiflexor. The leg and joint control involved in the ankle controller as sensory inputs of the G_I and G_C are integrated to generate the motor neuron outputs. The loading contact information $\Theta(\frac{d(G_I)}{dt})$ activates the ipsilateral plantarflexor and reciprocally inhibits the dorsiflexor. A significant difference in ankle reflexive controller is that the sensory signal of the foot unloading $\Theta(-\frac{d(G_I)}{dt})$ elicits another plantarflexor. The dorsiflexor is excited by the contralateral foot contact signal $\Theta(\frac{d(G_C)}{dt})$. The joint has two stretch receptors. A local reflex arises to inhibit the motor neurons when the thresholds of the angular position are reached.

Sensory feedback from ground contact

The generation of walking gait depends primarily on the ground contact information which provides the phase status. The ground uncontact information is first used in our reflexive controller for the ankle control. It should be noted that as the switch sensor is placed at the heel of the foot it detects the heel contact rather than the toe contact. The load and unload of the leg generate the impulses to elicit the reflexes according to:

$$\begin{aligned} G_{HS} &= \Theta(\dot{G}) \\ G_{HO} &= \Theta(-\dot{G}) \\ G &= \begin{cases} 1 & F < \theta_F \\ 0 & \text{otherwise} \end{cases} \end{aligned} \tag{4.16}$$

Where G_{HS} is an impulse signal of HS, G_{HO} is an impulse signal of HO, F is real-time voltage signal from the microswitch sensor in the foot and θ_F is the threshold to define the foot contact statue G.

Stretch receptors

Stretch receptors contribute significantly to animal locomotion control. The stretch receptors in the joint give rise to a local reflex to reset the phase when the joint reaches the extreme positions. The extensor/plantarflexor sensor neuron inhibits its output according to:

$$B_E = \begin{cases} 1 & \phi < \theta_{ES} \\ 0 & \text{otherwise} \end{cases} \tag{4.17}$$

Where ϕ is the real-time angular position. θ_{ES} is the threshold of the extensor reflex.

Similarly, the output of the flexor and dorsiflexor motor neuron is modelled by:

$$B_F = \begin{cases} 1 & \phi > \theta_{FS} \\ 0 & \text{otherwise} \end{cases} \tag{4.18}$$

Where ϕ and θ_{FS} are similar to Eq. 4.17.

Motor outputs generation

The motor outputs are generated by convolving the summation of sensory feedback signals with filter functions. The motor output of the ankle plantarflexor consists of two activations triggered by different sensory inputs, as seen in Eq. 4.19 and 4.20, with I defining the ipsilateral leg and C representing the contralateral leg. These outputs are simply summed to give the overall motor output for the plantarflexor in the control model, Eq. 4.21.

$$U_{L/R,\ A,\ P_{HS}} = B_{L/R,\ A,\ P_{HS}} \cdot g_{L/R,\ A,\ P_{HS}} \cdot H_{L/R,\ A,\ P_{HS}} * (\omega_{GI \to L/R,\ A,\ P_{HS}} \cdot G_{I_{HS}}) \tag{4.19}$$

$$U_{L/R,\ A,\ P_{HO}} = B_{L/R,\ A,\ P_{HO}} \cdot g_{L/R,\ A,\ P_{HO}} \cdot H_{L/R,\ A,\ P_{HO}} * (\omega_{GI \to L/R,\ A,\ D_{HO}} \cdot G_{I_{HO}}) \tag{4.20}$$

$$U_{L/R,\ A,\ P} = U_{L/R,\ A,\ P_{HC}} + U_{L/R,\ A,\ P_{HO}} \tag{4.21}$$

The contralateral ground contact $G_{C_{HS}}$ triggers the ankle dorsiflexor, which is modelled as:

$$U_{L/R,\ A,\ D} = B_{L/R,\ A,\ D} \cdot g_{L/R,\ A,\ D} \cdot H_{L/R,\ A,\ D} * (\omega_{GC \to L/R,\ A,\ D} \cdot G_{C_{HS}}) \tag{4.22}$$

The motor outputs of flexors and extensors in hips and knees are the same as those in the previous model in Chapter 3:

$$\begin{aligned}
U_{L/R,\,H,\,F} &= B_{L/R,\,H,\,F} \cdot g_{L/R,\,H,\,F} \cdot H_{L/R,\,H,\,F} * (\omega_{GC \to L/R,\,H,\,F} \cdot G_{C_{HS}}) \\
U_{L/R,\,H,\,E} &= B_{L/R,\,H,\,E} \cdot g_{L/R,\,H,\,E} \cdot H_{L/R,\,H,\,E} * (\omega_{GI \to L/R,\,H,\,E} \cdot G_{I_{HS}}) \\
U_{L/R,\,K,\,F} &= B_{L/R,\,K,\,F} \cdot g_{L/R,\,K,\,F} \cdot H_{L/R,\,K,\,F} * (\omega_{GC \to L/R,\,K,\,F} \cdot G_{C_{HS}}) \\
U_{L/R,\,K,\,E} &= B_{L/R,\,K,\,E} \cdot g_{L/R,\,K,\,E} \cdot H_{L/R,\,K,\,E} * (\omega_{GI \to L/R,\,K,\,E} \cdot G_{I_{HS}} \\
&\quad + \omega_{B_{IH \to L/R,\,K,\,E}} \cdot \Theta(-\dot{B}_{I,\,H,\,F}))
\end{aligned} \tag{4.23}$$

The values of the motor outputs are then multiplied by a motor rotation direction indicator constant s and a servo amplifier coefficient α. The voltages applied to the joint motors are as following:

$$\begin{aligned}
V_{L/R,\,H} &= s_{L/R,\,H} \cdot \alpha_{L/R,\,H} \cdot (U_{L/R,\,H,\,F} - U_{L/R,\,H,\,E}) \\
V_{L/R,\,K} &= s_{L/R,\,K} \cdot \alpha_{L/R,\,K} \cdot (U_{L/R,\,K,\,F} - U_{L/R,\,K,\,E}) \\
V_{L/R,\,A} &= s_{L/R,\,A} \cdot \alpha_{L/R,\,A} \cdot (U_{L/R,\,A,\,P} - U_{L/R,\,A,\,D})
\end{aligned} \tag{4.24}$$

Where s is $+1$ or -1, which indicates the signs of the motor voltages of flexors and extensors in the joint, depending on the polarity of the motors. α represents a servo amplifier coefficient.

4.2.5 Summary

There is no CPG working as a natural oscillation generator in the reflexive controller. Rhythmic patterns are generated by a closed-loop system with an interplay of neuronal and mechanical control where the interaction between the environment and mechanical system is sent as sensory feedback to the neuronal control. The system does not involve any kind of precise position control algorithm. The control of one step is described as follow:

1. The ipsilateral ground contact $G_{I_{HS}}$ triggers the extensors of the ipsilateral leg while the ankle of the ipsilateral leg plantarflexes to rotate the foot towards the ground.

2. The ipsilateral hip rotates forwards like an inverted pendulum before the heel of the stance leg is lifted off the ground. The dorsiflexion of the ankle is driven passively by the hip motion during the phase. When the unloading of the heel $G_{I_{HO}}$ occurs, the ipsilateral ankle plantarflexor is triggered to push the foot off the ground.

3. When the contralateral foot touches the ground, the trigger signal $G_{C_{HS}}$ activates ankle dorsiflexion so the foot clears the ground coinciding with the ipsilateral hip and knee flexions.

4. The $\Theta(-\frac{d(B_{I,H,F})}{dt})$ sends an impulse to elicit the knee extensor when the ipsilateral hip achieves its AEA position. The robot straightens the knee before the foot contacts the ground. One stride finishes and a new stride starts.

4.3 Robot design

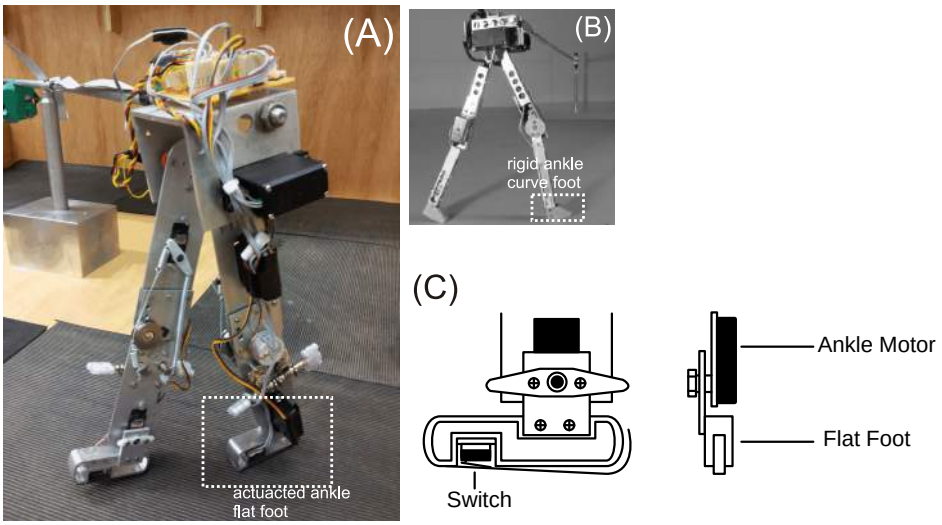

Figure 4.9: The mechanical design of the RunBot III. (A) RunBot III with the actuated ankle joint. (B) The original RunBot with the rigid ankle joint [5]. (C) Picture of the ankle-foot design.

The RunBot III has a 0.3 m height from foot to hip joint axis and a total weight of 552 g. It has two legs, two feet and a small torso body attached with the boom for constraining its walking in a planar circle. The robot consists of six actuated joints: two hip joints, two knee joints and two ankle joints. The hips and ankles are directly actuated by DC servo motors HS-625MG (Hitec RCD, USA) and HS-85+MG (Hitec RCD, USA) respectively. The compliant knees are actuated by DC servo motors HS-85+MG (Hitec RCD, USA) via springs (ENTEX STOCK SPRINGS, UK). All built-in pulse width modulation circuits are disconnected and control voltages are applied directly to the motors. The motor positions are measured via potentiometers. The output voltages are sent to a Linux-running computer through two D/A acquisition devices (USB-DUX, Incite Technology Ltd, UK). The boom can rotate freely in all three axes (pitch, roll and yaw). A summary of the robot is detailed in Tab. 4.4.

The most significant change in the mechanical design of our robot is the ankle-foot part. The curved feet with the rigid ankles were replaced with flat feet with actuated ankle joints as seen in Fig.4.9C. A microswitch sensor (Maplin, UK) is placed in the foot to detect the foot contact with the ground. The foot surface is supplemented with a rubber pad with high

Table 4.4: Specification of RunBot III

Parameters	Value
Mass (g)	552
Dimension of thigh (width, thickness, height) (cm)	4 ×0.2× 11
Dimension of shank (width, thickness, height) (cm)	4 ×0.2× 10
Dimension of foot (width, thickness, height) (cm)	6 × 1× 1
Total height (cm)	30

friction and appropriate shock absorbing capability.

In summary, we established a fully actuated bipedal robot while keeping the same mechanical designs of the hip and knee as in the RunBot II described in Chapter 3.

4.4 RunBot III walking experiments

In this section, we will describe the experiments performed with the RunBot III using the reflexive controller with ankle control.

4.4.1 Experimental setup

The robot is controlled by a real-time Linux computer, which receives sensory feedback from the sensors and commands the motor outputs to all motors via D/A data acquisition devices (USB-DUX D, Incite Technology Ltd, UK). The sampling rate is 200 Hz. Eight input channels are used to measure the motor positions ($\phi_{L/R,H/K/A}$) and ground contact information ($F_{L/R}$) respectively. The control programme was written with C++ language using the comedi and QT library. Six analogue outputs ($V_{L/R,H/K/A}$) are sent through a power amplifier with a gain of 2.3 and then sent to the six motors respectively. It should be noted that two D/A data acquisition devices are used because one USB-Dux D device has only four analogue outputs.

The RunBot III is used to validate the bio-inspired novel reflexive controller in regard of human-like walking with key characteristics, such as joint kinematics. The ankle is particularly interesting in the controller, as the ankle has been identified as a major power generator for human walking [196]. Its influence on human walking has been investigated in numerical studies [196, 197, 198, 199]. The functional impacts of the ankle push-off and ankle plantarflexion at the initial stance were examined in the experiments.

4.4.2 Parameter optimisation

All hip and knee parameters have already been optimised in the experiments of the RunBot II (Chapter 3 Section 3.3.1). Therefore, this experiment was concerned with the ankle parameters. The servo amplifier coefficient of the ankle $\alpha_{L/R,\ A}$ was set to 2. The function of the dorsiflexion initiated by contralateral HS is to clear the foot off the ground. It is the only ankle movement during the swing phase. The ankle movement is relatively simple as there is no environment interaction between the foot and the ground. However, the response of ankle dorsiflexion is not always sufficient for foot clearance. There is a tendency for toe stubbing to occur when increasing the time constant of $\tau_{L/R,\ A,\ D}$ of the transfer function $H_{L/R,\ A,\ D}$ for the ankle dorsiflexion. The optimal value of the time constant $\tau_{L/R,\ A,\ D}$ is set to 0.0637 ($fc_{L/R,\ A,\ D}$ = 2.5 Hz) and the weight value of $\omega_{GI\rightarrow L/R,\ A,\ D}$ is set to 1 by trial and error.

Once the foot clearance is achieved, the ankle control in the stance phase needs to be established. A smooth foot roll-over during the early stance phase can be achieved by coupling the values of the weight parameter $\omega_{GI\rightarrow L/R,\ A,\ P_{HC}}$ and the response of the transfer function $\tau_{L/R,\ A,\ P_{HS}}$. Basically, a faster response of the transfer function and a larger weight parameter would result in a faster foot rolling toward to the ground. To simplify the condition, the time constant $\tau_{L/R,\ A,\ P_{HS}}$ for the ankle plantarflexion after HS is set to a constant value (0.0955, $fc_{L/R,\ A,\ P_{HS}}$ = 1.6 Hz). Likewise, the time constant $\tau_{L/R,\ A,\ P_{HO}}$ of transfer function $H_{L/R,\ A,\ P_{HO}}$ is set to 0.1658 ($fc_{L/R,\ A,\ P_{HO}}$ = 0.96 Hz). Parameter values are detailed in Appendix B.

4.4.3 Results

Snapshots of one stride of the RunBot III are shown in Fig. 4.10 (top). At (a), the right foot heel strikes the ground where the stance phase of the right leg (red) is initiated, while the HS signal excites the swing phase of the left leg (green). Thus the extensors and plantarflexor of the right leg (red) are elicited and the flexors and dorsiflexor of the left leg (green) are activated. At (b) and (c), the right hip and knee continue to extend so that the whole limb rotates like an inverted pendulum and the right foot rotates forwards to the ground. Meanwhile, when the left hip flexes forwards, the left knee and left ankle flexes/dorsiflexes to make the foot clear the ground. At (d) the right heel is lifted off the ground which triggers the ankle plantarflexion for ankle push-off. At (e) the left foot contacts the ground and the two legs switch their swing and stance roles. At (f) the right leg (red) is in the early swing phase. At (g) the hip reaches its AEA which causes the inhibition of the knee flexor and excitation of the knee extensor. At (h) and (i) the right knee continues to extend until the leg is straight. At (j) the right foot heel strikes the ground again and the situation goes back to (a).

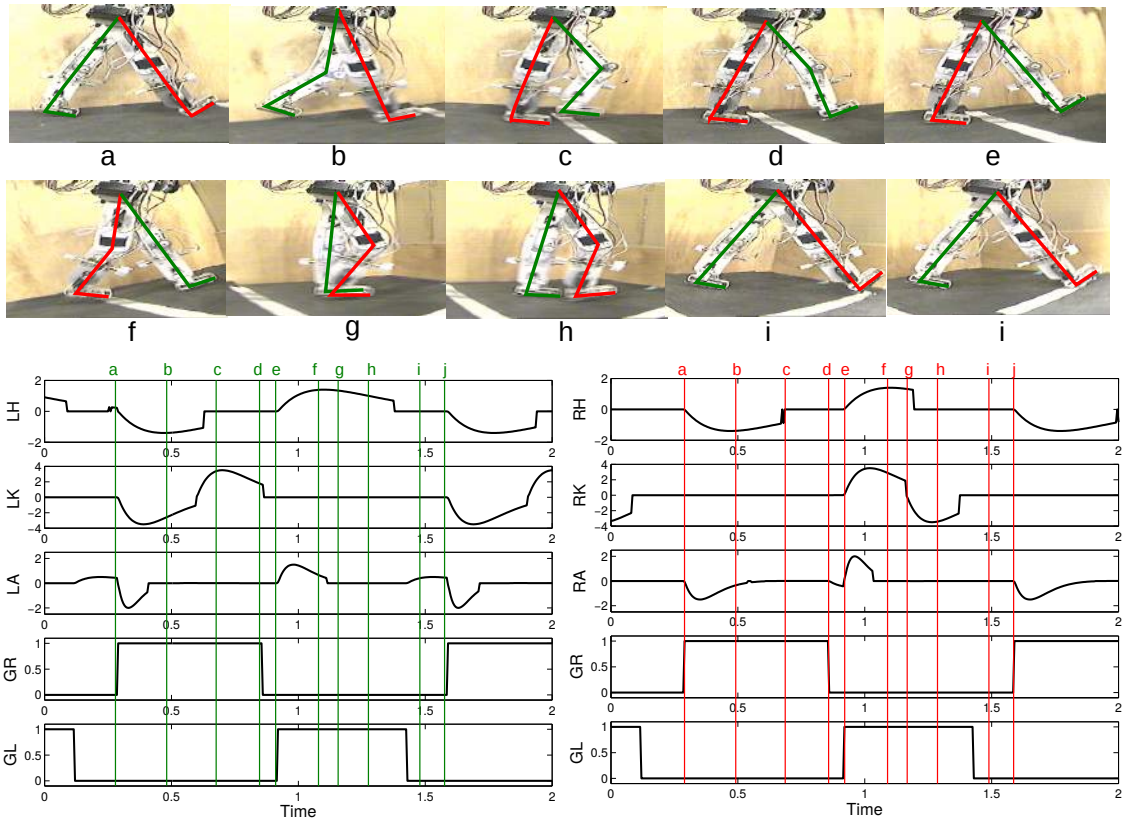

Figure 4.10: One stride of the RunBot III. Top: frames captured from a video file of the robot walking. Bottom: the control voltages of the right leg and left leg and the ground contact information (GL and GR). (a): foot touch down on right. (b)-(c): the right foot heel-strike triggers the extensors of the right leg and flexors of the left leg. (d): The plantarflexion on the right in response to the heel off. (e): Ground contact on the left. (f)-(g): The right leg initiates the swing phase while the left leg is in stance phase. (h): When the right hip reaches its AEA, the right knee starts to extend in (i). (j): The right foot contacts the ground again and one stride finishes.

The relationship between the velocity of hip extension and ankle push-off

The ankle plantarflexor group provides a strong contribution to ankle push-off [196]. The LG muscle generates the energy delivered to the leg [198], demonstrating that the role of the ankle plantarflexors is to initiate the swing phase [200]. A study in humans has shown that the ankle plantarflexors play a significant functional role in compensating the less efficient hip extensor [201]. To examine whether the same mechanism exists in the RunBot III, the coupling effect between the hip velocity and the ankle plantarflexor velocity at HO to the walking performance of the robot was studied in the experiment.

The robot was driven by various values of the servo amplifier coefficient of the hip $\alpha_{L/R,H}$ (from 1.3 to 1.6 with a step of 0.1), which interacts with the ankle plantarflexor at HO by varying value of the weight $\omega_{GI\rightarrow L/R,\ A,\ P_{HO}}$ (from 0 to 1.25 with a step of 0.25). The robot obtained stable walking with all couplings of the two parameters. The ankle plantarflexes

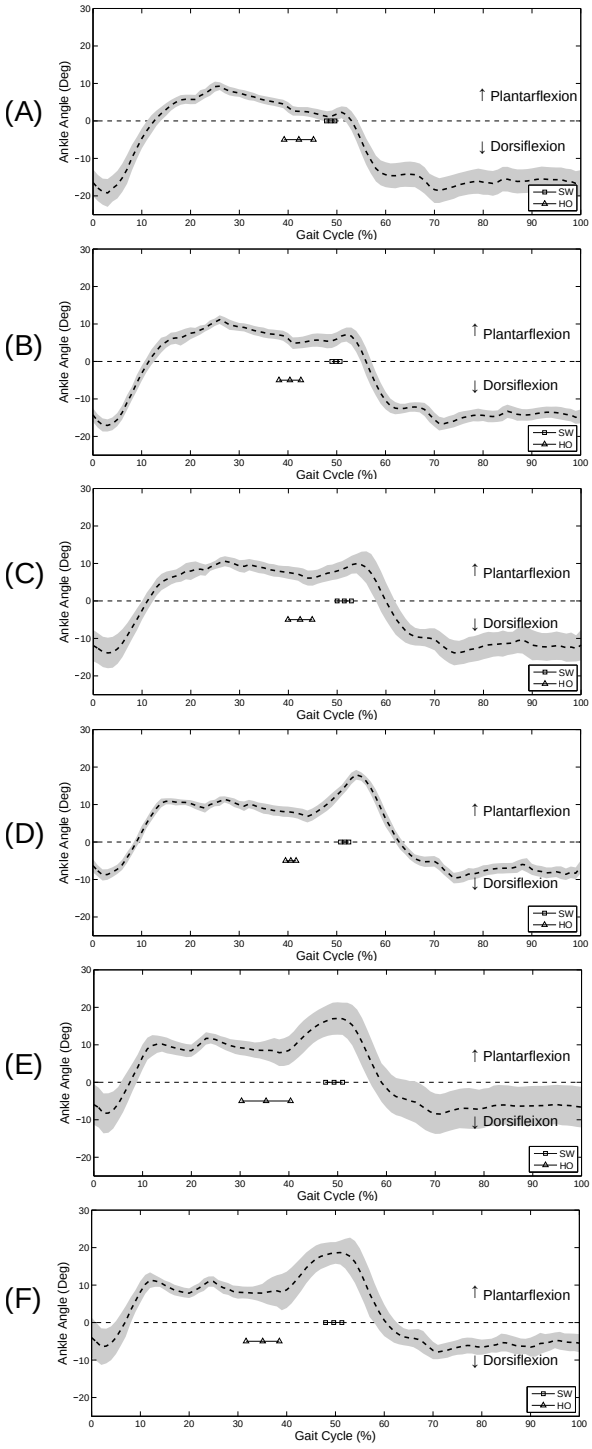

Figure 4.11: Comparison between ankle angular motions with various values of $\omega_{GI\rightarrow L/R,\ A,\ P_{HO}}$ during the gait cycle. The figures showed averages with a standard deviation in one gait cycle. (A): $\omega_{GI\rightarrow L/R,\ A,\ P_{HO}} = 0$. (B): $\omega_{GI\rightarrow L/R,\ A,\ P_{HO}} = 0.25$. (C): $\omega_{GI\rightarrow L/R,\ A,\ P_{HO}} = 0.5$. (D): $\omega_{GI\rightarrow L/R,\ A,\ P_{HO}} = 0.75$. (E): $\omega_{GI\rightarrow L/R,\ A,\ P_{HO}} = 1$. (F): $\omega_{GI\rightarrow L/R,\ A,\ P_{HO}} = 1.25$. Note here $\alpha_{L/R,\ H} = 1.5$

further while the value of the weight $\omega_{GI\rightarrow L/R,\ A,\ P_{HO}}$ increases as seen in Fig. 4.11. When the value of $\omega_{GI\rightarrow L/R,\ A,\ P_{HO}}$ equals to 0, the robot walks with a lack of ankle plantarflexor at

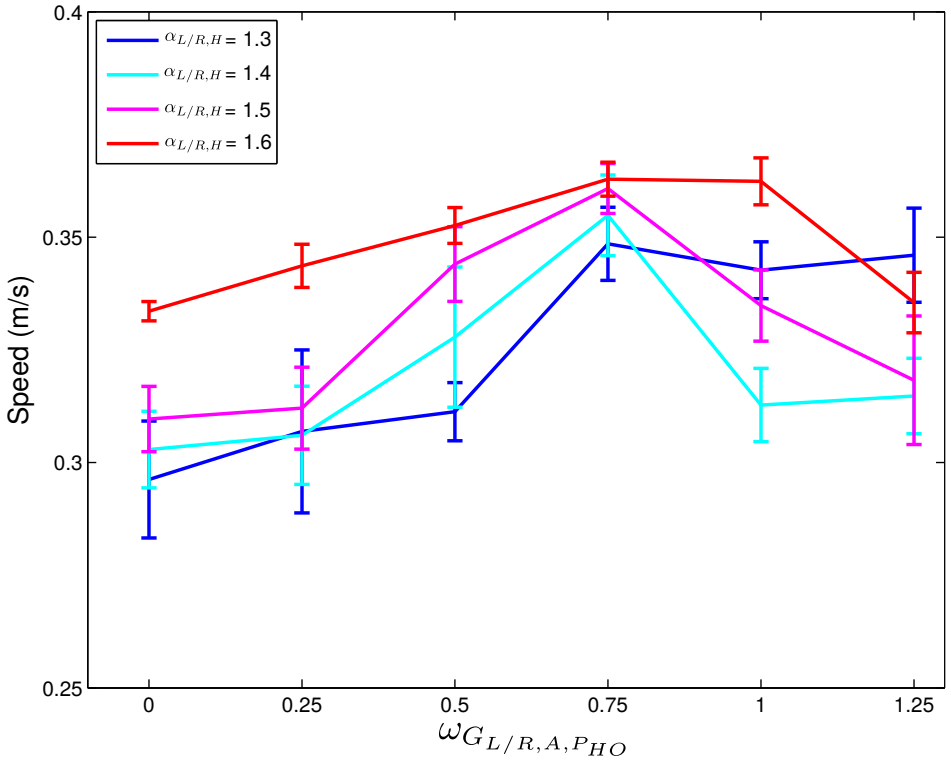

Figure 4.12: The speed results as a function of the weight of ankle plantarflexor at HO $\omega_{GI\rightarrow L/R,\ A,\ P_{HO}}$ and the servo amplifier coefficient of hip $\alpha_{L/R,\ H}$.

HO. An early HO happens during gait cycle when the $\omega_{GI\rightarrow L/R,\ A,\ P_{HO}}$ increases, however, the parameter does not affect the occurrence of the contralateral HS in the gait cycle. The phenomenon might be explained by the lack of the toe joint. The ankle plantarflexion after HO contributes to body forward progression while the forefoot firmly touches the ground in humans, facilitating the transition from the stance phase to the swing phase. In our robot the whole foot is lifted by the ankle plantarflexion as a rigid segment, thus the foot may be lifted off the ground before the contralateral foot contacts the ground. This results in "jumping", less stable walking and slower speed. Fig. 4.13 shows that the $\omega_{GI\rightarrow L/R,\ A,\ P_{HO}}$ significantly affects the stability of limit cycle walking. Therefore, a higher velocity of ankle plantarflexion does always not mean a faster speed, Fig 4.12.

It has been observed in Fig. 4.12 that the ankle push-off contributes significantly to the increase in walking speed of the robot. It is also found that increasing ankle push-off may help to compensate for a weak hip extensor and let the robot achieve a faster speed. This is shown in Fig.4.12, where the robot walks faster with a lower hip velocity and a higher ankle push-off velocity compared to the robot walking with a higher hip velocity and a lower ankle push-off velocity. For instance, the robot walks with a faster speed (0.3484 ± 0.0081 m/s) when the $\omega_{GI\rightarrow L/R,\ A,\ P_{HO}}$ and $\alpha_{L/R,\ H}$ are set to 0.75 and 1.3 respectively, compared to the walking speed (0.3118 ± 0.0087 m/s) when $\omega_{GI\rightarrow L/R,\ A,\ P_{HO}}$ is 0.25 and $\alpha_{L/R,\ H}$ is 1.5. There is a trade-off between the ankle push-off velocity and the hip extensor velocity. The

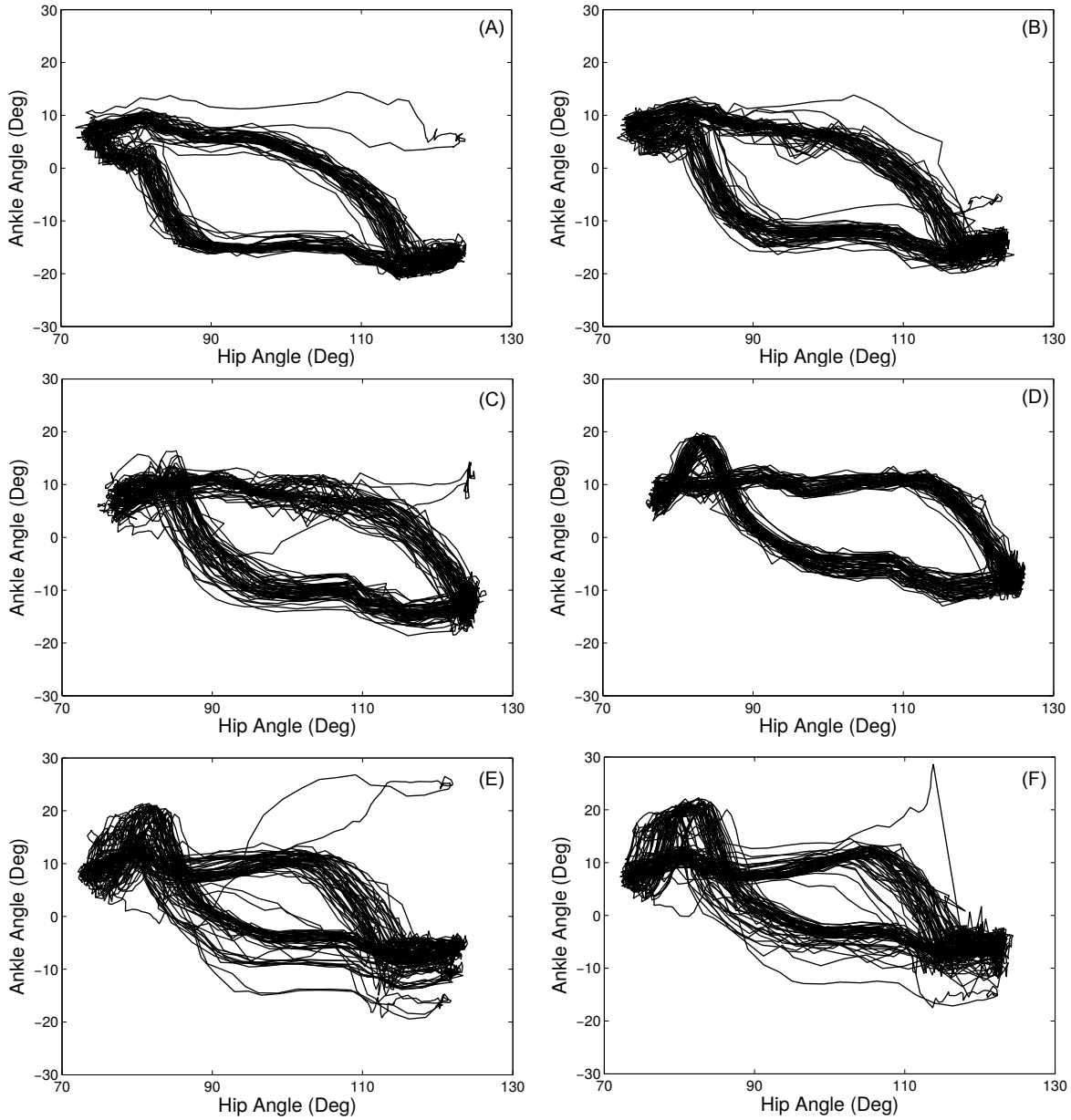

Figure 4.13: The plots of ankle angular motion versus hip angular motion with various values of $\omega_{GI\rightarrow L/R,\ A,\ P_{HO}}$ during the gait cycle. (A): $\omega_{GI\rightarrow L/R,\ A,\ P_{HO}} = 0$. (B): $\omega_{GI\rightarrow L/R,\ A,\ P_{HO}} = 0.25$. (C): $\omega_{GI\rightarrow L/R,\ A,\ P_{HO}} = 0.5$. (D): $\omega_{GI\rightarrow L/R,\ A,\ P_{HO}} = 0.75$. (E): $\omega_{GI\rightarrow L/R,\ A,\ P_{HO}} = 1$. (F): $\omega_{GI\rightarrow L/R,\ A,\ P_{HO}} = 1.25$. Note here $\alpha_{L/R,\ H} = 1.5$

result is consistent with the finding in human studies that ankle push-off would propel the centre of gravity forward and decrease the need for a hip extension during stance [196].

The "roll-off" effect of ankle plantarflexion

Perry et al. [202] states that the generation of forward velocity in gait is characterised by a roll-off effect with a controlled fall moving the body over the foot. As there is no precise position trajectory control involved in our reflexive controller, the fine tuning parameters of

the ankle plantarflexor excited by the ipsilateral HS is important to achieve stable walking pattern for the RunBot III. The ankle plantarflexes the foot towards the ground while the leg rotates forward in the early stance phase. Two parametres were chosen to investigate the coupling relationship between the ankle plantarflexor and the hip extensor during the early stance phase: one is the weight of the plantarflexor at the HS ($\omega_{L/R,\ A,P_{HS}}$), and the other one is the servo amplifier coefficient of the ipsilateral hip ($\alpha_{L/R,\ H}$). It has been found that stable gait can be achieved within a considerably large range of the parameters $\omega_{L/R,\ A,P_{HS}}$ and $\alpha_{L/R,\ H}$ as shown in Fig. 4.14. A large value of the weight $\omega_{L/R,\ A,P_{HS}}$ means a high velocity of ankle plantarflexion, which might result in an excessive forward velocity in gait and even an uncontrolled fall during the stance phase. The robot performed a "jumping" walk due to the excessive ankle plantarflexion. As it requires more time to let the robot respond to the disturbance and regain the stability, the robot performed a slow speed with a large weight value (Point S in Fig. 4.14). On the other hand if the $\omega_{L/R,\ A,P_{HS}}$ is too small, it would cause insufficient ankle roll-over movement. Thus, the robot would fail to support the body and maintain balance during the mid-stance phase because the foot would not fully make contact with the ground. The velocity of the ankle plantarflexion would affect the stability of walking and furthermore influence the time of the stride and walking speed.

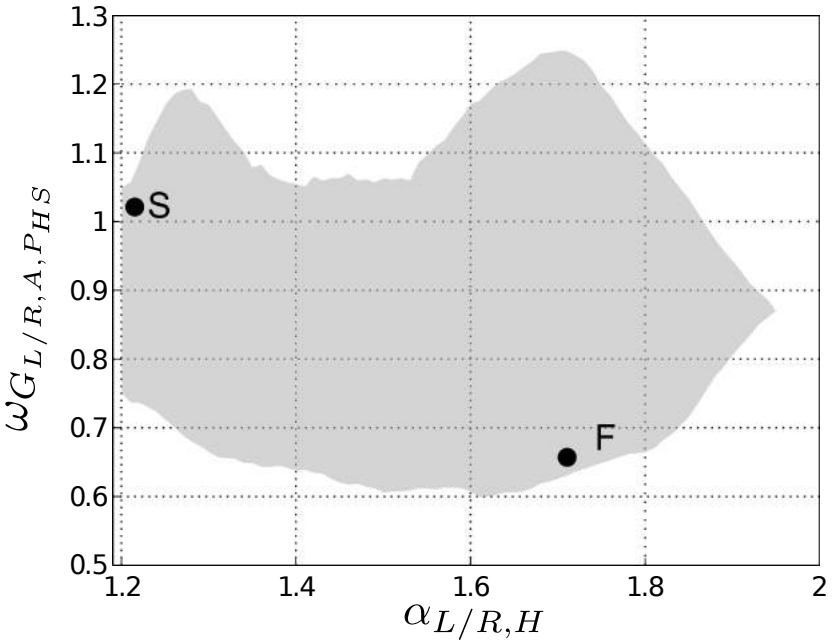

Figure 4.14: The area plot of stable walking as a function of the weight of ankle plantarflexor $\omega_{L/R,\ A,P_{HS}}$ and the servo amplifier coefficient $\alpha_{L/R,\ H}$. The grey area represents the parameter combinations in which the RunBot III performs a stable walking in at least 5 cycles. Point F represents the fastest speed while point S indicates the slowest speed achieved in the experiment.

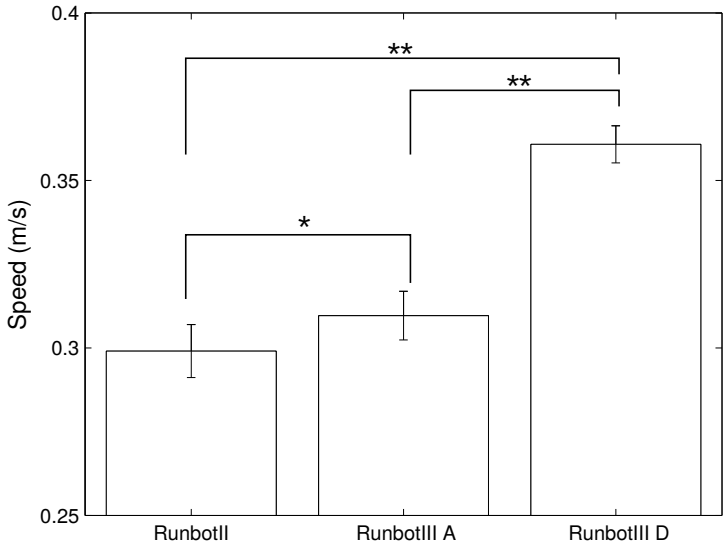

Figure 4.15: Speed comparison between the RunBot II and RunBot III without ankle push-off ($\omega_{L/R,\ A,P_{HO}} = 0$) and with proper ankle push off ($\omega_{L/R,\ A,P_{HO}} = 0.75$). where $* :\ p < 0.05$. $** :\ p < 0.001$

Comparison to the RunBot II

The main difference in mechanism between the RunBot II and RunBot III is the addition of actuated ankle joints. All parameters of the hip and knee joints are set the same in the two control models. The walking performances are compared to their different speed results in Fig. 4.15. First, ankle actuation contributes significantly to walking speed comparing to the rigid ankle (p $<$0.05). The RunBot III walks faster ($>$0.3 m/s) than the RunBot II ($<$0.3 m/s). Second, ankle push-off is a more significant factor to increasing speed rather than the ankle plantarflexion during the early stance phase (p $<$0.001). Proper ankle push-off increases walking speed by 16.13% compared to the speed without ankle push-off.

Comparison to human subject data

The robot's joint angles were qualitatively compared to human kinematic data obtained from Vaughan et al. [156]. A comparison of hip and knee motions between the robot and human subject has been discussed in Chapter 3. Thus, Fig. 4.16 only shows a comparison between the human subject and the robot's walking, for the sagittal hip and ankle joints. All data is normalised to one gait cycle (0 - 100%) since the length of time and sampling frequency are different for human and robot data.

The robot's cycle walking shows common features of human gait. The angular magnitudes are similar for human subject and the robot. The extension in the hip occurs after HS while

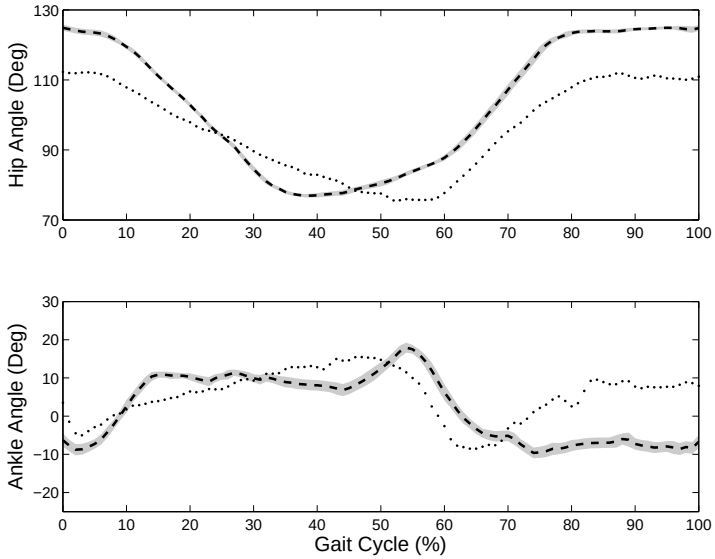

Figure 4.16: The comparison between the robot sagittal angles and human subject angles during one gait cycle. The averages (dashed line) with standard deviation (gray shaded) across one gait cycle of the robot and human movement (dotted line) Vaughan et al. [156] are shown in one plot.

the ankle performs a slight dorsiflexion at the early stance phase (0 - 10%) due to body weight acceptance. The ankle reaches the peak of plantarflexion at the late stance through early swing (50 - 60%). One significant difference is that the robot ankle is passively driven with the hip after the foot fully contacts the ground, so a slight passive dorsiflexion can be observed during the mid-stance phase. Another difference is that the robot does not have ankle plantarflexion to place the foot to a nearly natural position during swing after foot clearance with ankle dorsiflexion.

4.5 Summary

In this chapter, we implemented a new neural control architecture with ankle control and described the experiments and results performed with the RunBot III. The ankle consists of two plantarflexors during stance and one dorsiflexor during swing driven by different muscles. The ankle controller is inspired by the concept that there is a causal relationship between foot sensory feedback and muscle activation during gait walking. The ipsilateral foot contact signal was chosen to activate the ankle plantarflexions at HS and after HO. The contralateral foot contact signal initiates the swing phase of the leg and triggers the ankle dorsiflexion. RunBot III is still a bipedal dynamic walker with a purely reflexive robotic controller. It does not compute explicit trajectories but uses the simplified biologically inspired controller and the appropriate dynamic mechanism to establish a stable walking performance.

We pointed out that the weight of the plantarflexor at HS ($\omega_{L/R,\ A.\ P_{HS}}$) is significantly affected by the velocity of the hip extensor $\alpha_{L/R,\ A}$. We also examined various values of the weight of the ankle push off after HO $\omega_{L/R,\ A,\ P_{HO}}$, and how it contributes to the walking speed. We compared the walking performances between the two version of robots, indicating the essential role of the ankle during walking gait. Last but not the least we compared the walking behaviour of the robot to the human subject by showing the similarities in several aspects and pointing out the differences.

Chapter 5

Reliability Test of A Gait Phase Detection System

5.1 Introduction

FES has been utilised to help subjects with walking deficiencies since the early 1960s [120]. Electrical stimulation systems consist of an electrical stimulator sending electrical charges to the selected muscles of the legs, which cause artificial contractions of the stimulated muscle during walking. The correct timing of the stimulations in the gait cycle is essential for an effective functional stimulation [126]. The simplest method of controlling the onset and offset of the stimulations is to manually press a push-button [117], which in practical use is limited to indicate one single event during a gait cycle. Human walking is a sophisticated process with the interaction between CNS and PNS. As electrical stimulation artificially replaces the functional role of the CNS to control muscle contraction, sensory feedback is essential to coordinate the timing of stimulations. Artificial sensor systems ranging from simple foot switches to inclinometers, goniometers, gyroscopes, accelerometers, and biological sensory signals including EMG, afferent nerve signals, have been adapted into FES systems [124, 125, 127, 203]. Despite these efforts, the available methods are not suitable for the FES control transferred from the reflexive robotic controller described in Chapter 4.

In this chapter, I present a new reliable real-time gait phase detection system for FES walking system where control principles are adapted from the robotic controller. In the reflexive robotic controller, the foot contact and hip AEA signals are integrated to generate control voltages to drive the joint flexors/extensors during walking. Therefore, a sensor combination of FSRs embedded in the shoe insole and sensor containing a gyroscope and an accelerometer is used in our gait phase detection system. A rule-based gait phase detector is proposed by using the foot contact information and the sagittal hip angle signals to detect in real time the transitions between five gait phases during walking. The performance of the gait phase

detection system was tested in the experiment with 10 able-bodied subjects, and the results are discussed in the following sections.

5.2 Methods

5.2.1 Hardware

The gait phase detection system uses two types of sensors: 1) three FSRs that measure the foot load forces on the insole during walking, and 2) a 9-axis motion tracking microelectromechanical system device that is used to provide the sagittal hip angle by measuring the velocity and acceleration of the thigh in 3-axis. The sensory signals were sampled at a frequency of 100 Hz and processed in a C++ programme running on a Linux-operation laptop via serial ports as shown in Fig. 5.1

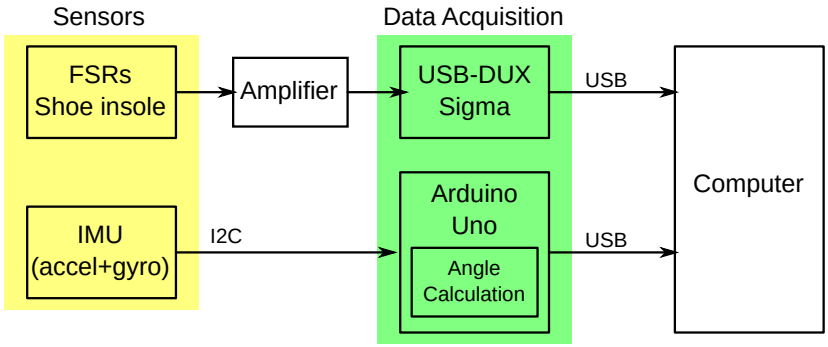

Figure 5.1: The block diagram of data acquisition system. The signals from FSRs are fed into a preamplifier and then a USB-DUX Sigma data acquisition device. The raw data from IMU is read by an Arduino Uno through I2C interface while an Arduino programme is running for angle calculation. The data taken by the data acquisition devices is then fed into a computer for further processing.

Foot contact measurement

The FSRs (FSR 402, Interlink Electronics Inc., USA) were small flat resistors with diameter of ϕ 13 mm. Resistance changes with applied force nonlinearly. Fig. 5.2 shows the positions of four FSRs: underneath the heel, first metatarsal head, fifth metatarsal head, and the big toe. These served to capture the force exerted by the foot on the insole during walking [204]. However, only three FSRs (the heel, the first and fifth metatarsal heads) were used to indicate whether weight was applied to the heel or forefoot as the force signals underneath the metatarsal heads are more reliable than the force signal under the toe in human walking study [190]. The insoles were custom-made to various shoe sizes. A preamplifier was developed in previous research [190], and was connected to the USB-DUX Sigma data acquisition device

(Incite Technology Ltd, UK) directly as shown in Fig. 5.2. The whole device was compact and lightweight to be worn on the participant's waist. The device amplified and transmitted data from two instrumented insoles. These insoles were connected to the preamplifier via ribbon cable as shown.

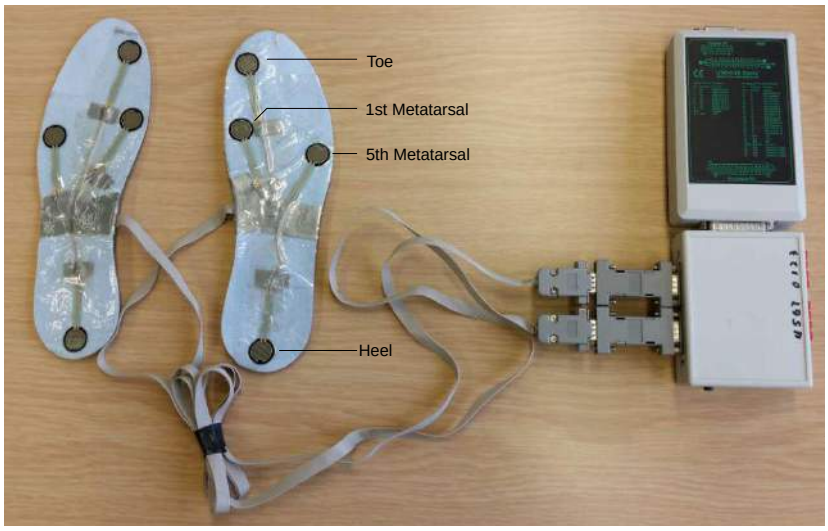

Figure 5.2: The FSRs insoles connects to the EMG/FSRs preamplifier which is connected to the USB-DUX Sigma data acquisition device via a D-connector. The whole equipment is compact for easy wearing for the participant during walking.

Sagittal hip angle measurement

The information about sagittal hip anglular position is important because the parameter is used to determine the phases in the swing phase. In this study, the angle measurement is realised using a motion sensor, which is MPU-9150 (InvenSense, CA, USA), and a low cost data acquisition card, which is Arduino Uno (Arduino).

The Arduino Uno is a universal microcontroller and has been widely used for various projects. It has an easy to use development environment and is designed to be easy to interface all kinds of sensors. The Arduino consists of the ATmega328 microcontroller and has an operating voltage of 5V. The microcontroller ATmega328 has 32 KB flash memory, as well as 2 KB of SRAM and 1 KB of EEPROM. The Arduino has 6 analog input pins and 14 digital I/O pins while the microcontroller has a clock speed of 16MHz.

The sensor chosen for the motion tracking was the MPU-9150. The sensor gives 9-axis of measurement including an accelerometer, a gyroscope and a magnetometer. Only a combination of an accelerometer and gyroscope from the MPU-9150 was used for the angle calculation in the study. The MPU-9150 runs on 2.375-3.46V. The voltage regulator of the Arduino can take an input of 5V and provide an output of 3.3V which powers the MPU-9150. The wiring is as shown in Fig. 5.3. Raw values from gyroscope and accelerometer

were easily read through register addresses.

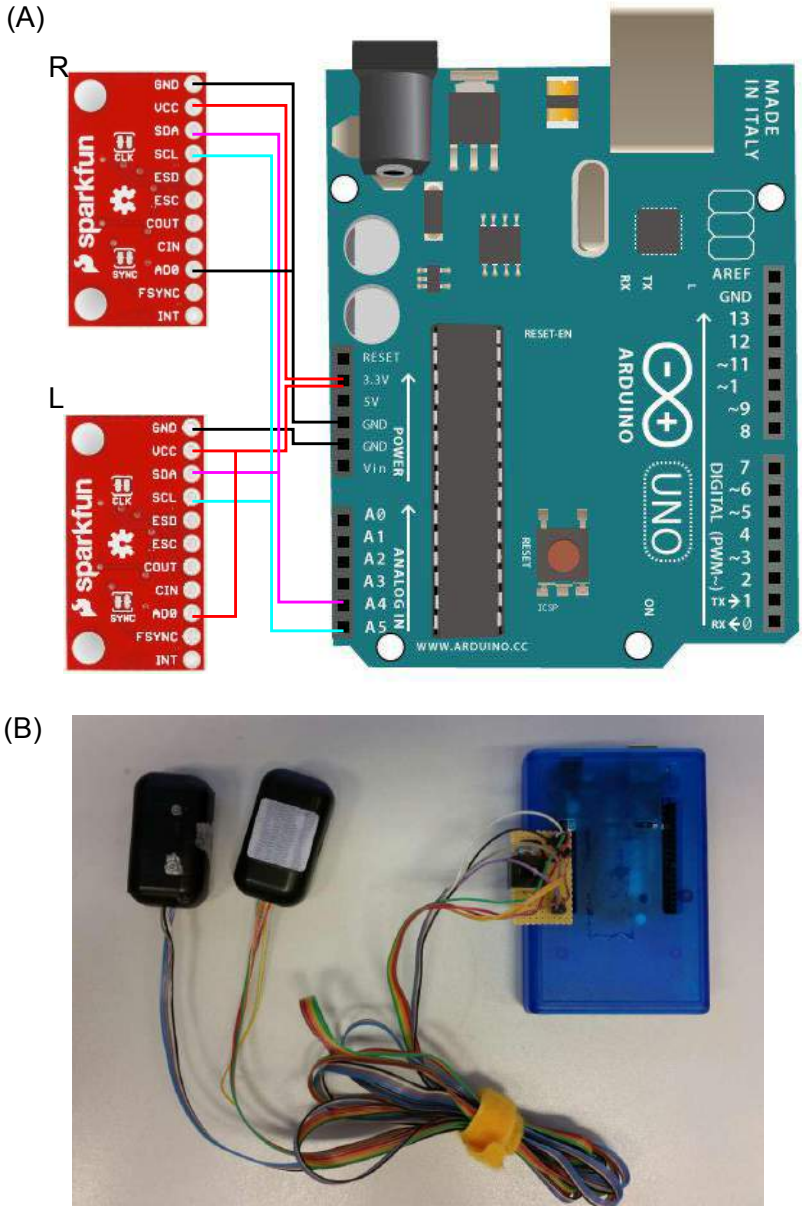

Figure 5.3: (A) Cable wiring between two motion tracking devices and an Arduino Uno. (B) Picture of two enclosured MPU9150 devices and an Arduino Uno board.

Each motion tracking device was required to be placed at the lateral side of the thigh as shown in Fig. 5.4. Therefore, the sagittal hip angle is defined as the angle along the y-axis in the x-y plane. The offsets of the sensors were calibrated first. Gyroscope ($g_{x/y/z}$) and accelerometer ($a_{x/y/z}$) values were converted from these raw reading values after calibration using Eq. 5.1.

$$\begin{aligned} g_{x/y/z} &= (r^{gyro}_{x/y/z} - g^{offset}_{x/y/z}) \cdot s_{gyro} \\ a_{x/y/z} &= (r^{accel}_{x/y/z} - a^{offset}_{x/y/z}) \cdot s_{accel} \end{aligned} \tag{5.1}$$

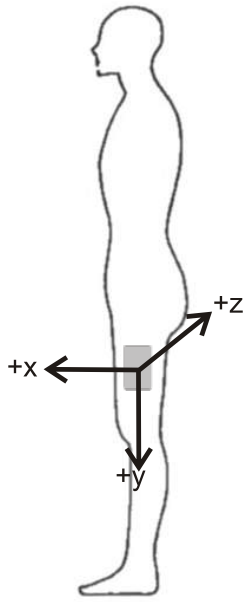

Figure 5.4: A motion tracking device MPU9150 is placed at the lateral side of the thigh. y-axis is vertical to the ground. The sagital hip angle is the angle along y-axis in the x-y plane.

The range of gyroscope measurement was set in $\pm 250°/s$, and the range of accelerometer was $\pm 2g$. The resolution of the microcontroller is 16 bits. Hence the gyroscope sensitivity s_{gyro} was 0.076295 and the accelerometer sensitivity s_{accel} was $6.1036e-05$.

Forward-Eulers' integration method was used to calculate the angle using the gyroscope as:

$$\phi_y^{gyro}(t) = g_y \cdot \triangle T + \phi_y^{gyro}(t-1) \tag{5.2}$$

where ϕ_y^{gyro} was the angle along y-axis calculated from gyroscope measurement. g_y was gyroscope value on the y-axis. $\triangle T$ was the time between current measurement and last measurement. The sampling rate of the application embedded in Arduino Uno is 100 Hz, thus $\triangle T$ is a constant value (0.01 s).

The angle calculated by using accelerometer was as

$$\phi_y^{accel}(t) = tan^{-1}\frac{a_y}{\sqrt{a_x^2 + a_z^2}} \tag{5.3}$$

where $-\infty \leqslant \frac{a_y}{\sqrt{a_x^2 + a_z^2}} \leqslant \infty$, $-\frac{\pi}{2} \leqslant \phi_y^{accel} \leqslant \frac{\pi}{2}$

To reduce noise drift, the final angle was obtained by a weighted integration of the angles

calculated using the gyroscope and the accelerometer respectively.

$$\phi_y = (w \cdot \ \phi_y^{gyro} + \phi_y^{accel})/(1+w) \tag{5.4}$$

where w was set to 20.

The angle ϕ_y was used in the integration of the gyroscope to avoid the drift, therefore, Eq.5.2 was rewritten to

$$\phi_y^{gyro}(t) = g_y \cdot \triangle T + \phi_y(t-1) \tag{5.5}$$

The angle signal ϕ_y was used to estimate the spatial position of the thigh. The placement of the motion tracking device MPU9150 was adjusted to obtain approximate zero degrees output when the participant stood straight and still.

5.2.2 Algorithm for gait phase detection

The gait phase detection system divided the gait cycle in five different gait phases, namely, HS, FF, HO, Early Swing (ESW) and Late Swing (LSW) phases. The frequency of the programme was set to 100 Hz, equal to the sensor sampling frequency. The system implemented an IF-THEN type finite state machine. The input data were signals from motion tracking devices and FSRs, and output data was phase states. All input data were first translated into binary signals by implementing a threshold method, Eq. 5.6.

$$\begin{aligned} G_H &= \begin{cases} 1 & F_H > \theta_{FH} \\ 0 & \text{otherwise} \end{cases} \\ G_T &= \begin{cases} 1 & F_T > \theta_{FT} \\ 0 & \text{otherwise} \end{cases} \\ \Phi_H &= \begin{cases} 1 & \phi_H > \theta_H \\ 0 & \text{otherwise} \end{cases} \end{aligned} \tag{5.6}$$

where G_H is a binary signal from the force signal of the heel (F_H), Φ_H is a binary signal from the sagittal hip angle signal (ϕ_H). Two FSRs were used under the 1st and 5th metatarsal head since the foot load is usually not symmetrical. So F_T is the maximal value of these two force signals, and G_T is a binary signal from the final force signal of the forefoot (F_T). $\theta_{FH/FT/H}$ are the threshold values. The force thresholds were set at 30% of the maximum activity, and the hip angle threshold was set at 80% of the maximum angle.

The set of rules is presented in Fig. 5.5. The binary signal of hip angle Φ_H was only used in the swing phase when G_H and G_T equaled to zero, where Φ_H distinguished the swing phase between ESW and LSW phases. The HS phase is the period when the heel of the foot contacts the ground ($G_H = 1$, $G_T = 0$). The FF phase is the period during which the entire foot touches the ground ($G_H = 1$, $G_T = 1$). The HO phase is the period usually following the FF phase, during which the forefoot is in contact with the ground and the heel is lifted off the ground ($G_H = 0$, $G_T = 1$). An example of gait phase detection during one subject's walking is shown in Fig. 5.6.

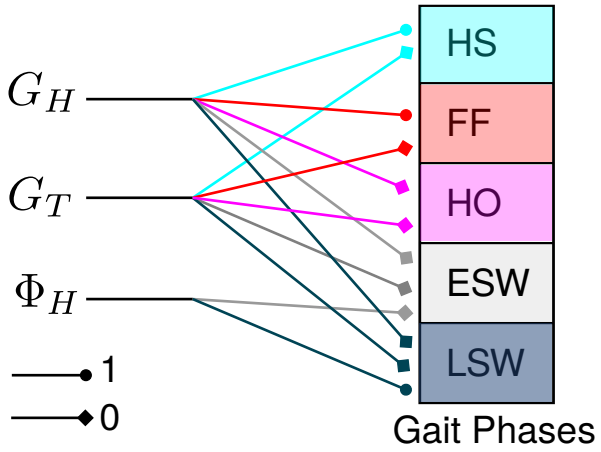

Figure 5.5: The rule defining five gait phases in one gait cycle. The binary signals from the foot contact and hip angle are encoded as 1 when the values are above the thresholds, otherwise are 0. The start of the swing phase is determined by detecting the foot off the ground ($G_H = 0$ and G_T = 0), while the Φ_H differentiates between the ESW and LSW phases. The HS is the early period of the stance phase when the heel starts to contact the ground ($G_H = 1$ and $G_T = 0$). The FF is the middle period of the stance phase when the foot is flat on the ground ($G_H = 1$ and $G_T = 1$). The ho is the late stance phase when the heel is lifted off the ground ($G_H = 0$ and $G_T = 1$).

Event impulses were generated during transitions between gait phases as shown in Fig. 5.7. Four types of events would be required for the FES control, I_{HS}, I_{HO}, I_{TO} and I_{LSW}. A summary of the rules generating these impulses is given below.

I_{HS}: The HS impulse indicates the initial foot contact with the ground which is the start of the stance phase. In normal gait, the heel usually contacts the ground first. However, subjects with a pathological walk may establish the foot contact with the forefoot.

I_{HO}: The HO impulse occurs when the FSR underneath the heel is not pressed and the front part of the foot still touches the ground. This event indicates the transition from the middle stance phase (FF) to the late stance phase during walking.

I_{TO}: The TO impulse indicates the transition from the stance phase (usually the HO phase) to the ESW phase, where the swing phase is when the foot is lifted off the ground so that no FSRs are pressed.

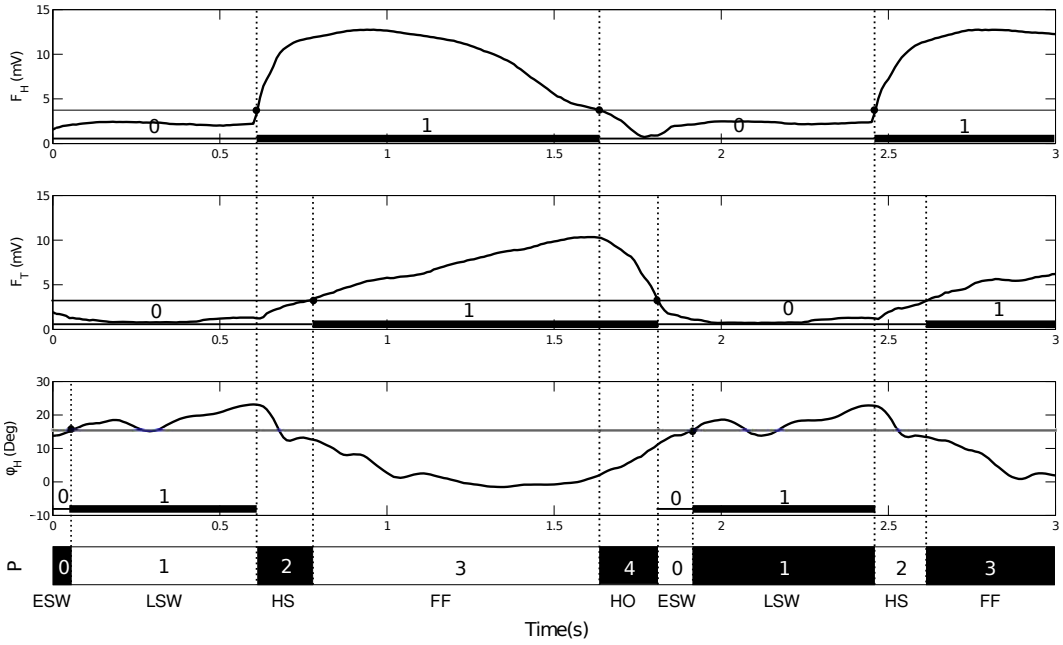

Figure 5.6: The force signals (F_H and F_T) and hip angle signal ϕ_H are translated into binary signals by given threholds. Gait phases is determined by the rules with the inputs of binary coded sensory signals. Normal human walking repeats five gait phases in a sequence.

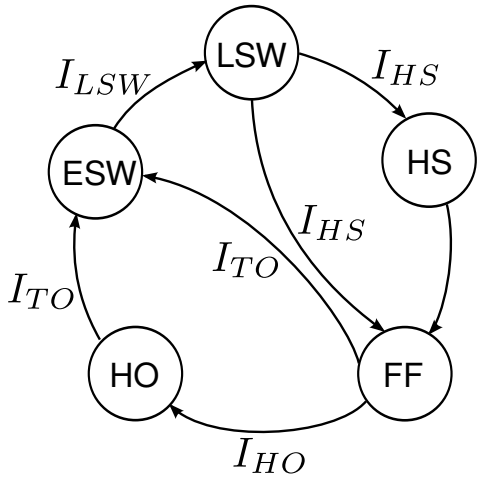

Figure 5.7: The gait phase detection system divides the gait cycle into five gait phases: Heel Strike (HS), Flat Foot (FF), Heel Off (HO), Early Swing (ESW) and Late Swing (LSW). The arrows illustrate the transitions between the gait phases, while event impulses are generated.

I_{LSW}: The LSW impulse indicates the transition from the ESW phase to the LSW phase when the hip angle ϕ_H reaches its threshold during the swing phase.

In summary, the structure of gait phase detection system is shown in Fig. 5.8. The sensory signals from the FSRs embedded in the shoe insole and the motion tracking device MPU9150 are the inputs of the system. The sensory signals are binary encoded with the threshold function. The gait cycle is divided into five gait phases by the rules illustrated in Fig. 5.5.

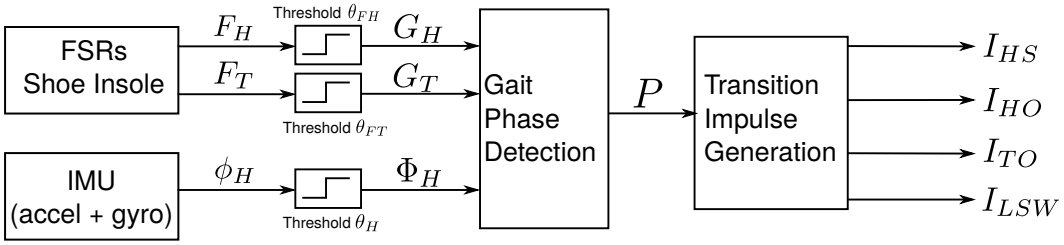

Figure 5.8: The diagram of the gait phase detection system is shown in the figure. The foot contact signals (F_H and F_T) and hip sagittal hip angle (ϕ_H) were measured from the FSRs shoe insoles and motion tracking sensor. The input signals were transferred to binary signals by the adaptive thresholds. Gait phases were defined by the set-up rules. The event impulses ($I_{HS/HO/TO/LSW}$) were generated at the transition between gait phases.

The event impulses presenting the phase transitions are generated as shown in Fig. 5.7. These impulses are the final output of the system.

5.2.3 Participants and ethics

Ten healthy participants with no known orthopaedic, metabolic, neurological impairment or pain that could influence their natural walking pattern, volunteered to take part in the study. These included six males and four females with a mean age of 27.6 years (range 22-44 years). Table. 5.1 outlines the details of the participants in the study. Ethical approval for the study was provided by College of Science and Engineering Ethics Committee at the University of Glasgow. All participants were fully informed of the procedure of the experiment and written consent was obtained prior to the study.

Table 5.1: Participant information of gait-phase detection system reliability test study. Subject ID were randomly assigned to each subject.

Subject ID	Gender	Age	Height (m)	Shoe size (UK)
A	F	24	165	4
B	M	27	180	11
C	F	22	166	4
D	M	28	184	9
E	M	44	173	8
F	M	24	174	8
G	F	27	157	3
H	F	25	158	4.5
I	M	27	176	9.5
J	M	28	182	9

5.2.4 Experiment protocol

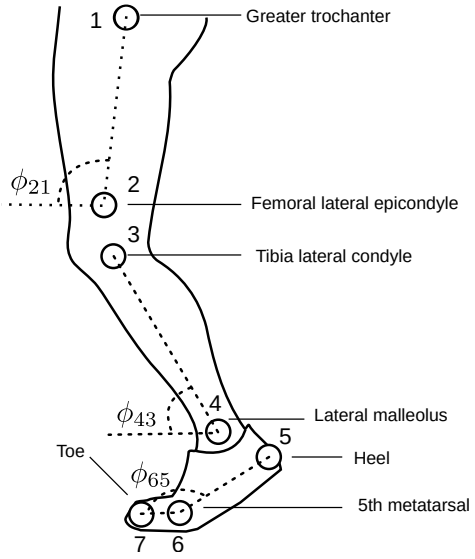

Figure 5.9: Positions of the retro-reflexive markers that were placed on the subject's heel, big toe, 5th metatarsal, lateral malleolus, tibia lateral condyle, femoral lateral epicondyle and greater trochanter to allow the camera to track their trajectories in the experiment.

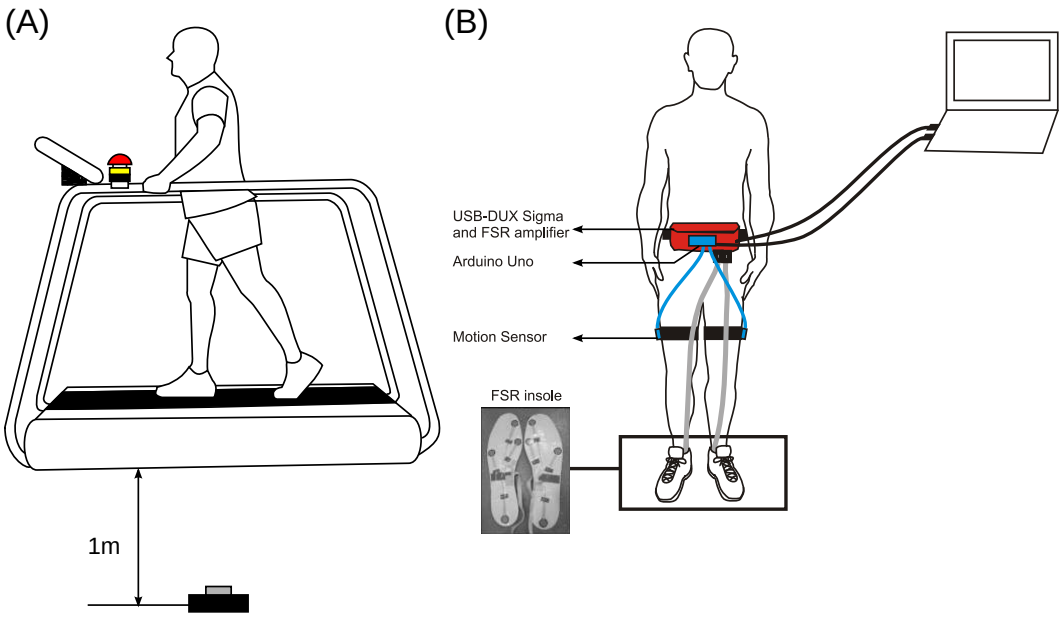

Figure 5.10: Experiment setup for data capture. (A) The subject walked on the treadmill while the camera captures the trajectories of retro-reflexive markers at 1m away. (B) The subject wore the data acquisition devices on their waist with the FSR insoles in their shoes and motor tracking sensors placed on the thighs. A laptop was used to record data. Video capture was controlled via a mobile app.

To validate the performance of gait phase detection system, the output was compared with the measurement obtained with an optical motion analysis programme. The programme tracked and measured the trajectories of retro-reflexive markers placed on the participant's

lower limb in the sagittal plane. The placements of the retro-reflexive markers are shown in Fig. 5.9. A high-speed camera (GoPro HERO3+, GoPro Inc., CA, USA) was utilised to track the markers with a sampling rate of 60 Hz. The trajectories of the markers were used to generate a "reference" gait phase signal to validate the accuracy of the output of the gait phase detection system.

Participants were required to wear flat-soled training shoes and shorts. Anthropometric data including shoe size, height and age were required when every participant arrived. The FSRs insoles were placed in the shoes, the data acquisition devices were worn around their waist, and motion tracking devices were placed on each thigh respectively, as shown in Fig. 5.10B. Each participant was instructed to perform three treadmill walking trials: (i) at a slow speed (1 km/h); (ii) at a fast speed (3 km/h) (iii) at a self-selected comfortable speed in a range of 1 to 3 km/h. Each trial lasted 3 minutes. A Key click sounds marked the start and the end of data recording in each trial for easy data and video tracking synchronisation for the investigator. A schematic diagram of the experimental setup is as shown in Fig. 5.10A.

5.2.5 Optical motion analysis

The motion analysis was programmed with the help of the image processing toolbox in Matlab (Matlab 2014a, The MathWorks, Massachusetts, USA). The data flow diagram of image processing is shown in Fig. 5.11. Each frame was calibrated and converted into a binary image. The centres of the retro-reflexive markers were calculated using the Moore-Neighbor tracking algorithm [205]. After the trajectories of seven retro-reflexive markers were calculated through every frame, as shown Fig.5.12, the data were filtered by a 4th order low-pass Butterworth filter with cut-off frequency of 4 Hz [206]. Then kinematic data can be further processed using Eq. 5.7.

$$\begin{aligned} \phi_{hip} &= \phi_{21} \\ \phi_{knee} &= \phi_{hip} - \phi_{43} \\ \phi_{ankle} &= \phi_{43} - \phi_{65} + 90^{\circ} \end{aligned} \tag{5.7}$$

A gait cycle was divided into four phases in the optical motion tracking system. These are HS, HO, ESW and LSW phases. The FF phase was not considered here because it is difficult to determine the condition in the frame due to individual variability. The positions of the retro-reflexive markers on the foot were used to define the status of the foot placement as shown in Fig. 5.13. The HS phase initiates when the x-axis position of the heel (x5) gets its minimal value. When the vertical displacement between the heel and 5th metatarsal head (y6-y5) rises and achieves the threshold $\theta_{y_6-y_5}$, the HO phase starts. Similarly, the displacement between the 5th metatarsal head and toe along y-axis (y7-y6) is utilized to

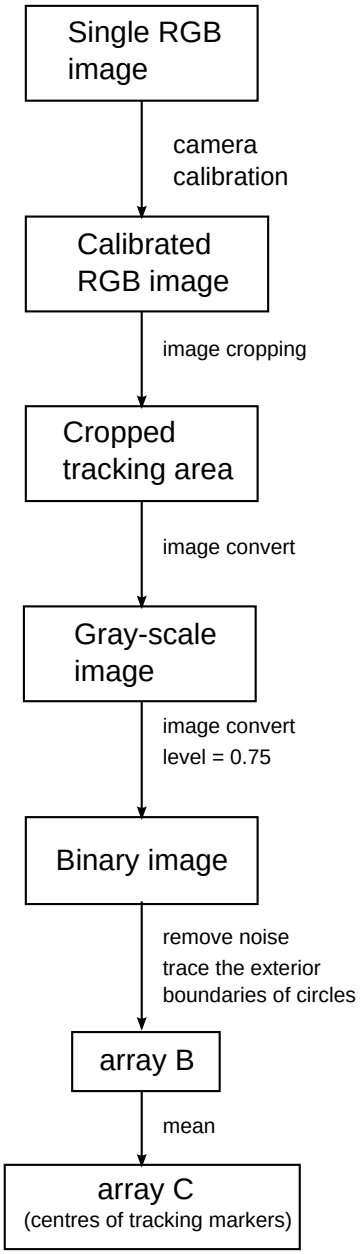

Figure 5.11: Data flow diagram of image processing for tracking the markers. Every single frame from video capture is calibrated to remove the distortion caused by the camera lens. The background is cropped out to remain main tracking area. Then the cropped image is converted to a gray-scale image and the gray-scale image is converted into a binary image with an optimal threshold value of approximately 0.75 through a trial and error approach. The bwboundaries function with the Moore-Neighbor tracking algorithm is used to trace the exterior boundaries of the markers after removing noise. A cell array B returns from the bwboundaries function, which contains all the points at the boundaries of the markers. The centres are calculated by averaging the positions of points. And the centre positions of the markers are stored in an array C.

define the beginning of the ESW phase. The LSW phase initiates when the hip angular position (ϕ_{hip}) reaches its threshold in the swing. Based on these rules, the reference output

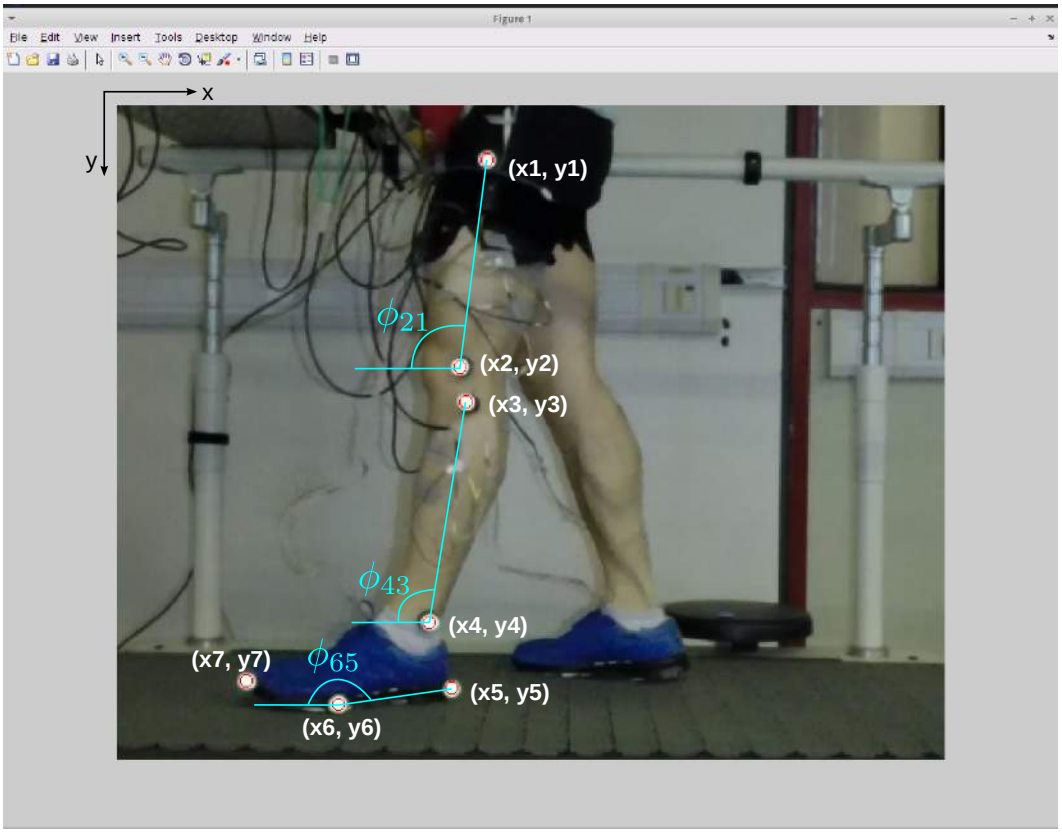

Figure 5.12: A frame plot with trajectory tracking process. Seven retro-reflexive markers were tracked in this frame. The kinematic data (hip, knee and angle angle) can be calculated according to the marking positions. Notation: (x1, y1) = the greater trochanter; (x2, y2) = the femoral lateral epicondyle; (x3, y3) = the tibia lateral condyle; (x4, y4) = the lateral malleolus; (x5, y5) = the heel; (x6, y6) = the 5th metatarsal; (x7, y7) = the big toe.

was generated as shown in Fig. 5.13. All threshold values may need to be adjusted for each subject.

The event impulses are then generated from the transitions between the phases based on the rules described in Section 5.2.2.

5.3 Results

5.3.1 Comparison of the gait phase detection system with a motion analysis system

The gait phase detection system performance was validated with an optical motion analysis system. A typical example is shown in Fig. 5.14 where FSRs signals (F_H and F_T), the sagittal hip angular signal (ϕ_H) and phase output signal (solid line in the bottom plot) were recorded during participant's walking. The reference signal (dashed line in the bottom plot) generated

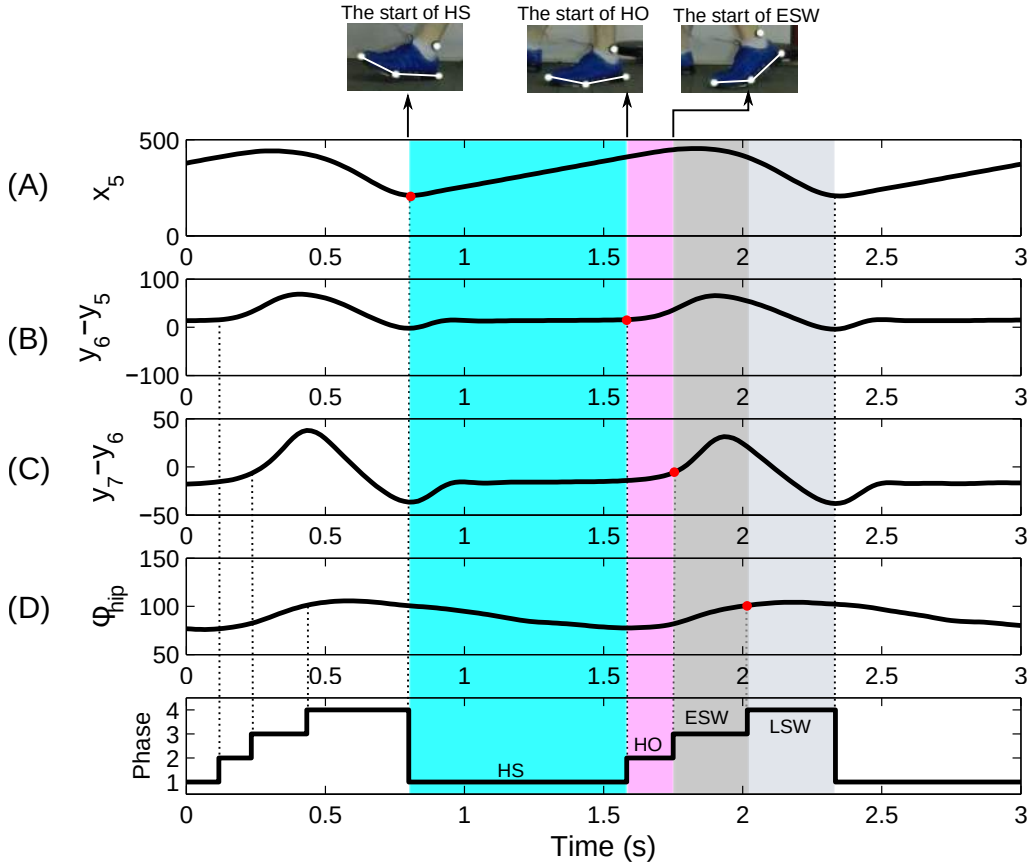

Figure 5.13: A subject's walking with a self-selected speed was tracked in a sequence of video frames. (A) The minimum value of the heel marker position along x-axis indicates the start of the heel-strike phase. (B) When the y-axis displacement between the heel and 5th metatarsal head achieves its threshold, the HO phase begins. (C) Reaching the threshold of the y-axis displacement between the 5th metatarsal head and toe means the foot is off the ground and the ESW phase initiates. (D) The LSW phase starts when the hip angle reaches its threshold. Notation: HS = heel strike, HO = heel off, ESW= early swing, LSW = late swing. The unit of the position data is pixel.

from the synchronised optical measurements of the markers' trajectories is compared with the output signal. The output signal correlated well with the reference signal. The time delay of the output signal was observed, however, the delay was less than 20 ms, which indicates the optical motion analysis system could be utilised as a reference system for verifying the performance of the gait phase detection system. Note here, only the impulses generated at transitions between phases, namely I_{HS}, I_{HO}, I_{TO} and I_{lSW}, were compared. Gait cycle was divided inversely by the event impulses only for the performance comparison between the optical motion analysis system and the gait phase detection system. Therefore, the HS and FF phase detected by the gait phase detection system is detected as one phase also called HS.

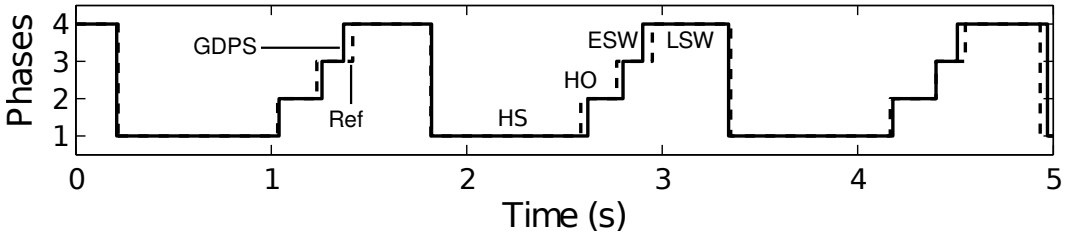

Figure 5.14: An example of gait phase detection system (GPDS) performance compared with the motion analysis system. The phase output signal (solid line) for a sequence of 5 seconds treadmill walking of a subject was obtained by the system through the inputs of foot contact and hip angle signals. The reference gait phase signal (dashed line) extracted from the markers' trajectories was used to evaluate the reliability of the gait phase detection system.

5.3.2 Treadmill walking trials with different speeds

The results of the experiments showed the excellent reliability of the gait phase detection system for treadmill walking with various speeds (See Table. 5.2). A total of 2339 steps (608 at slow speed, 1003 at fast speed, 718 at self-selected speed) for ten able-bodied participants was recorded. The system detected three events (HO, TO, and LSW) in all recorded steps under different speeds correctly, while it failed in 2 steps with slow speed, 14 steps with fast speed and 8 steps with self-selected speed in HS detection which yields the success rate of 99.67%, 98.60% and 98.89%, respectively. An example of sensory signals and phase output signals in 5 seconds of treadmill walking at slow and fast speed of a participant is as shown in Fig. 5.15. It was observed that the walking pattern of the participant at fast speed (Fig. 5.15 B) was different compared to that of the participant's walking at slow speed. For instance, the HS phase was much shorter and the subject performed a larger hip motion with faster speed. The subject had an obvious asymmetric foot contact at 1st and 5th metatarsal heads, which became more pronounced as walking speed increased. The asymmetric forefoot contact could cause false HS detections. A typical example of failed detection of another participant's walking is shown in Fig. 5.16. The participant lost foot contact at 1st metatarsal head and had an unexpected trough of the F_{M5} at 5th metatarsal head in HO phase. A toe contact ($G_T = 1$) was detected again following an early-swing phase ($G_T = 0$ and $G_H = 0$), thereafter a false impulse I_{HS} was generated. False HS detection happened in three subjects at fast speed, and in only one subject at slow speed and self-selected speed due to their gait patterns.

5.4 Summary

In this chapter, a new gait phase detection system specially designed for FES walking system was presented. The real-time system reliably identified the transitions between phases and

Table 5.2: The detection results of the experiments.

Types	Total Steps		Detection Success Rate (%)
Slow Speed (1km/h)	608	HS	99.67
		HO	100.00
		TO	100.00
		LSW	100.00
Fast Speed (3km/h)	1003	HS	98.60
		HO	100.00
		TO	100.00
		LSW	100.00
Self-selected Speed (1.5-2.5 km/h)	718	HS	98.89
		HO	100.00
		TO	100.00
		LSW	100.00

generated the event impulses. The system consists of three FSRs embedded in a shoe insole and a miniature motion tracking device placed at the lateral side of the thigh. The 3-axis gyroscope's and 3-axis accelerometer's outputs measured by the motion tracking device were used to calculate the sagittal hip angle while the FSRs detected the foot contact with the ground. The sampling rate of the sensor signals and gait phase detection algorithm was 100 Hz. The performance of the gait phase detection system was evaluated using an optical motion analysis system. Ten able-bodied subjects participated in the test of the system by performing various walking speeds (slow, fast and self-selected). The success rate for all speeds for detecting the impulses (I_{HO}, I_{TO}, I_{LSW}) was 100%. The system generated a few false impulses of foot contact I_{HS} in 3 subjects, however, the accuracy rate was still over 98%. The false detection of I_{HS} might be caused by the subject's walking style, for instance, foot over-pronation, or not customised placements of FSRs in the shoe insole. False detections mostly occurred due to unstable forefoot contact during a subject's walking at a fast speed in this experiment. A test on patients with gait disability can be worthwhile in future work. As the individuals with spinal cord injury walk at a limited speed [207] and the asymmetric forefoot contact has been considered in our gait phase detection system, the system performance on patients is expected to be efficacious. The potential use of this setup for neural prosthetic applications will be discussed in the next chapter.

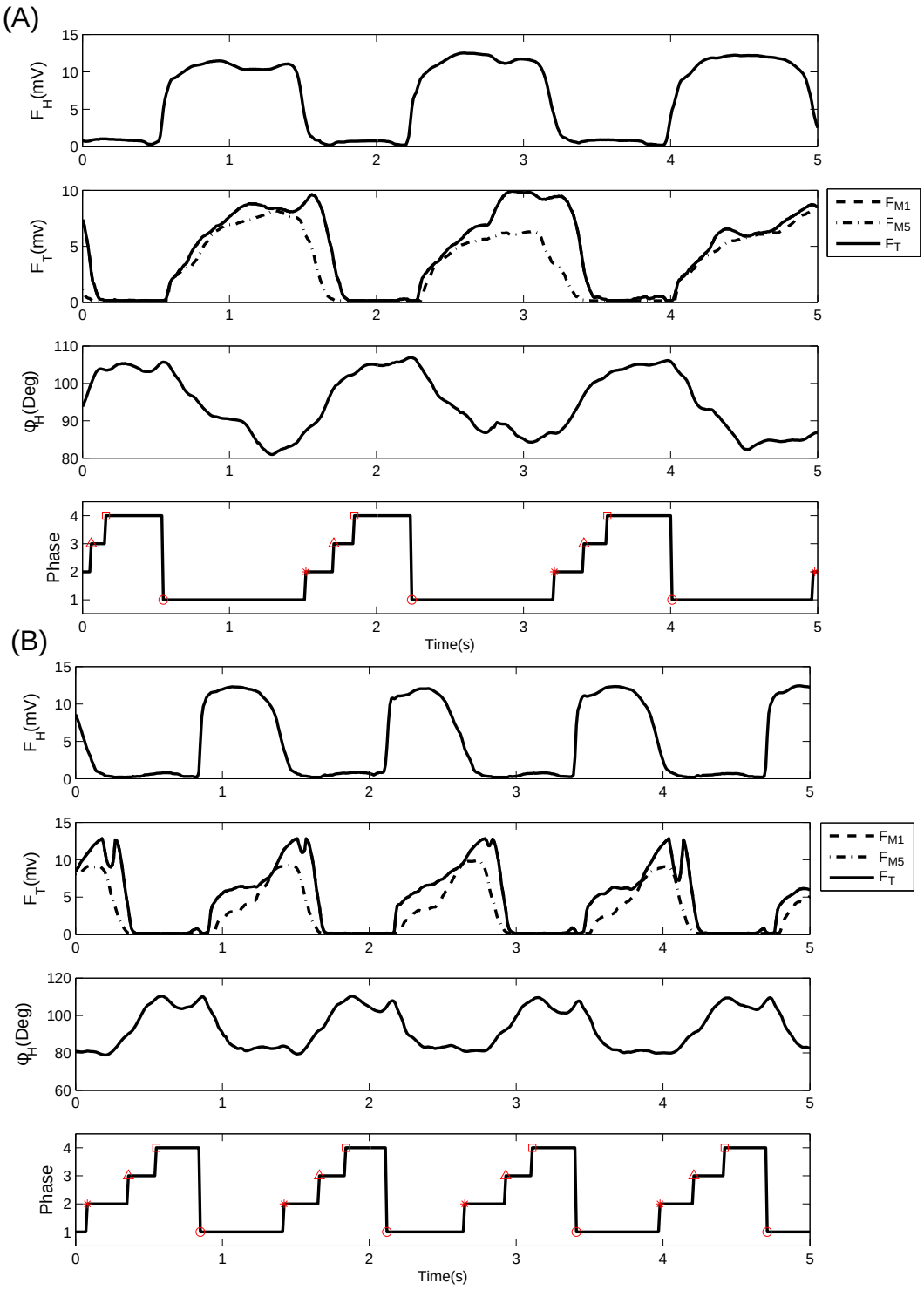

Figure 5.15: The performance of the gait phase detection system when a subject walked on the treadmill with the slow and fast speed. (A) The sensory signals and phase output signal at slow speed. (B) The sensory signals and phase output signal at fast speed. We observed obvious differences in the subject's walking with different speeds. The subject had a shorter period of foot contact during the stance phase and moved the hip in a larger range when he/she walked with a fast speed. The system successfully detected all phases. (Note, red circle = I_{HS}, red star = I_{HO}, red triangle = I_{TO}, red square = I_{LSW})

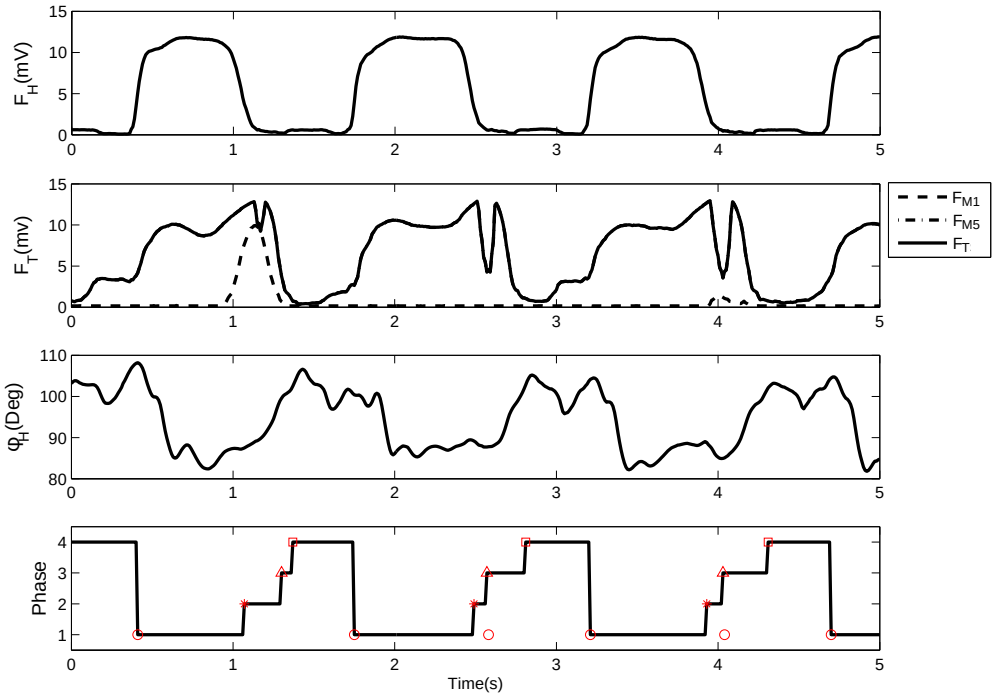

Figure 5.16: An example of failed detections happened during a subject's walking. The FSRs sensor at the 1st metatarsal head failed to detect the contact with the ground while the force signal F_{M5} at the 5th metatarsal head had a trough during the HO phase. The unstable forefoot contact with the FSRs caused false generations of the HS I_{HS}. (Note, red circle = I_{HS}, red star = I_{HO}, red triangle = I_{TO}, red square = I_{LSW})

Chapter 6

Functional Electrical Stimulation System Inspired by Reflexive Control Principles

We have presented a robotic reflexive controller derived from human walking in Chapter 4, which has been successfully implemented in the RunBot III. The results showed the efficiency of exploring biologically inspired approaches to robotics [155] since the human is an "ultimate robot" [176]. On the other hand, the robot was used as a realistic model to verify the biologically inspired control approach for a better understanding of human walking. As the human is regarded as an ideal robot [176], we assume that the same control model can be applied to control systems for human walking.

FES is the application of electrical stimuli to muscles to produce functional limb movements. The human muscles are viewed as actuators of joints in robotics. FES systems are so-called neural prostheses [114]. In this chapter, the robotic reflexive controller was transferred to an FES controller for walking. The FES controller was successfully implemented in an FES walking system by employing a new approach to obtain stimulation sequences for individual muscles using foot contact information from the gait phase detection system as described in Chapter 5. The feasibility and reliability of the system were evaluated in experiments with able-bodied subjects. A significant positive effect of the FES system on walking was observed in most subjects. Several recommendations for further work were highlighted in the conclusion.

6.1 A novel controller for multichannel FES system

We propose here that robotic control can share a similar structure with FES control as shown in Fig. 6.1 containing sensors, actuators and a controller. The "Sensor" block represents the interaction between the control system and the environment and provides input signals to the controller. The control output voltages/stimulation sequences are applied to motors/muscles, therefore, actuate the movements of the lower limbs.

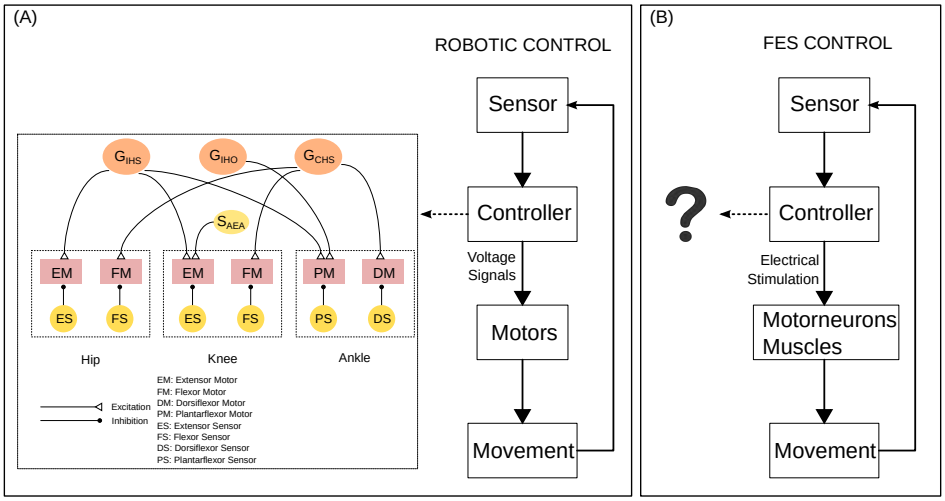

Figure 6.1: A model of a hierarchical controller for functional electrical stimulation (B) is created based on the robotic reflexive controller (A). The muscle functions replace the motor functions in the robotic control, while the same sensory feedbacks are used for triggering the stimulation on muscles. Therefore, the first question we need to answer is how to transfer the robotic reflexive controller to a muscular reflexive controller.

The reflexive controller described in Chapter 4 has a hierarchical structure with two levels of control as seen in Fig. 6.1A. Ground contact information is the main trigger signal for driving the flexor/extensor of each joint while the hip AEA activates the knee extensor in the late swing phase. At the bottom level of control, local reflexes in each joint prevent hyperflexion/hyperextension. As before, no precise position control algorithm is involved in this robotic control model. The same approach can be applied to our FES controller for human walking as shown in Fig. 6.1B. The foot contact information and hip sagittal angular position are used as the input signals. On the output side, selected muscles replace the functions of motors. The muscles are stimulated by automatically generated electrical stimulation sequences and drive the lower limb movement. Fig. 6.2 illustrates the overall structure of the FES walking system. The first question we are going to discuss is how to replace motor actuators with muscle functions.

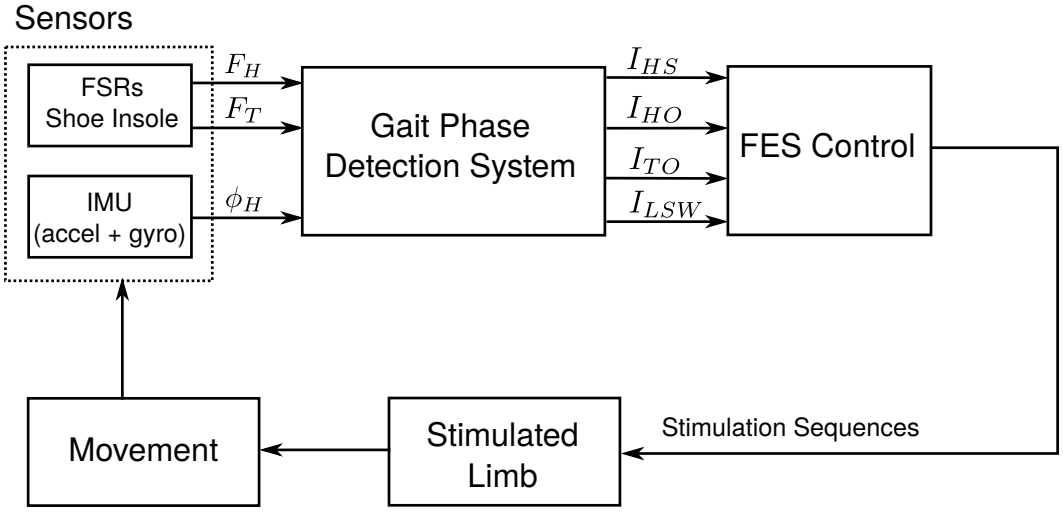

Figure 6.2: The structure of a closed-loop FES walking system. The gait phase detection system generates required impulses with sensory inputs of foot contact and hip sagittal angle signals. The stimulation sequence for each muscle is generated by the FES controller described in the previous section. The stimulated muscles could drive the limb movements while the sensors detect the interaction with the environment and the FES parameters are updated in real time.

6.1.1 Muscle functions corresponding to motor functions

Four muscles were selected, namely TA, LG, BF and RF on each leg, as the same muscles were chosen in previous human walking study [139]. The motor functions in the robotic reflexive controller were assigned to the selected muscles. Before going into the details, the difference between the anatomical and dynamic function of the muscle needs to be illustrated at first.

The direction of the torque exerted by a muscle is determined by the muscle's anatomical position. The anatomical function of a muscle is defined in extreme caution when anatomy alone is used. For multiple joint movements, a muscle acting on one joint would accelerate all joints regardless spanned or not. For instance, the soleus muscle can not only accelerate ankle plantarflexion as its anatomical definition but also the knee extension. Biarticular muscles can have multiple functions of actions. For instance, gastrocnemius muscle, which is responsible for knee flexion and ankle plantarflexion, can perform different functions depending on the position of the body and the interaction with the environment. The biarticular muscle effect on the different joints is not always constant but varies due to the changing of muscle moment arms on the joints according to different postures [208]. Thus, the muscle function could vary in different motor tasks, or even during a single motor task. This kind of muscle function is so called "dynamic function". Induce Acceleration (IA) analysis has been widely utilised to analyse dynamic muscle functions during normal gait [1, 198, 209], where some biarticular muscles were found to have the potential to induce a joint motion in

the opposite way to their anatomical definitions [210]. The dynamic or "counter-intuitive" function of a muscle should be concerned rather than its anatomical function in the FES treatment for a specific motor task, such like walking [211]. A dominant function can be determined for each muscle group during gait as following.

1. The TA is an uniarticular muscle that is responsible for ankle dorsiflexion.

2. The LG muscle generates the ankle plantarflexion and induces the acceleration of flexion at the hip and knee joints. The contribution of muscle to body support by accelerating the mass centre upward and forward indicates that the function of LG as a plantarflexor of the ankle is more significant than a flexor of the hip and knee [212]. Therefore the primary function of the LG is to extend the ankle.

3. In studies of dynamic muscle function during gait in IA analysis [1, 213], the RF was found to contribute to hip and knee extension during the stance phase, which agrees to the distal anatomical definition of the RF as a knee extensor, but conflicts its proximal anatomical definition as a hip flexor. This "counter-intuitive" function was also studied in the experiment with able-bodied subjects [211], where electrical stimulation was applied to the RF during pre-swing or after toe-off randomly during normal walking. A significant reduction in knee flexion and hip flexion was observed, which was assumed that the knee extension of the RF dominated its hip flexion as the RF diminishes hip and knee flexion during the early swing phase. Therefore, the dominant function of the RF we consider in the FES walking system is knee extension.

4. The BF muscle is a hybrid muscle consisting of long and short heads of origin. The BF long head arises from the ischial tuberosity while the BF short head starts on the posterior aspect of the femur. Both heads end on the head of the fibula and lateral tibial condyle [214]. The BF short head has a greater contribution to knee flexion than the long head of BF in human walkings studies [215, 216]. As knee flexion is considered as the main function of the BF, the short head of BF is more concerned when placing the electrodes. The muscle has a remote effect on the hip joint to induce hip flexion [1]. It assists in accelerating hip flexion for initiating the swing phase during gait [209]. The secondary induced dynamic function of BF short head acts as a weak hip flexor.

The muscle functions are summarised in Table 6.1. Most muscles have the same induced dynamic function as their anatomical definitions. "Counter-intuitive" functions were found in the RF where the muscle acts as a hip extensor rather hip flexor [1, 213] and the BF short head since this muscle should not act on the hip. As shown in Table 6.1, muscle functions are then related to motor functions corresponding to their dynamic functions. The TA performs as an ankle dorsiflexor while the LG acts as an ankle plantarflexor. The BF short head is

responsible for knee flexion and also hip flexion as its remote effect on the hip joint [1]. The knee and hip extension are activated by the RF.

Table 6.1: Summary of anatomical, dynamc muscle function and corresponding motor function [1]

	Anatomical Function	Induced Function	Motor Function
Tibialis Anterior	AD	AD	AD
Lateral Gastrocnemius	AP KF	AP KF	AP
Biceps Femoris Short Head	KF	KF **HF**	KF HF
Rectus Femoris	KE **HF**	KE **HE**	KE HE

Bold type indicates counter-intuitive function. AD = Ankle Dorsiflexion, AP = Ankle Plantarflexion, KF = Knee Flexion, KE = Knee Extension, HF = Hip Flexion, HE = Hip Extension.

6.1.2 The FES control principles

The muscular reflexive controller is shown in Fig. 6.3A. Two changes were made in order to transfer the controller from robot to human. First, in the robotic reflexive controller, the contralateral HS was used to indicate the initiation of the swing phase due to lack of a complex foot-ankle design in the RunBot III. The HS of the contralateral leg was replaced by the TO information to represent the start of the swing phase in human gait as shown in Fig. 6.1A. Second, the existence of local reflex loops in the spinal CNS of humans means that there is no need to include a local reflex circuit in the FES controller. The bottom level of the robotic reflexive controller is therefore excluded in Fig. 6.3A.

The hierarchical structure of the FES control is illustrated in Fig. 6.3B. The states (S) control the electrical stimulation on/off of muscle thereby timing and coordinating the stimulated muscle activations in the FES system. In the low level of the FES control, a 2nd order low-pass Butterworth filter function is used as a transfer function to generate impulse response triggered by specific event impulse. The impulse response is then normalised by the coefficient g to be between 0 and 1. The FES amplitude current is regulated to a range from the minimum threshold current c_{min} to the maximum threshold current c_{max}. Thus, the generation of stimulation sequences for each muscle is expressed as:

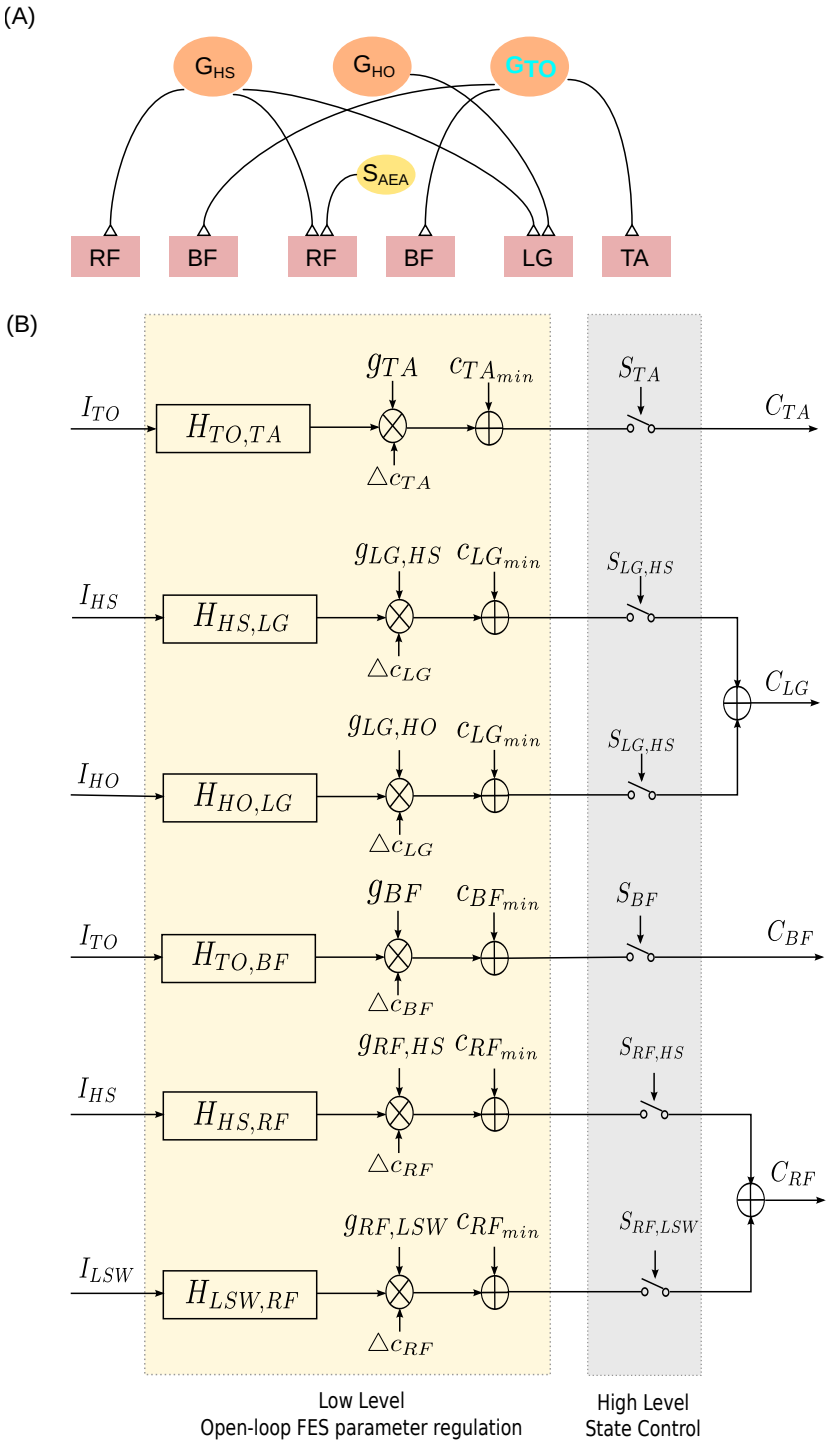

Figure 6.3: (A) The muscular reflexive controller is created based on the robotic reflexive controller where muscles replace the functions of motors in the robot according to their muscle dynamic functions. (B) The FES control with the hierarchical structure. The high level of the control is the state control for timing and coordination of the FES to the muscles in the walking system. The current amplitudes are first generated by event impulse through an open-loop transfer function H and regulated to a range in the low level of the control.

$$
\begin{aligned}
C_{TA} =& (g_{TA} \cdot H_{TA,\,TO} * I_{TO} \cdot \triangle_{c_{TA}} + c_{min,\,TA}) \cdot S_{TA} \\
C_{LG} =& (g_{LG,\,HS} \cdot H_{LG,\,HS} * I_{HS} \cdot \triangle_{c_{LG}} + c_{min,\,LG}) \cdot S_{LG,\,HS} \\
&+ (g_{LG,\,HO} \cdot H_{LG,\,HO} * I_{HO} \cdot \triangle_{c_{LG}} + c_{min,\,LG}) \cdot S_{LG,\,HO} \\
C_{BF} =& (g_{BF} \cdot H_{BF,\,TO} * I_{TO} \cdot \triangle_{c_{BF}} + c_{min,\,BF}) \cdot S_{BF} \\
C_{RF} =& (g_{RF,\,HS} \cdot H_{RF,\,HS} * I_{HS} \cdot \triangle_{c_{RF}} + c_{min,\,RF}) \cdot S_{RF,\,HS} \\
&+ (g_{RF,\,lSW} \cdot H_{RF,\,lSW} * I_{LSW} \cdot \triangle_{c_{RF}} + c_{min,\,RF}) \cdot S_{RF,\,LSW}
\end{aligned}
\tag{6.1}
$$

where H is the transfer function which convolves with the impulse input I to generate the response output. g is the gain coefficient to normalise the response output to the range between 0 and 1. c_{max} is the maximal threshold current that can produce maximally stimulated muscle contraction, and c_{min} is the minimal threshold current that can elicit visual muscle contraction. $\triangle c$ is the difference between the c_{min} and c_{max}. The values of c_{max} and c_{min} for each muscle will be measured in the preparation session of the experiment. The state function S switching the stimulation on and off is determined by gait phases as described in Eq. 6.2.

In summary, the FES control principles are illustrated as follows and Fig. 6.4:

1. HS: When the foot heel strikes the ground, the RF and LG are activated for the hip and knee extension and ankle plantarflexion respectively during the stance phase.

2. HO: The electrical stimulation is applied on the LG at HO so that the muscle contraction leads to the ankle plantarflexion to push the foot off the ground. The LG stimulation also accelerates the knee flexion to lift the leg.

3. TO: The swing phase starts while the foot lifts off the ground. The BF is electrically stimulated to flex the knee and hip joint, while the TA is activated by electrical stimulation to dorsiflex the ankle for clearing the foot with the ground during the swing phase. The LG stimulation is switched off so that the TA is not oppositely affected.

4. LSW: When the hip reaches its AEA position, the signal triggers the electrical stimulation on the RF to drive the knee extension during the late swing phase.

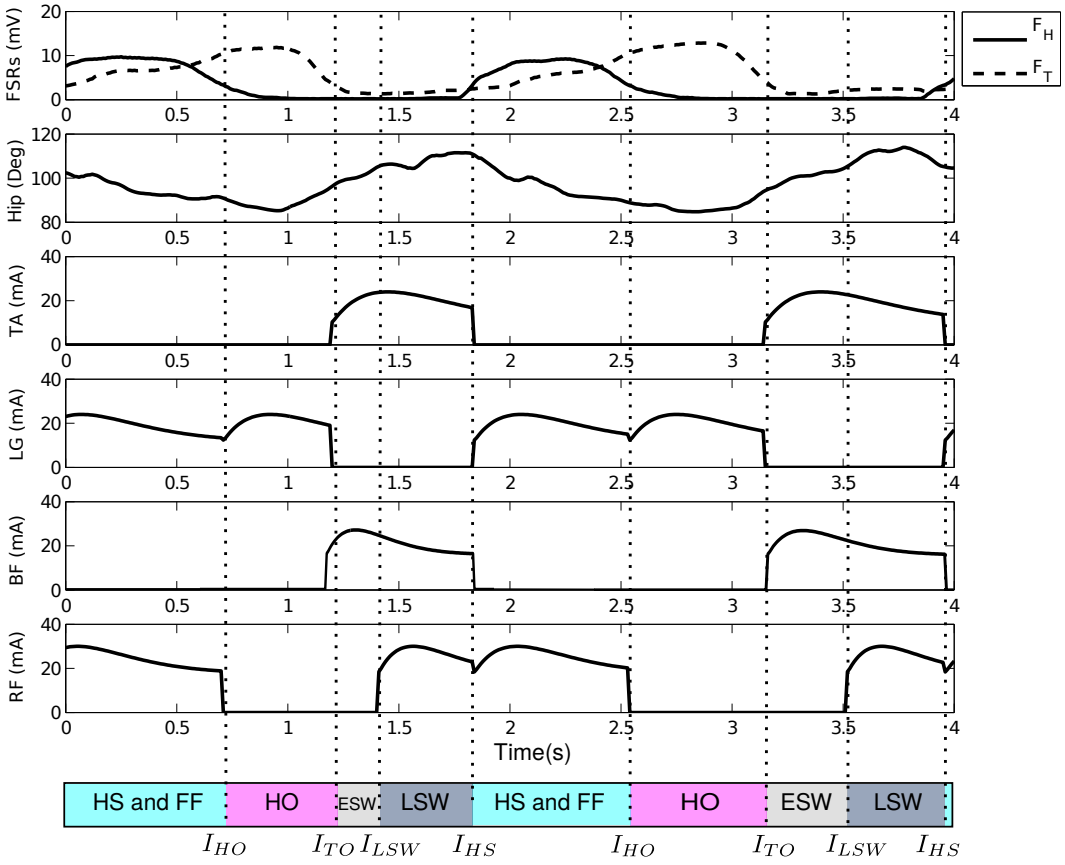

Figure 6.4: A sequence of 4s showing consecutive strides recorded during an FES session in one subject. The top two plots show the real-time processed signals from the FSRs and hip sagittal angle measurement. The bottom four plots show the stimulation sequences for four muscles based on the FES controller. Note: HS = Heel Strike, FF = Flat Foot, HO = Heel Off, ESW = Early Swing, LSW = Late Swing.

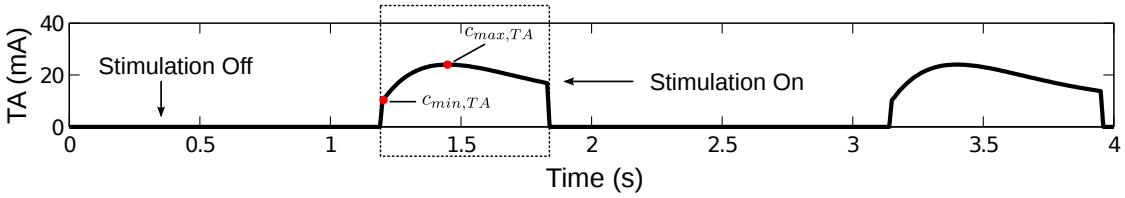

Figure 6.5: Illustration of electrical stimulation pattern to the TA muscle during gait walking derived from Fig. 6.4. The stimulation is switched on at the TO event. The current intensity is generated based on Eq. 6.1. The current rises from the minimal threshold current $c_{min,\,TA}$ to the maximal threshold current $c_{max,\,TA}$ and then descends to $c_{min,\,TA}$. The HS event indicating the initiation of the stance phase switches off the stimulation.

$$
\begin{aligned}
S_{TA} &= \begin{cases} 1 & \text{phase = ESW or LSW} \\ 0 & \text{otherwise} \end{cases} \\
S_{BF} &= \begin{cases} 1 & \text{phase = ESW or LSW} \\ 0 & \text{otherwise} \end{cases} \\
S_{LG,\,HS} &= \begin{cases} 1 & \text{phase = HS} \\ 0 & \text{otherwise} \end{cases} \\
S_{LG,\,HO} &= \begin{cases} 1 & \text{phase = HO} \\ 0 & \text{otherwise} \end{cases} \\
S_{RF,\,HS} &= \begin{cases} 1 & \text{phase = HS} \\ 0 & \text{otherwise} \end{cases} \\
S_{RF,\,LSW} &= \begin{cases} 1 & \text{phase = LSW} \\ 0 & \text{otherwise} \end{cases}
\end{aligned}
\tag{6.2}
$$

For example, the stimulation sequence of the TA muscle is as shown in Fig. 6.5. The impulse input I_{TO} triggers the stimulation. The electrical current applied to a muscle rises from the minimal threshold current $c_{min,\,TA}$, achieves the maximal threshold current $c_{max,\,TA}$ as the peak, and then descends. The occurrence of the event impulse I_{HS} representing the transition from the swing phase to the stance phase will switch off the TA stimulation.

6.1.3 System setup

The connection of the PC, stimulator and gait phase detection system is illustrated in Fig. 6.6. The stimulator, A/D data acquisition devices in the gait phase detection system are connected to the PC via USB ports.

The surface electrical stimulator (RehaStim, HASOMED, Germany) has 8 isolated stimulation channels. The range of current is from 0 to 126 mA. The pulse width can be set between 20 to 500 μs. The frequency of the stimulation can be set in a range from 0 to 140 Hz. Each channel of the stimulator is controllable in real time by the programme running in the PC. Thus, the universal stimulator can be applied to various FES applications.

The gait phase detection system has been described in detail in Section 5.2 of Chapter 5. The USB-DUX Sigma device (Incite Technology Ltd, UK) has 16 analogue inputs where six channels were utilised to measure the force data from the FSRs embedded in the shoe insoles. The Arduino Uno was used to communicate with two motion tracking devices (MPU9150,

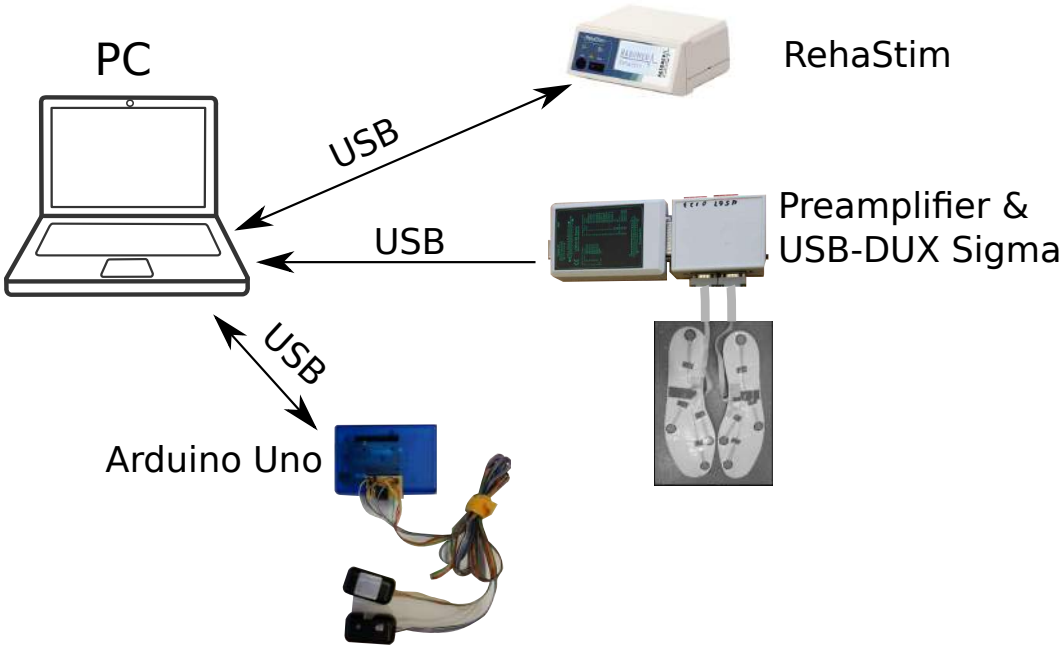

Figure 6.6: Hardware connections of the FES system. The stimulator, USB-DUX Sigma and Arduino Uno device are connected to the PC via USB ports.

InvenSence, CA, USA) via I2C for the hip angular measurement in the sagittal plane. The Arduino Uno was programmed to calculate the hip angles and send the values to the PC.

Graphical User Interface

The stimulator and data acquisition devices were implemented in the FES system. The programme was written with Comedi [217] and Qt [218] libraries in the C++ language, and able to run under the Linux operation system (Ubuntu 14.04). In the system, the pulse width is held constant and the current for eight channels are automatically generated by the FES control model during walking. The stimulation and all parameters are controlled by the GUI of the system as shown in Fig. 6.7.

Current status of foot contact and hip angular positions of both legs are displayed at the top right of the panel. One gait cycle is divided into four gait phases, namely HS, FF, HO and TO by the FSRs signals (Chapter 5). Different background colors indicate different gait phases, where cyan = the HS phase, red = the FF phase, magenta = the HO phase, lightgray = the TO phase. Directly below the foot contact status is the hip sagittal angles as indicated for the left and right hip.

The constant stimulation pulse width and frequency need to be set up prior to the stimulation in the panel. The hip AEA threshold can be adjusted respectively for each limb during the stimulation. The “Start” button at the bottom right of the panel starts the automatic

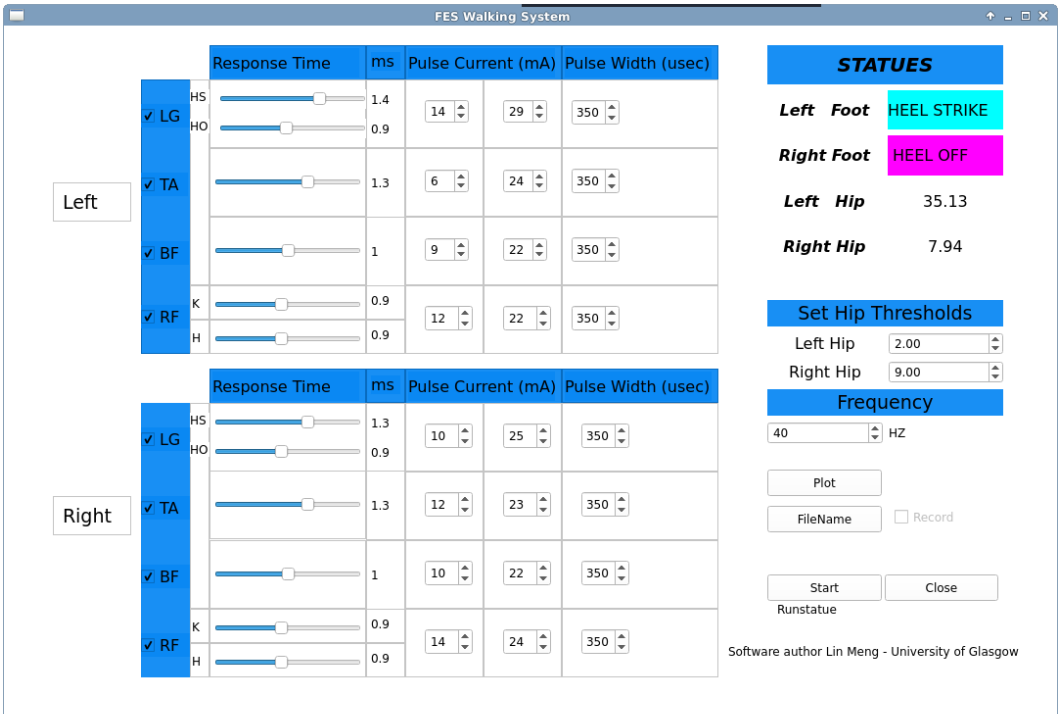

Figure 6.7: The GUI of the FES walking system.

stimulation and stops the stimulation when the button is pressed a second time. The text font below the button indicates the status of the stimulation.

A sub-window can be activated by pressing the "Plot" button. The plots of stimulation current for each muscle and phase state, including foot contact and hip AEA values, in the last 5 seconds can be viewed in the window as shown in Fig. 6.8.

The stimulation of each muscle is selectable in the panel. Three parameters of each muscle including the maximal threshold current, the minimal threshold current and the response time of filter function, need to be set up manually. The settings allow the researcher to individually set up the stimulation mode for each subject.

In summary, the GUI is designed so that all the control parameters and settings of the system can be accessed through the panel. The user-friendly interface allows researchers to use the system in the gait rehabilitation for spinal cord injuries in future research.

6.2 Experimental Setting

Experiments were designed to evaluate the reliability and repeatability of FES walking system. The behaviour of the system was only evaluated on able-bodied subjects. The performance of treadmill walking when stimulations were applied to the muscles was compared to normal treadmill walking.

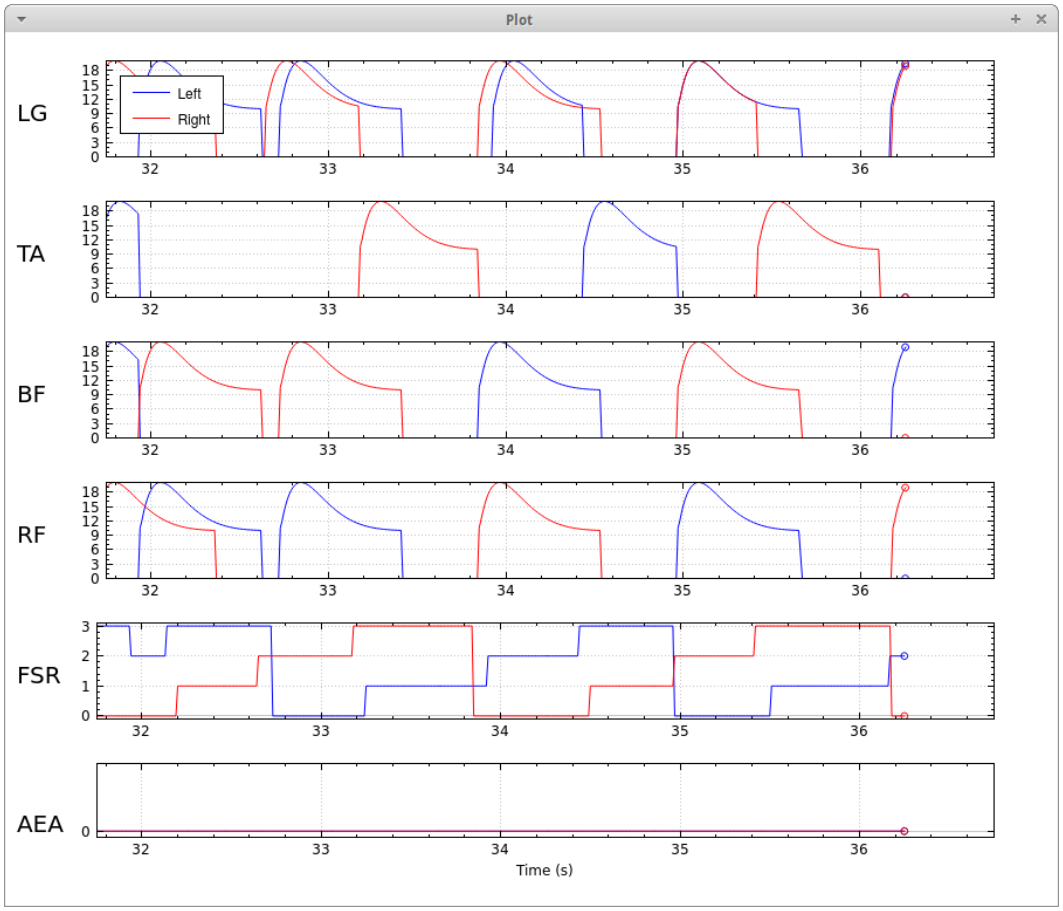

Figure 6.8: The real-time plot of stimulation sequences for each muscle and sensory input consisting of FSR contact status and hip AEA status. Signals pertaining to the left leg are drawn in blue while red lines indicate the right leg.

6.2.1 Participants

Seven able-bodied individuals with no known gait impairments participated in this study. The subjects (five males, two females) had an average age of 28.7 ± 7.9 year and were 1.75 ± 0.08 m in height. The detailed information about the subjects is shown in Table. 6.2. The University of Glasgow College of Science and Engineering Ethics Committee approved the protocol, and written informed consent was obtained from each subject before the experiment.

6.2.2 FES setup

Four muscle groups were stimulated in this study: RF, BF (short head), LG and TA of both legs, in order to augment knee flexion/extension and ankle flexion/extension. Stimulation of the RF and BF aims to induce hip flexion/extension. Two sizes of FES electrodes (Platinum electrodes, Nidd Valley Medical Ltd) were chosen. The larger electrodes (5×9cm) were used for the stimulation of the RF and BF, and the smaller ones (3×5cm) were utilised for

Table 6.2: Participant information of the test study of FES walking system. Subject ID was randomly assigned to each subject.

Subject ID	Gender	Age (years)	Height (m)
A	F	22	1.66
B	F	23	1.65
C	M	27	1.76
D	M	28	1.84
E	M	44	1.73
F	M	28	1.82
G	M	24	1.74

the stimulation of the TA and LG. All electrodes were carefully placed at the appropriate locations that led to sufficiently stimulated muscle contraction of the desired muscle groups. The positions of the electrodes in each subject is shown in Fig. 6.9.

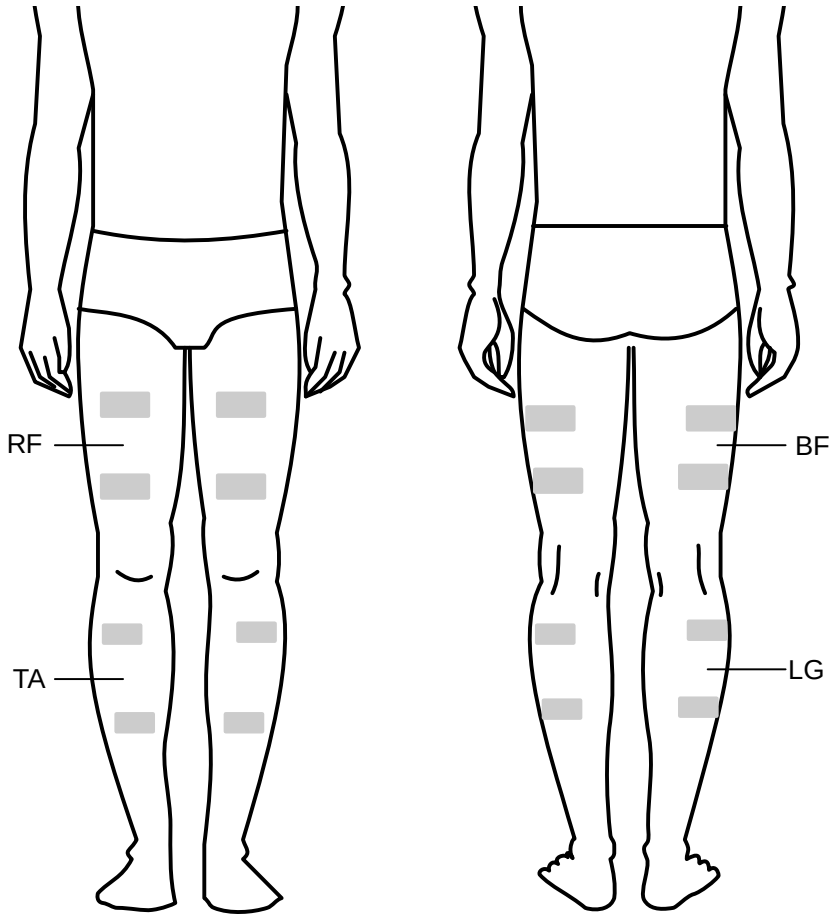

Figure 6.9: Illustration of stimulation electrode locations for each subject. The four muscle groups are chosen in the study. Two muscles are on the thigh - the RF in the front and BF at the back. The remaining two muscles are the TA and LG on the shank.

The frequency of the stimulation was set to 40 Hz, and the pulse width was 350 μs. The stimulation sequences were generated by Eq. 6.1. Prior to the stimulation session, the stimulation current parameters were tested and determined in the set-up session. These parameters are Perception Threshold Current (PTC), Minimal Threshold Current (MinTC) and Maximal Threshold Current (MaxTC). The PTC is defined as the current threshold at which the presence of a stimulus is perceived [219]. The MinTC (c_{min}) indicates the minimum current evoking a visible muscle contraction. The MaxTC (c_{max}) represents the maximum current that the subject can tolerate. These parameters were determined for each muscle by increasing the electrical current from 0 mA in steps of 1 mA. The subject was asked to judge the perception of the stimulation. The investigator determined the values of MinTC and MaxTC. The values of parameters are detailed in Appendix D.

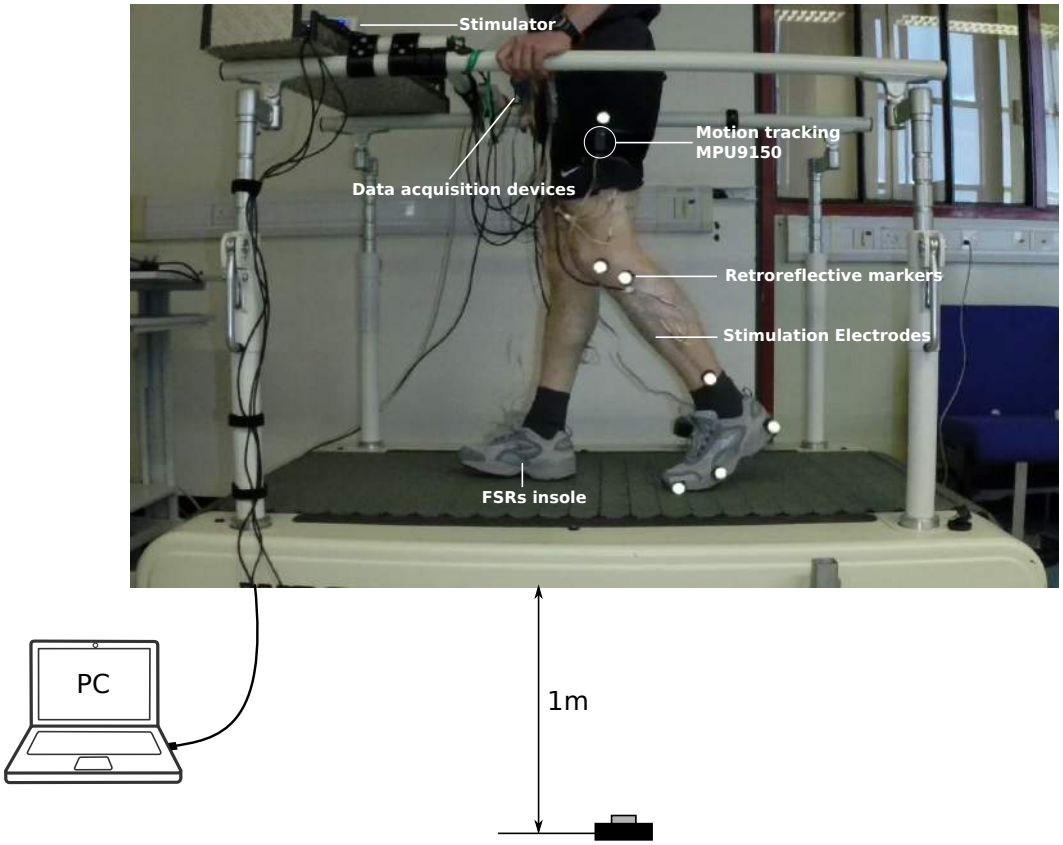

Figure 6.10: Schematic of the experimental setup: Subject walking on the treadmill during muscle stimulation. All devices including the stimulator and data acquisition devices are connected to a PC which runs the control programme while the subject wears the FSRs insoles in the shoes and motion tracking MPU9150 on the lateral side of the thigh. A high-speed video camera is used to capture the kinematic motion by tracking retro-reflective markers placed on the lower limb. The force contact signals from the FSRs, the sagittal hip angles calculated by Arduino Uno, and stimulation current intensity for each muscle are also recorded during the experiment.

The gait detection devices were worn on the waist and the motion tracking devices were placed on the lateral side of the thigh in a set orientation so that they could track the move-

ments of hips in the sagittal plane. The FSRs embedded insoles were worn in the shoes. FES electrodes were located on the four muscles of each leg. Fig. 6.10 shows the arrangement of the 8-channels FES walking system in the experiment. This data and the stimulation current intensity of each muscle were recorded with a sampling rate of 100 Hz during the sessions.

Kinematic data of the left leg were collected with a high-speed (60 Hz) video camera during treadmill walking. Retro-reflective markers were used for motion capture. The placement of the markers was unchanged during sessions. The markers were placed on the toe, 5th metatarsal head, heel, lateral malleolus, tibia lateral condyle, femoral lateral epicondyle, and greater trochanter of the lateral side of left leg. The ankle, knee and hip joints were calculated by the trajectories of the markers as described in Chapter5, Section 5.2.5.

6.2.3 Procedure

All experiments were conducted in the Centre of Rehabilitation Engineering Laboratory. Subjects were instructed to walk on the instrumented treadmill (Woodway, UK) at a self-selected comfortable speed which between 1 and 3 km/h (details in Table 6.3). Each subject was asked to:

1. Walk normally on the treadmill at their self-selected speed for 3 minutes.
2. Walk on the treadmill while the electrical stimulation of each muscle was tested and the time constant of transfer function was determined individually.
3. Walk on the treadmill with electrical stimulation applied to all eight muscles of both legs at the same speed chosen in session 1 for 1 minute, where c_{max} and c_{min} are set as the MaxTC and MinTC values measured prior to the session respectively for each muscle.

Table 6.3: Self-selected speed for each subject

Subject ID	A	B	C	D	E	F	G
Speed (km/h)	1.5	1.7	1.6	2.2	1.6	1.8	2.0

6.2.4 Data analysis

The kinematic data calculated from the motion capture system was synchronised with the other recorded data. For each trial, individual gait cycles were extracted from the data sequence. One gait cycle was considered as the interval between consecutive heel strikes of

the left foot. The heel strikes were detected by the gait phase detection system. Each gait cycle was resampled and time-normalised to 0 - 100% with 101 samples. All kinematic data including hip, knee and ankle angle were calculated for each stride. From each walking trial, 30 strides were obtained.

Gait phases can be determined from the motion capture system according to the foot position with the ground and hip angular position as detailed in Appendix D. The gait phase detection results from the motion capture system were compared to that from the gait phase detection system for the reliability test.

The maximum and minimum angles of the hip, knee and ankle were also found from the kinematic data in each trial. The angular ranges of the sagittal hip, knee and ankle were calculated by subtracting the maximum joint angle with the minimal joint angle. These values were used to evaluate the kinematic significant difference between conditions for each subject by using two-sample t-test (Matlab2014a, The MathWorks, Massachusetts, USA). To reduce the probability of obtaining significance by chance, the acceptable level of significance was adjusted for the number of comparisons [220]. Therefore, the critical p-value was set to $p < 0.004$.

6.3 Results

6.3.1 The reliability test

Strides of 1 minute walking were randomly extracted from the trial of 3 minutes treadmill walking when no stimulation was applied to muscles. Similarly, strides were extracted from the trial of 1-minute treadmill walking when stimulation was applied to 8 selected muscles of both legs. The predicted stimulation triggering events were compared to the recorded ones so that the reliability and repeatability of the control system could be estimated. Table 6.4 summarises the results of two conditions for each subject. The count of trigger events in experimental data and a number of false trigger events are shown in Table. 6.4.

Table 6.4 shows the excellent performance of the gait phase detection system in normal walking. No false trigger events were observed in Subject B-G during normal treadmill walking, and only subject A had 3 false HS, 1 missing HO and 1 false TO detection in total 41 strides. The gait phase detection system performance is less stable during treadmill walking with stimulation applied to the selected muscles compared to the performance during the voluntary treadmill walking without stimulation. In stimulation mode, one subject (subject F) showed no false events in the stimulated treadmill walking. Three subjects (subject A, D, G) only had a few false events. Although the remaining three subjects experienced more false events detected by the FSRs in the shoe insole, the precision rate is still over 75%.

Table 6.4: Results of stimulation trigger events of the FES walking system for seven subjects during experiments. Number of false triggers in shown in parenthesis. Notation: HS = Heel Strike, HO = Heel Off, TO = Toe Off, lSW = late Swing.

Subject	No Stim				Stim			
	HS	HO	TO	AEA	HS	HO	TO	LSW
A	42(3)	40(1)	41(1)	41(0)	42(1)	41(0)	41(0)	41(0)
B	31(0)	31(0)	31(0)	31(0)	33(4)	23(5)	30(4)	29(0)
C	38(0)	38(0)	38(0)	38(0)	36(2)	31(3)	49(15)	34(0)
D	39(0)	39(0)	39(0)	39(0)	41(0)	41(0)	43(2)	41(0)
E	33(0)	32(0)	32(0)	32(0)	31(8)	31(0)	42(8)	31(0)
F	32(0)	33(0)	33(0)	32(0)	29(0)	29(0)	30(0)	30(0)
G	38(0)	37(0)	37(0)	37(0)	40(1)	39(0)	40(1)	41(0)

The false events occurred due to the unreliable force measurement underneath the heel and forefoot. The motion tracking of the sagittal hip angular position has excellent reliability in the system with an accuracy rate of 100%.

6.3.2 A comparison of normal treadmill walking and stimulated treadmill walking

The FES influenced the stride frequency of the subjects. The three subjects (subject B, C, E) had fewer strides in 1-minute treadmill walking with stimulation compared to 1-minute treadmill walking without stimulation (Table. 6.4) at the same self-selected treadmill speed. The results indicated that the stimulation triggered at false events would hinder the gait walking. On the other hand, three out of four subjects (subject A, D, G) had the same number or more strides in 1 minute of stimulated treadmill walking, which suggested the stimulation at correct events would facilitate the walking for able-bodied subjects. For the study of the significant effect of FES on the walking, three subjects (subjects B, C, E) were excluded in this study.

The FES has a significant effect to the stride time of all subjects as shown in Fig. 6.11. A significant shorter stride time was achieved by subjects D and G. The LG stimulation after the HS decreased the early stance phase, while the FES on the LG at the ankle push-off significantly decreased the late stance phase in three of four subjects. The results indicated that the FES for ankle plantarflexion contributes to accelerating the transition from the stance phase to the swing phase, which would increase the stride frequency and, therefore, the

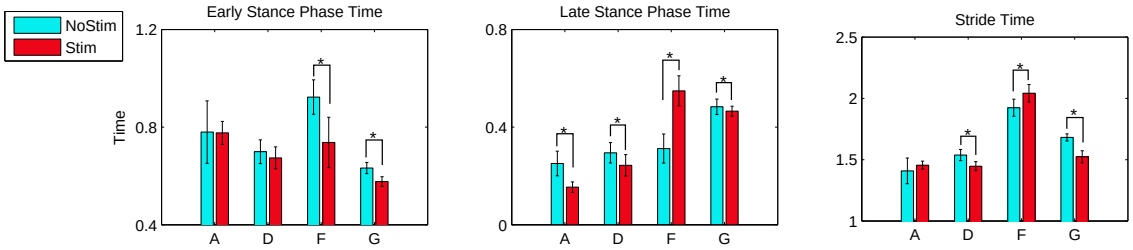

Figure 6.11: Comparing early stance phase time, late stance phase time and stride time in condition (no stimulation vs stimulation). Stride time is the time between two successive HS events. Early stance phase time is defined as the time period from the HS to the HO event. Late stance phase time is the period of time from the HO to the TO event. two-sample t-test is used to evaluate the significant difference in conditions (* = $p < 0.004$, n = 30).

walking speed.

Joint movements were analysed in the sagittal plane for each subject. The comparison of joint angles in conditions of walking with and without stimulation is shown in Fig. 6.12. All subjects (subjects A, D, F, G) achieved a similar gait pattern with the FES during the voluntary treadmill walking, which indicates the FES does not have negative effects on the subject walking. Moreover, differences in joint movements were also noted in Fig. 6.12. The minimum, maximum and range of joints were estimated for the ankle, knee and hip in the gait cycle. Quantitatively, the condition (no stimulation or stimulation) has a significant effect on kinematics as shown in Fig. 6.13 (values are listed in Appendix. D).

Ankle movement

As shown in Fig. 6.12, all male subjects (subjects D, F, G) obtained a higher peak of ankle plantarflexion when the stimulation was applied on the LG muscle during ankle push-off, while subject A performed a significantly smaller ankle plantarflexion within the gait cycle. Moreover, three of four subjects achieved a significantly larger ankle dorsiflexion in the swing phase due to the stimulation applied on the TA. The ankle movement when the LG and TA were stimulated during the treadmill walking was found to be significantly different to the ankle movement without stimulation by comparing the three parameters as shown in Fig. 6.13.

Knee movement

We observed less knee extension in the stance phase since the stimulation applied on the LG muscle does not only generate the ankle plantarflexion but also accelerates the knee flexion during the late stance phase. Two subjects performed a higher peak angle of knee flexion during the swing phase while the other two subjects obtained a smaller maximum knee flexion angle in the same phase. Hence, no positive effect on the knee flexion can be concluded in the experiment. However, quantitatively, the FES has significant effects on these gait variables as seen in Fig. 6.13.

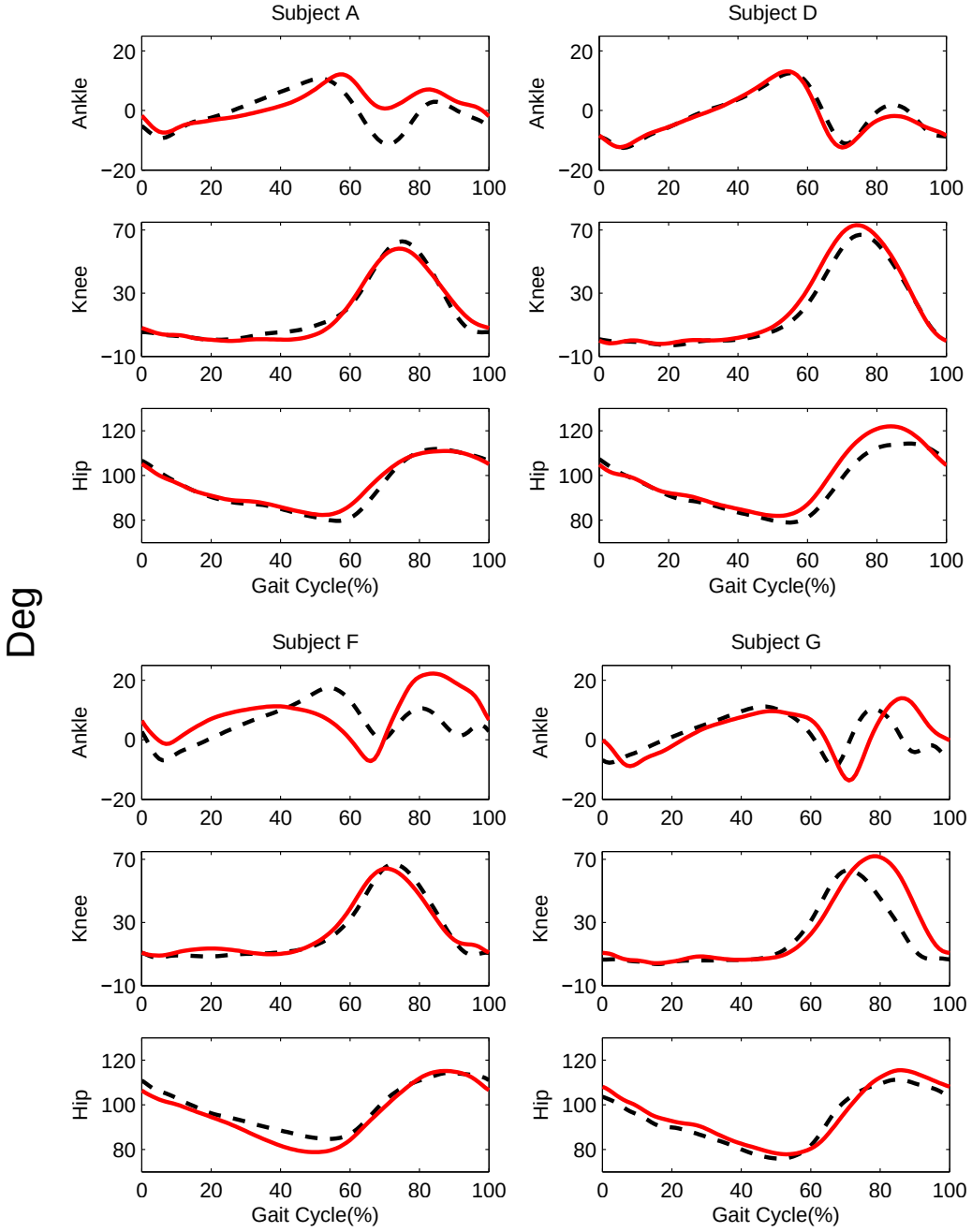

Figure 6.12: Comparing kinematic data of ankle, knee and hip in each condition (no stimulation vs stimulation). Black dashed lines represent the average joint curves in treadmill walking without stimulation while red solid lines show the average joint curves in treadmill walking with stimulation.

Hip movement

The results show that hip movement was significantly affected by the FES applied to the BF and RF muscle for all subjects. A wider range of the hip movement was obtained by three subjects (subject D, F, G) and two of three subjects performed significantly larger hip flexion in the swing phase, Fig. 6.13. Three subjects performed less hip extension during the stance

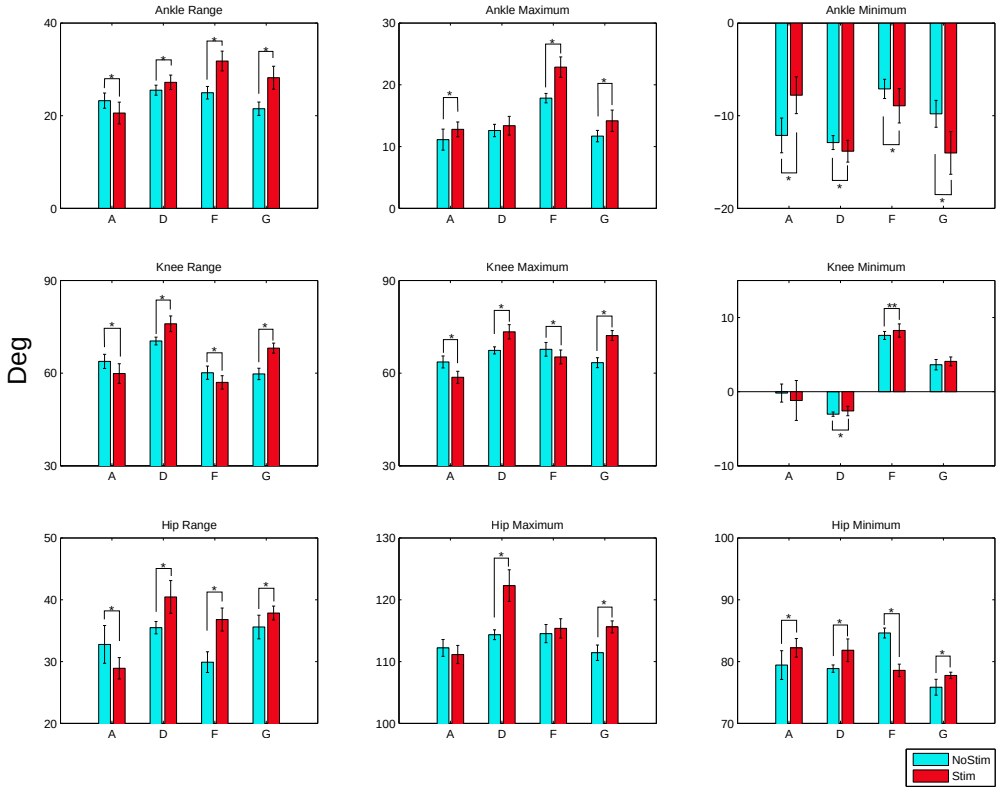

Figure 6.13: Comparison of kinematic parameters in both conditions. Two-sample t-test is used to evaluate the significant difference between the conditions. * = p <0.004, n = 30.

phase, which indicates that the FES accelerates the initiation of the swing phase and thus causes the increase in the stride frequency.

The results showed that the FES has a significant influence on the walking pattern of able-bodied subjects. Most subjects can perform a larger ankle dorsiflexion and hip flexion during the swing phase, which indicates that the FES walking system would help patients with pathological walks to lift the leg off the ground during the swing phase through facilitating the ankle dorsiflexion and hip flexion. The FES to the LG also contributes to ankle push-off following the HO event. The ankle push-off would accelerate the transition from the stance phase to the swing phase and would also contribute to less hip extension in the late stance phase. It was unexpected that three subjects obtained less knee extension in the stance phase while all subjects reported to the author that the FES of the RF does contribute to the knee extension. The phenomenon might be explained that because the LG muscle was electrically stimulated after the HS event for body loading, the induced dynamic function of the LG to the knee flexion would accelerate the knee flexion. The effect of the FES walking system during the early stance phase needs to be studied further on more able-bodied subjects or patients.

6.4 Summary

The RunBot III implemented with the reflexive controller, biologically inspired by the causal relationship between muscle activation and foot contact sensory feedback in the human walking study, establishes stable bipedal walking. The results in Chapter 4 illustrate the advantages of applying bio-inspired principles to the robot control. Otherwise, the RunBot III is regarded as a realistic biomechanical model to help us understand the theory of human walking and validate the feasibility of the reflexive control model. Therefore, in this chapter, we proposed a novel FES reflexive controller transferred from the robotic reflexive controller to the lower limb control during human walking. The four muscles chosen in human walking study are selected, namely the TA, LG, BF and RF, to replace the motor functions, described in Section 6.1.1. In the new FES reflexive controller (Section 6.1.2), foot contact information is the main sensory input to trigger the electrical stimulations on muscles while the hip AEA signal is used to trigger the stimulation of the RF muscle for the knee extension during the late swing phase. Same with the robotic controller, no precise trajectories control is involved in the stimulation controller.

An FES walking system implemented with the muscular reflexive controller is also presented in this chapter (see Section 6.1.3). The system consists of a programmable stimulator and a gait phase detection system (Chapter 5). A GUI window allows set up of all parameters and monitoring current status in real-time. In future clinical research, the GUI can help clinical researchers to customise the stimulation pattern for each individual patient.

Seven able-bodied subjects participated in the experiment aiming to investigate the reliability and effectiveness of the FES walking system. The experiment comprises of two trials, normal treadmill walking and treadmill walking with the FES when all eight muscles of both legs were stimulated in corresponding gait phases. In the reliability test, false event detection occurred in the stimulated treadmill walking of three subjects. Less strides were performed in all three subjects in 1 minute, indicating the significance of the timing of FES. These subjects were excluded in the effectiveness study because the FES system would impede the walking if electrical stimulation is triggered at wrong events. However most of time the FES walking system performed correct phase detections. The kinematic data in the stimulated walking of these subjects still showed that positive effects of the FES on the walking, such as larger ankle plantarflexion at the ankle push-off and larger ankle dorsiflexion during the swing phase. The FES system showed positive improvement of the strides in the other four subjects. This means that the expected stimulation pattern of the FES walking system is fundamentally correct. In the effectiveness study, the significant differences of kinematic parameters in conditions of normal treadmill walking and stimulated treadmill walking were found in all subjects, indicating the significant effect of the system on the walking pattern. Some essential effects of the FES walking system were also observed in our experiment.

Firstly, the system can accelerate the transition from the stance phase from the swing phase. Secondly, it contributes to lifting the leg and clearing the foot off the ground during the swing phase. Last but not least, the stimulation on the LG and RF plays a significant role in body support during the stance phase.

Overall, the FES walking system shows a significant effect on the walking and an excellent reliability within different able-bodied subjects with various self-selected walking speed in the experiment. The FES walking system will be applied to clinical research of gait rehabilitation for patients with SCI.

Chapter 7

Discussion

In this thesis, a novel reflexive robotic controller based on the causal relationship between muscle activities and foot contact information derived a human study was created to generate a stable and coordinated limit cycle walking pattern. The biologically inspired reflexive controller was used in the RunBot III. The achievement of stable stepping of the robot demonstrates that the foot contact information is essential to locomotion movement. The bio-inspired control mechanism was exploited with the dynamics of the robot for stepping generation without any precise trajectory control. Therefore, the first part of the research outlined in this thesis has shown that the interaction between biology and robotics benefits each other. The bio-inspired principles can be validated by the use of the robot. The same concept was applied to FES control for walking assistance. The development of a multi-channels FES walking system based on the reflexive control principles aimed to demonstrate that the biologically inspired control method could be used as a simple, adaptive and robust approach in FES control. The second part of the research emphasised in this thesis has illustrated the feasibility of the approach. An evaluation of the techniques was implemented to test the reliability and effectiveness of the FES walking system in able-bodied subjects. This chapter also outlines the limitations and direction for future research.

7.1 From biology to robotics - RunBot III

Learning human biology has its unique benefits to creating the robotic control. Different levels of biological inspiration are available [155]:

1 Use knowledge of basic mechanical characteristics of animals, to determine leg degrees of freedom, or to configure the geometry of robots.

2 Examine and use typical sensory feedback to control leg movements.

3 Design controllers based on the architectural neural circuits underlying animal walking.

Biological inspiration in robotics has been a trend during the last decades. The concept of passive dynamic walking falls into level 1 above as the robots could achieve stable walking by their intrinsic dynamics of the mechanics with no actuation. The importance of mechanics to the system of bipedal dynamic walkers was demonstrated by McGeer [81]. Limit cycle walkers incorporate the characteristics of passive dynamic walkers with simple control principles. The simplest control model is to apply a small ankle or hip actuation at the initiation of the swing phase for the compensation of energy loss at HS [84, 221]. Through the addition of small actuators, the robots can walk on level ground. Foot contact signals are widely used to distinguish the stance and swing phase of the leg. Therefore, this kind of limit cycle walkers could be classified as level 2. The oscillator controller was inspired by principles of CPGs [95]. Most CPG models are used as a choice to substitute FSM methods including ZMP based control [104], HZD control [105, 106], vector map control [99, 101, 222] and virtual model control [102] among others. Although these CPG-based methods adapt the idea of CPG, the essence of these approaches is closer to level 2. The simple neural network only consists of neural coupled oscillator. For instance, a bipedal robot controlled by nonlinear oscillators which are reset by foot contact sensory feedback is able to achieve walking and running patterns by tuning the oscillator frequency and leg stiffness[94]. Moreover, Lewis et al. [223] proposed an inhibitory CPG network based on a burst spiking neural network. The CPG network formed a basic coordinating pattern for locomotion. Klein [110] developed a hierarchical neural model structured with CPG and reflex interaction. All these models are based on principles of the neural circuitry underlying human walking thus fall into level 3. However, more biology does not always mean a better solution in robotic engineering.

The biological system provides an extraordinary inspiration to robotic engineering as biology contains vast information and useful knowledge for robotics from neuroscience, biomechanism to a system of control. The question is how biology can and should be explored for robotics. Exact biological modeling is not feasible due to the complexity of the nervous system and thus of little interest. The goal of biological inspiration is to derive principles of the biological system and transfer them to robotic engineering. The embodied view suggests that “the neural models are embedded in an embodied system equipped with sensors and actuators enabling physical interaction with the environment” [224]. Passive dynamic walkers with the intrinsic dynamics of the mechanics are paradigmatic examples of self-stabilised systems: the robots can walk down a slope without control or actuation [81]. Neural control can be simplified through exploiting the dynamics by an appropriate mechanism. However, there is a gap between the artificial and biological system. The first important attempt is

to abstract biology principles. The principles do not only yield a better understanding of biological mechanisms but also would guide the construction of the artificial system.

In terms of all forms of locomotion, simplified neural control is associated with clever mechanical design. For instance, swimming can be produced by neural activity transmitted along a chain of coupled CPG oscillators in the spinal cord [225]. These concepts inspired a series of undulatory robots, such as swimming salamander, snake robots [226, 227]. The CPG models have been used in octopod, hexapod robots by the inspiration of the insect locomotion (reviewed in [113]). Moreover, neural control inspired by the CPG or reflex mechanisms has been also used for controlling bipedal walking robots [5, 94, 110, 223]. The key to the construction of all these robots is how to translate the neural activation into torque that drive individual limb segments, resulting in synchronised movements and coordinated locomotion. However, most of these approaches were based at the neural level.

Muscles provide actuation in humans. Muscle activity is convolutedly driven by the CNS and PNS. However, the interaction between CNS and PNS is complicated in biological systems. To create a minimalistic, linear and analogue control system for walking control, the transfer function between the CNS and PNS could be regarded as a black box. The transfer functions relating foot contact with muscle activity (EMG) from a population or individual have been calculated using adaptive filtering algorithm by Macleod [190]. The application of human transfer functions to the RunBot III has been shown to enable generating stable walking as there is a causal relationship between foot contact information and muscle activity during human walking [139]. However, there are several limitations in this study: Firstly, the human transfer functions were extracted from a population or individual subject based on the control of the RunBot II so that only the hip and knee motion were considered in the study. Secondly, the transfer functions need to be manually rescaled to a certain sample length in order to fit in the reflexive controller which has a limited adaptivity to different applications.

In this thesis, a novel approach to the abstraction of biological principles through relating the sensory information and motor activation during walking in a human study is proposed. A completely reflexive controller with ankle control was created from the biological inspiration. In contrast to the study of Macleod [190], the EMG signals were divided into strides, and each stride was scaled to a length of 101 samples to reduce the effect of speed. An adaptive filter with iterative learning optimisation algorithm was used to calculate filter response from a typical FSRs signal and the EMG signal. Impulse response resulted from the convolution of the FSR signal and the filter response as the foot contact is regarded as an impulse trigger in the RunBot. The relationship between the sensory input and the motor output was determined to each muscle function, and the muscle transfer functions were mapped into joint motions by using second order low-pass filter functions instead of using a curve fitting method. The advantage of using IIR filter function to represent the transfer function in the gait cycle is that the filter function increases the adaptability and efficiency of the system

to different control applications. The filter functions with the corresponding sensory signals that trigger the movements were extracted, and the novel and complete reflexive controller was created based on these biological principles.

7.1.1 Interpretation of data

The RunBot III was constructed and used to validate the bio-inspired technical principles. The robot does not involve any precise joint trajectories like all previous RunBots. To our knowledge, it is the first attempt to abstract the biological reflex principles from the human studies for controlling walking gait. The study presented a minimalistic reflexive locomotion model involved the ankle control which was inspired from the transfer functions relating the foot contact signal and muscle activity from the human experimentation. With experiments, we showed that the use of the control in the RunBot III enables the robot to perform a stable walking pattern.

7.1.2 Ankle functions

Our robot is not equipped with springs in the ankle joints in order to simplify the mechanical design. Two eminent features of ankle movement in the walking gait were examined in the experiments: one is the ankle plantarflexion in the early stance phase and the other one is the ankle plantarflexion in the late stance phase. Firstly, there is a "roll-off" effect of ankle plantarflexion during the initial stance phase. The ankle plantarflexion in this phase rotates the foot towards the ground while the hip rotates forward. The results demonstrate that an appropriate ankle velocity would provide a controlled "roll-off", which is consistent with results from humans [202]. Secondly, the ankle plantarflexion actively provides forward progression or push-off in the late stance phase [198]. In a simple bipedal locomotion model, an impulsive ankle push-off or a torque actuation at the hip enable the level walking. The compensation relationship between ankle push-off and hip extensor during walking gait has been shown in human studies [199, 201]. The results in Chapter 4 show that the hip velocity can be related to the ankle push-off velocity for determining the robot's speed in Fig 4.12. It suggests that there is also a similar trade-off between ankle push-off and hip extension in the RunBot III, where increasing the ankle push-off velocity could contribute to the compensation for the weak hip extensor.

Compared to the RunBot consisting of flat feet and compliant ankle joints with rotation and extension spring [194, 228], the ankle actuation at ankle push-off provides a proper propulsive force similar to humans. The time of HO is 40% while the heel lifted off at 46% of the gait cycle for the robot with the compliant ankle joint. The contralateral HS occur at 50% of the gait cycle for both robots. It suggests that the push-off decelerates the trunk and

increase the time between the HO and the contralateral HS [229]. The behaviour can not be observed in the passive ankle joint [194].

Moreover, the addition of the ankle joint significantly contributes to the walking speed of the robot by an increasing of 16% compared to the RunBot II with the rigid ankle. It emphasises the role of the ankle in the robot walking, especially ankle plantarflexions in the stance phase.

Comparison to human data

Robot behaviour can accentuate biological mechanisms of human walking. Therefore, it is necessary to compare the measured data to human gait data. Because the human kinematic experiments were not included in this study, we compared our results to data from the literature [156]. The ankle kinematic data during the robot's walking is qualitatively matched to human data as shown in Fig 4.16. Characteristics, angle range and timing of the ankle movement in the gait cycle were similar. The robot has a larger hip flex angle compared to the human subject due to the requirement to clear the swing leg off the ground. The RunBot III walking speed is scaled to leg length for the comparison to the human walking speed. The scaled robot walking speed is 1.16 leg-length/s, which is approximately close to the scaled human normal walking speed (1.13 leg-length/s) where a human subject with an average height (1.75m) walks at an average speed (1.4 m/s) [230].

Overall, the results of the study demonstrate that the method of incorporating an appropriate mechanical design with a simplified biologically inspired control model is sufficient to construct a robotic system. The reflexive robotic controller integrates simple foot sensory feedback to adaptively coordinate the limb movements on a step-by-step basis and produce steady walking. The human-like characteristics of the robot walking suggest that the robotic system inspired from the human experimental study approximates the human nervous system.

7.1.3 Limitations

Some limitations to the present study need to be considered. The RunBot III was used as a tool for validating principles of a natural human control system for walking. Although its mechanical structure does not exactly follow the human biomechanics, the RunBot III is a planar robot without demonstrating lateral motion which might be important in gait rehabilitation. Moreover, the rigid foot segment in the robot is different to the complex foot-ankle joint in humans as the compliance of the ankle is not considered for the sake of simplicity. In the experiments, we observed that the robot did a "jump" with a large ankle push-off velocity because energy is injected into the system too quickly due to the lack of the compliant ankle joint. Increasing the ankle push-off velocity can increase the walking

speed while the walking speed would oppositely decrease when the velocity reaches a certain threshold. This phenomenon may be explained by the fact that the increasing velocity of ankle push-off over the threshold causes unpredicted disturbances which take the robot more time to regain stability, resulting in a slower walking speed. However, the RunBot III does allow to test the reflexive control system based on the principles of the human natural system derived from the experimental data. It helps us to make the conclusions on the suitability of the approach before the development of a gait rehabilitation system for human use.

The foot contact information is the main sensory feedback in the control system. It excites all except one motion in the locomotion control. The only exception is the hip AEA that is used for the control of the knee extension at the late swing phase. This technique is from the previous reflexive controllers of the RunBots, and not based on the recorded data from the human walking experiment. Moreover, because there is no sufficient toe contact due to the rigid foot design, the TO information indicating the initiation of the swing phase is not reliable in our robotic system. Therefore, the contralateral HS is used to trigger the flexors in the swing leg instead in the control model of the RunBot III, which is consistent with the previous controller.

7.2 From robotic to FES - Multichannel FES walking system

An ideal FES system is expected to work in parallel with the human motor system. The simplest FES walking system is based on an open-loop control, such like Parastep I [231], where no signal is directly fed back to the microcontroller for monitoring the current state. It is thus impossible to generate accurate and coordinated control of multiple muscle contractions in the open-loop control. Sensory feedback is essential to determine the current state, which allows the movement control and improves the efficiency of the system. Two types of sensory signals could be used in FES control: biological sensory signals, like EMG, electroneurogram (ENG), Electroencephalography (EEG), and artificial sensory signals measured from sensors ranging from FSR to gyroscope, accelerometer, etc [122, 126, 127, 132, 232]. The common methods in FES control can fall into several categories including dynamic controller [233], finite state controller [131, 234] and artificial networks [163, 235]. However, these control methods have issues to be utilised in practical FES applications: Firstly, complicated algorithms for trajectories control always imply a high computational requirement. Secondly, it is difficult to apply the system to a human due to stimulation latency, muscle spasticity, voluntary control and muscle fatigue during the stimulation. This is also why the open-loop controller remains the most common in commercial markets. To the author's knowledge, no method has managed to generate movement perfectly in synchrony with the

human motor system as an ideal FES system would require. However, researchers found that biologically inspired methods are promising to realise the final aim.

The purpose of FES is to compensate for neuromotor system pathologies through using neural prostheses. The artificial control system is required to control the electrical stimulation on muscles based on sensory feedback. In the last decade, hierarchical control of locomotion has been adapted for real-time control of locomotion with FES assistive systems. The hierarchical structure usually has 2 (or more than 2) levels and combines the switch control and continuous control. The top level of the structure determines the stimulation state of muscles while the low level adjusts the stimulation parameters. The finite state control (FSC) method has been widely used for coordination control in multiple joint FES systems [234, 236] as it is an appropriate and effective technique for automatic determination of the FES coordination to multiple muscles. Most FES systems apply constant stimulation sequences to muscles in the stimulation period [122, 125, 127, 132, 237, 238], where the low level of hierarchical control is an open loop control. Regulating parameters such as pulse width and current value with precise control of stimulated muscle force, torque, kinematic or kinetic data during locomotion have also been studied in [235, 239]. For instance, artificial neural network algorithm was used to modulate pulse width with input data like force and angle signals [235]. However, neural network controlled FES usually requires offline or online training and the learning outputs are biased only fitting to individual subjects. These techniques are rarely used in practical FES systems due to the terms of muscle spasticity and fatigue during the stimulation.

In this study, we newly proposed an FES walking assistive system with a novel hierarchical controller. The hierarchical control model was inspired by human reflexive mechanism abstracted from the human walking experiments. The control model has been simplified and validated with a use of the realistic model - the RunBot III. The robot managed to generate an adaptive gait pattern based on self-stabilising dynamic mechanics. The rules have been well set-up and there is no necessity to learn from human biology again, which significantly simplifies the processing procedure. The results demonstrate that human robotics interaction is a powerful strategy to investigate FES locomotion controllers. Robotics study contributes to extract simple and fundamental control model from the complicated human neuromuscular system.

The biological FES control has the potential to enhance the FES system in several aspects. Firstly, an appropriate stimulation pattern can be easily generated to produce the desired joint movement based on the sensory feedback of foot contact information and hip sagittal angle signals. Secondly, there is no precise trajectories control involving in the FES control, which makes the controller easy to implement in practical FES assistive devices. Thirdly, the transfer functions extracted from the muscle activation and foot contact information were, to the author's knowledge, firstly used to transfer linear inputs into muscle stimulation sequences.

It is a simple but robust method to determine the output of the FES control in the low level based on the time of gait phases without precise control.

7.2.1 Postive effects on walking

The concept of the interaction between robotic and human control has been demonstrated with the implementation of the novel FES control into a FES walking system with significant success. It has been found in the experiment (described in Chapter 6 Section 6.3) that there are significant differences between voluntary and stimulated treadmill walking of able-bodied subjects. The comparison results suggest that the FES walking system has a significantly positive effect on the subjects' walking pattern:

1. **Ankle Plantarflexion**. Studies about FES on hemiparetic patients have shown that stimulating plantarflexor muscles for walking assistance results in a significant increase in paretic propulsion [240]. Forward propulsion during the late stance phase can be positively affected by applying electrical stimulation to the plantarflexor muscles on the paretic leg during walking. All subjects obtained a greater ankle plantarflexion angle during the late stance phase under the stimulation, which indicates that our FES walking system has a positive effect on increasing the forward propulsion at ankle push-off by electrically stimulating the plantarflexor muscle LG.

2. **Ankle Dorsiflexion**. One common problem in spinal cord injured patients with gait deficits is foot drop during the swing phase. A special class of FES devices have been developed particularly for drop foot correction [241]. In the experiment, six of seven subjects achieved a greater peak dorsiflexion during the swing phase. It suggests that the stimulation on the dorsiflexor muscle through the FES walking system could have the same orthotic effect for foot drop correction to the patients.

3. **Knee**. The FES to RF can positively affect the knee extension during walking gait [237, 242]. Meanwhile, a greater knee flexion is expected to help patients to clear foot over the ground during the swing phase, which has been observed that the knee is being more flexed in the early swing phase in FES assisted walking [238]. In our experiment, a greater peak knee angle during the swing phase was found in two of four subjects. The set-up rule for the knee extension triggered by the hip AEA might affect the maximal knee flexion angle in the swing phase, which needs further experiments to verify the assumption. Besides, a smaller knee extension during the stance phase was noticed in three of four subjects. It could be explained by the application of stimulation to the ankle plantarflexor muscle after HS which might increase the knee flexion[240]. Overall, no significant effect on knee motion can be concluded from the results.

4. **Hip**. A smaller hip extension in the stance phase was observed in three of four subjects as the stimulation of the ankle plantarflexor muscle after HO accelerates the initiation of the swing phase. The use of FES increased hip flexion and excursion in three of four subjects. This finding is in line with kinematic changes in FES-assisted walking for incomplete spinal cord injured patients [238].

Although the FES walking system has not been applied to gait rehabilitation for SCI patients, the results in able-bodied subjects implicate positive effects of the system. Ankle dorsiflexion, knee and hip flexion during the swing phase and knee extension during the stance phase are emphasised in FES systems for patients to obtain reciprocal walking [237, 238, 240, 241, 242]. As these kinematic characteristics are significantly affected by the FES walking system in the experiment, the system shows the great potentiality of gait assistance or retraining for patients with SCI.

7.2.2 Limitations

There are some limitations to the present FES walking system which need to be considered. Although learning from biologically inspired robotic control system provides a simple method for FES control, lateral movement is not demonstrated which will be an essential consideration in a successful overground gait rehabilitation system. However, the idea behind the reflexive control system based on human data is that walking is a repetitive motion regulated by sensory feedback. A simple and basic model validated by the RunBot III has been successfully used in the FES control. The results in Chapter 6 demonstrated the feasibility of the biological inspired robotic approach as an FES rehabilitation strategy for human walking.

Ankle plantarflexion during the initial stance phase provides active resistance for rotating the shank forward by lengthening the plantarflexor muscles (eccentric contraction) contributing to knee and ankle stability [197]. Compared with isometric and concentric contraction, eccentric contraction has its unique mechanism from the low-level nervous system [243], like the stretch reflex. FES to the plantraflexors for weight acceptance is rarely considered in FES walking systems. Some systems stimulated the dorsiflexors after HS in a short period [24, 127, 244]. To follow the robotic reflexive controller, the ankle plantarflexor LG was stimulated after HS with various current intensity generated by FES control. However, no significant effect was observed in the experiment comparing voluntary walking and FES walking, and a few subjects lifted the heel off the ground too early due to the stimulation. More sophisticated FES control to ankle movement according to the foot contact information is worth to be further considered.

Only averaged transfer functions from a population of subjects were studied to create a reflexive controller. The EMG transfer functions triggered by foot contact information was mapped to filter functions for motor movement control. The same filter functions are used in FES control. It will be interesting to compare the effect on walking between FES with variable current intensities and FES with constant current intensity to further provide valid evidence for using filter functions in FES control.

7.3 Significance

The work outlined in this thesis demonstrates an early stage in the development of a rehabilitation device for improving gait ability of individuals with imcomplete Spinal Cord Injury (iSCI). Although the FES walking system was not applied in the rehabilitation experimentation which would demonstrate clearly a contribution to this community, the developed control strategy was successfully implemented in the FES walking system and applied in the experiment on able-bodied subjects.

Human walking is hierarchically controlled at several levels of the CNS. The mechanism in the spinal cord provides the basic control units for efficient locomotion organization, which is mostly focused by robotics engineers to derive their inspiration from biologically inspired control methods. Initially, it was necessary to study the natural locomotion dependent on the interaction with the environment. The control strategy and transfer functions learned from the human natural control of locomotion in the experiment was applied to the RunBot III. The concept of the RunBot was the inspiration of the whole project. Using the robot has provided useful information during the preliminary experimentation. For instance, the foot contact information was the most important feedback in the walking locomotion. Foot contact signals could be used to trigger the flexors of the contralateral leg and the extensors of the ipsilateral leg except the knee extension at the late swing phase is activated by the ipsilateral hip AEA. Transfer functions derived from human data were successfully used in generating a stable walking cycle [139]. A completely reflexive controller with the addition of the ankle control was created based on the derived transfer functions from the human study. The successful establishment of the artificial system inspired from biology with the embodiment demonstrates the method is sufficient to extract biological principles for control use. It avoided to endanger users or add the complexity of individual compensation in the control model.

The control strategy with transfer functions was applied to an FES walking system. The feasibility of the system to produce stepping was demonstrated in able-bodied subjects. To the author's knowledge, this was the first attempt to apply a robotic approach to FES control. Duysens et al. [176] stated that human is the "ultimate robot". The control of human walking

is an excellent challenge for robotics. The bipedal robots can be designed and controlled based on studies of human walking and its neural control basis [110, 155]. The present study in the thesis verifies the hypothesis that the biologically inspired robotic approach could be used to control a neural prosthesis, i.e., FES systems. This suggested that this approach based on human robot interaction would be promising for creating a simple and adaptive control for different aims and applications.

7.4 Future work

The thesis developed the FES walking system to improve walking function, yet some technical improvements need to be solved before conducting a study with iSCI patients.

1. Development of the hardware. The current measurement devices can be replaced by a wireless solution for sensory measurement of the FSRs signals and hip sagittal angle via Bluetooth communication. This could significantly increase the practicability of the whole system. It could also be an important step to commercialise the system in future by making the programme software available on different platforms including Windows, Linux, OS X, etc. The prototype design has been finished as shown in Fig.7.1, but has not been implemented in the FES system yet. Further work is still needed.

2. Determining parameters of the filter functions: The time period of the filter function is determined by the time length of the gait phase in the present study. The parameters were manually set up by the researchers for individual subjects in the experiment. It will be promising to use a machine learning algorithm to adaptively determine these parameters for individuals in real time.

3. Intention to initiate the gait walking implemented in the FES system: The present study focuses on the spinal level of control which is the automatic level of walking without awareness. The FES control can be integrated with the intention detection for initiating the FES.

FES has great potential for functional use in patients with iSCI as they still preserve some sensor and motor functions. Although the context and level of patient need to be carefully considered and selected due to the fact that not all the SCI patients can benefit from FES treatment. In the next stage, the therapeutic and orthotic effects of the use of FES on incomplete spinal cord injured patients would be studied by evaluating the specific parameters, like gait parameters, blood flow, energy consumption, etc. An individualised FES gait programme for patients with iSCI will be established.

Figure 7.1: Photography of a Bluetooth module. The module will be used in the FES walking system in the next stage to measure the FSR signals and hip angles. This development will reduce the number of cables used in the system and significantly increase the portability of the whole system.

The main contribution in this thesis is to demonstrate a novel method to create FES control based on a human study by using the robot as a test tool. This is supported by the theory that the interaction between robotics and biology has benefits for each other. The same approach would be used to improve an FES control model by including more muscles stimulated for walking. Besides, the study about the causal relationship between the muscle activity and the sensory feedback, in this case, foot contact information, would be applied to investigate the relationship between muscle activity and sensory feedback in other locomotions, which would be sufficient in transferring the biological principles into real-world applications, such as robotic and FES control.

In summary, a few technical aspects in the system should be developed, which would promote the system into a commercial product in future. The application of the FES walking system to patients with iSCI can promote the study about the improvement in ambulatory function that can be achieved using this treatment, which would further highlight the feasibility of this approach.

Appendix A

Parameters in RunBot II

Table A.1: Parameters of filter functions

$\tau_{L/R,\ H,\ F/E}$	$t_{L/R,\ H,\ F/E}$	$g_{L/R,\ H,\ F/E}$	$\tau_{L/R,\ K,\ F/E}$	$t_{L/R,\ K,\ F/E}$	$g_{L/R,\ K,\ F/E}$
0.289	0.175	74.5	0.177	0.107	45.5

Table A.2: Parameters of the thresholds of sensor neurons at each joint

	$\theta_{L,\ H}(Deg)$	$\theta_{R,\ H}(Deg)$	$\theta_{L,\ K}(V)$	$\theta_{R,\ K}(V)$
Extensor	85	65	3.50	3.90
Flexor	110	105	1.00	1.00

Note here, because RunBot II has an elastic knee structure, it is impossible to track knee joint angle. The motor position voltage is utilized as the way to judge if the knee joint approaches the threshold of the joint angle in Tab. A.2.

Table A.3: Parameters of servo amplifier gain $a_{L/R,\ H/K}$

$a_{L,\ H}$	$a_{R,\ H}$	$a_{L,\ K}$	$a_{R,\ K}$
1.50	1.50	3.40	3.40

Table A.4: Parameters of servo motor direction indicator $s_{L/R,\ H/K}$

$s_{L,\ H}$	$s_{R,\ H}$	$s_{L,\ K}$	$s_{R,\ K}$
-1	1	-1	1

Table A.5: Parameters in knee geometric model

l_m	l_{ps}	l_{bp}	r_m	d_{peg}
6	3	2	1.5	0.3

Appendix B

Parameters in RunBot III

$$\omega = \begin{array}{c} \\ G_I \\ G_C \\ B_{I,H} \end{array} \begin{array}{c} \begin{array}{ccccccc} L/R,H,F & L/R,H,E & L/R,K,F & L/R,K,E & L/R,A,D & L/R,A,P_{HC} & L/R,A,P_{HO} \end{array} \\ \begin{pmatrix} 0 & 1 & 0 & 0.3 & 0 & various & various \\ 1 & 0 & 1 & 0 & 1 & & \\ & & & 1 & & & \end{pmatrix} \end{array} \tag{B.1}$$

Table B.1: Parametres for stretch receptors

	$\theta_{L,\ H}(Deg)$	$\theta_{R,\ H}(Deg)$	$\theta_{L,\ K}(V)$	$\theta_{R,\ K}(V)$	$\theta_{L,\ A}(Deg)$	$\theta_{R,\ A}(Deg)$
ES	75	65	1.50	3.50	-10	-10
FS	120	100	4.00	1.00	15	15

Table B.2: parametres for filter functions

	$H_{L/R,\ H,\ F/E}$	$H_{L/R,\ K,\ F/E}$	$H_{L/R,\ A,\ P_{HC}}$	$H_{L/R,\ A,\ P_{HO}}$	$H_{L/R,\ A,\ D}$
τ (s)	0.18	0.10	0.06	0.10	0.04
g	85.89	37.94	28.46	37.94	18.99

Table B.3: parameters for servo amplifier coefficients and servo motor direction indicators

$\alpha_{L/R,\ H}$	$\alpha_{L/R,\ K}$	$\alpha_{L/R,\ A}$	$s_{L,\ H/K/A}$	$s_{L/R,\ H/K/A}$
1.50	3.00	2.00	1	-1

Appendix C

Supplementary plots for RunBot III

The ankle angular motions in one gait cycle and plots of ankle angle versus hip angle when various $\omega_{GI\rightarrow L/R,\ A,\ P_{HO}}$ and $\alpha_{L/R,\ H}$ were selected are given here.

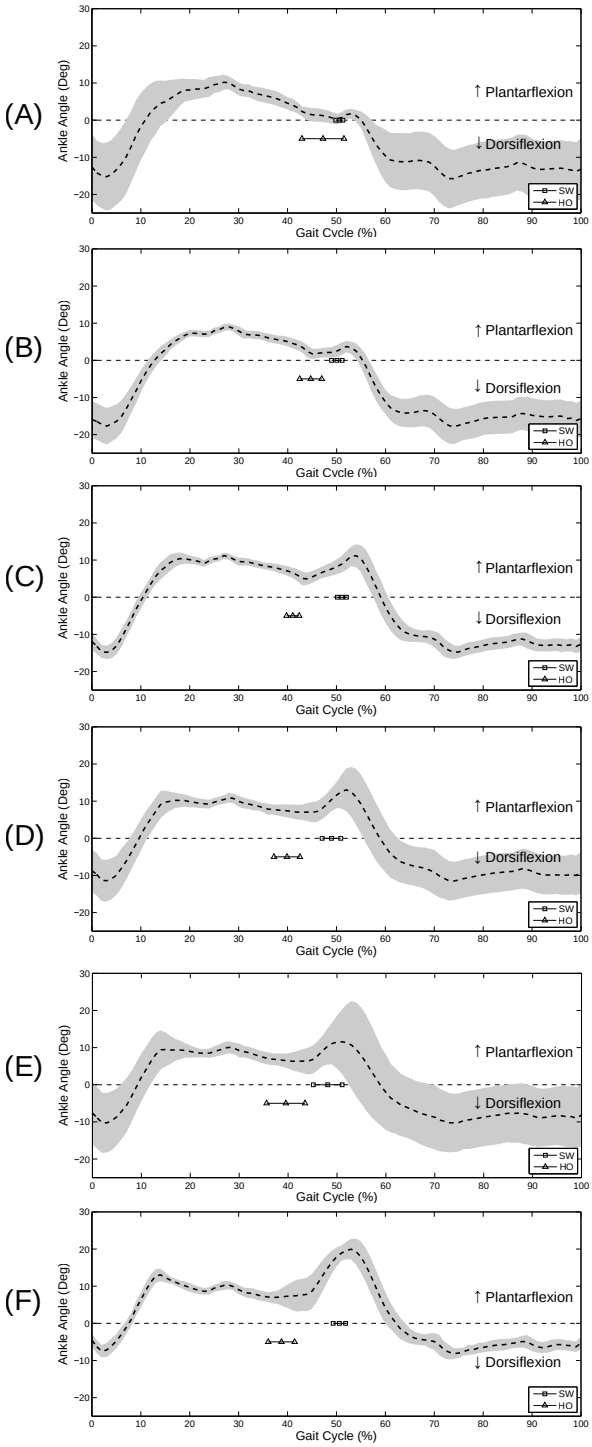

Figure C.1: Comparison between ankle angular motions with various values of $\omega_{GI \rightarrow L/R,\ A,\ P_{HO}}$ during gait cycle. The figures are shown averages with standard deviation in one gait cycle. (A): $\omega_{GI \rightarrow L/R,\ A,\ P_{HO}} = 0$. (B): $\omega_{GI \rightarrow L/R,\ A,\ P_{HO}} = 0.25$. (C): $\omega_{GI \rightarrow L/R,\ A,\ P_{HO}} = 0.5$. (D): $\omega_{GI \rightarrow L/R,\ A,\ P_{HO}} = 0.75$. (E): $\omega_{GI \rightarrow L/R,\ A,\ P_{HO}} = 1$. (F): $\omega_{GI \rightarrow L/R,\ A,\ P_{HO}} = 1.25$. Note here $\alpha_{L/R,\ H} = 1.3$

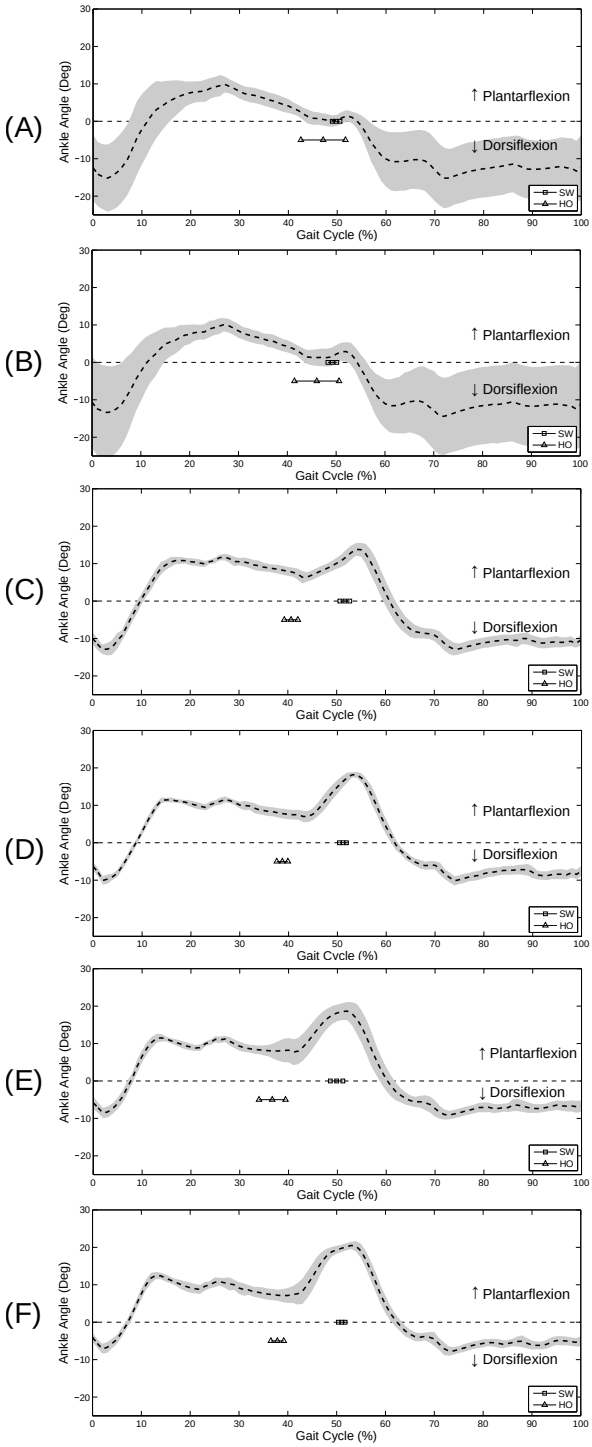

Figure C.2: Comparison between ankle angular motions with various values of $\omega_{GI \to L/R,\ A,\ P_{HO}}$ during gait cycle. The figures are shown averages with standard deviation in one gait cycle. (A): $\omega_{GI \to L/R,\ A,\ P_{HO}} = 0$. (B): $\omega_{GI \to L/R,\ A,\ P_{HO}} = 0.25$. (C): $\omega_{GI \to L/R,\ A,\ P_{HO}} = 0.5$. (D): $\omega_{GI \to L/R,\ A,\ P_{HO}} = 0.75$. (E): $\omega_{GI \to L/R,\ A,\ P_{HO}} = 1$. (F): $\omega_{GI \to L/R,\ A,\ P_{HO}} = 1.25$. Note here $\alpha_{L/R,\ H} = 1.4$

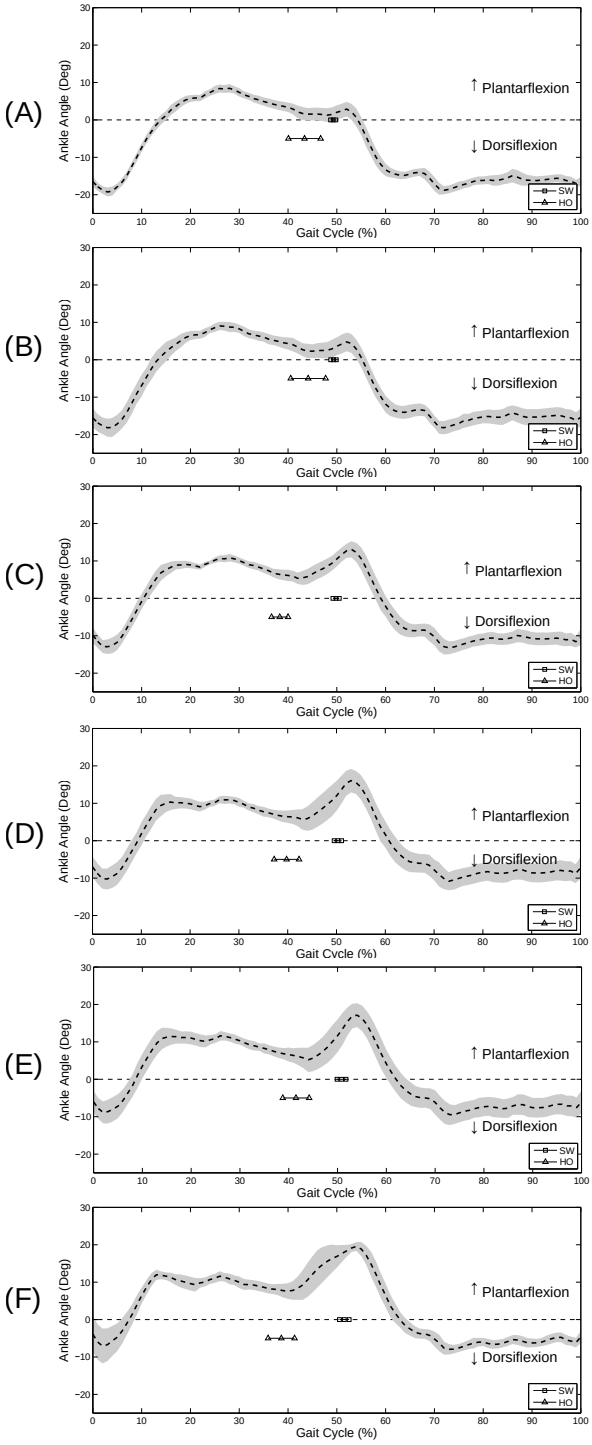

Figure C.3: Comparison between ankle angular motions with various values of $\omega_{GI \rightarrow L/R,\ A,\ P_{HO}}$ during gait cycle. The figures are shown averages with standard deviation in one gait cycle. (A): $\omega_{GI \rightarrow L/R,\ A,\ P_{HO}} = 0$. (B): $\omega_{GI \rightarrow L/R,\ A,\ P_{HO}} = 0.25$. (C): $\omega_{GI \rightarrow L/R,\ A,\ P_{HO}} = 0.5$. (D): $\omega_{GI \rightarrow L/R,\ A,\ P_{HO}} = 0.75$. (E): $\omega_{GI \rightarrow L/R,\ A,\ P_{HO}} = 1$. (F): $\omega_{GI \rightarrow L/R,\ A,\ P_{HO}} = 1.25$. Note here $\alpha_{L/R,\ H} = 1.6$

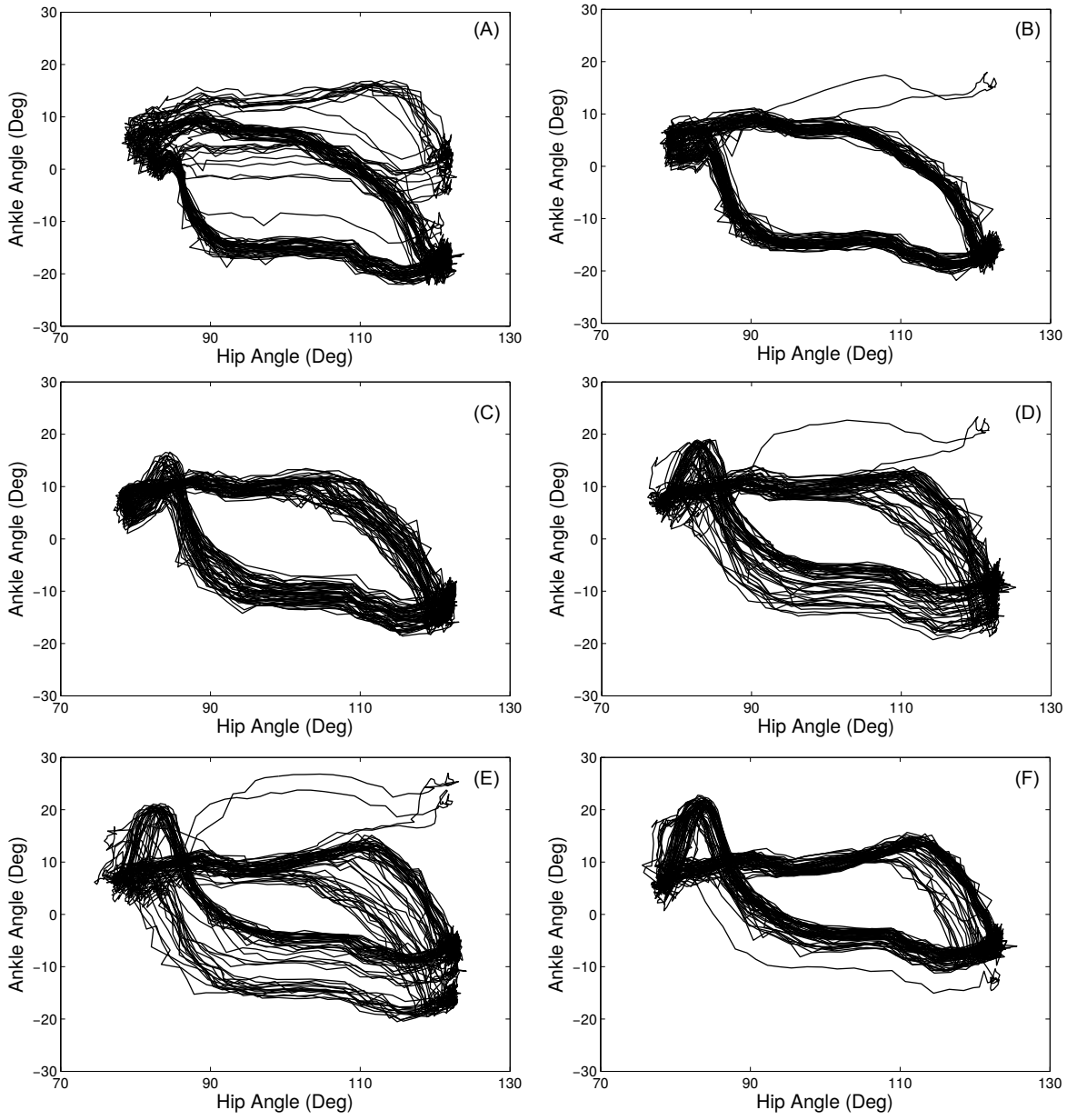

Figure C.4: The plots of ankle angular motion versus hip angular motion with various values of $\omega_{GI\rightarrow L/R,\ A,\ P_{HO}}$ during gait cycle. (A): $\omega_{GI\rightarrow L/R,\ A,\ P_{HO}} = 0$. (B): $\omega_{GI\rightarrow L/R,\ A,\ P_{HO}} = 0.25$. (C): $\omega_{GI\rightarrow L/R,\ A,\ P_{HO}} = 0.5$. (D): $\omega_{GI\rightarrow L/R,\ A,\ P_{HO}} = 0.75$. (E): $\omega_{GI\rightarrow L/R,\ A,\ P_{HO}} = 1$. (F): $\omega_{GI\rightarrow L/R,\ A,\ P_{HO}} = 1.25$. Note here $\alpha_{L/R,\ H} = 1.3$.

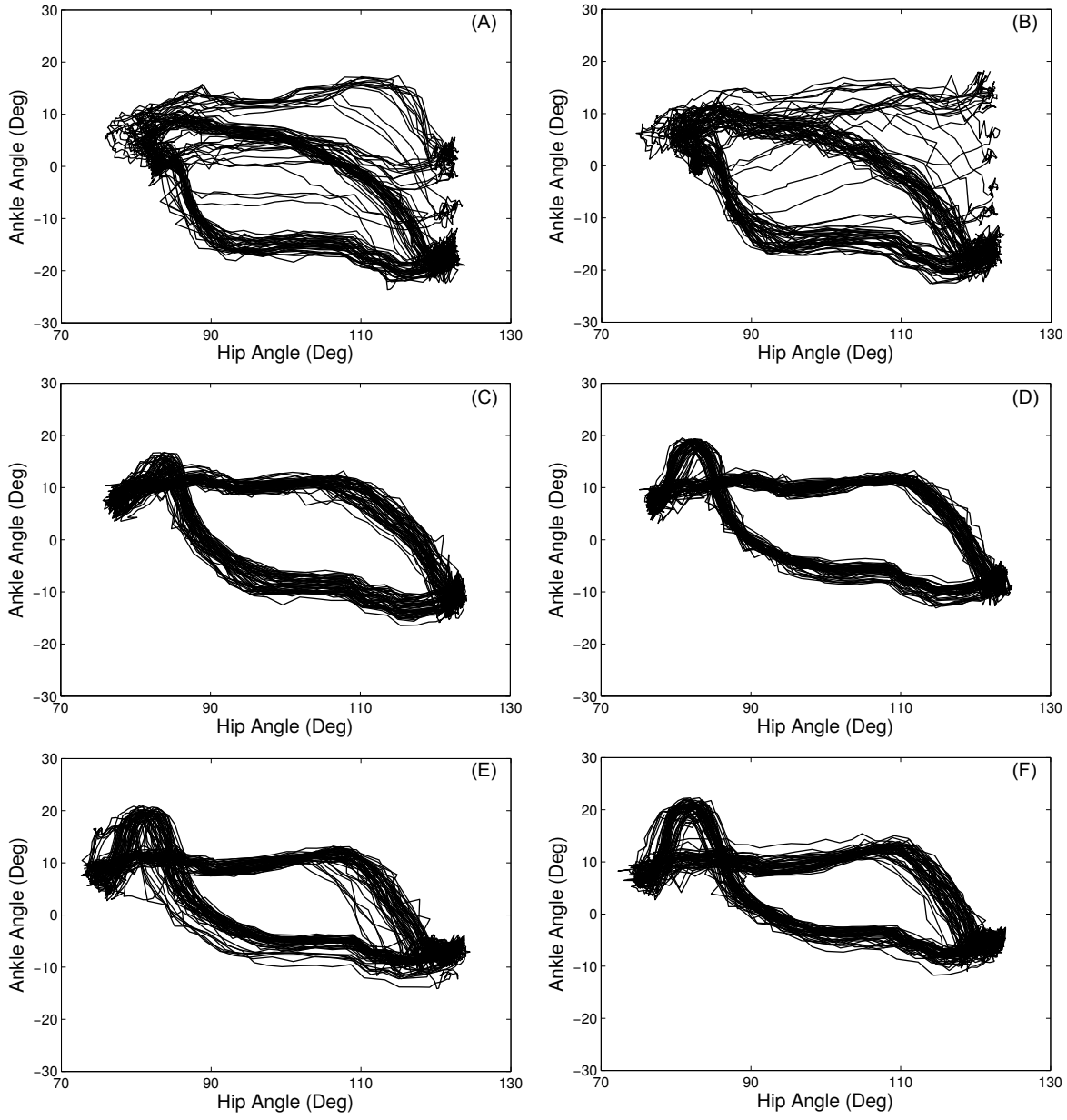

Figure C.5: The plots of ankle angular motion versus hip angular motion with various values of $\omega_{GI\rightarrow L/R,\ A,\ P_{HO}}$ during gait cycle. (A): $\omega_{GI\rightarrow L/R,\ A,\ P_{HO}} = 0$. (B): $\omega_{GI\rightarrow L/R,\ A,\ P_{HO}} = 0.25$. (C): $\omega_{GI\rightarrow L/R,\ A,\ P_{HO}} = 0.5$. (D): $\omega_{GI\rightarrow L/R,\ A,\ P_{HO}} = 0.75$. (E): $\omega_{GI\rightarrow L/R,\ A,\ P_{HO}} = 1$. (F): $\omega_{GI\rightarrow L/R,\ A,\ P_{HO}} = 1.25$. Note here $\alpha_{L/R,\ H} = 1.4$

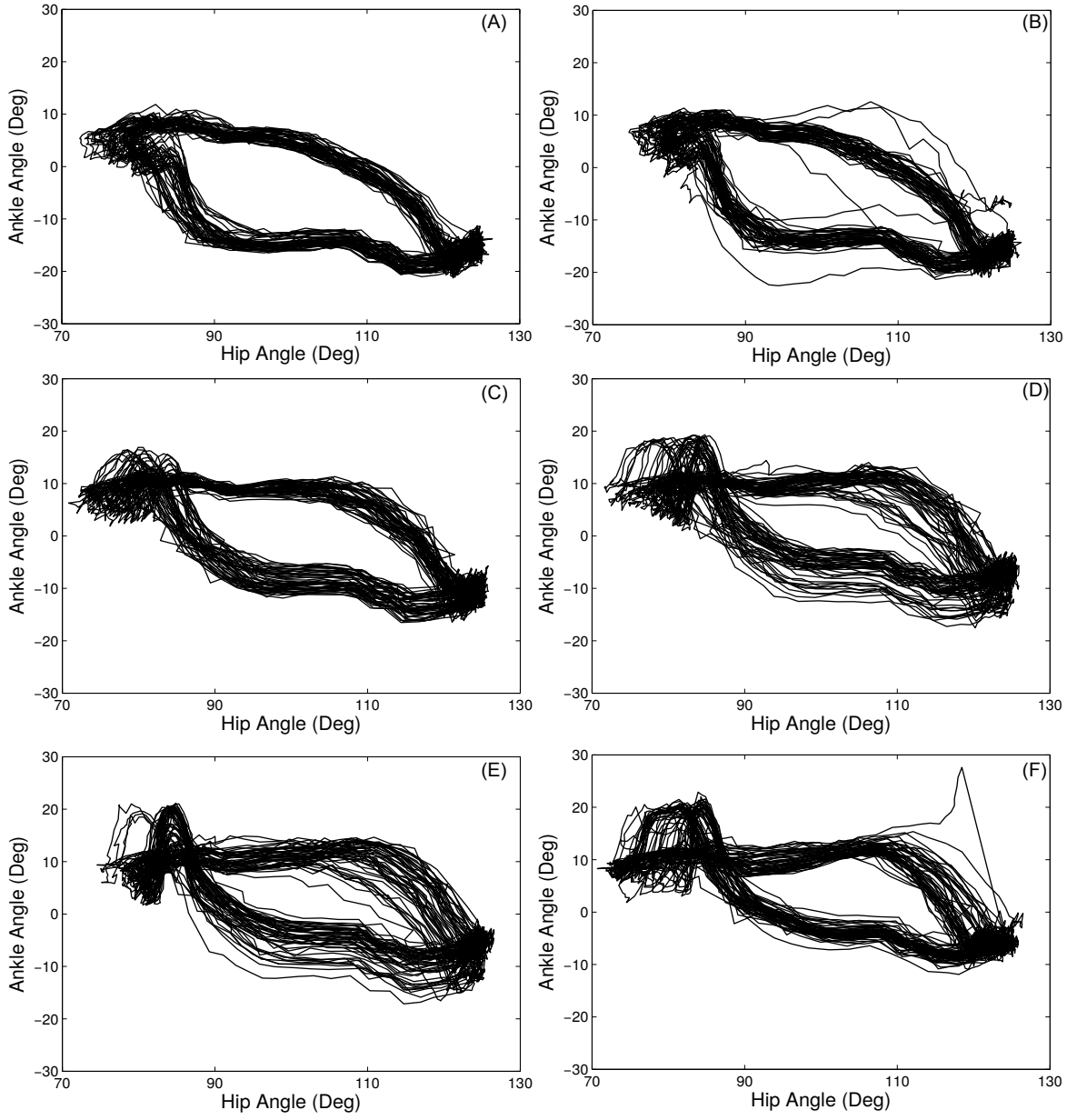

Figure C.6: The plots of ankle angular motion versus hip angular motion with various values of $\omega_{GI\rightarrow L/R,\ A,\ P_{HO}}$ during gait cycle. (A): $\omega_{GI\rightarrow L/R,\ A,\ P_{HO}} = 0$. (B): $\omega_{GI\rightarrow L/R,\ A,\ P_{HO}} = 0.25$. (C): $\omega_{GI\rightarrow L/R,\ A,\ P_{HO}} = 0.5$. (D): $\omega_{GI\rightarrow L/R,\ A,\ P_{HO}} = 0.75$. (E): $\omega_{GI\rightarrow L/R,\ A,\ P_{HO}} = 1$. (F): $\omega_{GI\rightarrow L/R,\ A,\ P_{HO}} = 1.25$. Note here $\alpha_{L/R,\ H} = 1.6$

Appendix D

Supplementary material of the FES experiment

Table D.1: parameters measured in the FES setup. Three parameters were measured for each muscle, namely Perception Threshold Current (PTC), Minimal Threshold Current (MinTC) and Maximal Threshold Current (MaxTC). Four muscles of each leg were chosen in the study. They are the Tibialis Anterior (TA), Lateral Gastrocnemius (LG), Biceps Femoris (BF) and Rectus Femoris (RF). The unit of the parameters is mA.

Subjects		LTA	LLG	LBF	LRF	RTA	RLG	RBF	RRF
A	PTC	4	3	5	4	4	4	4	4
	MinTC	10	16	15	15	12	11	18	15
	MaxTC	20	23	26	20	18	14	23	22
B	PTC	4	4	4	4	4	3	4	4
	MinTC	6	14	9	12	10	12	10	14
	MaxTC	24	29	22	22	23	25	22	24
C	PTC	4	4	4	4	4	4	5	5
	MinTC	8	8	10	10	6	7	10	10
	MaxTC	13	13	15	16	10	10	14	14
D	PTC	4	4	8	6	4	4	6	6
	MinTC	10	10	17	6	10	14	14	18
	MaxTC	15	15	23	18	23	23	25	26

E	PTC	4	4	6	5	4	4	6	6
	MinTC	8	8	14	14	8	8	14	14
	MaxTC	21	20	22	23	15	26	24	24
F	PTC	5	7	7	6	5	7	7	5
	MinTC	10	12	16	18	11	16	24	16
	MaxTC	24	24	27	30	24	27	30	30
G	PTC	4	4	6	4	4	4	6	4
	MinTC	13	6	14	12	14	10	11	10
	MaxTC	22	20	24	28	24	24	25	28

Table D.2: Time in seconds of early stance phase, late stance phase and stride in both conditions (no stimulation vs stimulation).

		A	D	F	G
Normal Treadmill Walking	Early Stance	0.7797 ± 0.1280	0.6993 ± 0.0487	0.9232 ± 0.0706	0.6323 ± 0.0227
	Late Stance	0.2510 ± 0.0505	0.2947 ± 0.418	0.3121 ± 0.597	0.4833 ± 0.0314
	Stride	1.4087 ± 0.1049	1.5373 ± 0.0455	1.9236 ± 0.0692	1.6813 ± 0.0293
Stimulated Treadmill Walking	Early Stance	0.7763 ± 0.0470	0.6740 ± 0.0450	0.7371 ± 0.1031	0.5770 ± 0.0199
	Late Stance	0.1543 ± 0.0213	0.2437 ± 0.436	0.5486 ± 0.0618	0.4653 ± 0.0205
	Stride	1.4550 ± 0.0327	1.4470 ± 0.0363	2.0414 ± 0.0715	1.5233 ± 0.0489

Table D.3: Means, standard deviation (SD) and statistical results for gait variables for all subjects for voluntary treadmill walking and FES-assisted treadmill walking.

Subject		Range of Ankle	Maximum of Ankle	Minimum of Ankle	Range of Knee	Maximum of Knee	Minimum of Knee	Range of Hip	Maximum of Hip	Minimum of Hip
A	NoStim	23.25 ± 1.65	11.12 ± 1.70	-12.13 ± 1.87	63.80 ± 2.29	63.62 ± 1.93	-0.19 ± 1.22	32.78 ± 3.05	112.21 ± 1.36	79.43 ± 2.33
	Stim	20.57 ± 2.34	12.79 ± 1.20	-7.79 ± 1.98	59.86 ± 3.18	58.67 ± 1.93	-1.19 ± 2.70	$28.92 \pm 1.73^{**}$	$111.14 \pm 1.46^{*}$	$82.22 \pm 1.50^{**}$
	p-value	$3.69E-06^{*}$	$4.91E-05^{*}$	$3.99E-12^{*}$	$8.85E-07^{*}$	$4.30E-14^{*}$	$6.83E-02$	$1.24E-07^{*}$	$4.93E-03$	$8.23E-07^{*}$
B	NoStim	18.41 ± 1.49	13.12 ± 1.14	-5.28 ± 1.73	51.64 ± 2.32	52.38 ± 2.86	0.74 ± 1.07	33.33 ± 1.01	108.50 ± 1.16	75.17 ± 1.16
	Stim	13.95 ± 1.52	15.33 ± 1.99	1.39 ± 1.97	39.64 ± 3.98	44.36 ± 3.93	4.72 ± 1.18	29.70 ± 1.73	105.96 ± 1.25	76.26 ± 1.31
	p-value	$2.99E-13^{*}$	$5.25E-02$	$1.19E-19^{*}$	$1.94E-09^{*}$	$1.73E-06^{*}$	$2.71E-20^{*}$	$1.96E-08^{*}$	$3.25E-11^{*}$	$5.50E-04^{*}$
C	NoStim	23.26 ± 1.36	6.41 ± 1.26	-16.84 ± 1.46	54.13 ± 2.75	49.14 ± 2.35	-4.98 ± 1.68	27.65 ± 1.56	104.89 ± 0.93	77.23 ± 1.12
	Stim	28.42 ± 5.80	4.61 ± 1.90	-23.80 ± 6.54	61.10 ± 4.24	56.96 ± 3.66	-4.98 ± 1.68	28.41 ± 4.20	107.76 ± 1.95	79.34 ± 3.59
	p-value	$1.41E-05^{*}$	$6.08E-05^{*}$	$4.35E-07^{*}$	$3.33E-10^{*}$	$5.60E-14^{*}$	$4.47E-02$	$3.60E-01$	$1.07E-09^{*}$	$3.18E-03^{*}$
D	NoStim	25.50 ± 1.07	12.60 ± 1.00	-12.91 ± 0.75	70.40 ± 1.26	67.37 ± 1.33	-3.03 ± 0.29	35.48 ± 1.00	114.35 ± 0.79	78.86 ± 0.59
	Stim	27.21 ± 1.56	13.38 ± 1.51	-13.83 ± 1.18	75.98 ± 2.54	73.38 ± 2.30	-2.60 ± 0.64	40.56 ± 2.65	122.29 ± 2.56	81.83 ± 1.83
	p-value	$7.38E-06^{*}$	$2.24E-02$	$5.99E-04^{*}$	$1.85E-15^{*}$	$1.24E-18^{*}$	$1.35E-03^{*}$	$1.32E-13^{*}$	$2.92E-23^{*}$	$1.13E-11^{*}$
E	NoStim	17.43 ± 0.97	10.09 ± 0.61	-7.34 ± 0.92	57.30 ± 1.36	64.73 ± 1.35	7.43 ± 0.82	29.01 ± 0.58	115.72 ± 0.52	86.70 ± 0.53
	Stim	20.91 ± 1.53	11.56 ± 0.71	-9.34 ± 1.52	57.51 ± 1.20	66.52 ± 1.07	9.01 ± 1.23	32.37 ± 1.27	118.43 ± 1.14	86.06 ± 0.94
	p-value	$4.98E-15^{*}$	$6.54E-12^{*}$	$6.90E-08^{*}$	$5.19E-01$	$4.34E-07^{*}$	$2.56E-07^{*}$	$4.27E-19^{*}$	$3.88E-17^{*}$	$1.84E-03^{*}$
F	NoStim	24.95 ± 1.36	17.84 ± 0.76	-7.11 ± 1.04	60.13 ± 2.14	67.72 ± 2.24	7.59 ± 0.53	29.90 ± 1.68	114.52 ± 1.48	84.62 ± 0.80
	Stim	31.79 ± 2.14	22.87 ± 1.65	-8.93 ± 1.86	57.00 ± 2.18	65.25 ± 2.25	8.25 ± 0.89	36.79 ± 1.87	115.37 ± 1.57	78.57 ± 1.01
	p-value	$2.33E-21^{*}$	$8.15E-22^{*}$	$1.86E-05^{*}$	$6.09E-07^{*}$	$7.67E-07^{*}$	$9.27E-04^{*}$	$1.12E-12^{*}$	$3.61E-02$	$1.79E-33^{*}$
G	NoStim	21.50 ± 1.43	11.70 ± 0.92	-9.80 ± 1.45	59.75 ± 1.84	63.39 ± 1.61	3.64 ± 0.70	35.59 ± 1.91	111.43 ± 1.25	75.84 ± 1.29
	Stim	28.20 ± 2.48	14.18 ± 1.73	-14.02 ± 2.30	68.10 ± 1.61	72.18 ± 1.59	4.08 ± 0.60	37.85 ± 1.13	115.61 ± 0.97	77.76 ± 0.52
	p-value	$1.43E-18^{*}$	$4.00E-09^{*}$	$8.85E-12^{*}$	$3.38E-26^{*}$	$4.56E-29^{*}$	$1.09E-02$	$6.57E-07^{*}$	$6.26E-21^{*}$	$3.22E-10^{*}$

* = $p < 0.004$

Bibliography

[1] S. A. Kimmel and M. H. Schwartz, "A baseline of dynamic muscle function during gait," *Gait & posture*, vol. 23, no. 2, pp. 211–221, 2006.

[2] S. C. Kirshblum, S. P. Burns, F. Biering-Sorensen, W. Donovan, D. E. Graves, A. Jha, M. Johansen, L. Jones, A. Krassioukov, M. Mulcahey *et al.*, "International standards for neurological classification of spinal cord injury (revised 2011)," *The Journal of Spinal Cord Medicine*, vol. 34, no. 6, pp. 535–546, 2011.

[3] E. P. Zehr and R. B. Stein, "What functions do reflexes serve during human locomotion?" *Progress in Neurobiology*, vol. 58, no. 2, pp. 185–205, 1999.

[4] D. G. Hobbelen, *Limit cycle walking*. TU Delft, Delft University of Technology, 2008.

[5] T. Geng, B. Porr, and F. Wörgötter, "Fast biped walking with a reflexive controller and real-time policy searching," *Advances in Neural Information Processing Systems*, vol. 18, p. 427, 2006.

[6] T. Geng, B. Porr, and B. Florentinwörgötter, "A reflexive neural network for dynamic biped walking control," *Neural Computation*, vol. 18, no. 5, pp. 1156–1196, 2006.

[7] T. Geng, "Fast biped walking with a neuronal controller and physical computation," Ph.D. dissertation, University of Stirling, 2007.

[8] J. Mehrholz, J. Kugler, and M. Pohl, "Locomotor training for walking after spinal cord injury," *The Cochrane Library*, 2008.

[9] K. L. Moore, A. F. Dalley, and A. M. Agur, *Clinically oriented anatomy*. Lippincott Williams & Wilkins, 2013.

[10] S. P. Burns, D. G. Golding, W. A. Rolle, V. Graziani, and J. F. Ditunno, "Recovery of ambulation in motor-incomplete tetraplegia," *Archives of Physical Medicine and Rehabilitation*, vol. 78, no. 11, pp. 1169–1172, 1997.

[11] K. S. Crozier, V. Graziani, J. Ditunno Jr, and G. J. Herbison, "Spinal cord injury: prognosis for ambulation based on sensory examination in patients who are initially motor complete." *Archives of Physical Medicine and Rehabilitation*, vol. 72, no. 2, pp. 119–121, 1991.

[12] V. Dietz and K. Fouad, "Restoration of sensorimotor functions after spinal cord injury," *Brain*, vol. 137, no. 3, pp. 654–667, 2014.

[13] V. Dietz, G. Colombo, L. Jensen, and L. Baumgartner, "Locomotor capacity of spinal cord in paraplegic patients," *Annals of Neurology*, vol. 37, no. 5, pp. 574–582, 1995.

[14] A. L. Behrman and S. J. Harkema, "Locomotor training after human spinal cord injury: a series of case studies," *Physical Therapy*, vol. 80, no. 7, pp. 688–700, 2000.

[15] M. Visintin and H. Barbeau, "The effects of body weight support on the locomotor pattern of spastic paretic patients." *The Canadian Journal of Neurological Sciences.*, vol. 16, no. 3, pp. 315–325, 1989.

[16] A. Wernig and S. Müller, "Laufband locomotion with body weight support improved walking in persons with severe spinal cord injuries," *Spinal Cord*, vol. 30, no. 4, pp. 229–238, 1992.

[17] A. Wernig, S. Müller, A. Nanassy, and E. Cagol, "Laufband therapy based on ?rules of spinal locomotion?is effective in spinal cord injured persons," *European Journal of Neuroscience*, vol. 7, no. 4, pp. 823–829, 1995.

[18] G. Colombo, M. Wirz, V. Dietz *et al.*, "Driven gait orthosis for improvement of locomotor training in paraplegic patients," *Spinal Cord*, vol. 39, no. 5, pp. 252–255, 2001.

[19] K. Ragnarsson, "Functional electrical stimulation after spinal cord injury: current use, therapeutic effects and future directions," *Spinal Cord*, vol. 46, no. 4, pp. 255–274, 2008.

[20] B. Kakulas, "Neuropathology: the foundation for new treatments in spinal cord injury," *Spinal Cord*, vol. 42, no. 10, pp. 549–563, 2004.

[21] P. Peckham, J. Mortimer, and E. Marsolais, "Alteration in the force and fatigability of skeletal muscle in quadriplegic humans following exercise induced by chronic electrical stimulation." *Clinical Orthopaedics and Related Research*, vol. 114, pp. 326–334, 1976.

[22] J. Chae and D. Yu, "Neuromuscular stimulation for motor relearning in hemiplegia," *Critical Reviews? in Physical and Rehabilitation Medicine*, vol. 11, no. 3&4, 1999.

[23] A. Kantrowitz, "Electronic physiologic aids," *Report of the Maimonides Hospital*, pp. 4–5, 1960.

[24] R. Kobetic and E. B. Marsolais, "Synthesis of paraplegic gait with multichannel functional neuromuscular stimulation," *IEEE Transactions on Rehabilitation Engineering*, vol. 2, no. 2, pp. 66–79, 1994.

[25] R. Kobetic, R. J. Triolo, J. P. Uhlir, C. Bieri, M. Wibowo, G. Polando, E. B. Marsolais, J. Davis, K. Ferguson, M. Sharma *et al.*, "Implanted functional electrical stimulation system for mobility in paraplegia: a follow-up case report," *IEEE Transactions on Rehabilitation Engineering*, vol. 7, no. 4, pp. 390–398, 1999.

[26] J. W. McDonald and C. Sadowsky, "Spinal-cord injury," *The Lancet*, vol. 359, no. 9304, pp. 417–425, 2002.

[27] J. B. Nielsen, "How we walk: central control of muscle activity during human walking," *The Neuroscientist*, vol. 9, no. 3, pp. 195–204, 2003.

[28] N. Bernstein, *The co-ordination and regulation of movements*. Pergamon-Press, 1967.

[29] T. G. Brown, "The intrinsic factors in the act of progression in the mammal," *Proceedings of the Royal Society of London B: Biological Sciences*, vol. 84, no. 572, pp. 308–319, 1911.

[30] A. Lundberg, "Multisensory control of spinal reflex pathways," in *Reflex Control of Posture and Movement: Proceedings of IBRO Symposium Held in Pisa, Italy, on September 11-14, 1978*, vol. 50. Elsevier, 1979, p. 11.

[31] S. Grillner, "Neurobiological bases of rhythmic motor acts in vertebrates," *Science*, vol. 228, no. 4696, pp. 143–149, 1985.

[32] B. Fedirchuk, J. Nielsen, N. Petersen, and H. Hultborn, "Pharmacologically evoked fictive motor patterns in the acutely spinalized marmoset monkey (callithrix jacchus)," *Experimental Brain Research*, vol. 122, no. 3, pp. 351–361, 1998.

[33] S. Rossignol, "Locomotion and its recovery after spinal injury," *Current Opinion in Neurobiology*, vol. 10, no. 6, pp. 708–716, 2000.

[34] S. Grillner and P. Zangger, "On the central generation of locomotion in the low spinal cat," *Experimental Brain Research*, vol. 34, no. 2, pp. 241–261, 1979.

[35] B. Bussel, A. Roby-Brami, O. Neris, and A. Yakovleff, "Evidence for a spinal stepping generator in man. electrophysiological study." *Acta Neurobiologiae Experimentalis*, vol. 56, no. 1, pp. 465–468, 1995.

[36] M. R. Dimitrijevic, Y. Gerasimenko, and M. M. Pinter, "Evidence for a spinal central pattern generator in humans," *Annals of the New York Academy of Sciences*, vol. 860, no. 1, pp. 360–376, 1998.

[37] H. Forssberg, "Ontogeny of human locomotor control i. infant stepping, supported locomotion and transition to independent locomotion," *Experimental Brain Research*, vol. 57, no. 3, pp. 480–493, 1985.

[38] S. Rossignol, *Neural Control of Stereotypic Limb Movements*. John Wiley & Sons, Inc., 2010.

[39] R. A. Kuhn, "Functional capacity of the isolated human spinal cord," *Brain*, vol. 73, no. 1, pp. 1–51, 1950.

[40] Y. Sqalli-Houssaini, J. R. Cazalets, and F. Clarac, "Oscillatory properties of the central pattern generator for locomotion in neonatal rats," *Journal of Neurophysiology*, vol. 70, no. 2, pp. 803–813, 1993.

[41] R. M. Harris-Warrick and A. H. Cohen, "Serotonin modulates the central pattern generator for locomotion in the isolated lamprey spinal cord," *Journal of Experimental Biology*, vol. 116, no. 1, pp. 27–46, 1985.

[42] S. Grillner, T. Deliagina, A. El Manira, R. Hill, G. Orlovsky, P. Wallén, Ö. Ekeberg, and A. Lansner, "Neural networks that co-ordinate locomotion and body orientation in lamprey," *Trends in Neurosciences*, vol. 18, no. 6, pp. 270–279, 1995.

[43] A. Cohen and P. Wallén, "The neuronal correlate of locomotion in fish," *Experimental Brain Research*, vol. 41, no. 1, pp. 11–18, 1980.

[44] T. G. Brown, "On the nature of the fundamental activity of the nervous centres; together with an analysis of the conditioning of rhythmic activity in progression, and a theory of the evolution of function in the nervous system," *The Journal of Physiology*, vol. 48, no. 1, p. 18, 1914.

[45] E. Marder and D. Bucher, "Central pattern generators and the control of rhythmic movements," *Current Biology*, vol. 11, no. 23, pp. 986–996, 2001.

[46] S. Grillner, "Control of locomotion in bipeds, tetrapods, and fish," in *Comprehensive Physiology*. John Wiley & Sons, Inc., 2011.

[47] H. Barbeau and S. Rossignol, "Recovery of locomotion after chronic spinalization in the adult cat," *Brain Research*, vol. 412, no. 1, pp. 84 – 95, 1987.

[48] M. Belanger, T. Drew, J. Provencher, and S. Rossignol, "A comparison of treadmill locomotion in adult cats before and after spinal transection," *Journal of Neurophysiology*, vol. 76, no. 1, pp. 471–491, 1996.

[49] L. Bouyer and S. Rossignol, "Contribution of cutaneous inputs from the hindpaw to the control of locomotion. ii. spinal cats," *Journal of Neurophysiology*, vol. 90, no. 6, pp. 3640–3653, 2003.

[50] S. Rossignol, R. Dubuc, and J.-P. Gossard, "Dynamic sensorimotor interactions in locomotion," *Physiological Reviews*, vol. 86, no. 1, pp. 89–154, 2005.

[51] J. Duysens, F. Clarac, and H. Cruse, "Load-regulating mechanisms in gait and posture: Comparative aspects," *Physiological Reviews*, vol. 80, no. 1, pp. 83–133, 2000.

[52] K. G. Pearson, J. E. Misiaszek, and K. Fouad, "Enhancement and resetting of locomotor activity by muscle afferents," *Annals of the New York Academy of Sciences*, vol. 860, no. 1, pp. 203–215, 1998.

[53] S. Grillner and S. Rossignol, "On the initiation of the swing phase of locomotion in chronic spinal cats," *Brain Research*, vol. 146, no. 2, pp. 269–277, 1978.

[54] J. Duysens and K. Pearson, "Inhibition of flexor burst generation by loading ankle extensor muscles in walking cats," *Brain Research*, vol. 187, no. 2, pp. 321–332, 1980.

[55] R. E. Kearney, M. Lortie, and R. B. Stein, "Modulation of stretch reflexes during imposed walking movements of the human ankle," *Journal of Neurophysiology*, vol. 81, no. 6, pp. 2893–2902, 1999.

[56] V. Dietz and J. Duysens, "Significance of load receptor input during locomotion: a review," *Gait & Posture*, vol. 11, no. 2, pp. 102–110, April 2000.

[57] T. Sinkjær, J. B. Andersen, M. Ladouceur, L. O. Christensen, and J. B. Nielsen, "Major role for sensory feedback in soleus emg activity in the stance phase of walking in man," *The Journal of Physiology*, vol. 523, no. 3, pp. 817–827, 2000.

[58] H. Hultborn and J. B. Nielsen, "Spinal control of locomotion – from cat to man," *Acta Physiologica*, vol. 189, no. 2, pp. 111–121, 2007.

[59] E. Eidelberg, J. Walden, and L. Nguyen, "Locomotor control in macaque monkeys," *Brain*, vol. 104, no. 4, pp. 647–663, 1981.

[60] J. G. Nicholls, A. R. Martin, B. G. Wallace, and P. A. Fuchs, *From neuron to brain*. Sinauer Associates Sunderland, MA, 2001, vol. 271.

[61] M. L. Shik and G. N. Orlovsky, "Neurophysiology of locomotor automatism," *Physiological Reviews*, vol. 56, no. 3, pp. 465–501, 1976.

[62] A. Lundberg, *Reflex control of stepping*. Universitetsforlaget, 1969, vol. 5.

[63] K. Akazawa, J. W. Aldridge, J. D. Steeves, and R. B. Stein, "Modulation of stretch reflexes during locomotion in the mesencephalic cat," *The Journal of Physiology*, vol. 329, no. 1, pp. 553–567, 1982.

[64] C. Capaday and R. Stein, "Amplitude modulation of the soleus h-reflex in the human during walking and standing," *The Journal of Neuroscience*, vol. 6, no. 5, pp. 1308–1313, 1986.

[65] J. Yang, R. Stein, and K. James, "Contribution of peripheral afferents to the activation of the soleus muscle during walking in humans," *Experimental Brain Research*, vol. 87, no. 3, pp. 679–687, 1991.

[66] J. F. Yang, M. J. Stephens, and R. Vishram, "Infant stepping: a method to study the sensory control of human walking," *The Journal of Physiology*, vol. 507, no. 3, pp. 927–937, 1998.

[67] M. Y. C. Pang and J. F. Yang, "The initiation of the swing phase in human infant stepping: importance of hip position and leg loading," *The Journal of Physiology*, vol. 528, no. 2, pp. 389–404, 2000.

[68] J. Donelan and K. Pearson, "Contribution of sensory feedback to ongoing ankle extensor activity during the stance phase of walking," *Canadian Journal of Physiology and Pharmacology*, vol. 82, no. 8-9, pp. 589–598, 2004.

[69] V. Dietz, "Spinal cord pattern generators for locomotion," *Clinical Neurophysiology*, vol. 114, no. 8, pp. 1379–1389, 2003.

[70] L. Jensen, T. Prokop, and V. Dietz, "Adaptational effects during human split-belt walking: influence of afferent input," *Experimental Brain Research*, vol. 118, no. 1, pp. 126–130, 1998.

[71] L. J. BOUYER and S. ROSSIGNOL, "The contribution of cutaneous inputs to locomotion in the intact and the spinal cat," *Annals of the New York Academy of Sciences*, vol. 860, no. 1, pp. 508–512, 1998.

[72] L. Bouyer and S. Rossignol, "Contribution of cutaneous inputs from the hindpaw to the control of locomotion. i. intact cats," *Journal of Neurophysiology*, vol. 90, no. 6, pp. 3625–3639, 2003.

[73] H. Forssberg, "Stumbling corrective reaction: a phase-dependent compensatory reaction during locomotion," *Journal of Neurophysiology*, vol. 42, no. 4, pp. 936–953, 1979.

[74] H. Forssberg, S. Grillner, and S. Rossignol, "Phase dependent reflex reversal during walking in chronic spinal cats," *Brain Research*, vol. 85, no. 1, pp. 103–107, 1975.

[75] J. Eng, D. Winter, and A. Patla, "Strategies for recovery from a trip in early and late swing during human walking," *Experimental Brain Research*, vol. 102, no. 2, pp. 339–349, 1994.

[76] E. Zehr, T. Komiyama, and R. Stein, "Cutaneous reflexes during human gait: electromyographic and kinematic responses to electrical stimulation," *Journal of Neurophysiology*, vol. 77, no. 6, pp. 3311–3325, 1997.

[77] J. Duysens, A. Tax, M. Trippel, and V. Dietz, "Phase-dependent reversal of reflexly induced movements during human gait," *Experimental Brain Research*, vol. 90, no. 2, pp. 404–414, 1992.

[78] A. Schillings, B. Van Wezel, and J. Duysens, "Mechanically induced stumbling during human treadmill walking," *Journal of Neuroscience Methods*, vol. 67, no. 1, pp. 11–17, 1996.

[79] V. Dietz, J. Quintern, G. Boos, and W. Berger, "Obstruction of the swing phase during gait: phase-dependent bilateral leg muscle coordination," *Brain Research*, vol. 384, no. 1, pp. 166–169, 1986.

[80] B. Conway, H. Hultborn, and O. Kiehn, "Proprioceptive input resets central locomotor rhythm in the spinal cat," *Experimental Brain Research*, vol. 68, no. 3, pp. 643–656, 1987.

[81] T. McGeer, "Passive dynamic walking," *The International Journal of Robotics Research*, vol. 9, no. 2, pp. 62–82, 1990.

[82] M. Garcia, A. Chatterjee, A. Ruina, and M. Coleman, "The simplest walking model: Stability, complexity, and scaling," *Journal of Biomechanical Engineering*, vol. 120, no. 2, pp. 281–288, 1998.

[83] S. H. Collins, M. Wisse, and A. Ruina, "A three-dimensional passive-dynamic walking robot with two legs and knees," *The International Journal of Robotics Research*, vol. 20, no. 7, pp. 607–615, 2001.

[84] S. H. Collins and A. Ruina, "A bipedal walking robot with efficient and human-like gait," in *Proceedings of the 2005 IEEE International Conference on Robotics and Automation*. IEEE, April 2005, pp. 1983–1988.

[85] M. Wisse, "Three additions to passive dynamic walking: actuation, an upper body, and 3d stability," *International Journal of Humanoid Robotics*, vol. 2, no. 04, pp. 459–478, 2005.

[86] M. Wisse and J. Van Frankenhuyzen, "Design and construction of mike; a 2-d autonomous biped based on passive dynamic walking," in *Adaptive motion of animals and machines*. Springer, 2006, pp. 143–154.

[87] M. Wisse, R. Schwab, A.L.and van der Linde, and F. van der Helm, "How to keep from falling forward: elementary swing leg action for passive dynamic walkers," *IEEE Transactions on Robotics*, vol. 21, no. 3, pp. 393–401, June 2005.

[88] Y. Hrmzl and G. Moskowitz, "The role of impact in the stability of bipedal locomotion," *Dynamics and Stability of Systems*, vol. 1, no. 3, pp. 217–234, 1986.

[89] I. Kato, S. Ohteru, H. Kobayashi, K. Shirai, and A. Uchiyama, "Information-power machine with senses and limbs," in *On Theory and Practice of Robots and Manipulators*, ser. International Centre for Mechanical Sciences. Springer Vienna, 1974, vol. 201, pp. 11–24.

[90] M. Vukobratović, "How to control artificial anthropomorphic systems," *IEEE Transactions on Systems, Man and Cybernetics*, no. 5, pp. 497–507, 1973.

[91] K. Hirai, M. Hirose, Y. Haikawa, and T. Takenaka, "The development of honda humanoid robot," in *IEEE International Conference on Robotics and Automation*, vol. 2. IEEE, May 1998, pp. 1321–1326.

[92] K. Kaneko, F. Kanehiro, S. Kajita, K. Yokoyama, K. Akachi, T. Kawasaki, S. Ota, and T. Isozumi, "Design of prototype humanoid robotics platform for hrp," in *IEEE/RSJ International Conference on Intelligent Robots and Systems*, vol. 3. IEEE, 2002, pp. 2431–2436.

[93] Y. Sakagami, R. Watanabe, C. Aoyama, S. Matsunaga, N. Higaki, and K. Fujimura, "The intelligent asimo: System overview and integration," in *IEEE/RSJ International Conference on Intelligent Robots and Systems*, vol. 3. IEEE, 2002, pp. 2478–2483.

[94] F. Iida, J. Rummel, and A. Seyfarth, "Bipedal walking and running with spring-like biarticular muscles," *Journal of Biomechanics*, vol. 41, no. 3, pp. 656 – 667, 2008.

[95] G. Taga, Y. Yamaguchi, and H. Shimizu, "Self-organized control of bipedal locomotion by neural oscillators in unpredictable environment," *Biological Cybernetics*, vol. 65, no. 3, pp. 147–159, 1991.

[96] S. Miyakoshi, G. Taga, Y. Kuniyoshi, and A. Nagakubo, "Three dimensional bipedal stepping motion using neural oscillators-towards humanoid motion in the real world," in *Proceedings., 1998 IEEE/RSJ International Conference on Intelligent Robots and Systems*, vol. 1, Oct 1998, pp. 84–89.

[97] J. Nakanishi, J. Morimoto, G. Endo, G. Cheng *et al.*, "Learning from demonstration and adaptation of biped locomotion," *Robotics and Autonomous Systems*, vol. 47, no. 2, pp. 79–91, 2004.

[98] S. Aoi and K. Tsuchiya, "Stability analysis of a simple walking model driven by an oscillator with a phase reset using sensory feedback," *IEEE Transactions on Robotics*, vol. 22, no. 2, pp. 391–397, April 2006.

[99] T. Matsubara, J. Morimoto, J. Nakanishi, M. aki Sato, and K. Doya, "Learning cpg-based biped locomotion with a policy gradient method," *Robotics and Autonomous Systems*, vol. 54, no. 11, pp. 911 – 920, 2006, planning Under Uncertainty in Robotics.

[100] L. Righetti and A. Ijspeert, "Programmable central pattern generators: an application to biped locomotion control," in *Proceedings 2006 IEEE International Conference on Robotics and Automation*, May 2006, pp. 1585–1590.

[101] G. Endo, J. Morimoto, T. Matsubara, J. Nakanishi, and G. Cheng, "Learning cpg-based biped locomotion with a policy gradient method: Application to a humanoid robot," *International Journal of Robotics Research*, vol. 27, no. 2, pp. 213–228, 2008.

[102] J. Pratt, C. Chew, A. Torres, P. Dilworth *et al.*, "Virtual model control: An intuitive approach for bipedal locomotion," *International Journal of Robotics Research*, vol. 20, no. 2, pp. 129–143, 2001.

[103] A. Seyfarth, F. Iida, R. Tausch, M. Stelzer *et al.*, "Towards bipedal jogging as a natural result of optimizing walking speed for passively compliant three-segmented legs," *International Journal of Robotics Research*, vol. 28, no. 2, pp. 257–265, 2009.

[104] J. Pratt, T. Koolen, T. de Boer, J. Rebula, S. Cotton, J. Carff, M. Johnson, and P. Neuhaus, "Capturability-based analysis and control of legged locomotion, part 2: Application to m2v2, a lower body humanoid," *The International Journal of Robotics Research*, vol. 31, no. 10, pp. 1117–1133, September 2012.

[105] H. Park, K. Sreenath, A. Ramezani, and J. Grizzle, "Switching control design for accommodating large step-down disturbances in bipedal robot walking," in *IEEE International Conference on Robotics and Automation*, 2012.

[106] K. Sreenath, H.-W. Park, and J. Grizzle, "Design and experimental implementation of a compliant hybrid zero dynamics controller with active force control for running on mabel," in *2012 IEEE International Conference on Robotics and Automation (ICRA)*. Saint Paul, MN: IEEE, May 2012, pp. 51–56.

[107] R. Q. van der Linde, "Passive bipedal walking with phasic muscle contraction," *Biological Cybernetics*, vol. 81, no. 3, pp. 227–237, 1999.

[108] H. Geyer, A. Seyfarth, and R. Blickhan, "Positive force feedback in bouncing gaits?" *Proceedings of the Royal Society of London B: Biological Sciences*, vol. 270, no. 1529, pp. 2173–2183, 2003.

[109] H. Geyer and H. Herr, "A muscle-reflex model that encodes principles of legged mechanics produces human walking dynamics and muscle activities," *IEEE Transactions on Neural Systems and Rehabilitation Engineering*, vol. 18, no. 3, pp. 263–273, 2010.

[110] T. J. Klein, "A neurorobotic model of humanoid walking," Ph.D. dissertation, The University of Arizona, 2011.

[111] B. Webb, "Can robots make good models of biological behaviour?" *Behavioral and Brain Sciences*, vol. 24, no. 06, pp. 1033–1050, 2001.

[112] A. J. Ijspeert, A. Crespi, D. Ryczko, and J.-M. Cabelguen, "From swimming to walking with a salamander robot driven by a spinal cord model," *Science*, vol. 315, no. 5817, pp. 1416–1420, 2007.

[113] A. J. Ijspeert, "Central pattern generators for locomotion control in animals and robots: a review," *Neural Networks*, vol. 21, no. 4, pp. 642–653, 2008.

[114] P. H. Peckham and J. S. Knutson, "Functional electrical stimulation for neuromuscular applications*," *Annual Review of Biomedical Engineering*, vol. 7, pp. 327–360, 2005.

[115] J. S. Knutson, G. G. Naples, P. H. Peckham, and M. W. Keith, "Electrode fracture rates and occurrences of infection and granuloma associated with percutaneous intramuscular electrodes in upper-limb functional electrical stimulation applications," *Journal of Rehabilitation Research and Development*, vol. 39, no. 6, pp. 671–684, 2002.

[116] S. P. Levine, R. L. Kett, M. Gross, B. Wilson, P. Cederna, and J. Juni, "Blood flow in the gluteus maximus of seated individuals during electrical muscle stimulation," *Archives of Physical Medicine and Rehabilitation*, vol. 71, no. 9, pp. 682–6, 1990.

[117] D. Graupe and K. H. Kohn, "Functional neuromuscular stimulator for short-distance ambulation by certain thoracic-level spinal-cord-injured paraplegics," *Surgical Neurology*, vol. 50, no. 3, pp. 202–207, 1998.

[118] L. Vodovnik, B. R. Bowman, and P. Hufford, "Effects of electrical stimulation on spinal spasticity." *Scandinavian Journal of Rehabilitation Medicine*, vol. 16, no. 1, p. 29, 1984.

[119] E. Beaumont, E. Guevara, S. Dubeau, F. Lesage, M. Nagai, and M. Popovic, "Functional electrical stimulation post-spinal cord injury improves locomotion and increases afferent input into the central nervous system in rats," *The Journal of Spinal Cord Medicine*, vol. 37, no. 1, pp. 93–100, January 2014.

[120] W. T. Liberson, H. J. Holmquest, D. Scot, and M. Dow, "Functional electrotherapy: stimulation of the peroneal nerve synchronized with the swing phase of the gait of hemiplegic patients." *Archives of Physical Medicine and Rehabilitation*, vol. 42, pp. 101–105, Feb 1961.

[121] A. Kralj, T. Bajd, and R. Turk, "Electrical stimulation providing functional use of paraplegic patient muscles," *Medical Progress Through Technology*, vol. 7, no. 1, pp. 3–9, April 1980.

[122] T. Bajd, A. Kralj, R. Turk, H. Benko, and J. Šega, "The use of a four-channel electrical stimulator as an ambulatory aid for paraplegic patients," *Physical Therapy*, vol. 63, no. 7, pp. 1116–1120, 1983.

[123] Y.-L. Chen, W. H. Chang, M.-K. Wong, F.-T. Tang, H.-I. Chen, C.-S. Huang, and T.-S. Kuo, "A treadmill apparatus with a computer-assisted functional electrical stimulation system and foot switch control for restoration of ambulation in stroke patients," in *Proceedings of the 19th Annual International Conference of the IEEE Engineering in Medicine and Biology Society*, vol. 4. IEEE, 1997, pp. 1785–1787.

[124] M. M. Skelly and H. J. Chizeck, "Real-time gait event detection for paraplegic fes walking," *IEEE Transactions on Neural Systems and Rehabilitation Engineering*, vol. 9, no. 1, pp. 59–68, 2001.

[125] R. Williamson and B. J. Andrews, "Gait event detection for fes using accelerometers and supervised machine learning," *IEEE Transactions on Rehabilitation Engineering*, vol. 8, no. 3, pp. 312–319, 2000.

[126] I. P. Pappas, T. Keller, S. Mangold, M. R. Popovic, V. Dietz, and M. Morari, "A reliable gyroscope-based gait-phase detection sensor embedded in a shoe insole," *IEEE Sensors Journal*, vol. 4, no. 2, pp. 268–274, 2004.

[127] J. Kojović, M. Djurić-Jovičić, S. Došen, M. B. Popović, and D. B. Popović, "Sensor-driven four-channel stimulation of paretic leg: Functional electrical walking therapy," *Journal of Neuroscience Methods*, vol. 181, no. 1, pp. 100–105, 2009.

[128] C. Lynch and M. Popovic, "Closed-loop control for fes: Past work and future directions," in *10th Annual Conference of the International FES Society*, 2005, pp. 2–4.

[129] D. B. Popović, "Advances in functional electrical stimulation (fes)," *Journal of Electromyography and Kinesiology*, vol. 24, no. 6, pp. 795–802, 2014.

[130] R. Tomović and R. B. Mcghee, "A finite state approach to the synthesis of bioengineering control systems," *Human Factors in Electronics, IEEE Transactions on*, no. 2, pp. 65–69, 1966.

[131] G. M. Lyons, P. H. Veltink, and P. C. Sweeney, "Finite state control of functional electrical stimulation for the rehabilitation of gait," *Medical and Biological Engineering and Computing*, vol. 38, no. 2, pp. 121–126, 2000.

[132] B. Andrews, R. Baxendale, R. Barnett, G. Phillips, T. Yamazaki, J. Paul, and P. Freeman, "Hybrid fes orthosis incorporating closed loop control and sensory feedback," *Journal of biomedical engineering*, vol. 10, no. 2, pp. 189–195, 1988.

[133] D. Popovic, R. Tomovic, and L. Schwirtlich, "Hybrid assistive system-the motor neuroprosthesis," *IEEE Transactions on Biomedical Engineering*, vol. 36, no. 7, pp. 729–737, 1989.

[134] C. Kirkwood, B. Andrews, and P. Mowforth, "Automatic detection of gait events: a case study using inductive learning techniques," *Journal of Biomedical Engineering*, vol. 11, no. 6, pp. 511–516, 1989.

[135] A. Kostov, B. J. Andrews, D. B. Popović, R. B. Stein, and W. W. Armstrong, "Machine learning in control of functional electrical stimulation systems for locomotion," *IEEE Transactions on Biomedical Engineering*, vol. 42, no. 6, pp. 541–551, 1995.

[136] S. Jonic, T. Jankovic, V. Gajic, and D. Popvic, "Three machine learning techniques for automatic determination of rules to control locomotion," *IEEE Transactions on Biomedical Engineering*, vol. 46, no. 3, pp. 300–310, 1999.

[137] I. P. Pappas, M. R. Popovic, T. Keller, V. Dietz, and M. Morari, "A reliable gait phase detection system," *IEEE Transactions on Neural Systems and Rehabilitation Engineering*, vol. 9, no. 2, pp. 113–125, 2001.

[138] S. K. Ng and H. J. Chizeck, "Fuzzy model identification for classification of gait events in paraplegics," *IEEE Transactions on Fuzzy Systems*, vol. 5, no. 4, pp. 536–544, 1997.

[139] C. A. Macleod, L. Meng, B. A. Conway, and B. Porr, "Reflex control of robotic gait using human walking data," *PloS ONE*, vol. 9, no. 10, p. e109959, 2014.

[140] D. Hobbelen, T. de Boer, and M. Wisse, "System overview of bipedal robots flame and tulip: Tailor-made for limit cycle walking," in *IEEE/RSJ International Conference on Intelligent Robots and Systems*. France: IEEE, September 2008, pp. 2486–2491.

[141] G. A. Pratt and M. M. Williamson, "Series elastic actuators," in *IEEE/RSJ International Conference on Intelligent Robots and Systems*, vol. 1. Pittsburgh, PA: IEEE, Aug 1995, pp. 399–406.

[142] J. Rummel, Y. Blum, H. Maus, C. Rode *et al.*, "Stable and robust walking with compliant legs," in *IEEE International Conference on Robotics and Automation*. Anchorage, AK: IEEE, May 2010, pp. 5250–5255.

[143] R. van der Linde, "Design, analysis, and control of a low power joint for walking robots, by phasic activation of mckibben muscles," *IEEE Transactions on Robotics and Automation*, vol. 15, no. 4, pp. 599 –604, aug 1999.

[144] K. Narioka and K. Hosoda, "Designing synergistic walking of a whole-body humanoid driven by pneumatic artificial muscles: An empirical study," *Advanced Robotics*, vol. 22, no. 10, pp. 1107–1123, 2008.

[145] R. Niiyama and Y. Kuniyoshi, "Design of a musculoskeletal athlete robot: A biomechanical approach," *Proc. of Climbing and Walking Robots and the Support Technologies for Mobile Machines (CLAWAR 2009)*, pp. 173–180, 2009.

[146] J. Grizzle, J. Hurst, B. Morris, H.-W. Park, and K. Sreenath, "Mabel, a new robotic bipedal walker and runner," in *American Control Conference*. St.Louis, MO: IEEE, June 2009, pp. 2030–2036.

[147] J. Rummel, Y. Blum, and A. Seyfarth, "Robust and efficient walking with spring-like legs," *Bioinspiration & Biomimetics*, vol. 5, no. 4, p. 046004, 2010.

[148] D. Owaki, M. Koyama, S. Yamaguchi, S. Kubo *et al.*, "A 2-d passive-dynamic-running biped with elastic elements," *IEEE Transactions on Robotics*, vol. 27, no. 1, pp. 156–162, 2011.

[149] R. E. Reeve and B. H. Webb, "New neural circuits for robot phonotaxis," *Philosophical Transactions of the Royal Society of London. Series A: Mathematical, Physical and Engineering Sciences*, vol. 361, no. 1811, pp. 2245–2266, 2003.

[150] D. T. Reilly and M. Martens, "Experimental analysis of the quadriceps muscle force and patello-femoral joint reaction force for various activities," *Acta Orthopaedica*, vol. 43, no. 2, pp. 126–137, 1972.

[151] T. A. Blackburn and E. Craig, "Knee anatomy:a brief review," *Physical Therapy*, vol. 60, no. 12, pp. 1556–1560, 1980.

[152] T. Van Eijden, E. Kouwenhoven, J. Verburg, and W. Weijs, "A mathematical model of the patellofemoral joint," *Journal of Biomechanics*, vol. 19, no. 3, pp. 219–229, 1986.

[153] T. Fukunaga, K. Kuo, Y. Kawakami, S. Fukashiro *et al.*, "In vivo behaviour of human muscle tendon during walking," *Proceedings of the Royal Society of London. Series B: Biological Sciences*, vol. 268, no. 1464, pp. 229–233, 2001.

[154] J. B. Nielsen and T. Sinkjær, "Afferent feedback in the control of human gait," *Journal of Electromyography and Kinesiology*, vol. 12, no. 3, pp. 213–217, 2002.

[155] R. D. Beer, R. D. Quinn, H. J. Chiel, and R. E. Ritzmann, "Biologically inspired approaches to robotics: What can we learn from insects?" *Communications of the ACM*, vol. 40, no. 3, pp. 30–38, 1997.

[156] C. L. Vaughan, B. L. Davis, and J. C. O'connor, *Dynamics of human gait*. Human Kinetics Publishers Champaign, Illinois, 1992.

[157] K. Olree and C. Vaughan, "Fundamental patterns of bilateral muscle activity in human locomotion," *Biological Cybernetics*, vol. 73, no. 5, pp. 409–414, 1995.

[158] G. Taga, "A model of the neuro-musculo-skeletal system for human locomotion," *Biological Cybernetics*, vol. 73, no. 2, pp. 97–111, 1995.

[159] V. Inman, H. Ralston, and F. Todd, *Human walking*. Williams & Wilkins, 1981.

[160] K. Pearson, "Common principles of motor control in vertebrates and invertebrates," *Annual Review of Neuroscience*, vol. 16, no. 1, pp. 265–297, 1993.

[161] A. Frigon and S. Rossignol, "Experiments and models of sensorimotor interactions during locomotion," *Biological Cybernetics*, vol. 95, no. 6, pp. 607–627, 2006.

[162] A. Prochazka, "Proprioceptive feedback and movement regulation," *Comprehensive Physiology*, 2010.

[163] B. Verdaasdonk, H. Koopman, and F. Helm, "Energy efficient and robust rhythmic limb movement by central pattern generators," *Neural Networks*, vol. 19, no. 4, pp. 388–400, 2006.

[164] J. Pratt and B. Krupp, "Design of a bipedal walking robot," in *Proc. SPIE*, vol. 6962, April 2008, p. 69621F.

[165] M. Locascio, J. Solomon, and M. Hartmann, "Linear reactive control of three-dimensional bipedal walking in the presence of noise and uncertainty," *Adaptive Behavior*, 2012.

[166] F. Iida, J. Rummel, and A. Seyfarth, "Bipedal walking and running with compliant legs," in *IEEE International Conference on Robotics and Automation*, Roma, April 2007, pp. 3970–3975.

[167] E. Petiot, C. Barrès, B. Chapuis, and C. Julien, "Frequency response of renal sympathetic nervous activity to aortic depressor nerve stimulation in the anaesthetized rat," *Journal of Physiology*, vol. 537, no. 3, pp. 949–959, 2001.

[168] J. Rose and J. G. Gamble, *Human walking*. Lippincott Williams & Wilkins Philadelphia, 2006.

[169] T. J. Klein and M. A. Lewis, "A physical model of sensorimotor interactions during locomotion," *Journal of Neural Engineering*, vol. 9, no. 4, p. 046011, 2012.

[170] T. Takuma and K. Hosoda, "Controlling the walking period of a pneumatic muscle walker," *International Journal of Robotics Research*, vol. 25, no. 9, pp. 861–866, 2006.

[171] G. T. Yamaguchi and F. E. Zajac, "A planar model of the knee joint to characterize the knee extensor mechanism," *Journal of Biomechanics*, vol. 22, no. 1, pp. 1–10, 1989.

[172] S. Mochon and T. McMahon, "Ballistic walking," *Journal of Biomechanics*, vol. 13, no. 1, pp. 49–57, 1980.

[173] S. Grillner, "Control of locomotion in bipeds, tetrapods, and fish," *Comprehensive Physiology*, 1981.

[174] C. Capaday, "The special nature of human walking and its neural control," *Trends in Neurosciences*, vol. 25, no. 7, pp. 370–376, 2002.

[175] E. P. Zehr and J. Duysens, "Regulation of arm and leg movement during human locomotion," *The Neuroscientist*, vol. 10, no. 4, pp. 347–361, 2004.

[176] J. Duysens, H. W. Van de Crommert, B. C. Smits-Engelsman, and F. C. Van der Helm, "A walking robot called human: lessons to be learned from neural control of locomotion," *Journal of Biomechanics*, vol. 35, no. 4, pp. 447–453, 2002.

[177] C. S. Sherrington, "Flexion-reflex of the limb, crossed extension-reflex, and reflex stepping and standing," *The Journal of physiology*, vol. 40, no. 1-2, p. 28, 1910.

[178] S. Degallier, C. Santos, L. Righetti, and A. Ijspeert, "Movement generation using dynamical systems: a humanoid robot performing a drumming task," in *IEEE-RAS International Conference on Humanoid Robots*. Genova: IEEE, Dec 2006, pp. 512–517.

[179] T. Mori, Y. Nakamura, M. Sato, and S. Ishii, "Reinforcement learning for cpg-driven biped robot," in *Proceedings of the national conference on artificial intelligence*, 2004, pp. 623–630.

[180] E. Torres and L. Garrido, "Automated generation of cpg-based locomotion for robot nao," *RoboCup 2011: Robot Soccer World Cup XV*, pp. 461–471, 2012.

[181] F. Gomez-Rodríguez, A. Linares-Barranco, L. Miró, S. Liu *et al.*, "Aer auditory filtering and cpg for robot control," in *IEEE International Symposium on Circuits and Systems*. IEEE, 2007, pp. 1201–1204.

[182] S. Collins, A. Ruina, R. Tedrake, and M. Wisse, "Efficient bipedal robots based on passive-dynamic walkers," *Science*, vol. 307, no. 5712, pp. 1082–1085, 2005.

[183] M. M. Rodgers, "Dynamic biomechanics of the normal foot and ankle during walking and running," *Physical Therapy*, vol. 68, no. 12, pp. 1822–1830, 1988.

[184] P. Crenna and C. Frigo, "Evidence of phase-dependent nociceptive reflexes during locomotion in man," *Experimental Neurology*, vol. 85, no. 2, pp. 336–345, 1984.

[185] J. B. Nielsen, "Motoneuronal drive during human walking," *Brain research reviews*, vol. 40, no. 1, pp. 192–201, 2002.

[186] R. Hayashi, A. Miyake, and S. Watanabe, "The functional role of sensory inputs from the foot: stabilizing human standing posture during voluntary and vibration-induced body sway," *Neuroscience Research*, vol. 5, no. 3, pp. 203–213, 1988.

[187] M. Magnusson, H. Enbom, R. Johansson, and I. Pyykkö, "Significance of pressor input from the human feet in anterior-posterior postural control: the effect of hypothermia on vibration-induced body-sway," *Acta Otolaryngol*, vol. 110, no. 3-4, pp. 182–188, 1990.

[188] M. Do, B. Bussel, and Y. Breniere, "Influence of plantar cutaneous afferents on early compensatory reactions to forward fall," *Experimental Brain Research*, vol. 79, no. 2, pp. 319–324, 1990.

[189] B. M. Van Wezel, F. A. Ottenhoff, and J. Duysens, "Dynamic control of location-specific information in tactile cutaneous reflexes from the foot during human walking," *The Journal of Neuroscience*, vol. 17, no. 10, pp. 3804–3814, 1997.

[190] C. A. Macleod, "Development of a reflexive control system for gait using human walking data," Ph.D. dissertation, University of Strathclyde, 2015.

[191] R. Drake, A. W. Vogl, and A. W. Mitchell, *Gray's anatomy for students*. Elsevier Health Sciences, 2014.

[192] N. Hamilton, W. Weimar, and K. Luttgens, *Kinesiology: Scientific Basis of Human Motion*, ser. Kinesiology: Scientific Basis of Human Motion. McGraw-Hill, 2012.

[193] H. Milner-Brown, R. Stein, and R. Yemm, "The contractile properties of human motor units during voluntary isometric contractions," *The Journal of Physiology*, vol. 228, no. 2, pp. 285–306, 1973.

[194] D. Renjewski and A. Seyfarth, "Robots in human biomechanics - a study on ankle push-off in walking," *Bioinspiration & Biomimetics*, vol. 7, no. 3, p. 036005, 2012.

[195] D. Hobbelen and M. Wisse, "Ankle actuation for limit cycle walkers," *International Journal of Robotics Research*, vol. 27, no. 6, pp. 709–735, June 2008.

[196] D. A. WINTER, "Energy generation and absorption at the ankle and knee during fast, natural, and slow cadences." *Clinical Orthopaedics and Related Research*, vol. 175, pp. 147–154, 1983.

[197] D. H. Sutherland, L. Cooper, and D. Daniel, "The role of the ankle plantar flexors in normal walking." *The Journal of Bone & Joint Surgery*, vol. 62, no. 3, pp. 354–363, 1980.

[198] R. R. Neptune, S. Kautz, and F. Zajac, "Contributions of the individual ankle plantar flexors to support, forward progression and swing initiation during walking," *Journal of Biomechanics*, vol. 34, no. 11, pp. 1387–1398, 2001.

[199] S. Nadeau, D. Gravel, A. B. Arsenault, and D. Bourbonnais, "Plantarflexor weakness as a limiting factor of gait speed in stroke subjects and the compensating role of hip flexors," *Clinical Biomechanics*, vol. 14, no. 2, pp. 125–135, 1999.

[200] T. F. Novacheck, "The biomechanics of running," *Gait & Posture*, vol. 7, no. 1, pp. 77–95, 1998.

[201] C. L. Lewis and D. P. Ferris, "Walking with increased ankle pushoff decreases hip muscle moments," *Journal of Biomechanics*, vol. 41, no. 10, pp. 2082–2089, 2008.

[202] J. Perry, J. R. Davids *et al.*, *Gait analysis: normal and pathological function.* Thorofare, New Jersey: SLACK Incorporated, 1992.

[203] S. Simcox, S. Parker, G. M. Davis, R. W. Smith, and J. W. Middleton, "Performance of orientation sensors for use with a functional electrical stimulation mobility system," *Journal of Biomechanics*, vol. 38, no. 5, pp. 1185 – 1190, 2005.

[204] M. Granat, D. Maxwell, C. Bosch, A. Ferguson, K. Lees, and J. Barbenel, "A body-worn gait analysis system for evaluating hemiplegic gait," *Medical Engineering & Physics*, vol. 17, no. 5, pp. 390–394, 1995.

[205] R. C. Gonzalez, R. E. Woods, and S. L. Eddins, *Digital Image Processing Using MATLAB*. New Jersey: Prentice Hall, 2004.

[206] M. W. Whittle, *Gait analysis: an introduction*, 4th ed. Butterworth-Heinemann, Dec 2006.

[207] H. J. van Hedel, M. Wirz, and V. Dietz, "Assessing walking ability in subjects with spinal cord injury: validity and reliability of 3 walking tests," *Archives of Physical Medicine and Rehabilitation*, vol. 86, no. 2, pp. 190–196, 2005.

[208] C. Stewart, N. Postans, M. Schwartz, A. Rozumalski, and A. Roberts, "An investigation of the action of the hamstring muscles during standing in crouch using functional electrical stimulation (fes)," *Gait & Posture*, vol. 28, no. 3, pp. 372 – 377, 2008.

[209] M. D. Fox and S. L. Delp, "Contributions of muscles and passive dynamics to swing initiation over a range of walking speeds," *Journal of Biomechanics*, vol. 43, no. 8, pp. 1450 – 1455, 2010.

[210] F. E. Zajac and M. E. Gordon, "Determining muscle's force and action in multi-articular movement." *Exercise and Sport Sciences Reviews*, vol. 17, no. 1, pp. 187–230, 1989.

[211] A. Hernndez, A. Lenz, and D. Thelen, "Electrical stimulation of the rectus femoris during pre-swing diminishes hip and knee flexion during the swing phase of normal gait," *IEEE Transactions on Neural Systems and Rehabilitation Engineering*, vol. 18, no. 5, pp. 523–530, Oct 2010.

[212] K. M. Steele, A. Seth, J. L. Hicks, M. S. Schwartz, and S. L. Delp, "Muscle contributions to support and progression during single-limb stance in crouch gait," *Journal of Biomechanics*, vol. 43, no. 11, pp. 2099 – 2105, 2010.

[213] R. S. Barrett, T. F. Besier, and D. G. Lloyd, "Individual muscle contributions to the swing phase of gait: An emg-based forward dynamics modelling approach," *Simulation Modelling Practice and Theory*, vol. 15, no. 9, pp. 1146 – 1155, 2007.

[214] W. G. Coole Jr and J. H. Gieck, "An analysis of hamstring strains and their rehabilitation," *Journal of Orthopaedic & Sports Physical Therapy*, vol. 9, no. 2, pp. 77–85, 1987.

[215] F. C. Anderson, S. R. Goldberg, M. G. Pandy, and S. L. Delp, "Contributions of muscle forces and toe-off kinematics to peak knee flexion during the swing phase of normal gait: an induced position analysis," *Journal of Biomechanics*, vol. 37, no. 5, pp. 731 – 737, 2004.

[216] S. R. Goldberg, F. C. Anderson, M. G. Pandy, and S. L. Delp, "Muscles that influence knee flexion velocity in double support: implications for stiff-knee gait," *Journal of Biomechanics*, vol. 37, no. 8, pp. 1189 – 1196, 2004.

[217] B. Porr, *Comedi Library*, 2015. [Online]. Available: http://www.linux-usb-daq.co.uk/comedi/doc_html/

[218] H. Nord and E. Chambe-Eng, *Qt*, 2015. [Online]. Available: http://www.qt.io/

[219] E. A. Pfeiffer, "Electrical stimulation of sensory nerves with skin electrodes for research, diagnosis, communication and behavioral conditioning: A survey," *Medical and Biological Engineering*, vol. 6, no. 6, pp. 637–651, 1968.

[220] F. Alton, L. Baldey, S. Caplan, and M. Morrissey, "A kinematic comparison of overground and treadmill walking," *Clinical Biomechanics*, vol. 13, no. 6, pp. 434–440, 1998.

[221] D. Hobbelen and M. Wisse, "Controlling the walking speed in limit cycle walking," *International Journal of Robotics Research*, vol. 27, no. 9, pp. 989–1005, 2008.

[222] M. Okada, K. Tatani, and Y. Nakamura, "Polynomial design of the nonlinear dynamics for the brain-like information processing of whole body motion," in *IEEE International Conference on Robotics and Automation*, vol. 2. IEEE, 2002, pp. 1410–1415.

[223] M. Lewis, F. Tenore, and R. Etienne-Cummings, "Cpg design using inhibitory networks," in *IEEE International Conference on Robotics and Automation*. IEE, April 2005, pp. 3682–3687.

[224] R. Pfeifer, M. Lungarella, and F. Iida, "Self-organization, embodiment, and biologically inspired robotics," *Science*, vol. 318, no. 5853, pp. 1088–1093, 2007.

[225] S. Grillner, "Biological pattern generation: the cellular and computational logic of networks in motion," *Neuron*, vol. 52, no. 5, pp. 751–766, 2006.

[226] A. Ijspeert and A. Crespi, "Online trajectory generation in an amphibious snake robot using a lamprey-like central pattern generator model," in *2007 IEEE International Conference on Robotics and Automation*. IEEE, April 2007, pp. 262–268.

[227] S. Hirose and E. F. Fukushima, "Snakes and strings: new robotic components for rescue operations," *The International Journal of Robotics Research*, vol. 23, no. 4-5, pp. 341–349, 2004.

[228] P. Manoonpong, T. Kulvicius, F. Wörgötter, L. Kunze, D. Renjewski, and A. Seyfarth, "Compliant ankles and flat feet for improved self-stabilization and passive dynamics of the biped robot - runbot?" in *11th IEEE-RAS International Conference on Humanoid Robots (Humanoids)*. IEEE, 2011, pp. 276–281.

[229] A. D. Kuo, "Energetics of actively powered locomotion using the simplest walking model," *Journal of Biomechanical Engineering*, vol. 124, no. 1, pp. 113–120, 2002.

[230] R. C. Browning, E. A. Baker, J. A. Herron, and R. Kram, "Effects of obesity and sex on the energetic cost and preferred speed of walking," *Journal of Applied Physiology*, vol. 100, no. 2, pp. 390–398, 2006.

[231] K. J. Klose, P. L. Jacobs, J. G. Broton, R. S. Guest, B. M. Needham-Shropshire, N. Lebwohl, M. S. Nash, and B. A. Green, "Evaluation of a training program for persons with sci paraplegia using the parastep® 1 ambulation system: part 1. ambulation performance and anthropometric measures," *Archives of Physical Medicine and Rehabilitation*, vol. 78, no. 8, pp. 789–793, 1997.

[232] G. Pfurtscheller, G. R. Müller, J. Pfurtscheller, H. J. Gerner, and R. Rupp, "'thought'–control of functional electrical stimulation to restore hand grasp in a patient with tetraplegia," *Neuroscience Letters*, vol. 351, no. 1, pp. 33–36, 2003.

[233] R. J. Vogelstein, F. Tenore, R. Etienne-Cummings, M. A. Lewis, and A. H. Cohen, "Dynamic control of the central pattern generator for locomotion," *Biological Cybernetics*, vol. 95, no. 6, pp. 555–566, 2006.

[234] P. Sweeney, G. Lyons, and P. Veltink, "Finite state control of functional electrical stimulation for the rehabilitation of gait," *Medical and Biological engineering and Computing*, vol. 38, no. 2, pp. 121–126, 2000.

[235] F. Sepulveda, M. H. Granat, and A. Cliquet, "Two artificial neural systems for generation of gait swing by means of neuromuscular electrical stimulation," *Medical Engineering and Physics*, vol. 19, no. 1, pp. 21–28, 1997.

[236] A. Mulder, P. Veltink, H. Boom, and G. Zilvold, "Low-level finite state control of knee joint in paraplegic standing," *Journal of Biomedical Engineering*, vol. 14, no. 1, pp. 3–8, 1992.

[237] T. Bajd, A. Kralj, M. Štefančič, and N. Lavrač, "Use of functional electrical stimulation in the lower extremities of incomplete spinal cord injured patients," *Artificial Organs*, vol. 23, no. 5, pp. 403–409, 1999.

[238] M. Ladouceur and H. Barbeau, "Functional electrical stimulation-assisted walking for persons with incomplete spinal injuries: changes in the kinematics and physiological cost of overground walking." *Scandinavian Journal of Rehabilitation Medicine*, vol. 32, no. 2, pp. 72–79, 2000.

[239] L. A. Johnson and A. J. Fuglevand, "Mimicking muscle activity with electrical stimulation," *Journal of Neural Engineering*, vol. 8, no. 1, p. 016009, 2011.

[240] T. M. Kesar, R. Perumal, D. S. Reisman, A. Jancosko, K. S. Rudolph, J. S. Higginson, and S. A. Binder-Macleod, "Functional electrical stimulation of ankle plantarflexor and dorsiflexor muscles effects on poststroke gait," *Stroke*, vol. 40, no. 12, pp. 3821–3827, 2009.

[241] A. Kottink, L. Oostendorp, J. Buurke, A. Nene *et al.*, "The orthotic effect of functional electrical stimulation on the improvement of walking in stroke patients with a dropped foot: A systematic review," *Artificial Organs*, vol. 28, no. 6, pp. 577–586, 2004.

[242] S. Khamis, R. Martikaro, S. Wientroub, Y. Hemo, and S. Hayek, "A functional electrical stimulation system improves knee control in crouch gait," *Journal of children's orthopaedics*, vol. 9, no. 2, pp. 137–143, 2015.

[243] R. M. Enoka, "Eccentric contractions require unique activation strategies by the nervous system," *Journal of Applied Physiology*, vol. 81, no. 6, pp. 2339–2346, 1996.

[244] U. Bogataj, N. Gros, M. Kljajić, and R. Aćimović-Janežič, "Enhanced rehabilitation of gait after stroke: a case report of a therapeutic approach using multichannel functional electrical stimulation," *IEEE Transactions on Rehabilitation Engineering*, vol. 5, no. 2, pp. 221–232, 1997.